

Comparison of *in vivo* solid-phase microextraction (SPME) to Folch
extraction of brain lipids in *Rattus norvegicus* using LC-MS

Cian Monnin

A Thesis

In

The Department

Of

Chemistry and Biochemistry

Presented in Partial Fulfilment of the Requirements

For the Degree of Master of Sciences (Chemistry) at

Concordia University

Montréal, Québec, Canada

May 2017

© Cian Monnin, 2017

Abstract

Comparison of *in vivo* solid-phase microextraction (SPME) to Folch extraction of brain lipids in *Rattus norvegicus* using LC-MS

Cian Monnin, M. Sc.

Lipidomics is the comprehensive study of the lipids present in an organism. To achieve high analytical sensitivity and good lipid coverage in global lipidomics, sample preparation, mobile phase composition, chromatographic separation, and data processing parameters must be optimized. Solid-phase microextraction (SPME) is a non-exhaustive, *in vivo* sample preparation method that has not previously been applied to lipidomics studies but that provides a promising alternative to microdialysis for *in vivo* lipid analysis. Before SPME can be successfully applied to lipidomic studies, it is important to increase the sensitivity of liquid chromatography-mass spectrometry (LC-MS) detection as much as possible. This was accomplished by comparing the effect of four different mobile phase additives on signal intensity using negative electrospray ionization (ESI): acetic acid, ammonium acetate, ammonium hydroxide and ammonium acetate with acetic acid. Acetic acid at a concentration of 3.5 mM outperformed the other additives tested causing a 42% increase in lipid coverage along with a 2-19-fold increase in signal compared to 10 mM ammonium acetate. The main disadvantages of acetic acid were (i) wide peak shape for two lipid classes: phosphatidic acid and phosphatidylserine and (ii) reduction of signal intensity for phosphatidylcholine and ceramide lipids. These results show that although basic pH promotes in-solution ionization, surface, electrochemical and gas-phase processes provide significant contributions to overall ESI efficiency thus resulting in enhanced ionization at acidic pH. Acetic acid is good choice of additive for negative mode ESI due its ability to increase formation of deprotonated adducts, low molecular volume, high-gas phase proton affinity, and capability for electrochemical reduction. Traditionally, lipids are extracted from brain tissue using the Folch method, a biphasic liquid-liquid extraction method that relies on chloroform/methanol solvent. In this study, SPME was compared to the Folch method to determine if it is a viable alternative. The main SPME parameters that affect extraction efficiency of *in vivo* SPME were evaluated for this application: extraction time, desorption time, and desorption solvent. Analysis of SPME extracts showed 147 and 613 features versus 1368 and 1161 detected in the Folch extract in positive mode and negative mode, respectively. Using LipidSearch 127 lipids in positive mode and 57 lipids in negative mode were identified in the SPME extracts verses 145 in positive mode and 99 in negative mode for the Folch extracts. This study represents the first step towards the development and inter-laboratory validation of *in vivo* SPME demonstrating its ability as a new and viable alternative to Folch extractions that can be used in lipidomics studies of the brains of alive, awake animals for the first time.

Acknowledgements

I would like to extend my deepest and most sincere gratitude to my supervisor, Professor Dajana Vuckovic, whose tireless enthusiasm, guidance and support I could not have done without.

I would like to thank my committee members, Professors Yves Gélinas and Vladamir Titorenko for the insights they shared.

It was a pleasure to work alongside my colleagues, Dmitri Sitnikov, Irina Slobodchikova, Parsram Ramrup, Hanieh Peyman, Mariana De Sá Tavares Russo, Rosalynde Sonnenberg, Alexander Napylov, and Ankita Gupta.

All my love to my family Fionnuala, Jean Paul, Darragh and Robin, and my partner, Delphine.

Contribution of Authors

Chapter 2

This chapter entitled “Improving negative ESI-LC-MS lipidomic analysis of human plasma using acetic acid as a mobile phase additive” authored by Cian Monnin, Parsram Ramrup, Carolann Daigle-Young and Dajana Vuckovic was submitted for publication to Rapid Communications in Mass Spectrometry on May 18, 2017.

C.M. performed all experimental work and data analysis for the comparison of acetic acid and ammonium hydroxide. C.M. and P.R. performed all experimental work and data analysis for the comparison of acetic acid and ammonium acetate. C.D-Y. assisted in data analysis for the comparison of acetic acid and ammonium acetate. C.M. and D.V. designed all experiments, interpreted results and co-wrote the manuscript. The version included here is the pre-peer review version which has been submitted to Rapid Communications in Mass Spectrometry. All authors reviewed and revised the manuscript.

Chapter 3

This chapter entitled “Comparison of *in vivo* solid-phase microextraction (SPME) to Folch extraction of brain lipids in *Rattus norvegicus* using LC-MS” authored by Cian Monnin, Clement Hamani, Germán Augusto Gómez-Ríos, Nathaly Reyes-Garcés, Ezel Boyacı, Barbara Bojko, Janusz Pawliszyn, Dajana Vuckovic is the first draft of manuscript in preparation that will be submitted for publication in autumn 2017.

C.M. performed all LC-MS analyses, Folch extraction, *ex vivo* SPME extraction time profile and SPME desorption experiments and analysis work. C.M and D.V. designed Folch extraction, *ex vivo* SPME extraction time profile and SPME desorption experiments. D.V. supervised all work performed at Concordia University. C.H. prepared brain tissue samples for Folch experiment and designed and supervised all *in vivo* animal studies at CAMH. G.A.G-R., N.R-G., and E.B. performed *in vivo* SPME sampling. G.A.G-R., N.R-G., E.B., B.B., and J.P. designed *in vivo* SPME experiment. G.A.G-R. also designed and prepared the micropositioner used for *in vivo* sampling in this work. J.P. supervised all work at the University of Waterloo and is the PI for this project. C.M. performed LC-MS analysis and data processing of *in vivo* SPME, including comparison to Folch described in this chapter. C.M. and D.V. interpreted results and co-wrote

this first draft of the manuscript, that is included in this thesis. All authors will review and contribute to the final version of the manuscript prior to manuscript submission.

Appendix B

This appendix entitled “Systematic Assessment of Seven Solvent and Solid-Phase Extraction Methods for Metabolomics Analysis of Human Plasma by LC-MS” authored by Dmitri G. Sitnikov, Cian S. Monnin and Dajana Vuckovic is the manuscript published in Scientific Reports 6, Article number: 38885 (2016)

D.G.S. and C.S.M. performed all experimental and analysis work. Specifically, C.S.M. performed MTBE extractions, data analysis using Agilent Mass Profiler Pro and manual curation of several data sets and formatting of images for final article. D.G.S. and D.V. designed the experiment, interpreted results and co-wrote the manuscript. All authors reviewed and revised the manuscript.

1. Introduction	1
1.1. Lipidomics	1
1.1.1. Glycerolipids	2
1.1.2. Glycerophospholipids	2
1.1.3. Sphingolipids	3
1.2. Lipid composition of brain	3
1.2.1. Human brain	3
1.2.2. Rat brain	6
1.2.3. Lipid composition of plasma	9
1.3. Sample preparation	9
1.3.1. Liquid-liquid extraction	9
1.3.2. In vivo sampling: Microdialysis	11
1.3.3. In vivo sampling: Solid-phase microextraction	12
1.3.4. SPME versus MD	15
1.4. Liquid chromatography-mass spectrometry for lipidomics	16
1.4.1. LC	16
1.4.2. Electrospray ionisation (ESI)	17
1.4.3. MS	20
1.4.4. Quadrupole-Time-of-Flight (QTOF)	22
1.4.5. Orbitrap	24
1.4.6. Data processing	26
1.5. Research objectives	30
2. Improving negative ESI-LC-MS lipidomic analysis of human plasma using acetic acid as a mobile phase additive	31
2.1. Abstract	31

2.1.1.	Keywords	32
2.2.	Introduction	32
2.3.	Experimental.....	35
2.3.1.	Chemicals.....	35
2.3.2.	Preparation of lipid standards	36
2.3.3.	Preparation of human plasma samples	36
2.3.4.	LC-MS analysis on LTQ Orbitrap Velos.....	36
2.3.5.	LC-MS analysis on Agilent 6550 iFunnel QTOF	37
2.3.6.	Post-column gas-phase addition of mobile phase additives on Agilent 6550 iFunnel QTOF using Dual AJS ESI source	38
2.3.7.	Data processing	39
2.4.	Results and Discussion.....	40
2.4.1.	Comparison of AmOH versus AA	40
2.4.2.	Additive introduction in gas-phase using dual spray configuration.....	41
2.4.3.	Additive introduction in mobile phase and effect of AmOH concentration.....	41
2.4.4.	Comparison of AA versus AmAc and AmAc with AA as mobile phase additives	46
2.4.5.	Does AA promote both deprotonation and acetate adduct formation?	49
2.4.6.	Effect of AA on chromatographic peak shape	52
2.4.7.	Examining gas-phase versus solution-phase contributions of AA to lipid ionization	52
2.5.	Conclusions	56
3.	Comparison of in vivo solid-phase microextraction (SPME) to Folch extraction of brain lipids in <i>Rattus norvegicus</i> using LC-MS	57
3.1.	Abstract	57
3.2.	Introduction	58
3.3.	Materials and methods	60
3.3.1.	Chemicals and materials	60

3.3.2.	Folch method for brain tissue samples	61
3.3.3.	SPME extraction time optimization	62
3.3.4.	SPME desorption time and desorption solvent optimization.....	62
3.3.5.	In vivo SPME sampling.....	63
3.3.6.	LC-MS/MS	63
3.3.7.	Data processing and analysis	64
3.4.	Results and discussion.....	65
3.4.1.	Ex vivo SPME extraction from brain tissue and evaluation of extraction time.....	66
3.4.2.	SPME desorption solvent and desorption time	75
3.4.3.	Folch lipid profile of hippocampus and nucleus accumbens brain regions.....	78
3.4.4.	In vivo SPME lipid profile of hippocampus	90
3.4.5.	Folch versus in vivo SPME.....	91
3.4.6.	Matrix effects	94
3.5.	Conclusions	97
4.	Conclusions and future work.....	98
4.1.	Conclusions	98
4.2.	Future work	100
	Appendix A Supplementary information for Chapter 2 and 3.	111
	Appendix B Systematic Assessment of Seven Solvent and Solid-Phase Extraction Methods for Metabolomics Analysis of Human Plasma by LC-MS.....	142

List of Figures

Figure 1.1 Chemical structures of three main lipid classes of interest in this thesis: (a) GP, (b) GL and (c) SP. Each panel lists the associated subclasses that belong to the class of interest and shows a structure of a representative lipid belonging to that class. (a) shows the three different sections of an aliphatic GP lipid (i) the hydrophobic acyl chains of varying length (ii) the glycerol backbone common to all GPs and GLs and (iii) the polar head group that characterises a specific GP lipid subclass. In this example, the head group is a choline meaning this lipid belongs to the GP subclass PC. (b) shows a TG, a glycerol backbone with three acyl chains. (c) shows a ceramide, a sphingosine backbone that has been N-acylated. Lipid structures obtained from LIPID MAPS^[34]4

Figure 1.2 Chemical structure of main glycerophospholipid subclasses showing common glycerol backbone bound to two acyl chains with a polar phosphate headgroup (a) PA, (b) PS, (c) PC, (d) PG, (e) PE and (f) PI. R1 and R2 represent acyl chains of varying length and varying degree of unsaturation. Lipid structures obtained from LIPID MAPS^[34]5

Figure 1.3 Chemical structure of main sphingolipid subclasses showing common sphingoid base backbone in (a) sphingosine. The addition of an amide-linked acyl chain in the sn-2 position leads to (b) Cer whereas (c) SM subclass has an amide-linked acyl chain in the sn-2 position and a phosphocholine head group in the sn-3 position. R represents amide-linked acyl chains of varying length and degrees of unsaturation. Lipid structures obtained from LIPID MAPS^[34]6

Figure 1.4 Lipid composition of rat cerebellum (orange, n=8) and hippocampus (green, n=8) regions. Shotgun lipidomic analysis of Bligh and Dyer brain tissue extracts using an Orbitrap fusion MS. Glucosylceramide (HexCer), sulfatide (SHexCer) the O- nomenclature denotes GP with an acyl chain bonded via a vinyl ether bond rather than an ester bond in the sn-1 position and are also known as plasmalogens figure reprinted from reference^[35] with permission from Springer publications7

Figure 1.5 Comparison of Folch to Bligh and Dyer method. Iverson et al^[48] prepared 45 samples with different total % lipid content using either Folch or Bligh and Dyer methods in duplicate. At low % lipid content, the two methods showed good agreement. Once lipid content increases above 2% (as is the case with brain tissue) the Bligh and Dyer method begins to significantly underestimate lipid content. Figure reproduced from reference^[48] with permission from publisher.11

Figure 1.6 SPME workflow for extraction of analytes from animal brain tissue. Figure from reference^[67] reprinted with permission from John Wiley and Sons publisher13

Figure 1.7 Comparison of *in vivo* SPME to MD for measurement of two neurotransmitters, serotonin and dopamine. (a) shows the change in serotonin levels as a function of time. SPME and MD both show an up regulation of serotonin (5-HT) after the administration of fluoxetine. (b) shows that dopamine (DA) levels remained constant as expected after the administration of 10 mg/kg of fluoxetine at t=0. Values reported are the mean ± standard deviation from n=12 rats. Sampling was 30 min for each time point for both MD and SPME. Figure reprinted from reference^[55] with permission from John Wiley and Sons.15

Figure 1.8 Schematic of electrospray ionization LC-MS interface in positive-ion mode.....18

Figure 1.9 High resolving power is required to distinguish lipids with the same nominal mass .20

Figure 1.10 Schematic of QTOF Figure reproduced from reference^[93] with permission from John Wiley and Sons.....23

Figure 1.11 Ion trajectory around the inner electrode of an orbitrap. “Reprinted with permission from A. Makarov. Electrostatic Axially Harmonic Orbital Trapping: A High-Performance Technique of Mass Analysis^[95]. Copyright 2000 American Chemical Society”25

Figure 1.12 Schematic of an LTQ Orbitrap Velos mass spectrometer. Figure reproduced from reference^[97] under the CC-BY 4.0 license28

Figure 1.13 Comparison of CID and HCD fragmentation of PC (34:1). (a) shows CID product spectrum of PC(34:1) $[M+H]^+$ 760.57 selected for fragmentation in plasma in positive mode ESI. This was obtained in the linear ion trap. The fatty acid composition of the PC has been determined via the CID fragmentation but the headgroup of the PC was not detected due to m/z cut-off of ion trap. Fragments giving compositional information of acyl chains: 478.59 -FA (18:1)(as ketene), 496.39 -FA (18:1). 522.49 -FA (16:0)(as ketene). Fragment identities obtained from^[35]. (b) shows HCD product spectrum of the same PC (34:1) which was obtained in Orbitrap after fragmentation in the HCD collision cell and confirms presence of the headgroup with m/z of 184.07.....27

Figure 1.14 De-isotoping and de-adducting is an important part of data processing to arrive at correct number of putative features. (a) shows a screenshot from SIEVE software, a mass list for a compound with MW 794.6218. The $[M+H]^+$, $[M+Na]^+$, and $[M+NH_4]^+$ have been highlighted. The software has labelled the isotope peaks, M+1, M+2 etc... as all belonging to one compound with the MW of 794.6218. (b) shows the spectrum of this compound with the $[M+NH_4]^+$ being the dominant adduct. There are 51 hits from a LIPIDMAPS search for lipids of this mass belonging to the GL, GP and PK lipid classes. Due to the $[M+NH_4]^+$ being the dominant adduct this is most likely TG (48:6).....29

Figure 2.1 Overview of experimental design for comparison of mobile-phase additives using either Orbitrap or QTOF. The stated additives were added directly into mobile phases A and B 40

Figure 2.2 Comparison of the influence of AA and AmOH on lipid signal intensity when (a) additive is introduced post-column in gas-phase using dual spray configuration and (b) additive is present directly in mobile phase. (a) shows the dependence of lipid signal intensity in Standard Mix I upon addition of AA or AmOH in gas-phase using either methanol or acetonitrile as solvent after lipid separation using CSH C₁₈ column. Normal calibration solution that was used

for reference values consists of internal calibrants dissolved in 95% acetonitrile, 5% water with 0.01% AA. All peak areas were normalized to this reference. (b) shows the dependence of lipid signal intensity of Internal Standard Mix 1 spiked into human plasma at 200 ng/mL concentration upon use of AA (0.02%) or AmOH (0.014-0.05%) in mobile phase. The analytes were separated using pH-stable C₁₈ EVO column. All peak areas were normalized to the peak areas obtained with 0.02% AA mobile phase. For both panels a and b, all data was acquired on QTOF and the results shown are for n=3 analyses.43

Figure 2.3 Summary of lipidomic results obtained from human plasma samples (n=2) analysed on QTOF using different mobile phase additives and EVO C₁₈ column. Ion maps for 0.02% AA (a) and 0.014-0.05% AmOH (b-d) show that AA provides higher lipid coverage and allows the detection of additional features absent in the AmOH ion maps. Total number of features is shown in top right corner of each panel, and shows that AA increased lipid coverage by 40%, 109% and 130% respectively when used as an additive compared to increasing concentrations of AmOH. (e) shows the effect of additive on number of features binned according to specific intensity ranges. All data presented was processed using MPP. Note: n=3 samples were injected, but one replicate was removed from further data processing due possible spiking of internal standards error.45

Figure 2.4 Comparison of the influence of 0.02% AA compared to 10 mM AmAc and 10 mM AmAc with 0.02% AA on the signal intensity of lipids in (a-b) Internal Standard Mix II spiked into plasma samples at final concentration of 100 ng/mL (n=4) and (c-d) human plasma after LipidSearch identification. (a) normalizing the peak area to 0.02% AA shows that 0.02% AA causes an increase in signal intensity for six of the lipids present: PI, LPC, PG, PS, PE, SM. Ceramide shows best signal intensity with 10 mM AmAc with 0.02% AA. (b) LSM (d17:1) was not detected in 0.02% AA and showed the highest signal intensity in 10 mM AmAc. (c) LipidSearch was used to identify lipids in plasma samples after isopropanol precipitation. Peak areas of all ions seen for each individual lipid belonging to a given subclass were then summed to give a total area for each subclass. These subclass total areas were then normalized to the mobile phase containing AA at 0.02% (v/v). AA causes significant increase in signal for 11 lipid

subclasses when compared to 10 mM AmAc as shown in (c). AA caused signal decrease for two lipid subclasses: ceramides and PC when compared to 10 mM AmAc (d). For all panels, all data was acquired on CSH C₁₈ and Orbitrap.48

Figure 2.5 Comparison of lipid coverage obtained with 0.02% AA (a), 10 mM AmAc (b) and 10 mM AmAc with 0.02% AA (c). The panels show ion maps of lipid features in plasma samples (n=4) after isopropanol precipitation detected with SIEVE. In addition to the criteria outlined above these ion maps only show features with RSD <30%. AA shows an increase of compared to AmAc (b).10 mM AmAc and 0.02% AA (c) shows the fewest number of features with 2077 using a CSH C₁₈ column on an Orbitrap MS.....50

Figure 2.6 Extracted ion chromatograms from plasma samples of lipids identified with LipidSearch (a) m/z 433.2356 corresponding to [M-H]⁻ ion of LPA (18:2) and (b) m/z 884.5415 corresponding to [M-H]⁻ of PI (18:1/20:4). The peak height for LPA increased from 4.23x10⁵ to 1.05x10⁶, a 2.4-fold increase when 0.02% AA was used as the additive, despite the increase in tailing. The peak height for PI (18:1/20:4) increased from 9.96x10⁴ to 9.5x10⁵, a 9.5-fold increase while peak shape quality is retained with 0.02% AA as the additive. Plasma samples separated with a CSH C₁₈ and analyzed on Orbitrap.53

Figure 2.7 The influence of AA in the gas phase on Internal Standard Mix I at a concentration of 200 ng/mL in 70% MeOH separated on a CSH column and analyzed on QTOF MS, n=3 analyses. Mobile phases with and without AA were used to assess the addition of AA in the gas phase. The auxiliary spray was used to introduce a solvent with or without AA present to evaluate the addition of AA in the gas phase.55

Figure 3.1 Example extraction time profiles of PS (17:0/17:0) (a-b), LPS (17:0)(c-f), LPC (17:0)(g-i) and TG d5 (17:0/17:1/17:0)(k) obtained from the extraction of lipid standard mix (a,c,e,g, and i) and from lipid standard spiked into brain tissue (b,d,f,h,j, and k) extracted with SPME using six different extraction times: 5 min, 15 min, 30 min, 1 hour, 2 hours, and 20 hours.

All extractions were performed in duplicate and analysed using a CSH C₁₈ column on an orbitrap73

Figure 3.2 Comparison of 5 min SPME performed *ex vivo* immediately after thawing intact brain and the following the 20 hour extraction at room temperature. (a) shows a sub section of Cer and CerP that were released after 20 hours. (b) shows PIs that were released after 20 hours and (c) shows Cer and CerP species that did not exhibit release after 20 hour77

Figure 3.3 Evaluation of (a) desorption time (b) a sequential desorption from 100% MeOH into 100% IPA including analysis of the combined MeOH and IPA desorptions in a single LC-MS analysis and (c) different combinations of MeOH and IPA (100% MeOH; 50:50 MeOH/IPA; 20:80 MeOH:IPA). LC-MS analysis performed using a CSH C₁₈ column on QTOF, n=3.80

Figure 3.4 Ion maps of *in vivo* SPME extracts of hippocampus region (n=3) in (a) positive ESI mode and (b) negative ESI mode. Data was processed using SIEVE. The sequential desorption into IPA reveals unique features that were not detected in the MeOH extract.81

Figure 3.5 Ion maps of Folch extracts of hippocampus (8 biological replicates, n=2 technical replicates per sample) and nucleus accumbens (4 biological replicates, n=2 technical replicates per sample) regions after Orbitrap LC-MS analysis in (a) positive ESI mode and (b) negative ESI mode. Data was processed using SIEVE with the following criteria features with >30% RSD in QC samples were excluded, features with retention time < 2 mins and >25 mins were excluded, features with MW >1200 were excluded. In addition, each feature also had to meet the following criteria: detected in 66% of samples for either region, good peak quality via manual inspection, and signal >5x that of blank.83

Figure 3.6 Comparison of lipid signal intensities observed for hippocampus and nucleus accumbens. The mean peak area of each of the identified lipid sub classes were summed. The sum of peak areas in the hippocampus region/sum of peak areas in the nucleus accumbens region

were compared. A value <0.5 (indicated by red dash) shows that significantly less of that subclass is observed in the hippocampus region while a value >2 (indicated by red dash) shows that significantly more of that lipid subclass is observed in the hippocampus region. Lipid areas were corrected using IS MIX II on a subclass basis. Folch extracts of hippocampus (8 biological replicates, $n=2$) and nucleus accumbens(4 biological replicates, $n=2$) regions were analysed on an using as CSH C_{18} column on an Orbitrap.88

Figure 3.7 The PCA plots from (a) positive ESI mode and (b) negative ESI mode of the Folch extracts of the two brain regions hippocampus $n=16$ (blue), nucleus accumbens (red) $n=8$ and QC (yellow) $n=5$. (H7 replicates omitted from positive mode PCA due to high RSD)89

Figure 3.8 (a-b) Composition of the hippocampus according to the number of lipid classes confidently identified with LipidSearch from the Folch Extraction and *in vivo* SPME in positive mode. According to LipidSearch SPME extracts contain mostly GL, 95%, while in Folch GPs make up 40% of the lipids. (c-d) show the same comparison but in negative mode. Here both methods show a similar % of GPs and SLs.93

Figure 3.9 Response of standard mix spiked post extraction to monitor matrix effects in Folch extracts (a-b) and *in vivo* SPME extracts (c-d).....96

List of Tables

Table 1.1 Lipid composition of human plasma. Plasma was obtained from 100 individuals between the ages of 40 and 50. Table adapted from reference ^[38] with permission from The American Society for Biochemistry and Molecular Biology	8
Table 1.2 Common adducts observed for lipid subclasses in positive and negative ESI adapted from reference ^[75] reprinted with permission from Elsevier	19
Table 1.3 Summary of headgroup ions observed for different GP subclasses	21
Table 1.4 Grading criteria used by LipidSearch	29
Table 2.1 Effect of additive on the formation of deprotonated [M-H] ⁻ ions and acetate adducts [M+CH ₃ COO] ⁻ . Peak areas are shown for Internal Standard Mix I spiked into plasma giving final concentration of 200 ng/mL (n=3). The deprotonated form of the lipid is the most abundant ion for five lipids: LPS, LPE, PG, PS and PE. The acetate adduct is the dominant form for PC, while LPC shows intense ions for both deprotonated ion and acetate adduct. LC-MS analysis was performed using C ₁₈ EVO column with additives present in the mobile phase at either 0.02% AA or 0.02% AmOH on QTOF MS.....	51
Table 2.2 Effect of additive on the formation of deprotonated [M-H] ⁻ ions and acetate adducts [M+CH ₃ COO] ⁻ . Peak areas are shown for Internal Standard Mix I spiked into plasma giving final concentration of 75 ng/mL (n=4). The deprotonated form is the most intense ion for four lipids: LPS, PG, PS and PE. The acetate adduct is the dominant form for PC. LPC shows a strong signal for both deprotonated form and the acetate adduct. LC-MS analysis was performed using CSH C ₁₈ on Orbitrap with mobile phase either containing 0.02% AA or 10 mM AmAc. LPE (17:1), although present in the mixture was not detected.....	51

Table 3.1 Summary of extraction times required to reach equilibrium in solvent and tissue samples for spiked non-endogenous lipids. *Degradation observed. †Release of PS was observed after 20 hours. ‡TG was not soluble in 20% MeOH.....74

Table 3.2 Number of putative lipids detected using *ex vivo* SPME from brain tissue and the effect of extraction time on lipid coverage. The data was obtained using SIEVE software with the criteria for the feature to be included being: detected in both replicates of samples for each time point, good peak quality via manual inspection, and signal >5-times that of the blank, features with retention time <2 min and >25 min excluded, and features with MW >1200 excluded, n=275

Table 3.3 Number of putative lipids detected from *in vivo* SPME from hippocampus region using SIEVE software, features with >30% RSD in QC samples excluded, the criteria for the feature to be included being: detected in 66% of samples for each region, good peak quality via manual inspection, and signal >5-times that of the blank, features with retention time <2 min and >25 min excluded, and features with MW >1200 excluded, n=380

Table 3.4 Number of putative lipids detected using SIEVE software in hippocampus (n=16) and nucleus accumbens (n=8) brain regions. The results shown are for high-quality data set whereby: features with >30% RSD in QC samples were excluded, features with retention time < 2 min and >25 min were excluded, and features with MW >1200 were excluded. In addition, each feature also had to meet the following criteria: detected in 66% of samples for either region, good peak quality via manual inspection, and signal >5-times that of blank.82

Table 3.5 Technical and biological variability of lipid measurement using Folch extraction method for hippocampus and nucleus accumbens brain regions. The table shows median %RSD of the signal intensity of all lipids detected in different biological and technical replicates of the Folch extractions of the hippocampus and nucleus accumbens regions to assess the heterogeneity of the tissue sample and repeatability of extraction procedure. *Low sample volume prevented analysis of the 2nd technical replicate of N3.86

Table 3.6 Top 10 compounds contributing most to negative mode PCA separation along x-axis along with tentative ID's queried from LIPID MAPS database that were downregulated in hippocampus with respect to nucleus accumbens.....90

Table 3.7 Top 10 compounds contributing most to negative mode PCA separation along x-axis along with tentative ID's queried from LIPID MAPS database that were upregulated in hippocampus with respect to nucleus accumbens.....90

Table 3.8 Comparison of species identified with the Folch extraction method (n=16) to *in vivo* SPME (n=3) method of the hippocampus region with LipidSearch in positive ESI mode on Orbitrap. Lipids were considered identified if they contained an A or B grade in one of the samples from each extraction92

Table 3.9 Comparison of species identified with the Folch extraction method (n=16) to *in vivo* SPME (n=3) method of the hippocampus region with LipidSearch in negative ESI mode on Orbitrap. Lipids were considered identified if they contained an A or B grade in one of the samples from each extraction92

List of Equations

Equation 1.1 Distribution coefficient.....	13
Equation 1.2 Amount of analyte extracted by SPME.....	14
Equation 1.3 Amount of analyte extracted by SPME when sample volume is large	14
Equation 1.4 Rayleigh limit	18
Equation 1.5 Mass resolving power.....	20
Equation 1.6 Mass accuracy in ppm	21
Equation 1.7 Oscillation frequency of ions around the inner electrode.....	24

List of Abbreviations

5-HT	serotonin
AA	acetic acid
ACN	acetonitrile
AGC	automatic gain control
AJS	dual Agilent jet stream
AmAc	ammonium acetate
AmF	ammonium formate
AmOH	ammonium hydroxide
BEH	ethylene-bridged-hybrid
BUME	butanol:methanol
C_o	initial concentration
C_f^∞	concentration of the analyte in fibre at equilibrium
C_s^∞	concentration of the analyte in sample at equilibrium
CE	cholesterol ester
Cer	ceramide
CID	collision induced dissociation
CSH	charged surface hybrid
Δm_{FWHM}	the difference in mass at full-width half-maximum.
DA	dopamine
DG	diacylglycerol
e	elementary charge
ϵ_o	permittivity of the surrounding medium
ESI	electrospray ionization
FA	formic acid
FtAc	fatty acyls
γ	surface tension of the droplet
GL	glycerolipid
GP	glycerophospholipid
HCD	higher-energy collision
HILIC	hydrophilic interaction liquid chromatography
HPLC	high performance liquid chromatography
IPA	isopropanol
K_{fs}	distribution coefficient
LOD	limit of detection
LC	liquid chromatography
LPA	lysophosphatidic acid
LPC	lysophosphatidylcholine
LPG	lysophosphoglycerol

LPE	lysophosphatidylethanolamine
LPI	lysophosphatidylinositol
LPS	lysophosphatidylserine
LSM	lysosphingomyelin
LLE	liquid-liquid extraction
m/z	mass-to-charge ratio
MD	microdialysis
MeOH	methanol
MG	monoacylglycerol
MS	mass spectrometry
MS/MS	tandem mass spectrometry
MTBE	methyl tert-butyl ether
NA	missing
NPLC	normal-phase liquid chromatography
PA	phosphatidic acid
PAN	polyacrylonitrile
PC	phosphatidylcholine
PDMS	poly(dimethyl siloxane)
PE	phosphatidylethanolamine
PEG	poly(ethylene glycol)
PG	phosphatidylglycerol
PI	phosphatidylinositol
ppm	parts-per-million
PS	phosphatidylserine
QTOF	quadrupole-time-of-flight
r	the radius of the droplet
RPLC	reversed-phase liquid-chromatography
R_s	mass resolving power
SM	sphingomyelin
SP	sphingolipid
sphingosine	2S,3R-D-erythro-2-amino-1,3-octadec-4E-ene-diol
SPME	solid-phase microextraction
TG	triacylglycerol
V_f	fibre coating volume
V_s	sample volume
Z_r	Rayleigh limit

1. Introduction

1.1. Lipidomics

Lipidomics is the study of chemically distinct molecules that are classified as lipids and the analysis of these compounds in biological systems^{[1][2]}. Lipidomics is a subset of metabolomics and is thus a constituent of the -omics sciences along with genomics, transcriptomics and proteomics. Lipids are hydrophobic or aliphatic compounds that are grouped into eight classes based on both their chemical properties and their biosynthetic context^[3]. Lipids play integral roles in an organism including cell signalling, energy storage and cell structure. Changes in lipid levels can also be indicative of health problems such as dyslipidaemia^[4], diabetes^[4], hereditary sensory neuropathy^[4], neurodegeneration (such as Parkinson's diseases and Alzheimer's disease)^[4-7], lysosomal storage disorders^[4], cystic fibrosis^[4], and cardiovascular disorders^[4,8]. To further elucidate lipids' roles in these diseases, the ability to identify and quantitate lipids is required. This makes lipidomic analysis critical to further our understanding of lipids' roles in the biology, biochemistry and molecular biology fields. Lipids also have the potential to be biomarkers for disease further cementing the necessity to be able to accurately identify and quantitate lipids. Lipids are chemically diverse and are thus divided into eight main classes: fatty acyls (FtAc), glycerolipids (GL), glycerophospholipids (GP), sphingolipids (SP), sterol lipids, prenol lipids, saccharolipids, and polyketides^[1,2]. Figure 1.1 shows three main classes of lipids (i) GP (ii) GL and (iii) SP included within the scope of this project. Lipid identification is hierarchically categorized into four parts (i) lipid subclass (ii) sum composition of acyl chains (iii) specific chain length and degree of unsaturation of acyl chains and (iv) structurally defined molecular lipid where the total information is known including double bond position, double bond conformation and acyl chain position. Figure 1.1 (a) shows a phosphatidylcholine (PC) and demonstrates the different levels of identification available when discussing lipids. The lipid class can be easily determined by precursor ion scanning in an MS/MS. The polar head group has a specific m/z associated with it. For example, the PC lipid in Figure 1.1 (a) will have a head group m/z of 184.1 in MS product spectrum after fragmentation of the protonated parent ion. Utilisation of a high-resolution MS allows elucidation of the total amount of carbons and degree of unsaturation in the acyl chains of the PC therefore allowing the determination of the sum composition. Determining the location of the acyl chain and double bond position requires a

more in depth analysis using techniques such as: MS^{3[9]}, ion mobility-MS^[9], and ozone-induced dissociation^[9,10]. Reaching this level of molecular identification is therefore a demanding and expensive task applicable only in a targeted context. It is not feasible in untargeted, global lipidomic studies where hundreds of lipids are detected and identified. In an untargeted approach lipids are typically reported as either (i) lipid headgroup along with sum composition of acyl chains or, if MS product ion spectrum contains this information, (ii) lipid headgroup with specific chain length and degree of unsaturation.

1.1.1. Glycerolipids

Glycerolipids have a glycerol backbone and between one and three acyl chains at the sn-1, sn-2 and sn-3 positions. They are named mono-, di- and triacylglycerols (MG, DG and TG respectively) depending on the number of acyl chains present. GLs play a major role in energy storage in the body, as they provide a way for the body to store energy in adipose tissue in times of excess until needed^[11,12]. TGs and DGs are also involved in signal transduction via the formation of lipid-derived signals: malonyl-Coenzyme A and long-chain acyl Coenzyme A^[13]. In the brain DGs are important signalling lipids that activate a number of proteins such as protein kinase C^[14].

1.1.2. Glycerophospholipids

Glycerophospholipids have a glycerol backbone similar to GLs. They differ in that they have a polar head group in the sn-3 position. These head groups are: PC, phosphatidic acids (PA), phosphatidylethanolamines (PE), phosphatidylserines (PS), phosphatidylglycerols (PG), and phosphatidylinositols (PI). In the sn-1 and sn-2 position acyl chains are present. PA is the simplest GP as it has only a phosphate headgroup. PC has a choline bound to the phosphate group. PE has an ethanolamine bound the phosphate group. PS has a serine bound to the phosphate headgroup. PG has a glycerol bound to the phosphate group. Finally, PI has an inositol attached to the phosphate group. Generic structures of the GPs can be seen in Figure 1.2. Each of these GPs also have a lyso- form where one of the acyl chains has been cleaved off. GPs play an important structural role as components of cell membranes, and PCs are the most abundant phospholipid in membrane bilayers^[14]. GPs are also involved in cell signalling such as: membrane trafficking, cytoskeletal organisation, and glucose metabolism^[15]. PIs are heavily involved in signalling pathways in the brain and have been studied in relation to Alzheimer's disease^[16].

1.1.3. Sphingolipids

Sphingolipids are found in all mammalian cells and are involved in both structure and cell signalling^[17]. The simplest SP is sphingosine which consists of a sphingoid base backbone, a feature common to all SP. Sphingoid bases consist of a long aliphatic chain (typically 18 carbons long) with 2-amino-1,3 diol headgroup^[18]. The most common configuration of this sphingoid base is sphingosine (*2S,3R-D-erythro-2-amino-1,3-octadec-4E-ene-diol*) (Figure 1.3 (a)). In addition to the sphingoid base, a ceramide lipid (Cer) has an amide-linked acyl chain in the sn-2 position and a H atom in the sn-3 position (Figure 3 (b)). In addition to the sphingoid base, a sphingomyelin (SM) lipid has an amide-linked acyl chain in the sn-2 position and a phosphocholine (PC) in the sn-3 position (Figure 3 (c)). SPs are involved in different biological roles in the brain such as but not limited to: apoptosis^[19–21], cell proliferation^[22], migration^[23] and vasoconstriction^[24,25]. SPs are associated with a number of neurological disorders including: Krabbe, Metachromatic leukodystrophy, Tay-Sachs and Gucher types 2 and 3^[17].

1.2. Lipid composition of brain

The two regions of the brain focused on in this study are the hippocampus and the nucleus accumbens. The hippocampus is involved in memory and suffers damage in people with Alzheimer's disease^[26,27]. It is also involved in depression and has been the region of focus in depression studies^[28,29]. The nucleus accumbens is related to motivation and reward and is of interest in addiction studies^[30–32].

1.2.1. Human brain

A typical human brain will vary in lipid content from 36% (grey matter) to 81% (myelin)^[33]. O'Brien *et al.*^[33] found that lipid content of grey matter in a 55-year old consists of approximately 44.7% GP, 12% SP, and 31.3% cholesterol with 12% being uncharacterized. Post-mortem examination by Söderberg *et al.*^[5] of different brain regions in individuals suffering from Alzheimer's disease and healthy controls determined that the hippocampus region of healthy subjects was 17 ± 1.6 (mg/g wet weight) GPs. In another study focusing on Alzheimer's disease, Chan *et al.*^[7] examined the prefrontal cortex and entorhinal cortex of human brains and found cholesterol to be the most abundant lipid at around 50 mol%. The most abundant GP present

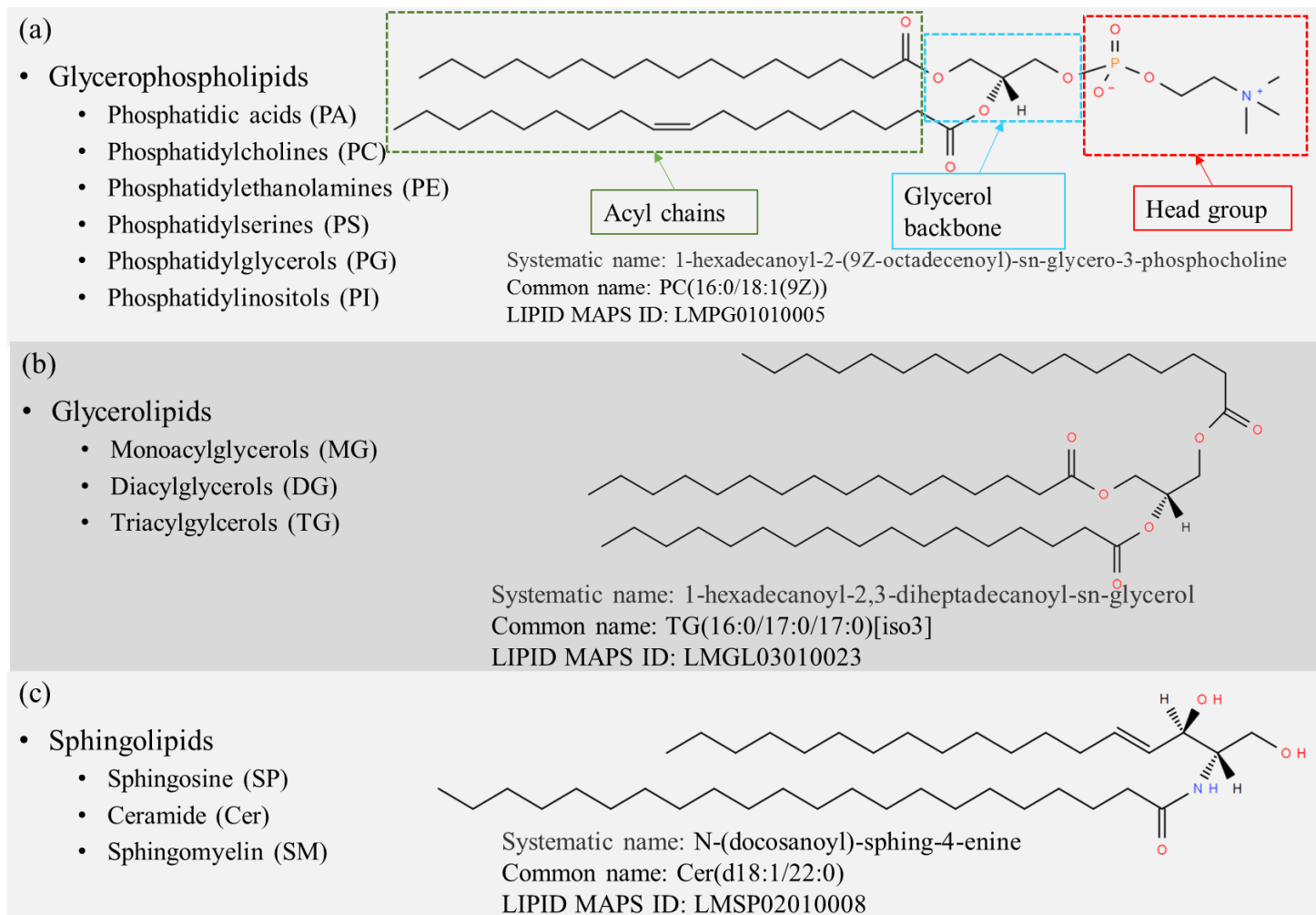
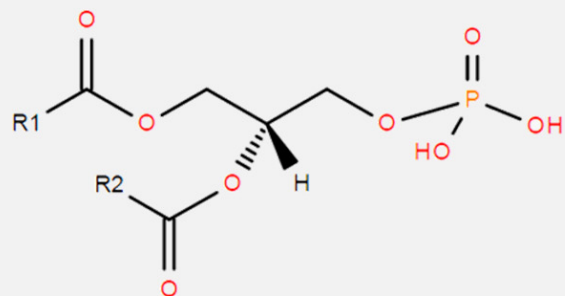
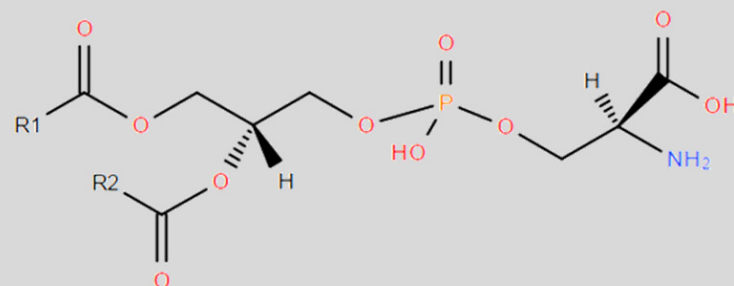


Figure 1.1 Chemical structures of three main lipid classes of interest in this thesis: (a) GP, (b) GL and (c) SP. Each panel lists the associated subclasses that belong to the class of interest and shows a structure of a representative lipid belonging to that class. (a) shows the three different sections of an aliphatic GP lipid (i) the hydrophobic acyl chains of varying length (ii) the glycerol backbone common to all GPs and GLs and (iii) the polar head group that characterises a specific GP lipid subclass. In this example, the head group is a choline meaning this lipid belongs to the GP subclass PC. (b) shows a TG, a glycerol backbone with three acyl chains. (c) shows a ceramide, a sphingosine backbone that has been N-acylated. Lipid structures obtained from LIPID MAPS^[34].

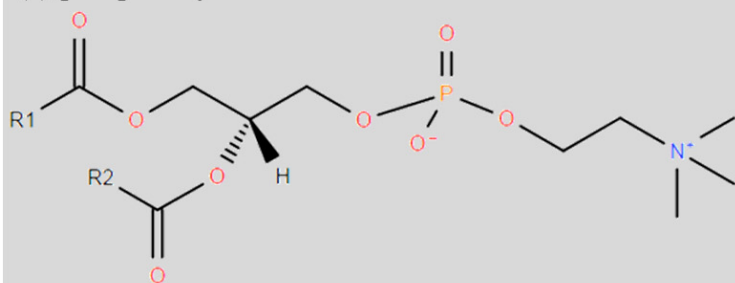
(a) phosphatidic acid



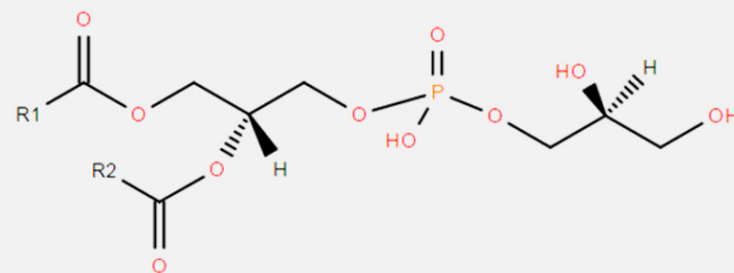
(b) phosphatidylserine



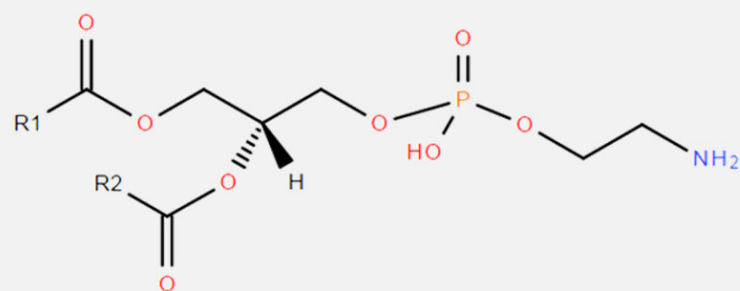
(c) phosphatidylcholine



(d) phosphatidylglycerol



(e) phosphatidylethanolamine



(f) phosphatidylinositol

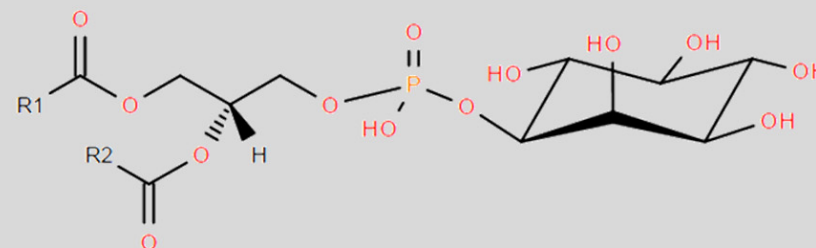


Figure 1.2 Chemical structure of main glycerophospholipid subclasses showing common glycerol backbone bound to two acyl chains with a polar phosphate headgroup (a) PA, (b) PS, (c) PC, (d) PG, (e) PE and (f) PI. R1 and R2 represent acyl chains of varying length and varying degree of unsaturation. Lipid structures obtained from LIPID MAPS^[34].

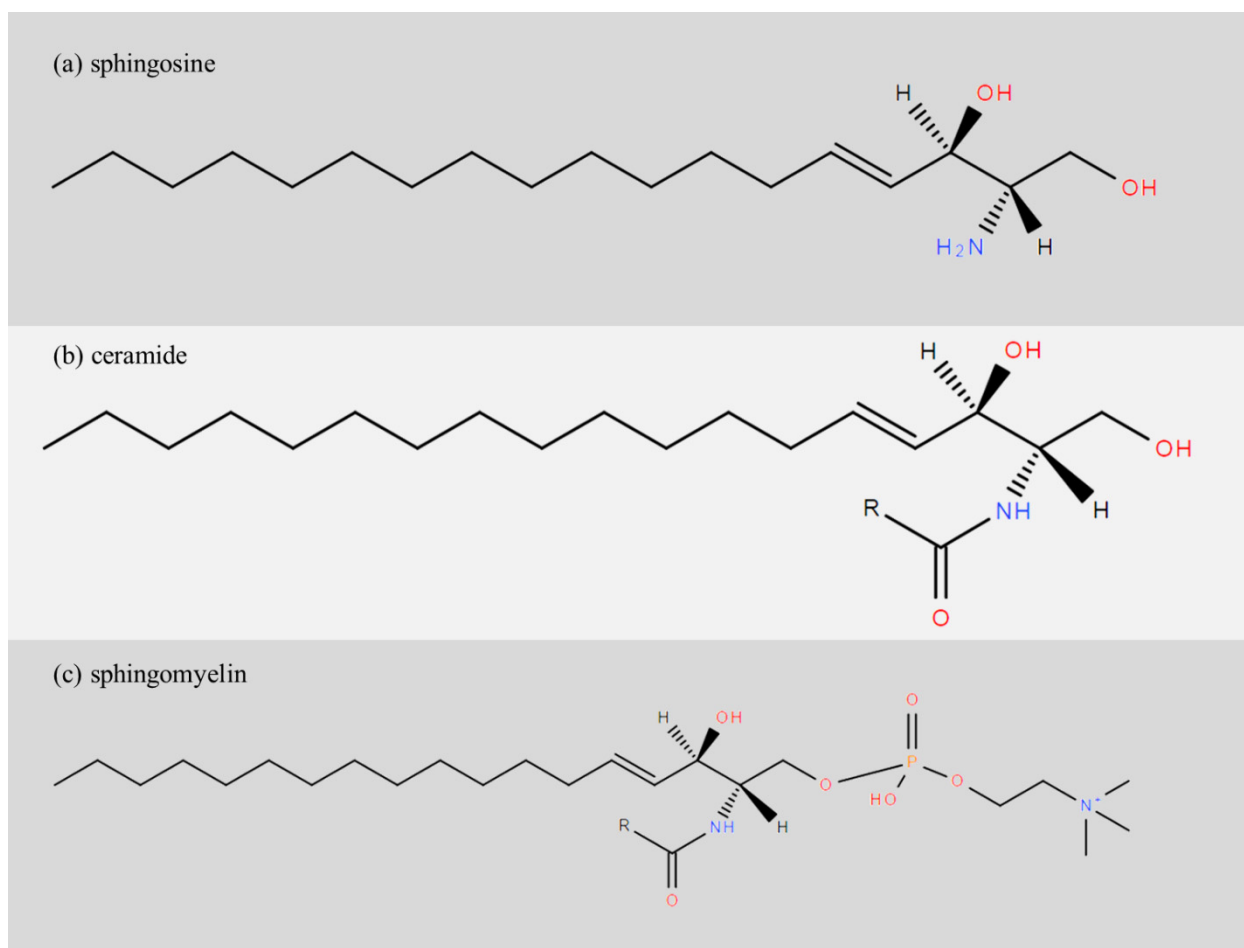


Figure 1.3 Chemical structure of main sphingolipid subclasses showing common sphingoid base backbone in (a) sphingosine. The addition of an amide-linked acyl chain in the sn-2 position leads to (b) Cer whereas (c) SM subclass has an amide-linked acyl chain in the sn-2 position and a phosphocholine head group in the sn-3 position. *R* represents amide-linked acyl chains of varying length and degrees of unsaturation. Lipid structures obtained from LIPID MAPS^[34].

was PC (16-18 mol%). Other studies have reported GP subclasses in brain tissue samples^[5,35–37] with PE and PC being the most abundant subclasses at around 60 mol% combined^[35,36]. The brain lipidomic heterogeneity is attributed to the considerable variations in lipid composition across different areas of the brain.

1.2.2. Rat brain

Almeida *et al.* performed an analysis of the lipidome of rat hippocampus and cerebellum regions using shotgun lipidomics^[35,36]. Their results show that PE and PC are the most abundant lipid

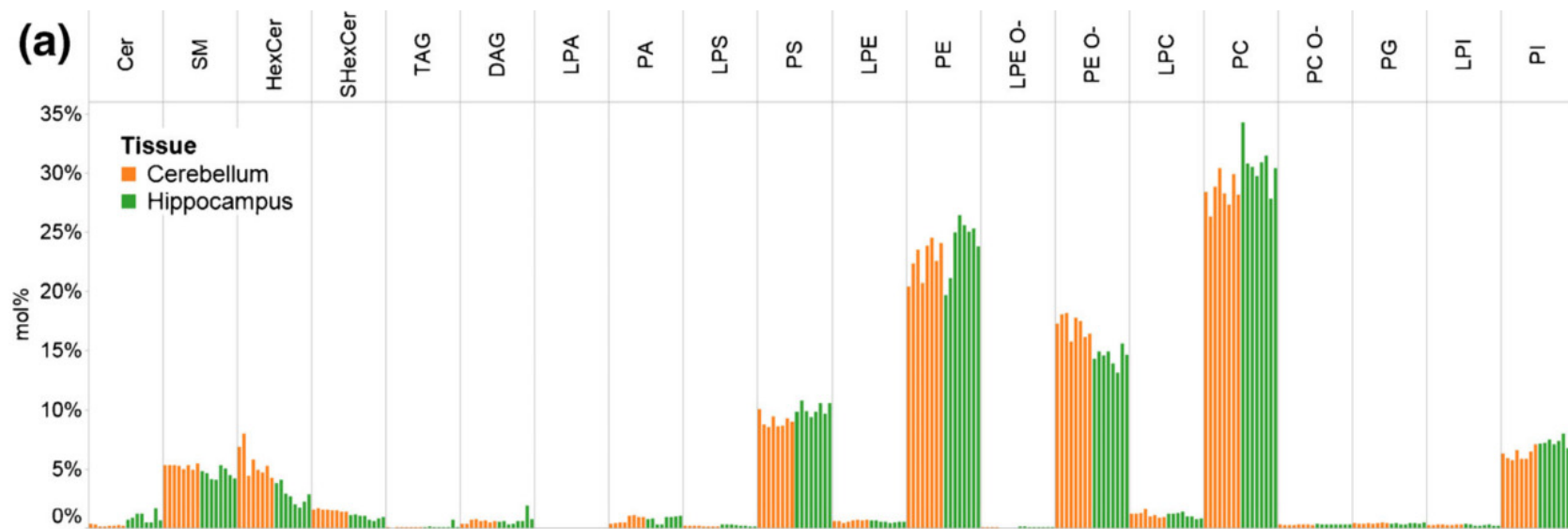


Figure 1.4 Lipid composition of rat cerebellum (orange, n=8) and hippocampus (green, n=8) regions. Shotgun lipidomic analysis of Bligh and Dyer brain tissue extracts using an Orbitrap fusion MS. Glucosylceramide (HexCer), sulfatide (SHexCer) the O-nomenclature denotes GP with an acyl chain bonded via a vinyl ether bond rather than an ester bond in the sn-1 position and are also known as plasmalogens figure reprinted from reference^[35] with permission from Springer publications

Table 1.1 Lipid composition of human plasma. Plasma was obtained from 100 individuals between the ages of 40 and 50. Table adapted from reference^[38] with permission from The American Society for Biochemistry and Molecular Biology

Lipid Category	Number of Species	Sum(nmol/mL)	Sum(mg/dL)
Fatty Acyls			
Fatty Acids	31	214	5.82
Eicosanoids	76	0.071	0.002
Total	107	214	5.82
Glycerolipids			
Triacylglycerols	18	1058	90.6
1,2-Diacylglycerols	28	39	2.36
1,3-Diacylglycerols	27	13	0.805
Total	73	1110	93.7
Glycerophospholipids			
PE	38	435	32.7
LPE	7	36.6	1.78
PC	31	1974	157
LPC	12	103	5.25
PS	20	7	0.559
PG	16	6.12	0.480
PA	15	2.50	0.173
PI	19	31.5	2.74
N-acyl PS	2	0.013	0.001
Total	160	2596	201
Sphingolipids			
Sphingomyelins	101	303.468	22.817
Monohexosylceramides	56	2.3135	0.18
Ceramides	41	11.586	0.732
Sphingoid bases	6	0.5678	0.02029
Total	204	318	23.7
Sterol Lipids			
Free Sterols	14	826	31.8
Esterified Sterols	22	2954	114
Total	36	3780	146
Prenol lipids			
Dolichols	6	0.025	0.003
Coenzyme-Q	2	4.59	0.394
Total	8	4.62	0.397
Grand total	588	8023	474

subclasses in the hippocampus region of rat brain, representing ~35 mol% and ~30 mol%, respectively. Figure 1.4 summarizes the composition of all lipid subclasses determined in this study. Green *et al.*^[39] examined the lipid profile of various regions of the brain including the nucleus accumbens region. They extracted lipids from brain tissue from Sprague-Dawley male rats using the Folch method. Using ¹H NMR and ESI-MS/MS they reported that the nucleus accumbens region consists of 19.6 mol% PC, 17.2 mol% PE, 16.5 mol% SL, 39.3 mol% cholesterol, and 8.9 mol% plasmalogens.

1.2.3. Lipid composition of plasma

Plasma is a biological sample that is easier to handle and obtain than brain tissue samples, so human plasma was used in initial LC-MS method development in this project as described in Chapter 2. Quehenberger *et al.*^[38] performed an extensive lipidomic profiling study of human plasma. Numerous extraction protocols were used specific to the class of lipids under examination: free fatty acids; eicosanoids; GL and cholesteryl esters; GP; SL; sterols; cardiolipin, dolichol and ubiquinone. In addition to tailored extraction methods for each subclass of lipids, different configurations of instruments were used for analysis including a variety GC-MS and LC-MS systems. The lipid composition of plasma, as obtained in this comprehensive, seminal study is given above in Table 1.1.

1.3. Sample preparation

1.3.1. Liquid-liquid extraction

Liquid-liquid extraction (LLE) is a widely used technique in lipidomics^[40-44]. Numerous LLE methods exist and use different solvent systems for different biological matrices. The octanol/water partition coefficient ($\log P$) for lipids ranges from 35 for the very hydrophobic TGs up to close to 0 for some of the LGP and fatty acids^[45]. Lipids with a high $\log P$ will be extracted with excellent recovery into solvents with a polarity index around 3, like chloroform, while lipids with low $\log P$ will be extracted with high recovery into solvents with polarity index around 6, like methanol (MeOH)^[45]. Using different ratios of these solvents, it is possible to extract lipids spanning the entire $\log P$ range of interest. For tissue samples, methanol/chloroform LLE methods known as Folch^[46] and Bligh and Dyer^[47] are the most commonly used. The Folch method is a widely used LLE method that uses an 8:4:3 (v/v/v) ratio of chloroform/methanol/water as the extraction solvent^[46]. It was first used by Folch in 1957 to

extract lipids from animal liver and muscle tissue^[46]. A 20-fold volume of 2:1 chloroform/methanol is added to tissue after which 0.9% NaCl is added. Two layers are formed: a lower organic layer that contains the lipids initially present in the tissue sample and an upper aqueous layer. Between these two layers is a protein disk interface. The organic layer is transferred to a new vial and after an evaporation and reconstitution step the extract can be analysed by LC-MS. In 1959, Bligh and Dyer modified the Folch method to a 1:2:0.8 (v/v/v) ratio of chloroform/methanol/water^[47]. Their method showed an increase in recovery of lipids from muscle tissue and reduced the amounts of solvent required and is considered a “green” method. The Bligh and Dyer method works well when the total lipid content of the sample is <2%^[48]. However, at higher lipid content, like brain tissue with lipid content of 36-81%^[33], the Bligh and Dyer method begins to underestimate the amount of lipids present^[48] as shown below in Figure 1.5. For plasma samples, in addition to the above-mentioned methods, the butanol:methanol (BUME) method^[49] and Methyl tert-butyl ether^[50] method (MTBE) LLE have also been applied. The MTBE method was shown to have similar extraction efficiencies to the Folch and to the Bligh and Dyer methods for extracting GPs, free cholesterol, cholesteryl esters and SPs from brain tissue^[50]. It has the advantage of the organic phase being the upper layer making sample handling easier as the protein interface does not have to be punctured as in the case of the Folch method. They do not report the ability of MTBE to recover GLs from samples^[50]. Sheng *et al.*^[51] assessed several different methods including MTBE and Folch for extracting lipids from the cyanobacteria *Synechocystis* PCC 6803 which is known to contain large amounts of DGs. They determined that the Folch method was the best choice for DG extraction due to its permeability, polarity, and interaction with hydrogen bonds due to the nature and location of DGs in cyanobacteria. Matyash *et al.*^[50] and Sheng *et al.*^[51] showed that MTBE and Folch provide comparable recoveries of GPs from tissue. Sheng *et al.*^[51] showed that Folch outperforms the MTBE method for the extraction of GLs from tissue. For these reasons the Folch method was chosen as the LLE sample preparation for extracting lipids from brain tissue in this thesis. The main disadvantage of the Folch method is that it requires the animal to be sacrificed to recover enough tissue to perform the extraction. In addition, when performing an extraction, the tissue is homogenised which destroys spatial information of the tissue sample. As an alternative to this LLE method, *in vivo* methods could be considered. Two *in vivo* methods that exist but have not been applied to *in vivo* lipidomic studies are microdialysis and SPME.

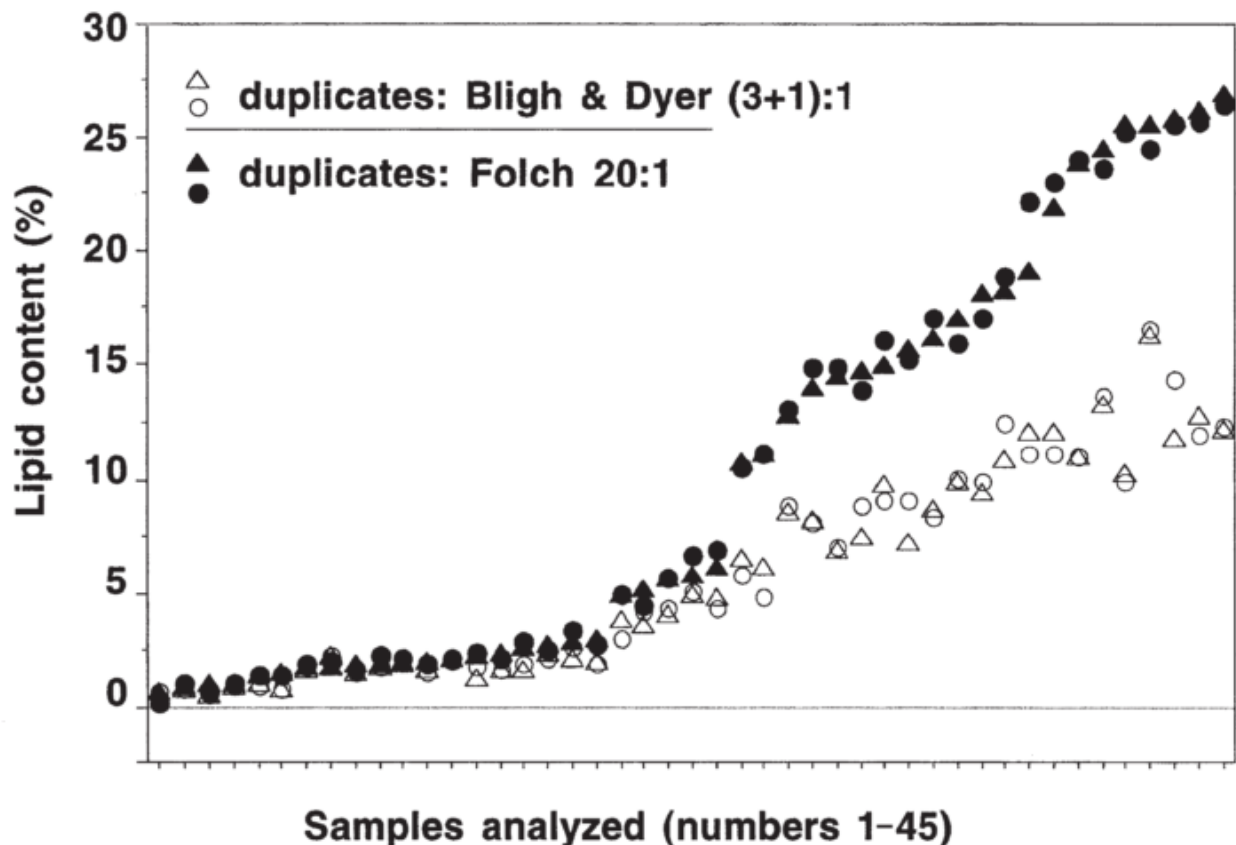


Figure 1.5 Comparison of Folch to Bligh and Dyer method. Iverson et al^[48]. prepared 45 samples with different total % lipid content using either Folch or Bligh and Dyer methods in duplicate. At low % lipid content, the two methods showed good agreement. Once lipid content increases above 2% (as is the case with brain tissue) the Bligh and Dyer method begins to significantly underestimate lipid content. Figure reproduced from reference^[48] with permission from the publisher.

1.3.2. *In vivo* sampling: Microdialysis

Microdialysis (MD) is a widely used technique that is used for *in vivo* studies in brains^[52-58]. This powerful sampling technique is often used when investigating the pharmacokinetics of drugs^[52,53,57] and temporal changes in neurotransmitters^[59-62]. The MD probe is introduced into a cannula that has been implanted in the brain of the subject. The MD probe is then continually perfused with an aqueous buffer which composition has been matched with the pH and ionic strength of the tissue surrounding the probe known as the perfusate. Flow rates for the perfusate span the range of 0.5-2.0 $\mu\text{L}/\text{min}$ ^[58]. The MD probe is made of a semipermeable, dialysis membrane with a molecular weight cut-off ranging from between 20-60 kDa^[58] that allows analytes to diffuse across it. Probes used in rat brain studies are typically 15 mm long with a

diameter between 200-500 μm ^[58]. The diffusion of analytes is governed by the concentration gradient that exists between the perfusate and the extracellular tissue^[52]. This concentration gradient can also be used to deliver compound in the extracellular tissue in a technique known as retrodialysis which can be used for calibration by loading a standard (with similar physiochemical properties as the analyte) in the perfusate. The standard crosses the membrane at the same rate as the analyte of interest. The resulting loss of this standard from the perfusate can be used to determine the rate and recovery^[58]. The dialysate is collected and analysed at appropriate intervals. MD allows measurement of unbound analytes in the extracellular fluid of tissue and gives real-time measurements of the therapeutically active (unbound) concentration of the drug^[52]. In online MD analysis sample collection and analysis are done in a continuous manner which reduces error associated with manual sample manipulation, exposure to air, and degradation^[58]. This can allow near real-time temporal resolution^[58]. High temporal resolution can give useful information about a drug's pharmacokinetics or neurotransmitter levels. Although MD is a useful *in vivo* technique it does not lend itself easily to lipidomics. The perfusate must match the surrounding conditions of the extracellular matrix of the brain and an organic solvent required to extract lipids would not be suitable for this task.

1.3.3. *In vivo* sampling: Solid-phase microextraction

Solid-phase microextraction (SPME) is a non-exhaustive, equilibrium based sampling technique. It combines extraction, pre-concentration, and reduction of sample complexity in one step. SPME can be applied to a number of different complex matrices including: environmental samples^[63], food samples^[64], and biological samples^[65]. SPME can be employed for *in vivo* sampling of biological fluids and tissues if biocompatible SPME fibres are used. The design of an SPME device for direct extraction is straightforward. A thin, metal fibre core with diameter of 200 μm has an extraction sorbent immobilized on a portion of the fibre (typically 2-15 mm long). This coating is 45 μm thick. With further miniaturization of the fibre dimensions, for example 50 μm support and 5-10 μm coating, excellent spatial resolution may be achieved. For *in vivo* sampling the coatings must be biocompatible and include: poly(dimethyl siloxane)(PDMS), polypyrrole, poly(ethylene glycol)(PEG) and polyacrylonitrile (PAN). In addition, the sorbent can contain C_{18} or other sorbents of interest but the sorbent surface must be covered by a layer of one of the biocompatible polymers to prevent the fouling of the coating *in vivo* and adverse reactions such as clot formation^[66]. The selection of coating is important since the selectivity of

each coating differs, thus leading to distinct analyte profiles. After a pre-conditioning step the fibre is introduced to a biological matrix either *in vivo* or *ex vivo*. The sorbent is in direct contact with the sample matrix. Analytes begin to move from the matrix to the coating until equilibrium is reached, provided enough time is given. After extraction, the fibre is removed and a quick wash step is performed. The fibre is then placed in a desorption solvent; in the case of lipids an organic solvent such as methanol or isopropanol is a suitable desorption solvent. After enough time has been given to ensure complete desorption, analysis via LC-MS can be performed. A typical *in vivo* workflow is shown below in Figure 1.6.

The distribution coefficient (K_{fs}) of an analyte governs the extent of the analyte's extraction from the sample and is described by equation 1.1^[66] where C_f^∞ and C_s^∞ are the concentrations of the analyte at equilibrium in either the fibre or the sample matrix, respectively.

$$K_{fs} = \frac{C_f^\infty}{C_s^\infty}$$

Equation 1.1 Distribution coefficient

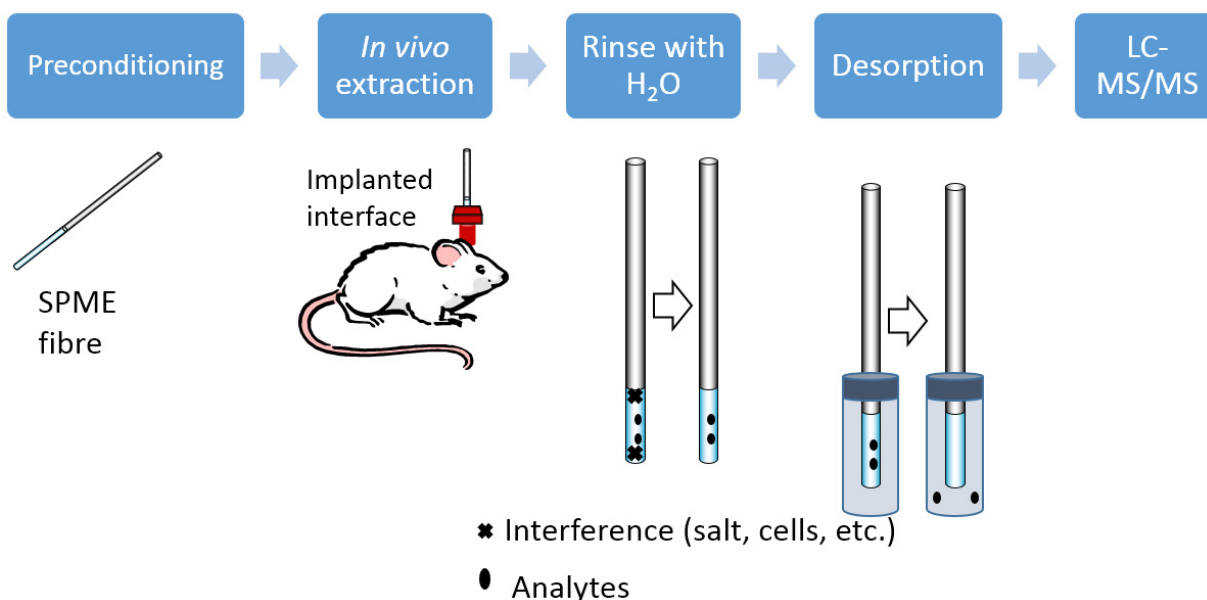


Figure 1.6 SPME workflow for extraction of analytes from animal brain tissue. Figure from reference^[67] reprinted with permission from John Wiley and Sons.

The amount of analyte extracted, number of moles (n), is given by equation 1.2^[66] where K_{fs} is the distribution coefficient of analyte between the fiber and the sample matrix, V_f is the fibre coating volume, V_s is the sample volume and C_o is the initial concentration of a given analyte in the sample.

$$n = \frac{K_{fs} \cdot V_f \cdot V_s \cdot C_o}{K_{fs} \cdot V_f + V_s}$$

Equation 1.2 Amount of analyte extracted by SPME

The amount extracted correlates to the amount in the system and can be independent of sample volume as shown in Equation 1.3^[66]. When $V_s \gg K_{fs} \cdot V_f$, the number of moles of analyte, n , becomes

$$n = K_{fs} \cdot V_f \cdot C_o$$

Equation 1.3 Amount of analyte extracted by SPME when sample volume is large

This means that the amount of analyte extracted is directly proportional to the initial concentration of the analyte in the sample. This also means that the exact volume of the sample does not have to be determined allowing for *in vivo* quantitation.

In vivo SPME has been successfully employed to measure concentrations of drugs and/or their metabolites in rats^[68,69], mice^[70], dogs^[71] and global metabolomic studies in circulating blood of mice^[67]. Bai *et al.* used SPME to monitor the accumulation of geosmin and 2-methylisoborneol, compounds produced by cyanobacteria, in live fish muscle^[72]. Focusing on lipidomics, only two studies to date have been reported. Birjandi *et al.* showed the ability of SPME to successfully extract fatty acids of varying degrees of unsaturation and length from human and fish plasma^[73]. In 2016, Birjandi *et al.* also demonstrated the ability of SPME to extract lipids from homogenized human hepatocellular carcinoma cell line cultures in a global lipidomic approach^[74]. The C₁₈ SPME stationary-phase was applied in a 96-well plate format using 60 min extraction time. This was followed by a quick rinsing in purified water and a desorption for 60 min into isopropanol(IPA)/MeOH (1:1). SPME was compared to the Bligh and Dyer method and provided a more comprehensive coverage of less abundant species like LPC, LPE, PS, PG, DG and CE. SPME also reduced the matrix effects observed when compared to Bligh and Dyer.

SPME has not yet been evaluated for *in vivo* lipidomics studies of either plasma or tissue in any animal model.

1.3.4. SPME versus MD

Cudjoe *et al.*^[55] administered fluoxetine, an antidepressant known to change the serotonin levels and not affect dopamine levels, to rats. Serotonin and dopamine levels were measured with both

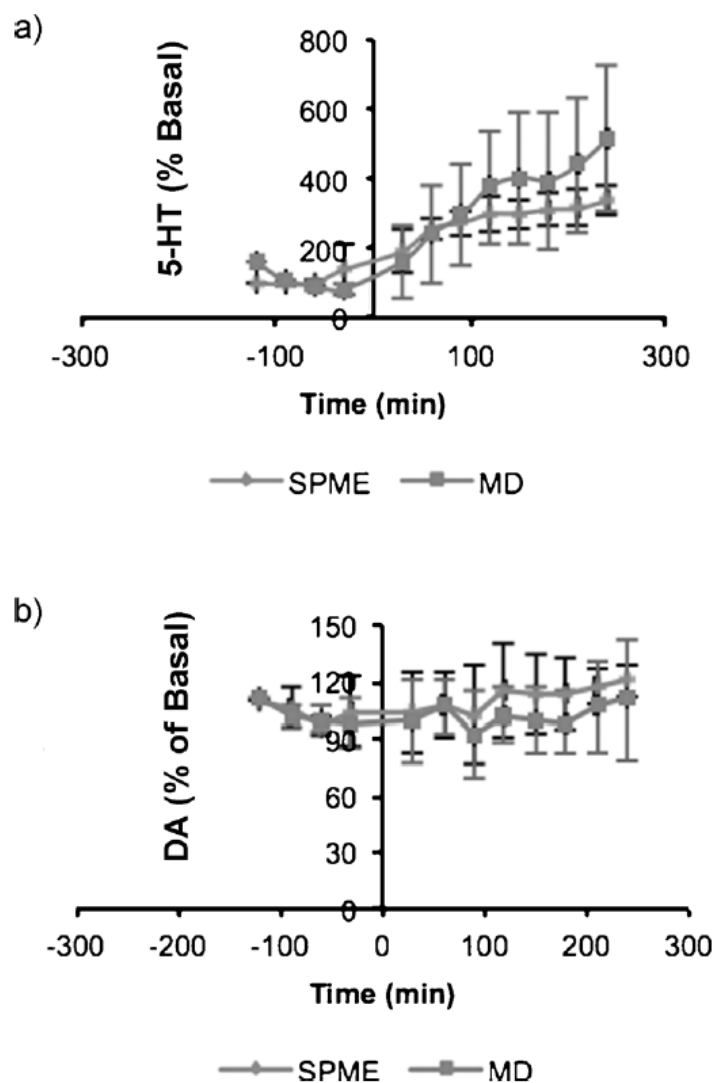


Figure 1.7 Comparison of *in vivo* SPME to MD for measurement of two neurotransmitters, serotonin and dopamine. (a) shows the change in serotonin levels as a function of time. SPME and MD both show an up regulation of serotonin (5-HT) after the administration of fluoxetine. (b) shows that dopamine (DA) levels remained constant as expected after the administration of 10 mg/kg of fluoxetine at $t=0$. Values reported are the mean \pm standard deviation from $n=12$ rats. Sampling was 30 min for each time point for both MD and SPME. Figure reprinted from reference^[55] with permission from John Wiley and Sons.

SPME and MD before and after drug administration. The same concentration trends were observed for both neurotransmitters using both *in vivo* methods, with serotonin showing an increase over time and dopamine showing no changes during the experiment. The observed trends can be seen below in Figure 1.7. MD had large error bars potentially due to matrix effects while in SPME this error was lowered. This demonstrates the ability of SPME to be used in conjunction with MD to observe temporal changes of both polar and non-polar compounds in living, awake animals. MD has better temporal resolution compared to SPME since MD can achieve near real-time temporal resolution while SPME requires longer extraction times. SPME has better spatial resolution with the fibres usually being smaller than the MD probes. MD cannot easily extract lipids as the solvents required to do so would interfere with the tissue surrounding the probe. Also, lipids would experience severe non-specific binding to the walls of the tubes required for MD due to their hydrophobicity. For these reasons, SPME was selected for evaluation as a potential *in vivo* method for lipidomic extraction.

1.4. Liquid chromatography-mass spectrometry for lipidomics

Direct infusion or shotgun lipidomics is a popular choice to analyse lipids due to its high-throughput. Unfortunately, it suffers from some inherent issues namely: inability to distinguish isomers, ion suppression, and difficulty with accurate quantification because of differences in fragmentation mechanisms that can occur even within the same lipid sub-class^[1,75]. Liquid-chromatography (LC) helps with the issues encountered when performing shotgun lipidomics. LC allows for separation of lipid classes determined by their physiochemical interactions with the various types of chromatographic stationary phases available.

1.4.1. LC

Three main chromatographic modes used for the separation of lipids are normal-phase LC (NPLC), reversed-phase LC (RPLC) and hydrophilic interaction LC (HILIC)^[75]. RPLC separates compounds on the basis of their hydrophobicity. Hydrophilic compounds elute early while hydrophobic compounds (long acyl chains) are retained and require increasing amounts of organic solvent to elute. Increased degree of unsaturation reduces retention time due to the π electron dipole in the double bond(s) reducing the hydrophobicity of the compound. Consequently, RPLC allows separation of lipids belonging to the same class but with different acyl chains and different number of double bonds. NPLC and HILIC separate compounds on the

basis of their hydrophilic nature. Lipids are therefore separated and grouped according to their subclass-specific polar head-group. This co-elution of species with the same head-group will lead to ion suppression, because the competition for charge at the ionization source will be increased. In addition, solvents typically used with NPLC such as hexane or heptane are not compatible with MS detection due to their low polarity which means they cannot be sprayed easily due to their low dielectric constant meaning they cannot be as easily polarized [76,77]. These suppression and compatibility issues are addressed with the use of RPLC which is why it was selected for use in this study. The column selected for this project was a Waters charged surface hybrid (CSH) C₁₈ which is used frequently in lipidomic studies [40,78–83]. C₁₈ is a typical reversed-phase stationary phase that consists of C₁₈ chains bound to a support. CSH C₁₈ column reduces tailing of basic compounds at low pH [84] by causing a reduction in the secondary interactions of basic compounds that occur with silanols in silica-based stationary phases due to incomplete capping. In addition to the CSH column, a Kinetex EVO C18 column was used as it is a pH stable column (with a pH range 1-12) suitable for use with ammonium hydroxide at high pH. C₁₈ chains are bound to ethane cross-linked silica in a core-shell configuration.

1.4.2. Electrospray ionisation (ESI)

An integral part of any MS instrument is the ionization source. For LC-MS, the LC effluent must be converted from liquid to gas and the neutral analytes must be charged. Electrospray ionisation (ESI) is a popular choice which has been around for more than 100 years [85,86]. It was widely applied to mass spectrometry as an ionization source in 1989 once the Fenn group showed its ability to successfully ionize large biomolecules without excessive fragmentation [87]. ESI is therefore known as a “soft ionization” technique due to minimal in-source fragmentation. ESI can be operated in either positive mode or negative mode. In positive-mode ESI, a positive charge is applied to the capillary tip and the entrance to the mass analyser has a negative charge applied to it. The opposite is true for an ESI operated in negative mode. The LC effluent enters the spray capillary. As the effluent leaves the spray tip it forms a Taylor cone. In positive-mode the spray droplets have a positive charge placed on them. Negative counterions in the solution will move towards the wall of the capillary due to the positive charge on the wall [88]. The effluent then forms an aerosol as it is sprayed from the capillary tip, shown in Figure 1.8. As the droplets fly towards the mass analyser entrance desolvation occurs due in part to a heated gas, typically N₂, that is introduced co-axially to the MS intake. As the droplets shrink in size the charge

density on the droplets increases. The coulombic repulsion surpasses the surface tension at the Rayleigh limit, given by Equation 1.4^[89].

$$z_R = \frac{8\pi}{e} \sqrt{\epsilon_0 \gamma r^3}$$

Equation 1.4 Rayleigh limit

where e is the elementary charge, ϵ_0 is the permittivity of the surrounding medium, γ is the surface tension of the droplet and r is the radius of the droplet. Once the Rayleigh limit is reached the droplet undergoes Coulomb fission creating smaller droplet(s). This process is repeated producing smaller and smaller droplets until finally gas phase ions are emitted. There are three theorized ESI mechanisms^[90,91]: (i) ion evaporation model where small ions are ejected from the spray droplet, (ii) charge residue model where a globular protein has a spray droplet shrink around it resulting in the charge residing in the protein and (iii) chain ejection model where an unfolded protein is ejected from the droplet whilst charge is placed on it. This study is focused on small molecules and will therefore only consider (i) the ion ejection model.

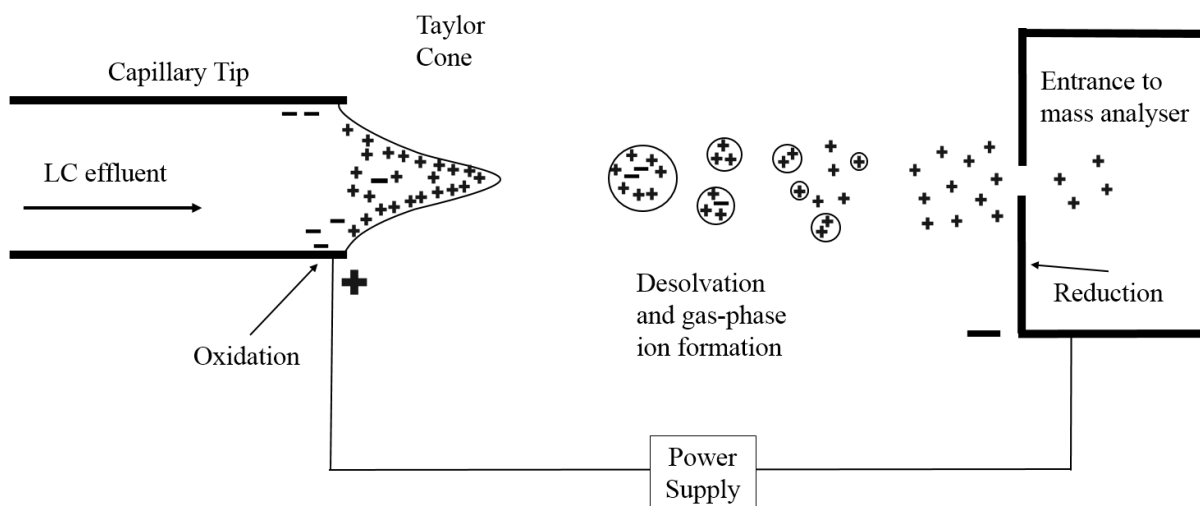


Figure 1.8 Schematic of electrospray ionization LC-MS interface in positive-ion mode.

Equation 1.4 demonstrates that the ability of a droplet to emit a gas phase ion is dependent in part on the properties of the mobile phase namely: surface tension and viscosity. A lower viscosity allows higher electrophoretic mobility of ions^[88]. In fact, there are a large number of mobile phase and mobile phase additive characteristics that affect ionisation including: volatility, conductivity, ionic strength, dielectric constant, electrolyte concentration, pH, and gas-phase reactions^[88]. However, ionization efficiency cannot be the only factor determining mobile phase selection as chromatographic separation must also be taken into account. This leads to careful consideration when choosing a mobile phase for LC-MS. Protonation, $[M+H]^+$, and deprotonation, $[M-H]^-$, are common types of ionisation that occur in positive-mode ESI and negative-mode ESI, respectively. In addition to protonation and deprotonation, ESI has also high propensity for adduct formation. Adducts such as ammonium, $[M+NH_4]^+$, sodium, $[M+Na]^+$, and potassium $[M+K]^+$ are common in positive mode ESI depending on the nature of analyte and mobile phase employed. In negative-mode ESI, the most common ions observed in addition to $[M-H]^-$ are acetate, $[M+CH_3COO]^-$, formate, $[M+HCOO]^-$, and chloride, $[M+Cl]^-$ adducts. Common adducts for the lipid subclasses of interest are given below in Table 1.2^[75].

Table 1.2 Common adducts observed for lipid subclasses in positive and negative ESI adapted from reference^[75] reprinted with permission from Elsevier

Lipid subclass	Positive mode	Negative mode
PC	$[M+H]^+$, $[M+Na]^+$	$[M-H]^-$, $[M+CH_3COO]^-$, $[M+HCOO]^-$
PE	$[M+H]^+$, $[M+Na]^+$	$[M-H]^-$
PG	$[M+H]^+$, $[M+Na]^+$, $[M+NH_4]^+$	$[M-H]^-$
PI	$[M+H]^+$, $[M+Na]^+$, $[M+NH_4]^+$	$[M-H]^-$
PS	$[M+H]^+$	$[M-H]^-$
PA	NA	$[M-H]^-$
SM	$[M+H]^+$	$[M+CH_3COO]^-$, $[M+HCOO]^-$
Cer	$[M+H]^+$, $[M+Na]^+$, $[M+NH_4]^+$	$[M-H]^-$, $[M+CH_3COO]^-$, $[M+HCOO]^-$
MG, DG, TG	$[M+Na]^+$, $[M+NH_4]^+$	NA

1.4.3. MS

Mass resolving power is an important aspect of any mass spectrometer especially in the case of lipids where there can be a lot of mass overlap. Resolving power of a mass spectrometer is given by the formula:

$$R_s = \frac{m}{\Delta m_{FWHM}}$$

Equation 1.5 Mass resolving power

Where m is the mass-to-charge ratio (m/z) and Δm_{FWHM} is the difference in mass at full-width half-maximum. Considering a low-resolution MS with $R_s = 800$ and a target compound with the mass of $824 \text{ Da} \pm 1$. Searching LIPID MAPS lipid database returns over 100 hits from eight different lipid classes. This would make the lipid very difficult to identify correctly. Conversely, if the same lipid was obtained using an MS with $R_s = 80,000$, searching LIPID MAPS lipid database returns 18 hits from two different classes. Each of these hits have the same exact mass

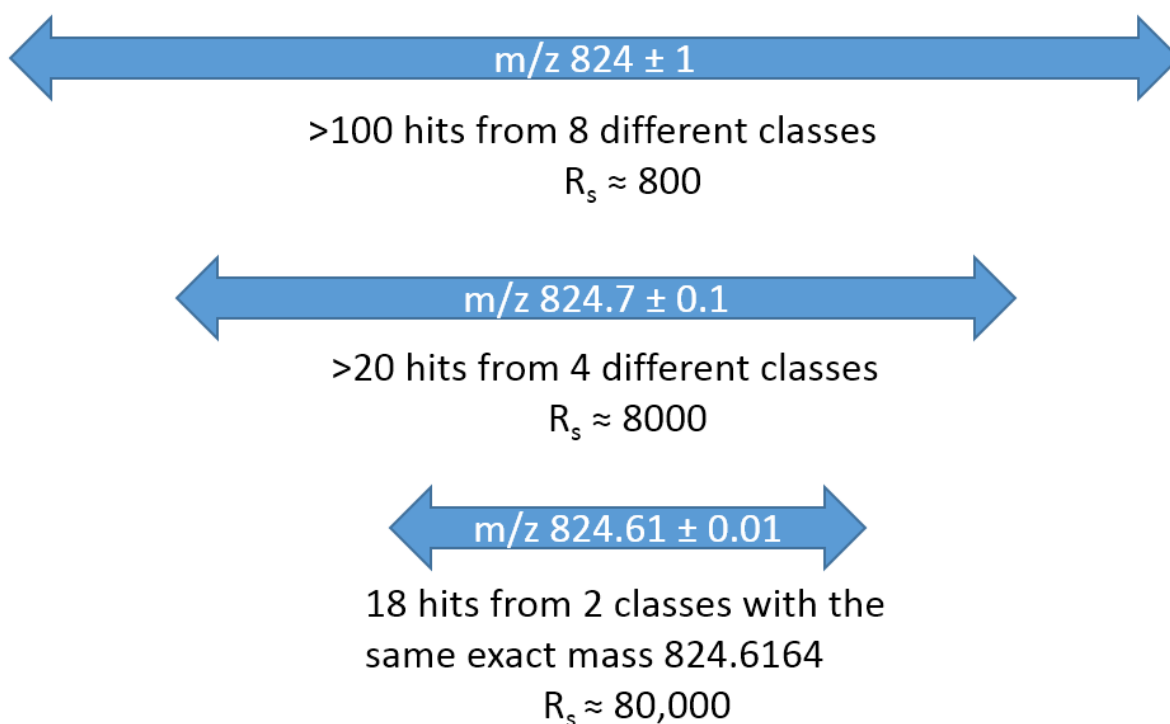


Figure 1.9 High resolving power is required to distinguish lipids with the same nominal mass

meaning that increasing the resolution further would not allow for the differentiation of these 18 compounds. A visual representation of this is given in Figure 1.9. Additional information like retention time and/or product ion spectrum could help correctly identify this compound. In addition to resolving power, mass accuracy is another important aspect of mass spectrometry. Mass accuracy is the deviation of the detected mass from the true mass of a compound and is usually reported in parts-per-million (ppm). Taking a compound's true mass to be 824.6894 Da and the detected mass of 824.6669 Da will give a mass accuracy of 27.28 ppm. This value can be obtained using the following formula:

$$\text{mass accuracy} = \frac{\Delta m}{m} \times 10^6$$

Equation 1.6 Mass accuracy in ppm

where m is the theoretical m/z of the compound and Δm is the difference between the observed m/z and the theoretical m/z . In addition to these two MS¹, factors lipids require MS/MS for identification. Fragments indicative of a certain lipid subclass are listed below in Table 1.3. Some of these fragments are shared by multiple subclasses like the 153 Da glycerol phosphate –H₂O fragment. In such cases, it is then necessary to compare MS/MS product spectra to a predicated product spectrum for that lipid and to match retention time to standards.

Table 1.3 Summary of headgroup ions observed for different GP subclasses

Lipid subclass	Fragment mass (Da)	Fragment
PA	153	glycerol phosphate –H ₂ O
PC	184	phosphocholine
PE	196	glycerol phosphoethanolamine –H ₂ O
PG	153	glycerol phosphate –H ₂ O
	227	glycerol phosphoglycerol –H ₂ O
PI	153	glycerol phosphate –H ₂ O
	241	cyclic inositol phosphate
PS	153	glycerol phosphate –H ₂ O
	87 (neutral loss)	serine

1.4.4. Quadrupole-Time-of-Flight (QTOF)

QTOF mass spectrometer is a hybrid mass spectrometer that combines a quadrupole mass filter with a time-of-flight mass analyser. In certain Agilent systems, like the 6550, after analytes are ionized in the ESI source, the ions pass through a hexabore transfer capillary where they are introduced to a Dual Ion Funnel system. This Dual Ion Funnel set up consists of a high-pressure funnel with a pressure between 7 and 14 Torr. The second low-pressure ion funnel is kept at a pressure of 1 to 3 Torr. Ions are focused by an RF voltage and accelerated by a DC voltage. This configuration helps to remove gas and neutral noise^[92]. The ions are then focused by an octapole. Following this is a quadrupole mass filter (Q1). This quadrupole is a set of four parallel metal rods. A radio frequency (RF) alternating voltage and a constant voltage are applied across the rods^[76]. These voltages set up an electric field that can allow only certain ions with a specific m/z to pass through. Ions that do not have the selected m/z end up colliding with rods and are neutralised. After Q1, selected ions enter a hexapole collision cell filled with non-reactive collision gas like He or N₂. In this collision cell precursor ions selected by Q1 are fragmented. The resulting fragment ions are then focused by another octapole before entering TOF mass analyzer. The ions then encounter an ion pulser in the TOF. The ion pulser is a series of plates which has a high voltage pulse applied which accelerates the ions through the drift tube orthogonally to their previous path. The ions travel through the drift tube which is under a strong vacuum as any collision here will cause deviation to the flight time of the ion leading to a reduction in mass accuracy. This drift tube has no electric or magnetic field present in it so the ions should all have the same kinetic energy applied to them that they gained from the ion pulser. Therefore, the ions will separate on the basis of their mass-to-charge ratio as the lighter ions will have a greater velocity than the heavier ions. However, the ions at the pulser do not have the exact same kinetic energy applied to them as ions that are closer to the ion pulser have a slightly greater kinetic energy applied to them. An electrostatic mirror device known as a reflectron is a way to combat these small differences in kinetic energy. The reflectron is a set of lenses that increase in electric potential. If two ions have the same m/z but different kinetic energy the ion with the higher kinetic energy will penetrate farther into the reflectron. As the ions travel into the reflectron they slow down and are eventually “reflected” towards the detector. Ions with the same m/z that initially had different kinetic energies now reach the start of the second drift region at the same time with the same kinetic energy^[76]. The reflectron improves resolving

power as the drift region is essentially doubled and the kinetic energies of ions with the same m/z are normalised. The ions then strike a microchannel plate detector with enough force to free electrons. The freed electrons are accelerated and hit a scintillator which emits photons when struck. The emitted photons then hit a photomultiplier tube which amplifies the signal and converts into an electronic signal. The analyte's time of

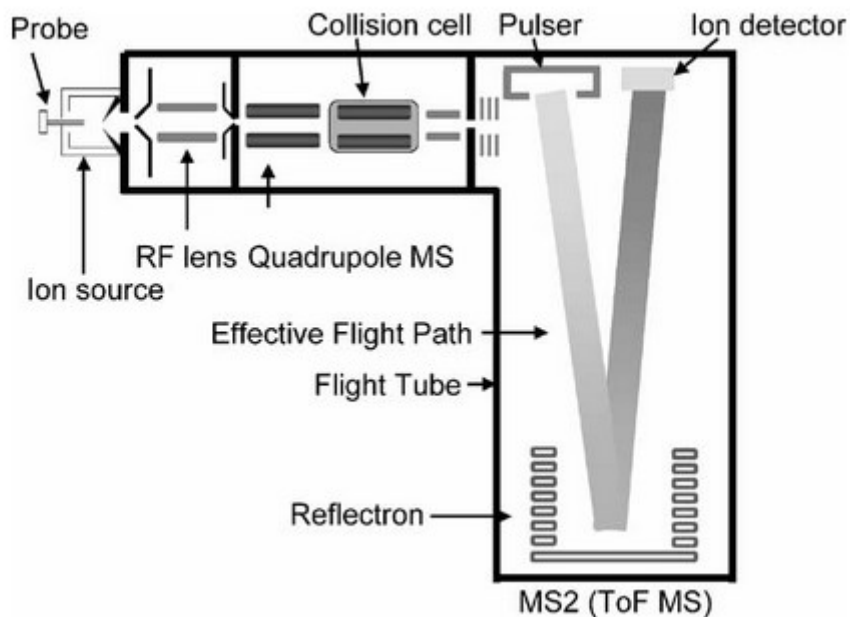


Figure 1.10 Schematic of QTOF Figure reproduced from reference^[93] with permission from John Wiley and Sons

flight through this drift tube is recorded and the m/z is deduced by the instrument. A QTOF is calibrated externally by measuring the time of flight of compounds whose mass is precisely known. The model of the QTOF used in this thesis was the Agilent 6550 iFunnel with a Dual Agilent Jet Stream (AJS) electrospray ionization source. This allows for the introduction of calibrant solution using an auxiliary spray. The inclusion of an internal calibrant in this auxiliary spray ensures that mass drifts are corrected in real time leading to better mass accuracy of 3-5 ppm^[94]. The AJS system (usually reserved for an internal calibrant solution that allows on-the-fly mass correction) allows for an additional solvent system to be introduced along side the regular ESI spray. The AJS system allowed for the examination of mobile phase additives introduced in gas-phase described in Chapter 2. In MS¹ mode all ions pass through the quadrupole to the detector and no fragmentation occurs. In MS² mode an m/z of interest is selected in Q1 and only

these ions pass through to the collision cell where they are fragmented, followed by analysis in TOF. MS/MS is required for identification of lipids as described in section 1.4.3. QTOF's maximum resolving power of 40,000 is not sufficient to resolve lipids that are close in MW. This requires the use of even higher resolution MS instrument, so the majority of the work reported in this thesis was performed on Orbitrap instrument. However, due to the availability of AJS spray configuration, QTOF was used to investigate the gas-phase effects of mobile phase additives examined and described in Chapter 2.

1.4.5. Orbitrap

The orbitrap is a high-resolution MS instrument with resolution of up to 1,000,000 achievable depending on the model. In this thesis, an orbitrap tandem mass spectrometer called the Linear Trap Quadrupole (LTQ) Orbitrap Velos was used which combines an ion trap and orbitrap mass analyzers, and offers maximum resolving power of 100,000. After ionization in the ESI source, ions enter the MS instrument and first pass through the S-lens which is a stacked ring ion guide where ions are separated from any neutrals. After several electrostatic lenses that further focus the ions, ions enter into a dual cell linear ion trap. The ions can be ejected from the ion trap either radially to a pair of electron multipliers or they can be ejected axially where the ions then pass through another focusing multipole and enter the curved trap (C-trap) where ions are collected and then pulse injected into the Orbitrap mass analyser in packets. The Orbitrap mass analyser consists of an inner spindle-shaped electrode and an outer barrel-shaped electrode as shown in Figure 1.11^[95]. As the ion packets enter the Orbitrap they experience radial and axial electric fields. The axial field accelerates the ions while the radial field puts them on a circular orbit around the inner electrode^[96]. Ions of the same m/z form rings around the inner electrode and the frequency of these rings in the z -direction is proportional to m/z of the ion as shown in Equation 1.7^[95] where ω is the frequency of oscillation in z direction, q is the charge, m is the mass and k is the force constant of the potential.

$$\omega = \sqrt{(q/m) k}$$

Equation 1.7 Oscillation frequency of ions around the inner electrode

The Orbitrap detects the image current of these ion rings and using a Fourier transformation converts the signal to a mass spectrum. A schematic of the Orbitrap used in this project can be seen in Figure 1.13. The time required to perform a scan in Orbitrap depends on the resolving

power selected, with high resolving power requiring ~ 1 sec per scan. Ion trap and Orbitrap mass analyzers can be operated individually, so while Orbitrap is acquiring an MS spectrum of precursor ions (MS^1), several data-dependent MS/MS scans can be performed in the faster LTQ either for user-selected target m/z or based on automatic selection by the instrument based on signal intensity or other criteria. The target ions are isolated and undergo CID fragmentation in the high-pressure cell of the LTQ. Following fragmentation in the high-pressure cell the ions are sent to the low-pressure of the LTQ and ejected radially to the electron multipliers to record product ion spectra (MS^2). This process can be fast, with the ability to record 6-10 MS/MS spectra per second. CID fragmentation in the ion trap is low-energy, and ion traps have a lower m/z cut-off determining which product ions can be stored at the same time as parent mass. Typically, ions with m/z less than $1/3$ m/z of parent ion will not be recorded. Both of these can affect lipid identification.

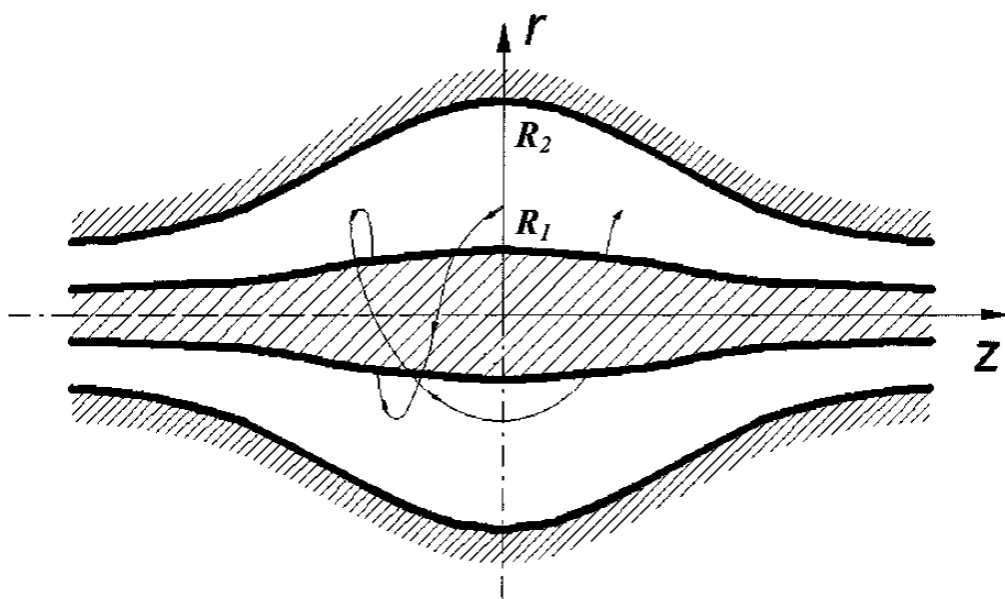


Figure 1.11 Ion trajectory around the inner electrode of an orbitrap. “Reprinted with permission from A. Makarov. *Electrostatic Axially Harmonic Orbital Trapping: A High-Performance Technique of Mass Analysis*^[95]. Copyright 2000 American Chemical Society”

The LTQ Orbitrap Velos also has a higher-energy collision cell (HCD). If this higher-energy CID is used, the parent ion of interest is selected in ion trap, fragmented in HCD cell and the resulting product ions are then injected into Orbitrap for detection^[97]. This allows the user to collect product ion spectrum of full m/z range desired and to acquire the product ion spectrum at

higher resolving power than MS/MS spectra acquired in ion trap. Combination of these two dissociation techniques can help boost confident identification. In Figure 1.12, the product spectra for both CID and HCD dissociation are shown. Figure 1.12 (a) shows that CID gives the fatty acid composition while (b) shows that HCD gives the polar head group. Combining the two allows the molecular lipid species, specific chain length and degree of unsaturation to be reported. An important aspect of the Orbitrap is the Automatic Gain Control (AGC). The AGC setting dictates the number of ions that are allowed to enter into Orbitrap. Typically, this is set at 10^6 . This AGC nullifies the issue of space charging and loss of mass accuracy and resolving power. Selecting a mass range that covers only the masses of interest is important to reduce the number of unwanted ions entering the Orbitrap. The unwanted ions will contribute to noise and reduce the signal-to-noise ratio of the signal of analytes of interest. The QTOF has a fast acquisition speed, good mass accuracy with internal calibration and has a medium resolving power of around 40,000. The Orbitrap has a slow acquisition speed although this can be adjusted at the cost of resolving power. Resolving power of the LTQ Orbitrap Velos is 100,000 and good mass accuracy <1 ppm with use of a lock mass can be achieved. The lock mass is a background signal of known mass that is frequently observed, e.g., steric acid with an m/z of 283.2643 in negative mode. The Agilent 6550 iFunnel QTOF was used for this project for method development when high resolution was not required and to assess the addition of additives via the auxiliary spray system. The Orbitrap was used for all plasma and brain analyses.

1.4.6. Data processing

In an untargeted method the large amounts of data generated by an LC-MS analysis must be processed with the aid of software. The main steps involved with untargeted data processing are: (i) feature detection, (ii) chromatographic alignment, (iii) de-isotoping and de-adducting, (iv) blank extraction, and (v) identification by comparison of MS/MS spectra to a database^[45,98]. De-isotoping is an important feature since ^{13}C makes up approximately 1.1% of the natural carbon on earth. This means that compounds with carbons will have isotope peaks with an intensity equal to $\#C \times 1.1\%$. The software takes this into account meaning it does not count $M+1$, $M+2$ etc. peaks as a separate feature but groups them into single feature. As mentioned in section 1.4.3, compounds can also form multiple adducts such as: $[\text{M}+\text{H}]^+$, $[\text{M}+\text{NH}_4]^+$, and $[\text{M}+\text{Na}]^+$. The software will also account for this and will look for these adducts and assign them to only one feature. SIEVE is software provided by ThermoScientific that executes operations (i) to (iv)

for Orbitrap raw MS files, while Profinder and MPP are similar software packages by Agilent Technologies that execute these operations for QTOF MS data. Although these software packages do a reasonably good job, the feature list obtained from the software is then also manually curated with the following criteria: (i) feature must be present in at least 66% of samples, (ii) must have good peak shape quality and adequate signal-to-noise ratio, and (iii) must be removed if present in blank in similar signal intensity. This results in a high quality curated

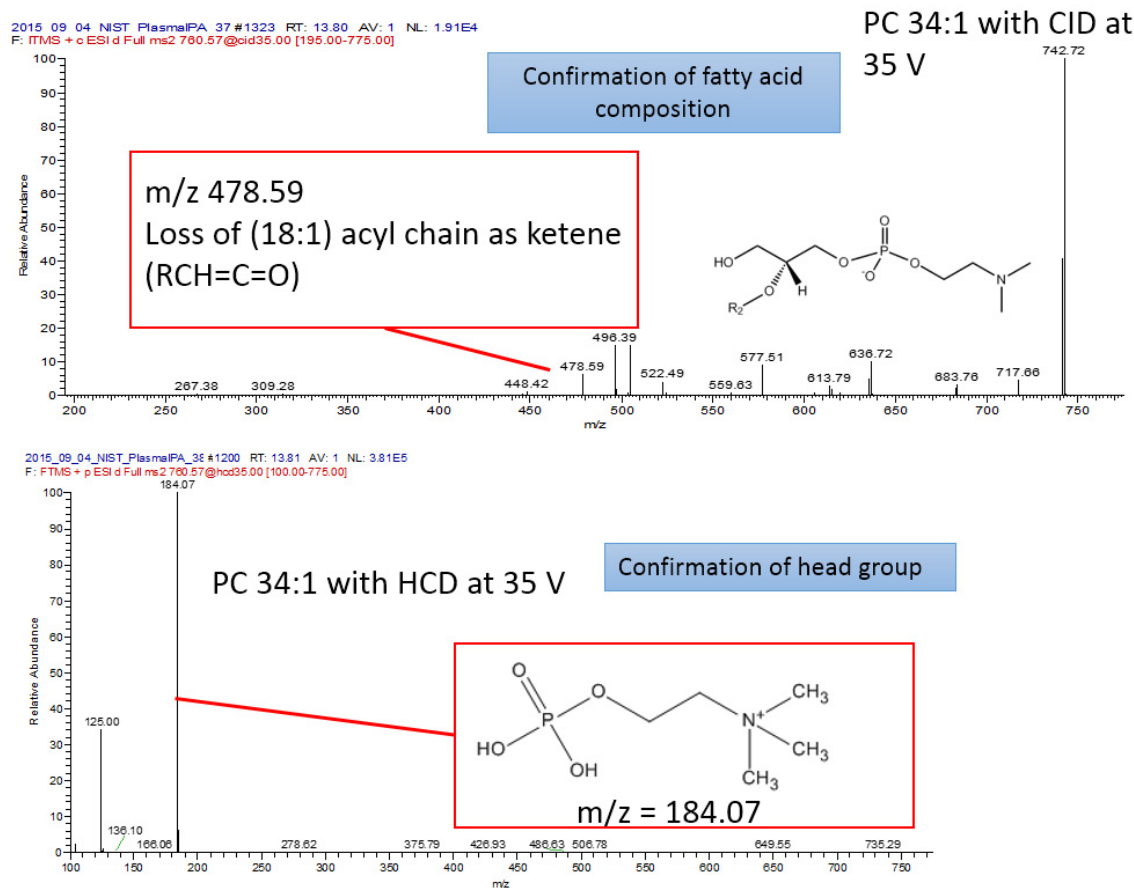


Figure 1.12 Comparison of CID and HCD fragmentation of PC (34:1). (a) shows CID product spectrum of PC(34:1) obtained in the linear ion trap. $[M+H]^+$ m/z 760.57 was selected for fragmentation in plasma in positive mode ESI. The fatty acid composition of the PC has been determined via the CID fragmentation but the headgroup of the PC was not detected due to m/z cut-off of ion trap. Fragments giving compositional information of acyl chains: 478.59 - FA (18:1)(as ketene), 496.39 -FA (18:1). 522.49 -FA (16:0)(as ketene). Fragment identities obtained from^[35]. (b) shows HCD product spectrum of the same PC (34:1) which was obtained in Orbitrap after fragmentation in the HCD collision cell and confirms presence of the headgroup with m/z of 184.07.

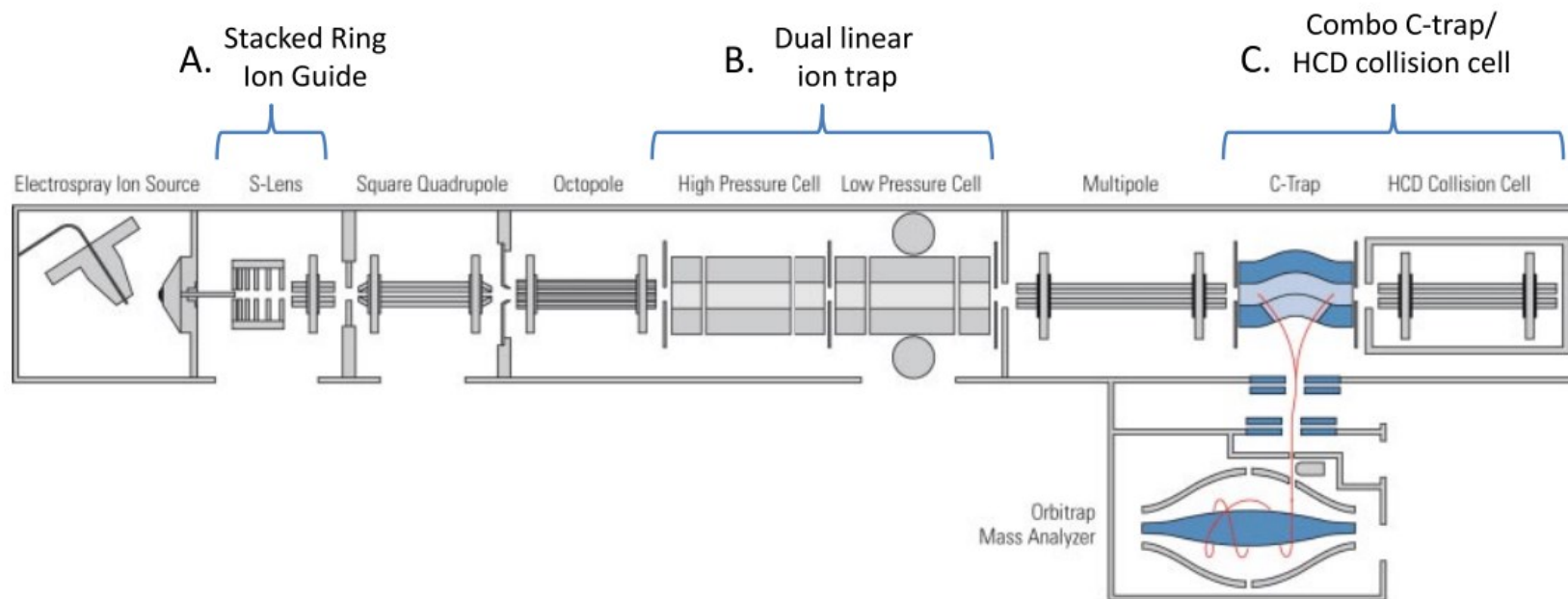


Figure 1.13 Schematic of an LTQ Orbitrap Velos mass spectrometer. Figure reproduced from reference^[97] under the CC-BY 4.0 license

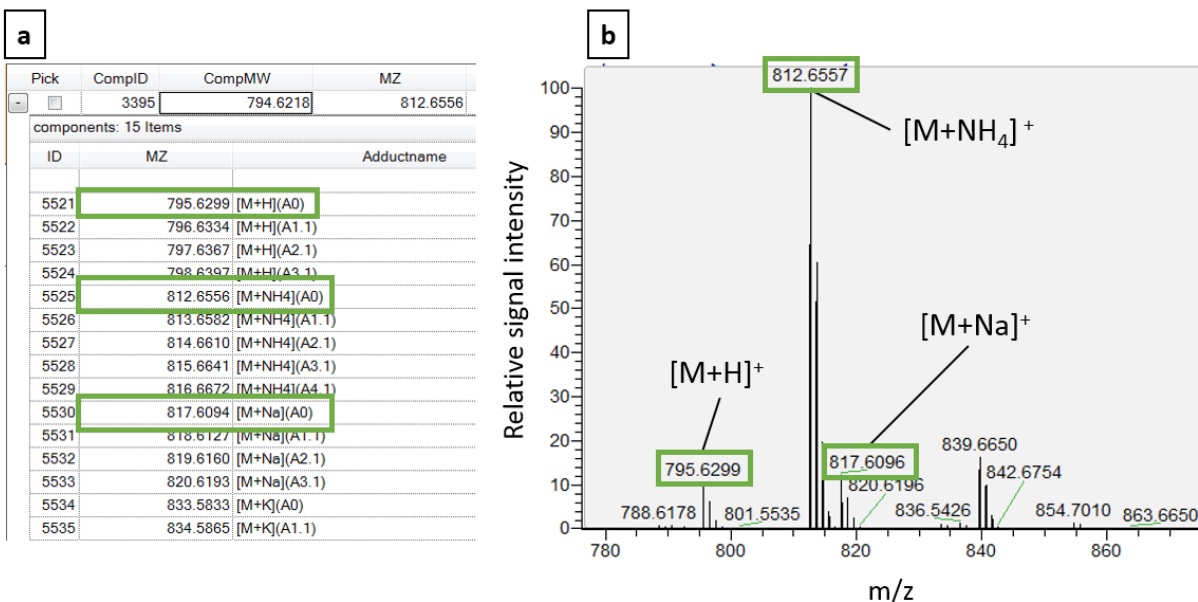


Figure 1.14 De-isotoping and de-adducting is an important part of data processing to arrive at correct number of putative features. (a) shows a screenshot from SIEVE software, a mass list for a compound with MW 794.6218. The $[M+H]^+$, $[M+Na]^+$, and $[M+NH_4]^+$ have been highlighted. The software has labelled the isotope peaks, M+1, M+2 etc... as all belonging to one compound with the MW of 794.6218. (b) shows the spectrum of this compound with the $[M+NH_4]^+$ being the dominant adduct. There are 51 hits from a LIPIDMAPS search for lipids of this mass belonging to the GL, GP and PK lipid classes. Due to the $[M+NH_4]^+$ being the dominant adduct this is most likely TG (48:6).

data set of putative metabolites or lipids. The LipidSearch software performs a feature detection step followed by an alignment step. Lipids are identified by comparing the parent mass and the product spectrum to a lipid library with predicted fragmentation patterns of >1.5 million lipids^[99]. Peaks are integrated and given a grade depending on level of identification. These grades range from A-D. Explanation of these grades is given in Table 1.4.

Table 1.4 Grading criteria used by LipidSearch

Grade	Criteria
A	Lipid class and fatty acid chain were completely identified
B	Lipid class and some fatty acid chains were identified
C	Lipid class or fatty acids were identified
D	Identification by other fragment (i.e. H ₂ O loss)

1.5. Research objectives

Extracting lipids from brain tissue requires the sacrifice of the animal to obtain enough tissue to perform traditional LLE methods such as the Folch method. An established *in vivo* method for sampling brain tissue, MD, exists. However, MD is limited to the analysis of polar compounds due to the nature of the perfusate required for sampling. Thus, currently there is no established *in vivo* method for sampling lipids from brain tissue. SPME has the potential to address this challenge. To be considered for future studies, its viability as a method of extracting lipids from brain tissue must be assessed. This project's main objective is to determine SPMEs capabilities by comparing it to the traditional Folch lipid extraction method. This study will evaluate and compare the lipid coverage of the two methods, and the matrix effects associated with both the methods. High sensitivity is required of the LC-MS since SPME is a non-exhaustive, microextraction technique. This requires that first the sensitivity of LC-MS detection is improved. To do this, different additives will be assessed to determine the additive that gives the greatest sensitivity of LC-MS detection in negative ESI mode. This will facilitate the detection of low abundance lipid species. Having increased the sensitivity of LC-MS detection in negative mode the SPME method can be optimized. This will be accomplished by evaluating different extraction times, desorption solvents, and desorption times. *In vivo* SPME fibres that have been used to extract lipids will be compared to Folch extractions of the hippocampus region of rats. This will allow an evaluation of the viability of SPME to extract lipids from brain tissue for the first time.

2. Improving negative ESI-LC-MS lipidomic analysis of human plasma using acetic acid as a mobile phase additive

Cian Monnin, Parsram Ramrup, Carolann Daigle-Young, Dajana Vuckovic

Department of Chemistry and Biochemistry, Concordia University, Montréal, Québec, Canada

Corresponding author: D. Vuckovic, Department of Chemistry and Biochemistry, 7141 Sherbrooke Street West, Montréal, Québec, Canada, H4B 1R6

email: dajana.vuckovic@concordia.ca

2.1. Abstract

Mobile phase additives in LC-MS are used to improve peak shape, analyte ionization efficiency and method coverage. Both basic and acidic mobile phases have been used successfully for negative ESI, but very few systematic investigations exist to date to justify the choice of mobile phase. Acetic acid was previously shown to improve ionization in untargeted metabolomics of urine, but has not been investigated in lipidomics. The goal of this study was to systematically compare the performance of acetic acid to other commonly employed additives in negative ESI-LC-MS lipidomics. The performance of acetic acid was compared to commonly utilized mobile phase additives in lipidomics: ammonium acetate, ammonium acetate with acetic acid and ammonium hydroxide using lipid standard solutions containing representatives of major mammalian lipid subclasses and isopropanol-precipitated human plasma. This design allowed comparison of the influence of additive and additive concentration on lipid signal intensity, lipid peak shape and lipid coverage in both simple and complex biological matrices using both Orbitrap and quadrupole-time-of-flight MS platforms with different ESI source designs. Ammonium hydroxide caused 2 to 1000-fold signal suppression of all lipid classes in comparison to acetic acid. In comparison to ammonium acetate, acetic acid increased lipid signal intensity from 2 to 19-fold for 11 lipid subclasses, and decreased ionization efficiency only for ceramide and phosphatidylcholine lipid classes which can be effectively ionized in positive ESI mode. The improved ionization efficiency using acetic acid also increased lipid coverage by 68% versus ammonium acetate additive. Acetic acid at a concentration 0.02% (v/v) is the suggested choice as a mobile phase additive for lipidomics and targeted lipid profiling with negative ESI-

LC-MS based on signal enhancement and improved lipid coverage compared to ammonium acetate, ammonium acetate with acetic acid, and ammonium hydroxide mobile phases.

2.1.1. Keywords

Negative electrospray ionization, mobile phase composition, acetic acid, ammonium acetate, ammonium hydroxide, lipidomics

2.2. Introduction

Reversed-phase (RP) liquid chromatography-mass spectrometry (LC-MS) is one of the most popular, modern approaches for lipidomics and targeted class-based lipid profiling. RP LC-MS allows for separation of lipids present in complex samples according to their headgroup, fatty acid chain length and number of double bonds^[100]. To achieve comprehensive coverage of lipids both positive and negative ESI mode are required^[79,101] because certain lipid subclasses are only detected in either positive electrospray mode (ESI⁺) or negative electrospray mode (ESI⁻). ESI⁺ is used for the detection of phosphatidylcholine (PC), lysophosphatidylcholine (LPC), lysophosphatidylethanolamine (LPE), phosphatidylethanolamine (PE), lysosphingomyelin (LSM), sphingomyelin (SM), ceramide (Cer), monoacylglycerol (MG), diacylglycerol (DG) and triacylglycerol (TG) lipid sub-classes. ESI⁻ provides better ionization efficiency for phosphatidic acid (PA), phosphatidylglycerol (PG), phosphatidylinositol (PI) and phosphatidylserine (PS) lipid sub-classes and their corresponding lyso forms (LPA, LPG, LPI and LPS).

In LC-MS, mobile phase additives are routinely used to improve peak shape, analyte signal and analyte coverage. The additives can act as ion-pairing agents by pairing with charged analytes resulting in a pseudo-neutral compound that can interact with the stationary phase whereas its charged counterpart cannot^[102] and/or to reduce tailing due to secondary interactions. This leads to sharper chromatographic peaks and reproducible retention times. Additives can also significantly increase ESI ionization efficiency of the analyte. Weak acids, such as acetic acid (AA), and formic acid (FA) are the most common mobile phase additives in ESI⁺ as the low pH of the solution facilitates protonation of the analytes. Salts are used in ESI⁺ at low concentrations to promote the formation of adducts such as $[M+Na]^+$ and $[M+NH_4]^+$ ^[103] for analytes for which the adduct formation is more favourable than protonation. However, for ESI⁻ there is no clear consensus as to the choice of the best additive and mobile phase pH as discussed in detail below.

In addition to ESI conditions, both mobile phase composition and analyte properties play important role in the ESI⁻ ionization process. The protic nature of methanol permits more effective solvation of deprotonated, negative ions than acetonitrile while its higher polarity and dielectric constant facilitate charge separation process in ESI and creation of thin layer of charge at the droplet surface^[104,105]. This makes protic solvents such as methanol preferred for ESI⁻. The analyte properties that best predict the ESI⁻ ionization efficiency for a given analyte include: (i) the number of hydrogen bonds the analyte can accept, (ii) the number of potential charge centres an analyte has and (iii) the polarity of the analyte although other studies also described the importance of pK_a /ionization degree in solution, number of free rotatable bonds and polar surface area^[104–106]. Additional class-specific studies also found significant influence of the pK_a /ionization degree in solution and anion charge delocalization^[107]. Despite the fact that there is currently no consensus regarding which parameters best describe ESI response for a given analyte, the studies to date converge that although analyte pK_a and mobile phase pH contribute to the extent of analyte ionization, the change of mobile phase pH may not result in expected change in ionization efficiency for a given analyte^[105,106,108,109] due to the fact that the ESI process is complex collection of solution-, surface-, and gas-phase reactions and equilibria. In particular, the ability of analyte to move to the droplet surface and be ejected from the surface play an important role in the overall extent of ionization. Recent study proposes classification of analytes as pH-dependent and pH-independent in ESI, but analyte physicochemical properties such as pK_a or degree of ionization could not accurately predict whether ionization process will be pH dependent for a given analyte^[106].

In ESI⁻ ammonium salts such as ammonium formate (AmF) and ammonium acetate (AmAc) are routinely used because they can facilitate deprotonation in the gas phase^[110]. Other studies favour basic mobile phase additives such as ammonium carbonate and ammonium hydroxide to promote solution-phase deprotonation^[108]. Yang *et al.* recently showed that basic pH was preferred for deprotonation of neutral compounds, while acidic compounds ionized better under acidic pH conditions^[111]. Such reports of “wrong-way-round” ionization have clearly shown that acidic mobile phases can also promote strong ionization in ESI⁻^[78,112,113], thus confirming that the influence of surface- and gas-phase processes is more significant than assumed in early studies and depends on both pH and ionic strength of electrosprayed solution^[114]. “Wrong-way-round ionization” is believed to be facilitated by the significant change of pH at the droplet surface

versus bulk solution due to charge enrichment in the surface layer and also possibly to favourable formation of charged ions due to application of ESI potential, causing different behaviour than in bulk solution^[105]. The superiority of acetic acid mobile phases has been shown for analytes such as amino acids (leucine, histidine) over basic mobile phases^[112]. Wu *et al.* examined the effect of weak acids ranging from formic to butyric acid on the ionization efficiency of four selective androgen receptor modulators^[115]. Their results show that AA outperforms other weak acids, acetate and formate salts and basic additives such as ammonium hydroxide and triethylamine, with maximum response observed for 1 mM concentration of AA. In a study of six acidic anti-inflammatory pharmaceuticals, AA was the best additive for fenoprofen, while basic triethylamine or ammonium carbonate mobile phases performed better for the other species tested in the concentration range of 5-20 mM^[113]. Weak acids such as AA can improve ESI⁻ ionization efficiency due to a number of favourable chemical and physical properties: (i) weak acid anions have a high gas-phase proton affinity, (ii) their only counterions are protons which can facilitate the reduction of other protons generated by the solvent into H₂ thus facilitating droplet charging, and (iii) weak acids with small molecular volume do not suppress the ionization of analytes^[115,116]. On the other hand, basic mobile phase additives such as ammonium hydroxide (AmOH) caused signal enhancement in ESI⁻ for a number of acidic analytes like cholic acid, a bile salt, and canrenoic acid, a prodrug which is metabolized to canrenone^[102]. In summary, there is currently no consensus in the literature regarding the optimal pH and/or additive to use for ESI⁻ which represents a critical gap in our knowledge. Current incomplete fundamental understanding of ESI⁻ process also does not allow us to predict with certainty the best additive for a given set of target analytes.

For omics studies, the situation is even more complicated due to a wide range of physicochemical properties of the analytes being measured. An extensive comparison of mobile phase additives for global metabolomics of urine showed AA in the concentration range of 0.2-1 mM significantly increased signal intensity across many metabolite classes and resulted in the highest number of metabolites detected in ESI⁻ when compared to FA (0.008 mM – 0.1% v/v), AmAc (1 mM) and AmF (1 mM)^[116]. A second study showed that 1 mM ammonium fluoride increases ionization efficiency (5.7-fold on average) in ESI⁻ compared to 5 mM AmAc pH 7 or 0.1% FA^[110]. This significant improvement in ionization efficiency also resulted in 2.5-fold increase in features detected, and these improvements were attributed to the fluoride anion's

strong proton affinity in the gas phase. These two studies clearly demonstrate that mobile phase selection can have an important effect on metabolite coverage, but provide conflicting results as to the choice of the best additive for ESI⁻.

The mobile phase additives commonly employed for lipid and lipidomics analysis in ESI⁻ include: 5-10 mM AmAc^[78,110,117,118], 5-20 mM AmF^[8,119,120], 0.02%-0.1% AA^[121,122], 0.2% FA^[110,121], and combinations of these salts and acids^[123]. The use of 0.05% AmOH was shown to give a higher signal for the anionic phospholipids, PG, PA, PS, PI (including their lyso forms) and the zwitterionic PE when compared to 10 mM AmAc^[124]. A systematic evaluation of mobile phase additives particular to global lipidomics was recently performed by Cajka and Fiehn^[79]. They examined AmF (10 mM), AmF/FA (10 mM, 0.1%), AmAc (10 mM), AmAc/AA (10 mM, 0.1%) and AmAc/FA (10 mM, 0.1%). They concluded that 10 mM AmAc was the best additive for ESI⁻; however, neither AA as an additive by itself nor AmOH were evaluated. Nazari and Muddiman compared the performance of 20 mM AmOH, 1 mM AA, 5 mM AmAc and 5 mM 2,2,2-trifluoroethanol for lipid ionization in imaging studies of liver tissue using polarity-switching ESI method^[125]. They concluded AA provided the best performance in terms of signal intensity, ESI stability and method precision. The use of different concentrations of additives, different analytical approaches (with and without LC separation) and different sample types for the evaluation precludes direct comparison of the existing studies. As a result, based on current literature it is not clear which additive provides the best performance for LC-MS lipidomics in ESI⁻.

Therefore, the goal of this study was to examine the performance of AA as a mobile phase additive for ESI⁻ LC-MS detection of lipids. This mobile phase additive was compared to the best additive proposed by Cajka and Fiehn^[79] (10 mM AmAc), 10 mM AmAc with 0.02% AA used by Uhl *et al.*^[123] and 0.05% AmOH proposed by Bang *et al.*^[124] using simple lipid standard mixtures and biologically-relevant human plasma extracts on two LC-MS instruments: Thermo LTQ-Orbitrap Velos and Agilent 6550iFunnel QTOF.

2.3. Experimental

2.3.1. Chemicals

LC-MS grade solvents and mobile phase additives were purchased from Sigma-Aldrich, Oakville, Ontario, Canada. Lipid standards PS (17:0/17:0), LPS (17:1), PC (19:0/19:0), PE

(17:0/17:0), PG (17:0/17:0), LPC (17:0), PE (12:0/13:0), PG (17:0/20:4(5Z,8Z,11Z,14Z)), PS (17:0/20:4(5Z,8Z,11Z,14Z)), PI (17:0/14:1(9Z)), LPA (13:0), sphingosine (SP) (d17:1), Cer (d18:1/25:0), SM (d18:1/12:0), LSM (d17:1), PA(17:0/20:4(5Z,8Z,11Z,14Z)) and LPE (17:1(10Z)) were purchased from Avanti Polar Lipids, Alabaster, AL, USA. Standard mixes also contained representative lipids from the TG, DG and MG classes however these are not detectable in ESI. Additional details including full lipid name, stock standard preparation and monoisotopic masses of ions observed are included in Appendix A, Tables A1-3.

2.3.2. Preparation of lipid standards

Lipid stock standard mix I for mobile phase comparison was prepared at concentration of 1 $\mu\text{g/mL}$ in 100% MeOH. This stock solution was diluted to 200 ng/mL in 50% MeOH before analysis. IS mix I was prepared at concentration of 6 $\mu\text{g/mL}$ in 100% MeOH and stored at -80°C . IS mix II was prepared at concentration of 400 ng/mL in 100% MeOH and stored at -80°C .

2.3.3. Preparation of human plasma samples

Citrated pooled human plasma (LOT#: BRH907831) was obtained from Bioreclamation IVT (Baltimore, MD, USA) and stored at -80°C prior to analysis. Four replicates were prepared for analysis on the Orbitrap. Lipids were extracted using a cold isopropanol protein precipitation method adapted from Sarafian *et al.*^[40]. Briefly, plasma was spiked with IS mix I to obtain concentration of 600 ng/mL. 450 μL of cold isopropanol was then added to 150 μL of plasma and vortexed for 1 minute. The samples were then incubated at -80°C for 1 hour, followed by centrifugation at 25,000 g at 4°C for 20 min to remove protein pellet. 100 μL of the resulting supernatant was finally diluted (1:1, v/v) with $\text{H}_2\text{O}/\text{MeOH}$ (1:1, v/v) containing IS mix II. This gave the final concentration of IS mix I in the extracts at 75 ng/mL and IS mix II at 100 ng/mL. A blank extract was prepared using purified water in place of plasma. Three replicates were prepared for analysis on the QTOF. They were prepared using the same protocol as the samples prepared for the Orbitrap but had IS mix I at a final concentration of 200 ng/mL and no IS mix II present.

2.3.4. LC-MS analysis on LTQ Orbitrap Velos

Three pairs of mobile phases were prepared. Mobile phase A1 consisted of 60:40 (v/v) water/methanol with 10 mM AmAc and 1 mM AA. Mobile phase B1 consisted of 90:10 (v/v) isopropanol/methanol with 10 mM AmAc and 1 mM AA. Mobile phase A2 consisted of 60:40

(v/v) water/methanol with 0.02% (v/v) AA. Mobile phase B2 consisted of 90:10 (v/v) isopropanol/methanol with 0.02% (v/v) AA. Mobile phase A3 consisted of 60:40 (v/v) water/methanol with 10 mM AmAc. Mobile phase B3 consisted of 90:10 (v/v) isopropanol/methanol with 10 mM AmAc. For preparation of mobile phases B1 and B3 the salt was first completely dissolved in methanol, followed by addition of isopropanol.

An Agilent 1200 LC system (Agilent Technologies, Santa Clara, CA, USA) connected to a LTQ-Orbitrap Velos (Thermo Fisher Scientific, Waltham, MA, USA) via a HESI source was used for comparison of three pairs of mobile phases described above. Separation was performed on a Waters XSelect CSH C₁₈ reversed phase column with dimensions: 130 Å, 2.5 μm, 2.1 mm x 75 mm (Waters, Milford, MA, USA). The refrigerated autosampler was set at 4°C and a column heater maintained at 55°C was used. The flow rate was 0.200 mL/min. The gradient program for all three mobile phase pairs was as follows: 0-2 min 20% B; 2-3 min 20%-80% B; 3-16 min 80%-95% B; 16-24 min 95% B; 24-24.1 min 95%-20% B; 24.1-37 min 20% B. Injection volume was 10 μL.

The ESI source parameters for the LTQ-Orbitrap Velos were: spray voltage: 3 kV, source temperature: 300°C, sheath gas flow rate: 10, Aux gas flow rate: 5, capillary temp: 275°C. A lock mass of 283.2643 (steric acid) was selected for internal mass calibration and S-Lens RF setting was 60%. Full MS¹ scan was performed with a m/z range of 280-1200, resolving power of 60,000 and AGC target of 1x10⁶ ions. This was followed by top 5 CID data-dependent-acquisition (DDA) for the 1st to the 5th most intense ion from the first scan event in the FTMS. The ion trap AGC MSⁿ target was 10,000. Dynamic exclusion settings were as follows: repeat count = 2, repeat duration = 20 seconds, and exclusion duration = 35 seconds. Collision energy of 35 V was used for DDA. To increase identifications, additional QC plasma injections were performed at the end of each batch using top 5 higher-energy collisional dissociation (HCD) DDA method for the 1st to the 5th most intense ion from the first scan event in the FTMS with a resolving power of 7,500 and AGC target of 50,000. Collision energy used for HCD was 55 V. Dynamic exclusion settings were the same as the CID settings above.

2.3.5. LC-MS analysis on Agilent 6550 iFunnel QTOF

Four pairs of mobile phases were prepared for the comparison of AmOH to AA. Mobile phase A1 consisted of 60:40 (v/v) water/methanol with 0.02% (3.5 mM) AA. Mobile phase B1

consisted of 90:10 (v/v) isopropanol/methanol with 0.02% (3.5 mM) AA. Mobile phase A2 consisted of 60:40 (v/v) water/methanol with 0.014% (3.5 mM) AmOH. Mobile phase B2 consisted of 90:10 (v/v) isopropanol/methanol with 0.014% (3.5 mM) AmOH. Mobile phase A3 consisted of 60:40 (v/v) water/methanol with 0.02% AmOH. Mobile phase B3 consisted of 90:10 (v/v) isopropanol/methanol with 0.02% AmOH. Mobile phase A4 consisted of 60:40 (v/v) water/methanol with 0.05% AmOH. Mobile phase B4 consisted of 90:10 (v/v) isopropanol/methanol with 0.05% AmOH.

An Agilent 1290 Infinity II UHPLC system was connected to an Agilent 6550 iFunnel QTOF MS instrument with a Dual Agilent Jet Stream (AJS) electrospray ionization source (Agilent, Santa Clara, CA, USA). The system also incorporated 1260 isocratic pump, which was used for continuous infusion of internal reference standard for internal mass calibration. The refrigerated autosampler was set to 4°C. Separation was performed on a Kinetex EVO C₁₈ reversed phase column with dimensions: 100 Å, 5 µm, 2.1 mm x 100 mm (Phenomenex, Torrance, CA, USA) thermostatted to 55°C. The flow rate was 0.250 mL/min. The gradient was as follows: 0-4 min 40% B, 4-6 min 40-65% B, 6-14 min 65% B, 14-18 min 65-80% B, 18-24 min 80-87% B, 24-24.5 min 87-95% B, 24.5-26 min 95% B, 26-26.1 min 95-40 %B, 26.1-32 min 40% B. Injection volume was 10 µL.

The Dual AJS ESI source parameters for the Agilent 6550 iFunnel QTOF MS were: drying gas temp: 275°C, drying gas flow rate: 15 L/min, sheath gas temp: 300°C, sheath gas flow: 12 L/min, capillary voltage: 3500 V, nozzle voltage: 500 V. MS scan was collected in the range of 100-1200 m/z with 1 spectra/s. Internal calibration was performed using the Dual AJS system using the calibrant masses of 112.03632 (purine) and 980.016375 (HP-0921 acetate adduct) from Agilent mass reference solution.

2.3.6. Post-column gas-phase addition of mobile phase additives on Agilent 6550

iFunnel QTOF using Dual AJS ESI source

Mobile phase with no additives present was prepared. Mobile phase A1 consisted of 60:40 (v/v) water/methanol and mobile phase B1 consisted of 90:10 (v/v) isopropanol/methanol. The dual AJS ESI source allows the introduction of a second spray that is usually used to add a reference standard mixture for internal mass calibration. This auxiliary spray allows the introduction of either AmOH or AA to the LC effluent within the ESI source therefore allowing the assessment

of the effect of introducing an additive in the gas phase. Four combinations of solvents with additives were assessed: (i) methanol with 0.02% AA, (ii) acetonitrile with 0.02% AA, (iii) methanol with 0.1% AmOH and, (iv) acetonitrile with 0.1% AmOH. Separation was performed on a Waters XSelect CSH C₁₈ reversed phase column with dimensions: 130Å, 2.5 µm, 2.1 mm x 75 mm. The same gradient as in the LC-MS analysis on Agilent 6550 iFunnel QTOF was used, see above.

2.3.7. Data processing

For samples run on QTOF, targeted data processing was performed on Agilent Masshunter software (TOF Quantitative Analysis B.07.00, Qualitative Analysis B.07.00), using 20 ppm extraction window for monoisotopic masses of interest. Deprotonated ion [M-H]⁻ and acetate adducts [M+CH₃COO]⁻ were considered for all lipid standards with the most intense ion used for signal intensity comparisons, as shown in Table 2.1 and Table 2.2. Any signal present in the blanks was subtracted and the final averaged peak areas across all replicates were compared. Untargeted data processing was performed using Agilent Profinder Software (B.08.00) and Agilent Mass Profiler Professional (B.14.00) with the following settings: peak filter = 600 counts, mass window = 15 ppm + 2 mDa, retention time tolerance = 5% + 1 min, molecular feature extraction score > 70, adducts: -H and +CH₃COO⁻ and, absolute intensity = 5000. The final datasets were then manually curated to meet the following criteria: minimum signal-to-noise ratio of 5 compared to the blank and metabolite must be present in 2 out of 3 samples. Features with retention time <1 min were omitted.

For targeted processing of Orbitrap data, Thermo Scientific Xcalibur (2.2 SP1.48) was used using the same criteria as for QTOF processing except a 10 ppm extraction. Thermo Scientific SIEVE (2.2 SP2) was used to process untargeted data with a minimum intensity = 5000. The final datasets were then manually curated to meet the following criteria: good quality peak shape (manual inspection), signal-to-noise ratio of 5 compared to the blank and, present in 3 out of 4 samples. Features with retention <2 min were omitted. Data from plasma samples after Orbitrap analysis were also processed using LipidSearch 4.1 to identify lipids. The high mass accuracy data from the MS¹ combined with the fragment MS² spectra are compared to a library of lipid ions and predicted lipid fragment patterns of over 1.5 million lipids^[99]. Data files with full scan and data-dependent-acquisition MS² spectra were searched using the “Product” search algorithm

with a precursor tolerance of 10 pm, a product tolerance of 0.5 Da, and m-Score threshold = 5. The alignment settings were: alignment method: Mean, R.T. tolerance = 0.25 min, toprank filter = on, main node filter = all isomer peaks, m-score threshold = 5.0. The resulting datasets were manually curated to meet the following criteria: lipids had to have an A or B grade in at least one of the samples, visually inspected for good peak quality, and minimum signal-to-noise ratio of 5 compared to the blank. The ID quality assigns each detected lipid one of the following grades: A: lipid class and fatty acid chain composition completely identified; B: lipid class identified and fatty acid chain partially identified; C: lipid class or fatty acid chain identified; D: identification by other fragment loss (H₂O loss). Only lipids identified with either an A or B grade were reported.

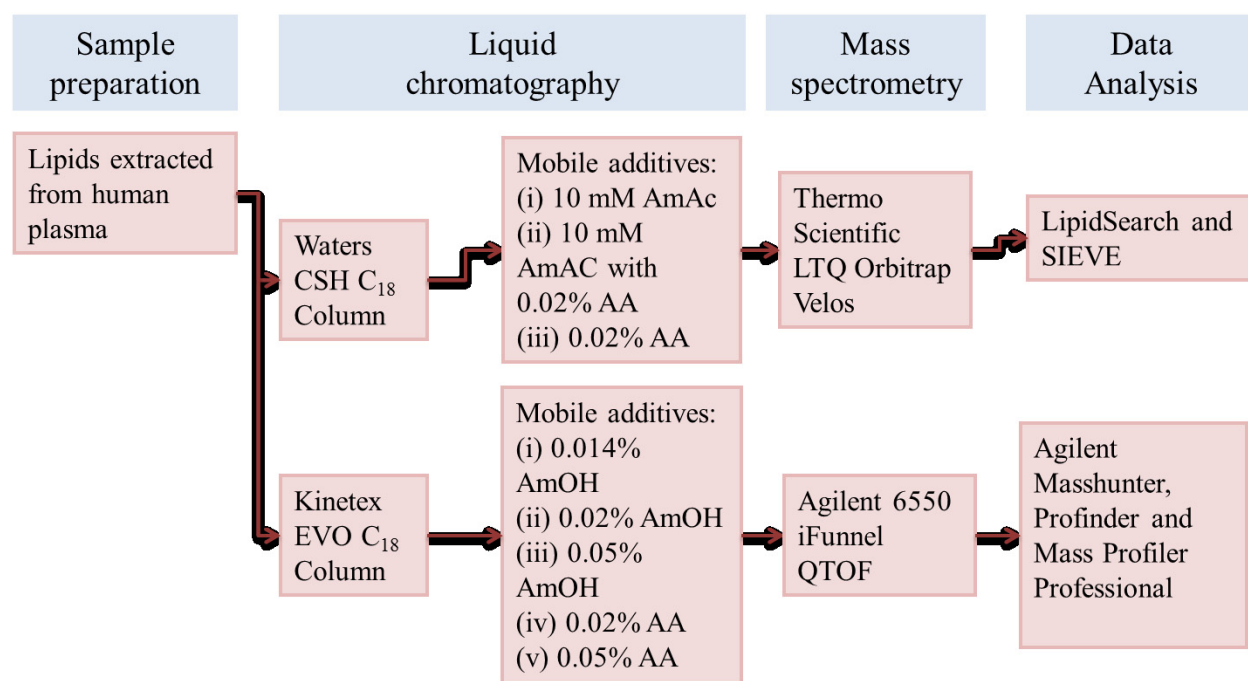


Figure 2.1 Overview of experimental design for comparison of mobile-phase additives using either Orbitrap or QTOF. The stated additives were added directly into mobile phases A and B

2.4. Results and Discussion

2.4.1. Comparison of AmOH versus AA

The comparison of AA and AmOH was performed in two ways: (i) post column addition using a dual spray ESI system to introduce AmOH or AA to the effluent from CSH C₁₈ column within the electrospray source and (ii) addition directly into mobile phase in combination with LC

separation using pH-stable Kinetic EVO C₁₈ column. This design allowed the distinction between gas-phase and solution-phase contributions of the additive to the lipid ionization process.

2.4.2. Additive introduction in gas-phase using dual spray configuration

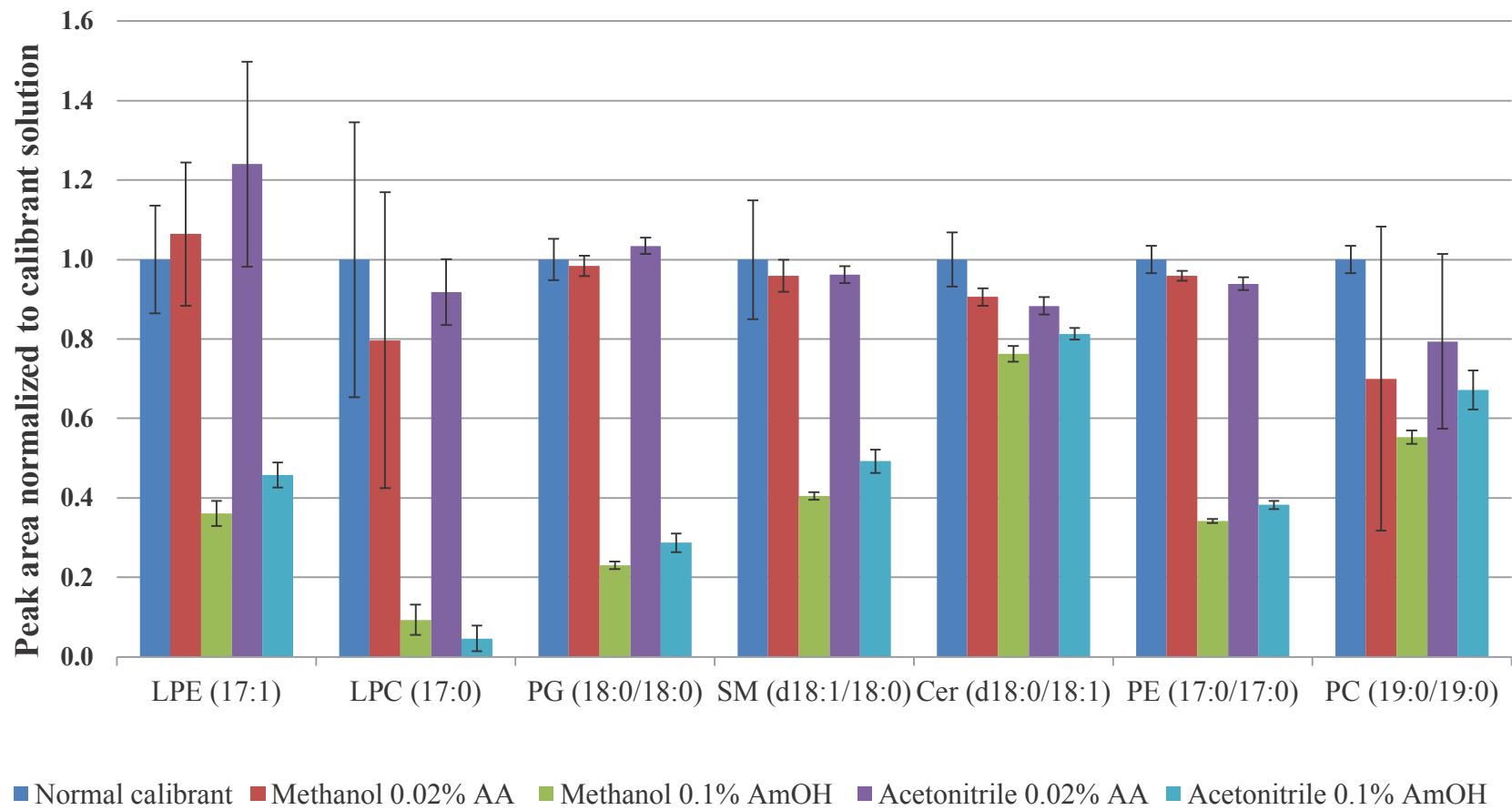
The hydroxide anion has a proton affinity of 1633.1 kJ/mol and the acetate anion has a proton affinity of 1457 kJ/mol^[126]. This suggests that the spray environment would have fewer protons when AmOH is present as an additive. Therefore, if the proton affinity of additive plays an important role in the overall ionization process, AmOH should allow for a more efficient ionization of the analytes. In this experiment, four different auxiliary sprays were tested: acetonitrile with 0.1% (v/v) AmOH, MeOH with 0.1% (v/v) AmOH, acetonitrile with 0.02% (v/v) AA and MeOH with 0.02% AA. The addition of AmOH in dual-spray configuration in the gas phase caused large suppression of signal intensity of the standard solution regardless of organic solvent as shown in Figure 2.2 (a) for all lipid subclasses except ceramides. As expected, there was no significant difference between the two solvents, MeOH and acetonitrile, used in the dual-spray. These solvents were added in gas-phase and the eluent from the column already contained protic solvents. These results clearly show that the presence of AmOH causes suppression when added in the post-column spray despite the fact that AmOH has a higher proton affinity and was present at a higher concentration than AA, 25 mM versus 3.5 mM.

2.4.3. Additive introduction in mobile phase and effect of AmOH concentration

Figure 2.1 summarizes the experiments that were performed to assess the performance of AmOH versus AA directly as mobile phase additives for lipidomics. Mobile phases with AA were prepared at a single concentration of 0.02% (v/v) [3.5 mM] because this was the optimal concentration of this additive in both our work on lipids and eicosanoids [data not shown] and metabolomics^[116]. As there is conflicting evidence about the use of ammonium hydroxide as mobile phase additive in negative ESI and no consensus on optimum concentration, the effect of AmOH concentration on lipid signal intensity and coverage was investigated in detail. Three different mobile phases were prepared at 0.014% (v/v) [3.5 mM], 0.02% (v/v), and at 0.05% (v/v) AmOH. This allowed for comparison of AA to AmOH using equimolar concentrations and equal % (v/v) concentrations. The pK_a of the amine groups in phospholipid headgroups ranges from ~9-11^[127]. The pK_a of the carboxylic acid groups ranges from ~2-5. The pK_{a1} of the

a

Response of standard mix I to postcolumn addition of AmOH and AA



b

Response of internal standard mix I in plasma to AmOH and AA in the mobile phase

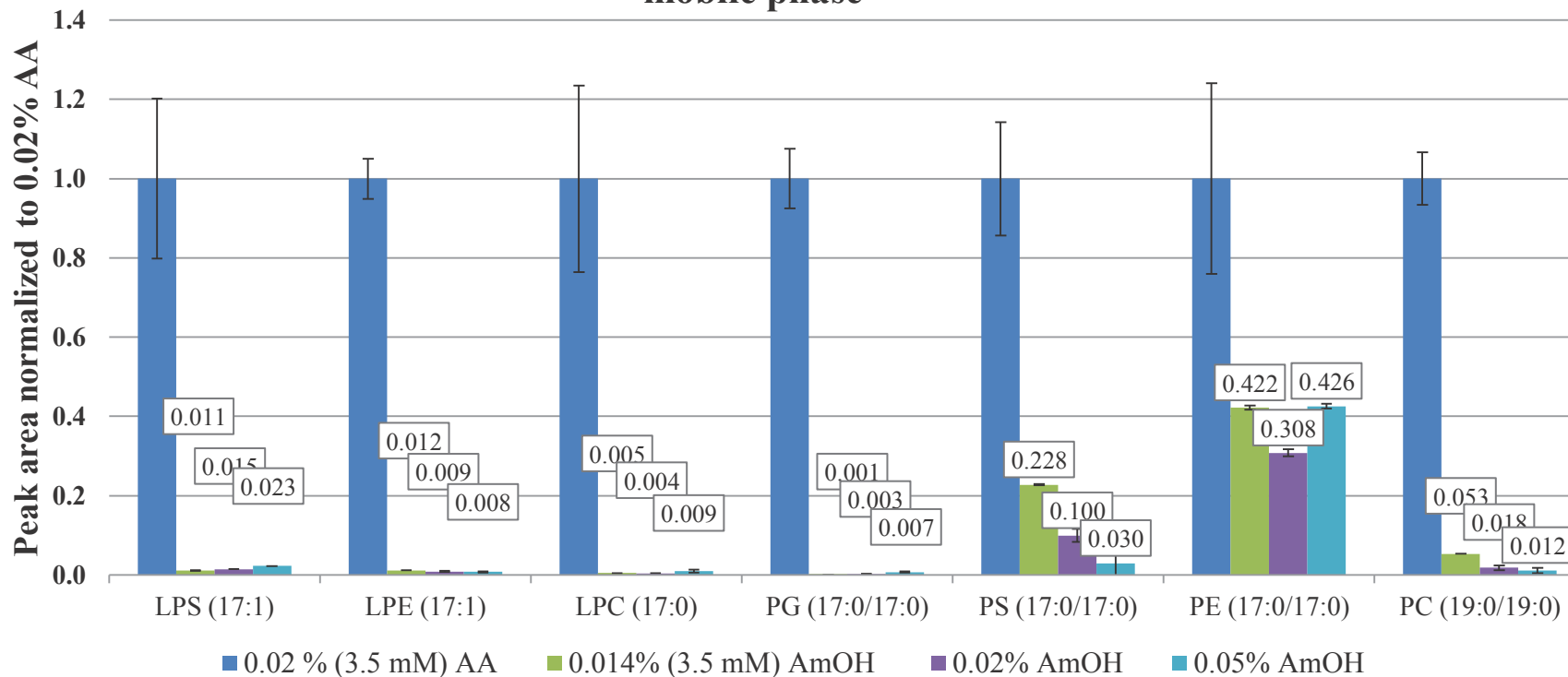
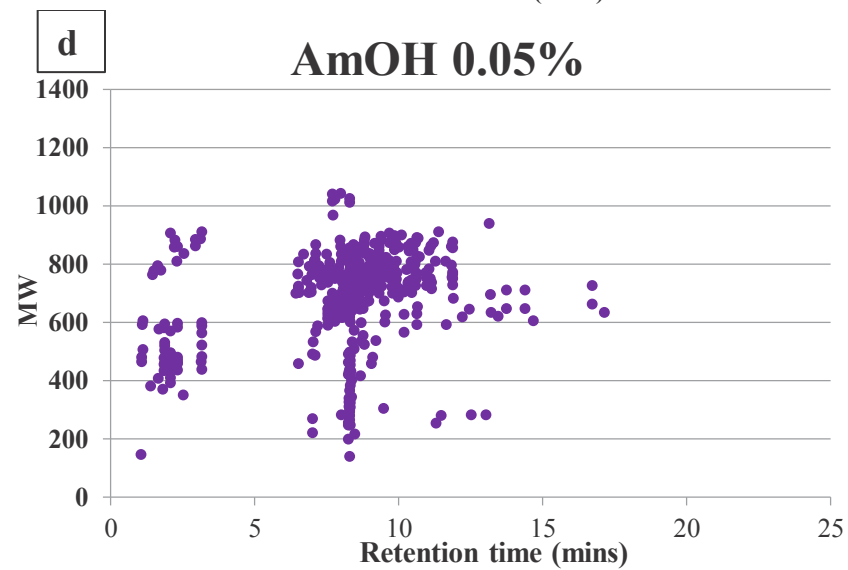
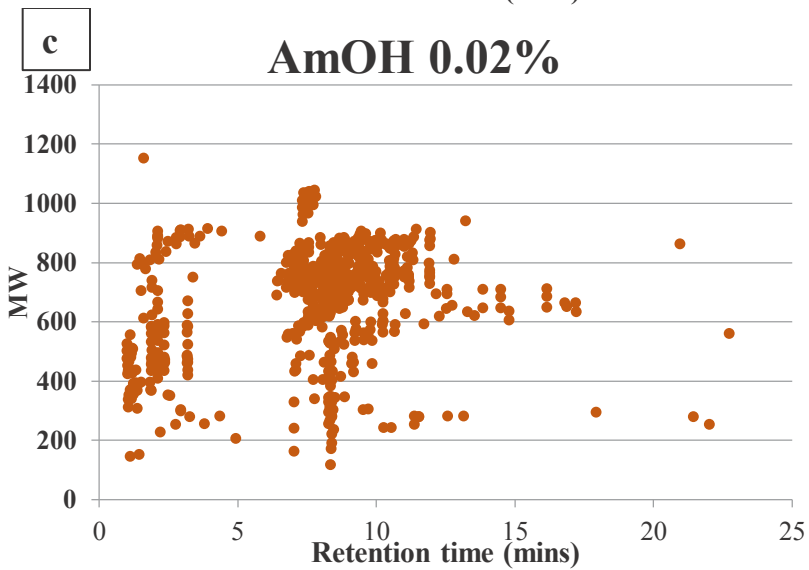
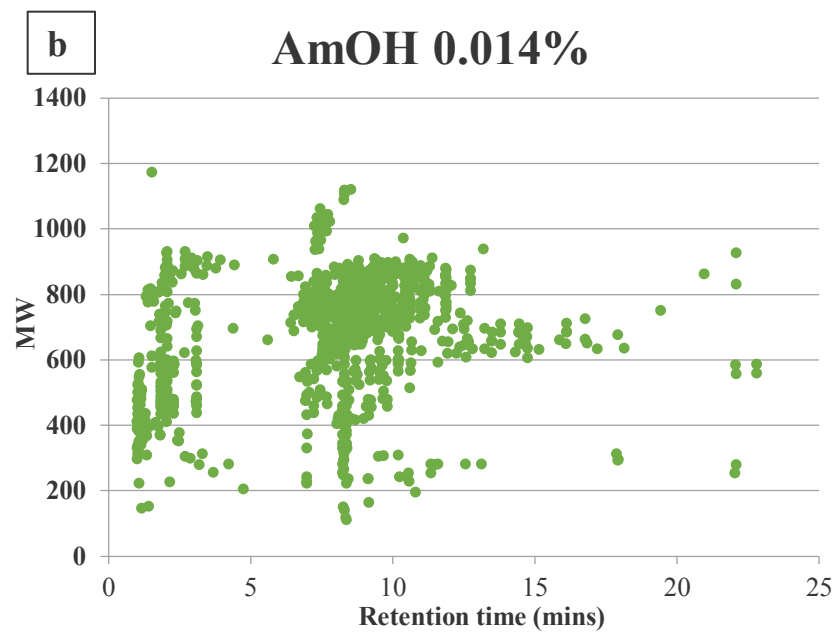
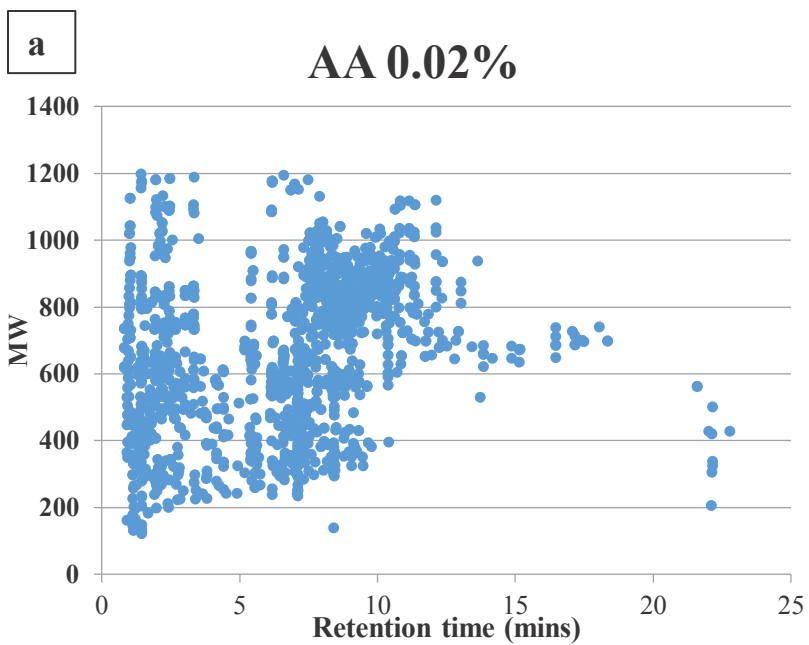


Figure 2.2 Comparison of the influence of AA and AmOH on lipid signal intensity when (a) additive is introduced post-column in gas-phase using dual spray configuration and (b) additive is present directly in mobile phase. (a) shows the dependence of lipid signal intensity in Standard Mix I upon addition of AA or AmOH in gas-phase using either methanol or acetonitrile as solvent after lipid separation using CSH C_{18} column. Normal calibration solution that was used for reference values consists of internal calibrants dissolved in 95% acetonitrile, 5% water with 0.01% AA. All peak areas were normalized to this reference. (b) shows the dependence of lipid signal intensity of Internal Standard Mix I spiked into human plasma at 200 ng/mL concentration upon use of AA (0.02%) or AmOH (0.014-0.05%) in mobile phase. The analytes were separated using pH-stable C_{18} EVO column. All peak areas were normalized to the peak areas obtained with 0.02% AA mobile phase. For both panels a and b, all data was acquired on QTOF and the results shown are for $n=3$ analyses.



e

Effect of AA and AmOH on signal intensity and number of putative lipids observed in human plasma

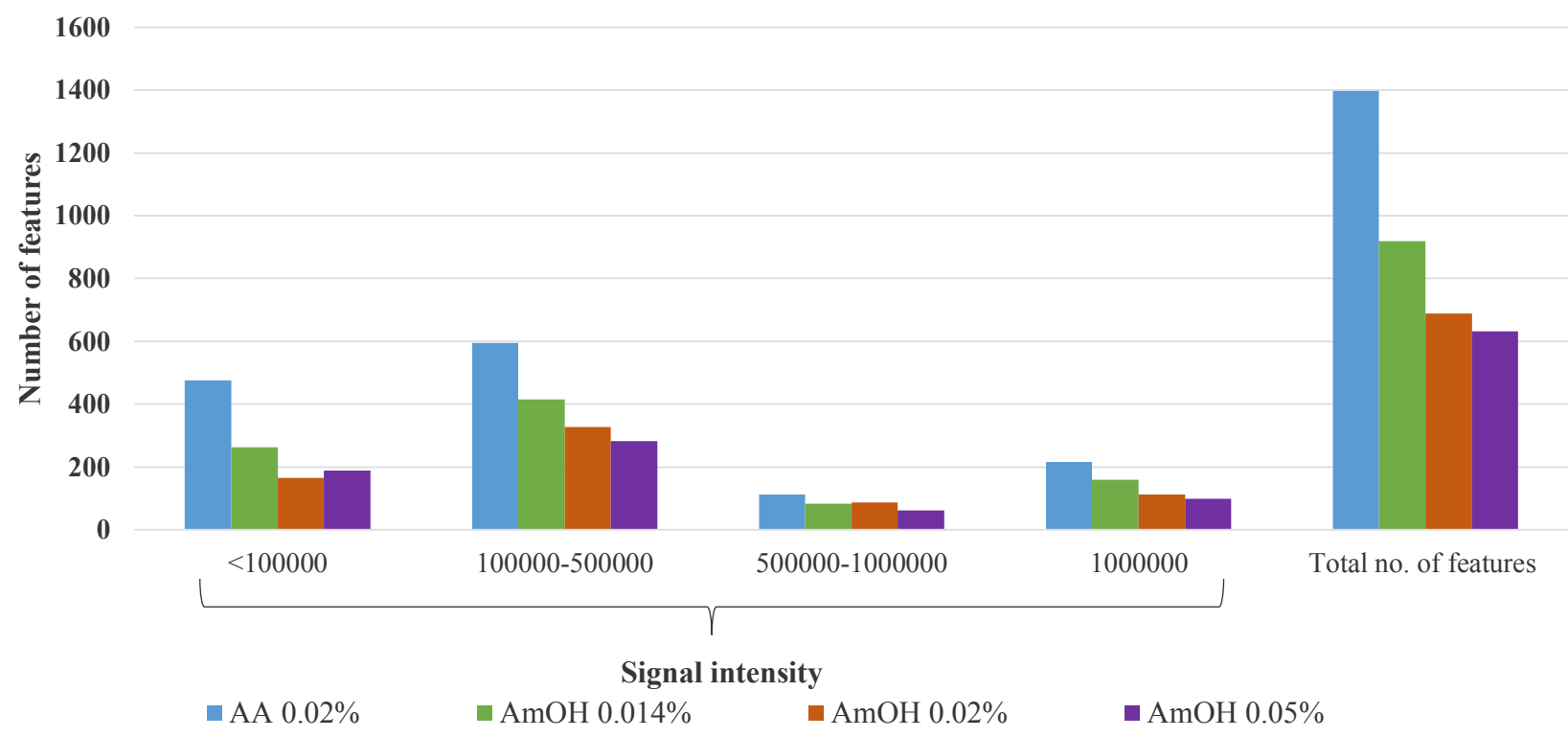


Figure 2.3 Summary of lipidomic results obtained from human plasma samples (n=2) analysed on QTOF using different mobile phase additives and EVO C₁₈ column. Ion maps for 0.02% AA (a) and 0.014-0.05% AmOH (b-d) show that AA provides higher lipid coverage and allows the detection of additional features absent in the AmOH ion maps. Total number of features is shown in top right corner of each panel, and shows that AA increased lipid coverage by 40%, 109% and 130% respectively when used as an additive compared to increasing concentrations of AmOH. (e) shows the effect of additive on number of features binned according to specific intensity ranges. All data presented was processed using MPP. Note: n=3 samples were injected, but one replicate was removed from further data processing due to possible spiking of internal standards error.

phosphate groups ranges from <1-6 while the pK_{a2} ranges from ~7-9^[127]. The pH of 0.1% AmOH is 12.4 which ensures that phospholipids would be present primarily in their anionic form. Therefore, if this is the most important contributing factor to overall ionization efficiency, basic additives such as AmOH should outperform AA in terms of ionization efficiency in negative ESI.

2.4.4. Comparison of AA versus AmAc and AmAc with AA as mobile phase additives

Buffer salts, such as AmAc, are a good choice for lipidomics when running analyses in positive mode as glycerolipids often form ammonium adducts^[128]. In ESI, AA produces protons rather than ammonium ions. These protons can form H_2 whereas ammonium ions cannot participate in electrochemical reduction. This electrochemical reduction of protons leads to an overall increase in negative charge on the spray droplets leading to a more effective ionization and higher metabolome coverage in previous work^[116]. However, this previous study did not examine whether lipids would show similar effects. Previous studies comparing the performance of the AmAc and AmF found that ammonium acetate provides less signal suppression than AmF for the same concentrations^[79,115,116].

Other studies, beyond the field of lipidomics, also found good performance of halogenated solvents, such as 2,2,2-trifluoroethanol or hexafluoroisopropanol for ESI- due to its capability for electrochemical reduction and high gas-phase affinity^[103,115]. However, in side-by-side comparison to acetic acid, 2,2,2-trifluoroethanol did not provide any additional improvement in signal intensity so was not selected for comparison in current study^[115,125].

Therefore, in this part of the work we compared the performance of 0.02% AA to 10 mM AmAc (which Cajka and Fiehn recently found to be the best additive for negative mode lipidomics^[79]) and to 10 mM AmAc with 0.02% AA to examine whether AA helps promote lipid ionization in comparison to ammonium acetate-containing mobile phases.

Figure 2.4 shows the signal intensity observed for Internal Standard Mix II in the three mobile phases tested. The results show 2.4 to 6.6-fold signal enhancement for PI, LPC, PG, PS, PE and SM classes in comparison to 10 mM AmAc, and 1.8 to 11.6-fold signal enhancement for the same lipid classes in comparison to 10 mM AmAc with 0.02% AA (Figure 2.4 (a)). In contrast,

ceramide shows the highest signal intensity in 10 mM AmAc with 0.02% AA. LSM (d17:1) was not detected in 0.02% AA and showed similar intensities in 10 mM AmAc and 10 mM AmAc with 0.02% AA as shown in Figure 2.4 (b).

Figure 2.4 (c-d) shows the effect of mobile phase additives on signal intensity per each subclass observed in plasma sample using lipid identifications made using LipidSearch software. Each subclass is shown with summed total peak area of all the ions observed for each of the different additives. These areas were then corrected for signal drift over the time required to complete these analyses and compared. Figure 2.4 (c) shows that AA as an additive improved signal up to 19-fold as in the case of LPI. Five sub-classes LPA, LPE, PA, PI and SM saw an increase of between 4- to 10-fold when compared to 10 mM AmAc. Three subclasses LPG, PG and LPS had no confidently identified lipids using ammonium acetate mobile phase additives and had 1-2 lipids identified for AA additive as shown in Supplementary Table A4. Comparing the performance of 0.02% AA with 10 mM AmAc with 0.02% AA, the results are similar to 10 mM AmAc except for PE class where 10 mM AmAc with 0.02% AA outperformed both 0.02% AA and 10 mM AmAc mobile phases. Comparing the performance of 10 mM AmAc and 10 mM AmAc with 0.02% AA, it is clear that the latter generally provides higher signal intensity as evident in Figure 2.4 (c-d). However, 0.02% AA mobile phase outperforms both AmAc mobile phases for the majority of lipids tested. Comparing Figure 2.4 (a) and Figure 2.4 (c-d) the results for most lipid subclasses agree well, except for PE where AA provides improvement in internal standard mix, but 10 mM AmAc with 0.02% AA outperforms 0.02% AA when summed intensities are taken into account. Supplementary Figure A1 shows the results for individual lipids that were successfully identified using LipidSearch using all three mobile phases. These results showed that the summed intensities provide good summary of the performance across the class, with individual lipids showing similar increases or decreases in signal intensity. This confirms that observed increases or decreases in signal intensity reported on per-class basis in Figure 2.4 are not due to huge enhancement or suppression of one member of that class, but are more generalizable trends. Figure 2.4 (c) also shows that LPC and PE classes are less sensitive to the exact nature of the additive than other lipid classes. There were two lipid classes: Cer and PC, where the signal in AA saw up to a 5-fold decrease when compared to AmAc and AA as shown in Figure 2.4 (d). These classes are typically analyzed in positive ESI, while negative ESI is used primarily for identification confirmation, specifically for identification of fatty acid

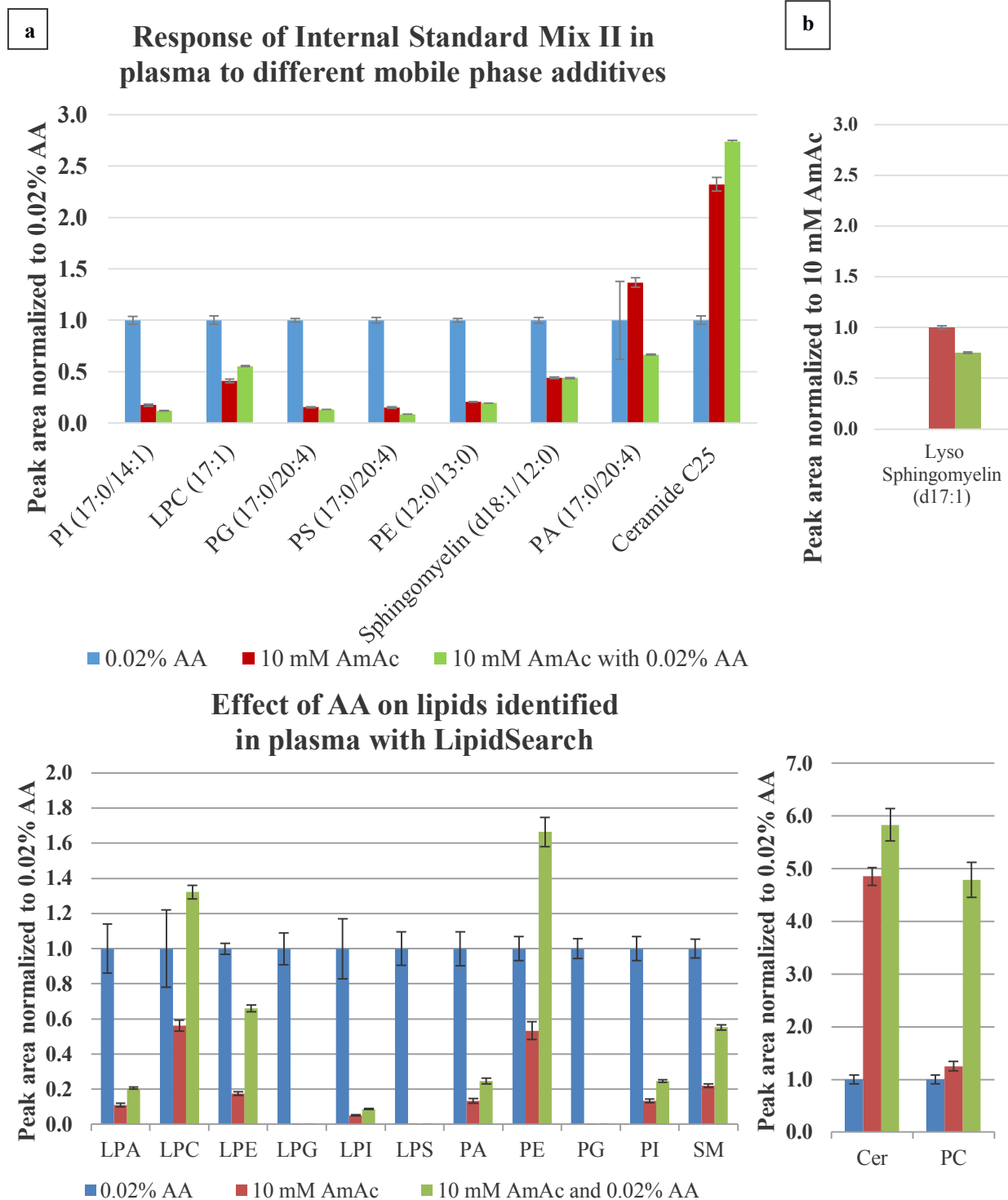


Figure 2.4 Comparison of the influence of 0.02% AA compared to 10 mM AmAc and 10 mM AmAc with 0.02% AA on the signal intensity of lipids in (a-b) Internal Standard Mix II spiked into plasma samples at final concentration of 100 ng/mL (n=4) and (c-d) human plasma after LipidSearch identification. (a) normalizing the peak area to 0.02% AA shows that 0.02% AA causes an increase in signal intensity for six of the lipids present: PI, LPC, PG, PS, PE, SM.

Ceramide shows best signal intensity with 10 mM AmAc with 0.02% AA. (b) LSM (d17:1) was not detected in 0.02% AA and showed the highest signal intensity in 10 mM AmAc. (c) LipidSearch was used to identify lipids in plasma samples after isopropanol precipitation. Peak areas of all ions seen for each individual lipid belonging to a given subclass were then summed to give a total area for each subclass. These subclass total areas were then normalized to the mobile phase containing AA at 0.02% (v/v). AA causes significant increase in signal for 11 lipid subclasses when compared to 10 mM AmAc as shown in (c). AA caused signal decrease for two lipid subclasses: ceramides and PC when compared to 10 mM AmAc (d). For all panels, all data was acquired on CSH C₁₈ and Orbitrap.

composition. The breakdown of the number of lipids identified for all classes in AA, AmAc or AmAc with AA mobile phases is shown in Supplementary Table A4. It shows a reduced number of Cer and PC was identified by LipidSearch using AA. For instance, with AA only 7 Cer were identified compared to 11 and 10 using the other additives. AA identified 19 PC lipids compared to 26 and 23 for 10 mM AmAc and 10 mM AmAc with 0.02% AA, respectively. In addition to using LipidSearch to perform lipid identifications, Thermo's SIEVE software was used to analyse the raw Orbitrap data to obtain the total number of putative lipids observed in each mobile phase. SIEVE algorithm includes de-isotoping and de-adducting, and thus resulted in a list of features that correspond to putative lipid species or compounds present. This list was then further manually curated to contain only features that showed up in at least 66% of the samples, had good peak shape quality, had >5 signal-to-noise ratio, and were not present in the blank leading to a high quality curated data set of putative lipids for each of the mobile phase additives. Figure 2.6 shows the resulting ion maps and total number of features detected in each mobile phase condition. AA outperformed both ammonium-acetate containing mobile phases with total of 3562 putative lipids, versus 2219 and 2077 for AmAc and AmAc with AA respectively. This represents 60% increase versus AmAc and 71% increase in lipid coverage over AmAc with AA. There was no significant difference in median RSD observed for n=4 plasma replicates with median RSD of 7%, 7% and 5% respectively for 0.02% AA, 10 mM AmAc and 10 mM AmAc with 0.02% AA, respectively. For all three mobile phases, 96-100% of putative lipids detected had RSD <30% demonstrating satisfactory performance in terms of repeatability.

2.4.5. Does AA promote both deprotonation and acetate adduct formation?

In negative ESI, ions are primarily formed by deprotonation or adduct formation with anions. Therefore, we also examined the propensity for the formation of deprotonated ion versus the

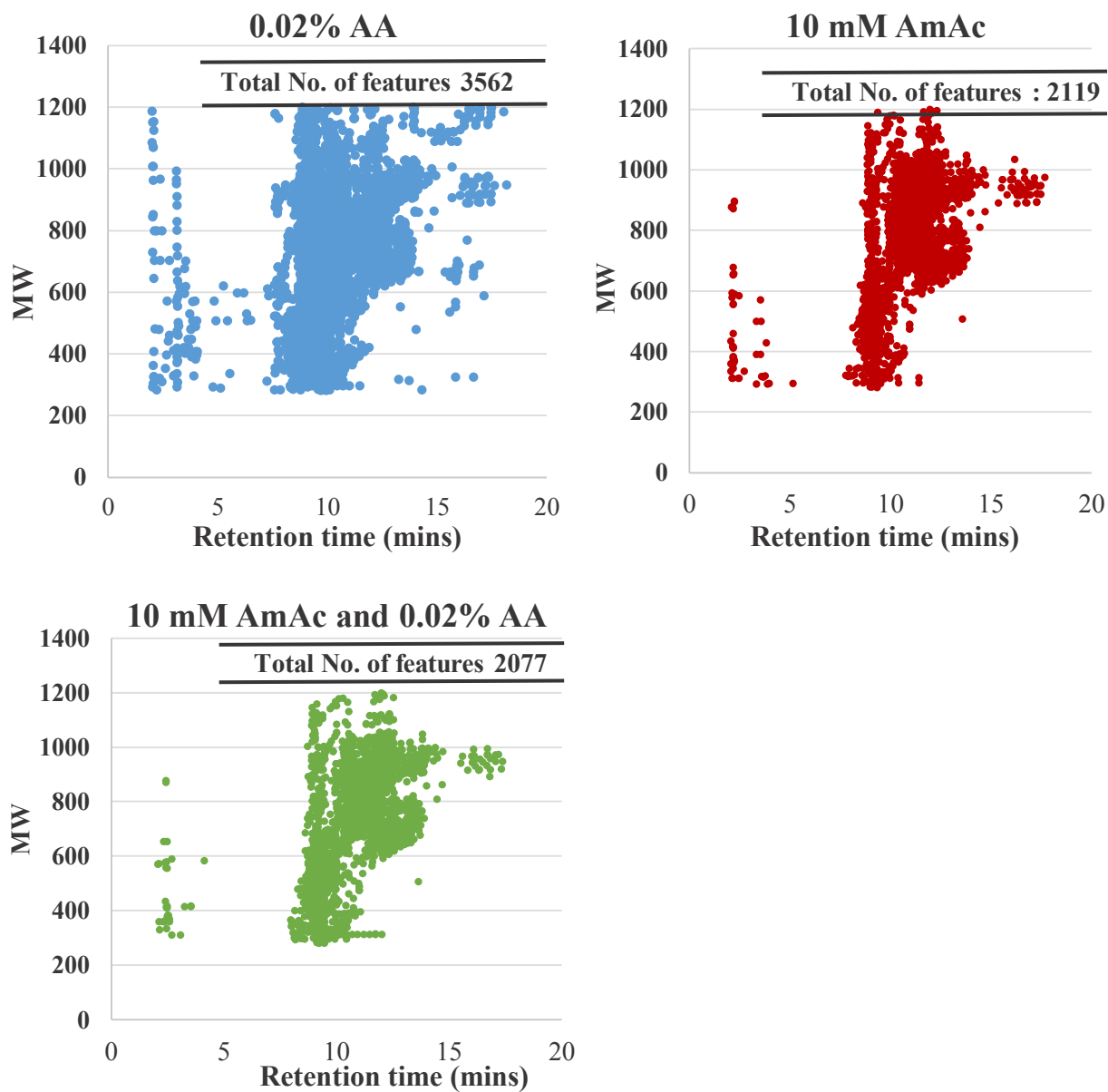


Figure 2.5 Comparison of lipid coverage obtained with 0.02% AA (a), 10 mM AmAc (b) and 10 mM AmAc with 0.02% AA (c). The panels show ion maps of lipid features in plasma samples (n=4) after isopropanol precipitation detected with SIEVE. AA shows an increase of compared to AmAc (b). 10 mM AmAc and 0.02% AA (c) shows the fewest number of features with 2077 using a CSH C₁₈ column on an Orbitrap MS.

Table 2.1 Effect of additive on the formation of deprotonated [M-H]⁻ ions and acetate adducts [M+CH₃COO]⁻. Peak areas are shown for Internal Standard Mix I spiked into plasma giving final concentration of 200 ng/mL (n=3). The deprotonated form of the lipid is the most abundant ion for five lipids: LPS, LPE, PG, PS and PE. The acetate adduct is the dominant form for PC, while LPC shows intense ions for both deprotonated ion and acetate adduct. LC-MS analysis was performed using C₁₈ EVO column with additives present in the mobile phase at either 0.02% AA or 0.02% AmOH on QTOF MS.

Lipid	0.02% AA				0.02% AmOH			
	[M-H] ⁻ Area	% RSD	[M+CH ₃ COO] ⁻ Area	% RSD	[M-H] ⁻ Area	% RSD	[M+CH ₃ COO] ⁻ Area	% RSD
LPS (17:1)	1.29E+06	20.2	ND		2.47E+04	1.2	ND	
LPE (17:1)	6.74E+06	5.1	5.02E+05	28.8	5.92E+04	10.2	ND	
LPC (17:0)	4.03E+05	23.5	2.25E+06	9.3	1.24E+04	6.9	ND	
PG (17:0/17:0)	1.51E+07	7.5	3.84E+03	12.0	6.50E+03	35.0	4.00E+04	13.7
PS (17:0/17:0)	6.21E+06	14.0	1.16E+05	10.2	4.45E+05	16.1	1.72E+05	5.1
PE (17:0/17:0)	5.32E+05	24.0	4.26E+03	87.0	1.77E+05	3.0	ND	
PC (19:0/19:0)	ND		7.70E+05	6.6	ND		8.67E+04	15.3

Table 2.2 Effect of additive on the formation of deprotonated [M-H]⁻ ions and acetate adducts [M+CH₃COO]⁻. Peak areas are shown for Internal Standard Mix I spiked into plasma giving final concentration of 75 ng/mL (n=4). The deprotonated form is the most intense ion for four lipids: LPS, PG, PS and PE. The acetate adduct is the dominant form for PC. LPC shows a strong signal for both deprotonated form and the acetate adduct. LC-MS analysis was performed using CSH C₁₈ on Orbitrap with mobile phase either containing 0.02% AA or 10 mM AmAc. LPE (17:1), although present in the mixture was not detected.

Lipid	0.02% AA				10 mM AmAc			
	[M-H] ⁻ Area	% RSD	[M+CH ₃ COO] ⁻ Area	% RSD	[M-H] ⁻ Area	% RSD	[M+CH ₃ COO] ⁻ Area	% RSD
LPS (17:1)	1.25E+06	12.2	ND		8.29E+05	5.6	ND	
LPC (17:0)	6.27E+06	2.5	8.50E+06	1.5	2.26E+06	3.4	2.76E+06	2.5
PG (17:0/17:0)	8.87E+06	5.4	6.45E+04	12.7	6.17E+05	8	ND	
PS (17:0/17:0)	6.10E+06	9.7	ND		3.88E+05	19.5	ND	
PE (17:0/17:0)	1.48E+06	5.1	9.39E+04	14.9	1.07E+06	4.9	2.85E+04	0.7
PC (19:0/19:0)	ND		2.72E+06	5.3	ND		1.45E+06	4.9

acetate adduct for different mobile phase compositions. The results of these evaluations are shown in Table 2.1 and Table 2.2 for AmOH and AmAc mobile phases respectively. The acetate adduct is the only adduct observed for PC (19:0/19:0) regardless of additive. For all the other lipids, the deprotonated ion is the most intense ion with the exception of LPC (17:1) where both the deprotonated form and acetate adduct have strong signal intensities in all mobile phases tested. These results confirm that the better performance of AA in comparison to AmOH and AmAc is not due to preferential formation of acetate adduct, but also the strong increase in the deprotonated ion. Kiontke *et al.* have previously shown that electrospray source configuration can impact even relative ion intensity obtained by different additives^[129], so in this work we compared AA performance on two different instrument platforms equipped with HESI and Jetstream sources from Thermo Scientific and Agilent Technologies, respectively. Our results comparing AA performance in the two sources confirm some differences in adduct formation. For instance, for PE on QTOF platform (Table 2.1) the acetate adduct represents 0.8% of [M-H]⁻ signal intensity, while on Orbitrap (Table 2.2) it represents 6.3%. For PS, adduct formation accounted for 1.8% on QTOF while no adduct signal was observed in Orbitrap. However, for both platforms the conclusions about most intense ion were comparable.

2.4.6. Effect of AA on chromatographic peak shape

The increase in signal for PA and LPA lipids comes at the cost of peak shape as the peaks for these species broaden and tail noticeably as shown in Figure 2.6 (a). The same is true for PS but the tailing and broadening are less pronounced. Peaks for other classes such as PI retain good chromatographic peak shape as shown in Figure 2.6 (b). The peak tailing for PA and LPA was observed on both CSH and EVO C₁₈ columns.

2.4.7. Examining gas-phase versus solution-phase contributions of AA to lipid ionization

Based on the literature to date, the beneficial performance of acetic acid as mobile phase additive for ESI⁻ can be attributed to both droplet surface and gas-phase contributions. For instance, Zhou and Cook proposed that in low ionic strength solutions at near-neutral pH protonation may occur

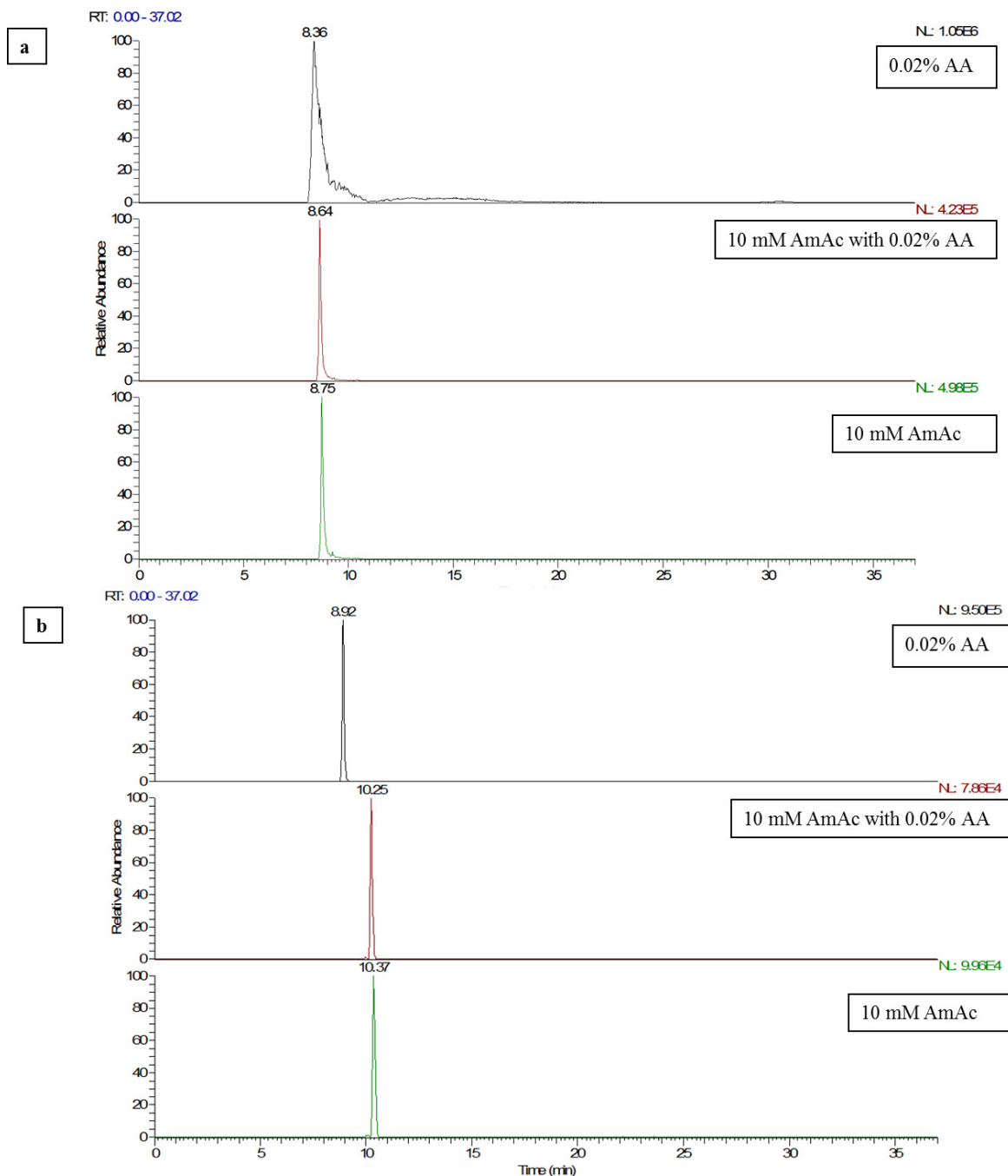


Figure 2.6 Extracted ion chromatograms from plasma samples of lipids identified with LipidSearch (a) m/z 433.2356 corresponding to $[M-H]^-$ ion of LPA (18:2) and (b) m/z 884.5415 corresponding to $[M-H]^-$ of PI (18:1/20:4). The peak height for LPA increased from 4.23×10^5 to 1.05×10^6 , a 2.4-fold increase when 0.02% AA was used as the additive, despite the increase in tailing. The peak height for PI (18:1/20:4) increased from 9.96×10^4 to 9.5×10^5 , a 9.5-fold increase while peak shape quality is retained with 0.02% AA as the additive. Plasma samples separated with a CSH C_{18} and analyzed on Orbitrap.

through charge localization in the thin surface layer of the droplet due to surface enrichment of protons^[114], which also leads to significant changes in local pH at the droplet surface. Similar mechanism may be possible in ESI⁻, where enrichment of anions may occur at the droplet surface, thus changing local pH. Hiraoka *et al.*^[130] and Mansoori *et al.*^[112] also provided evidence that the production of deprotonated ions is likely to proceed not only through the formation of OH⁻ anion through electrochemical reduction of H₂O but also via initial acetate adduct formation followed by CID in-source to form thermodynamically more stable [M-H]⁻ ion rather than acetate adduct. Our results could not distinguish between these two mechanisms so further fundamental studies and computational modelling studies are required to further understand why low concentrations of AA are beneficial for ESI⁻. However, Jetstream dual-spray source configuration allowed us to investigate the contribution of gas-phase to the overall ionization process.

Our results evaluating the effect of gas-phase contribution of AA to the ionization process do support the idea that gas-, surface-, and solution-phase contributions all play an important role but are also lipid-class dependent. Addition of AA in the gas phase provides a more robust signal as observed for PE and LPE and does contribute to signal increase as observed for PC as seen in Figure 2.7. The signal of analytes was far more dependent on AA in the mobile phase than the gas phase with lipids like PG not ionizing at in the absence of AA in the mobile phase. AA in the mobile phase had a pronounced effect on the signal of PC causing a signal increase of 44-fold compared to when there was no AA in either the gas phase or the mobile phase. Addition of AA in the gas phase did contribute to the increase in signal observed in PC. A 6-fold increase in signal was observed when comparing the addition of AA in the gas phase compared to when AA was absent in the gas phase and mobile phase. Addition of AA in the gas phase helps reduce the error on PE and LPE providing a more robust signal.

Overall, these results are in agreement with the results reported by Ehrmann *et al.* for ESI⁺, where solution-phase effect of the addition of AA to mobile phase was found to be more pronounced than gas-phase effect, as determined by more significant enhancement observed for poorly responsive analytes with higher pK_b values^[109]. All the analytes tested had higher gas-phase basicities than methanol used in mobile phase, and high gas-phase basicity by itself did not result in high electrospray response.

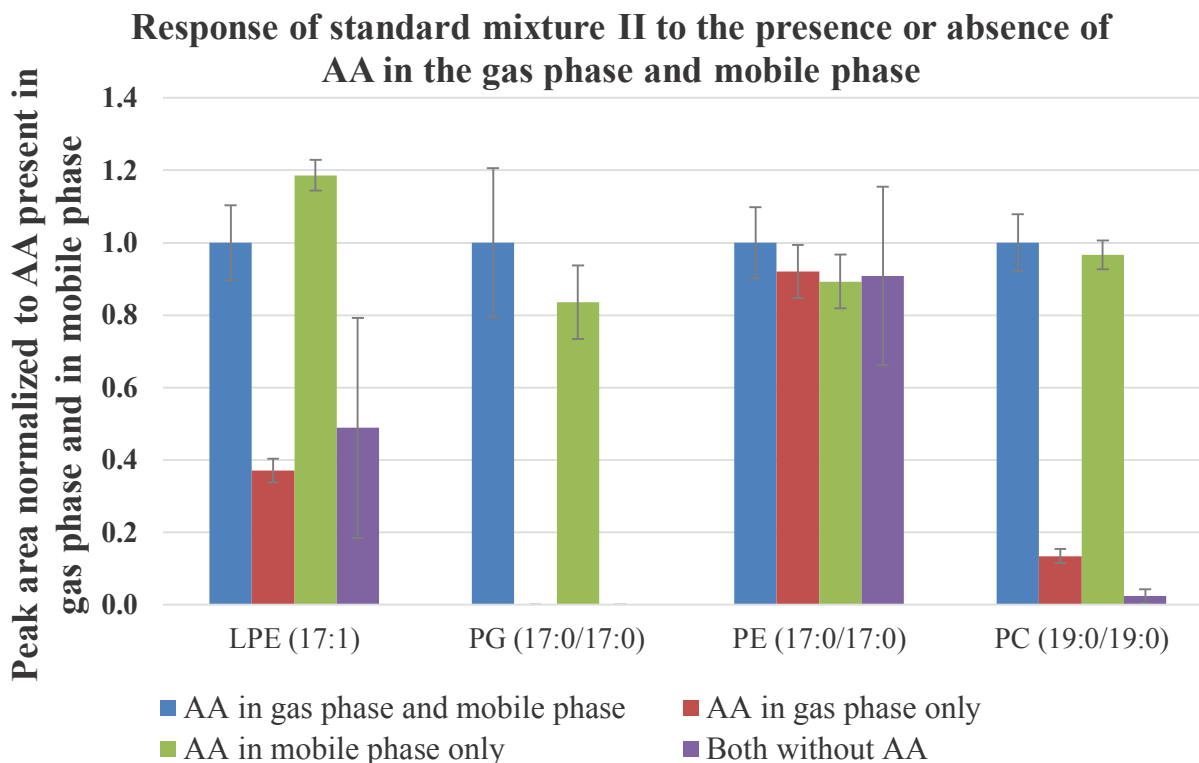


Figure 2.7 The influence of AA in the gas phase on Internal Standard Mix I at a concentration of 200 ng/mL in 70% MeOH separated on a CSH C₁₈ column and analyzed on QTOF MS, n=3 analyses. Mobile phases with and without AA were used to assess the addition of AA in the gas phase. The auxiliary spray was used to introduce a solvent with or without AA present to evaluate the addition of AA in the gas phase.

Our results support previous targeted and metabolomic studies that AA may be the optimal weak acid to use as modifier in ESI⁻. AA was previously found to outperform other weak acids such as formic, propionic and butyric because of its higher gas-phase proton affinity^[115]. AA's lower molecular volume causes less competition for space at the droplet surface compared to larger acids, and this low molecular volume effect is the most pronounced for the more hydrophilic analytes. Weak acids outperform basic additives because protons facilitate electrochemical reduction and charge separation at the spray tip. In addition, ammonium hydroxide in aqueous methanol solutions does not provide sufficient amount of stable anions to carry the negative charge^[103], thus possibly resulting in the poor performance observed in this study. Salts such as ammonium formate and acetate cannot facilitate either electrochemical reduction or deprotonation in solution-phase making them poor additives in ESI⁻. Zhang *et al.* found the best

response using AA at a concentration of 0.2-1 mM with small intensity decrease observed as AA concentration was increased to 5 mM ^[116]. They did not test 3.5 mM concentration that was used in our work, but this slightly higher concentration resulted in better repeatability over long analytical batches with negligible signal decrease over 1 mM concentration in our lab. Our results are also in line with previous study that found that optimal concentration of AA additive is approximately 1 mM with slight to no decrease observed for the four target analytes as AA concentration was increased to 10 mM ^[115].

2.5. Conclusions

A wide range of mobile phase additives are used in lipidomic studies in the literature. The results of this paper show that different additives can have significant impact on signal intensity and number of detected lipids. For lipidomic analysis of human plasma in negative mode ESI we would propose the use of 0.02% AA (v/v).

Acknowledgments;

The authors gratefully acknowledge financial support for this project from CQDM, Ontario Brain Institute (OBI), Brain Canada and participating members (as financial contributors) Pfizer Canada Inc. and Merck Canada Inc. for the project entitled “Solid phase microextraction-based integrated platform for untargeted and targeted *in vivo* brain studies.”.

3. Comparison of *in vivo* solid-phase microextraction (SPME) to Folch extraction of brain lipids in *Rattus norvegicus* using LC-MS

Cian Monnin, Clement Hamani, Germán Augusto Gómez-Ríos, Nathaly Reyes-Garcés, Ezel Boyacı, Barbara Bojko, Janusz Pawliszyn, Dajana Vuckovic

Department of Chemistry and Biochemistry, Concordia University, Montréal, Québec, Canada

Corresponding author: D. Vuckovic, Department of Chemistry and Biochemistry, 7141 Sherbrooke Street West, Montréal, Québec, Canada, H4B 1R6

email: dajana.vuckovic@concordia.ca

3.1. Abstract

Lipidomics is the comprehensive study of the lipids present in an organism. For over 60 years lipids have been extracted from brain tissue using the Folch method: an exhaustive, biphasic liquid-liquid extraction method that uses an excess of chloroform/methanol to extract lipids from the brain tissue sample. An alternative to LLE is solid-phase microextraction (SPME) which is a non-exhaustive, *in vivo* sample preparation method that uses a solid-phase sorbent immobilized on a thin fibre to insert and sample into the region of interest. This study aims to compare SPME to the Folch method to evaluate the capability of SPME to extract lipids from brain tissue. Parameters that affect *in vivo* SPME that were optimized include: extraction time, desorption time and desorption solvent. Using SIEVE, SPME extracts showed 147 and 613 features versus 1368 and 1161 detected in the Folch extracts in positive ESI mode and negative ESI mode, respectively. Using LipidSearch, SPME extracts showed 122 and 57 identified lipids versus 145 and 99 for the Folch extracts in positive ESI mode and negative ESI mode, respectively. The first step towards the development and inter-laboratory validation of *in vivo* SPME as a viable alternative to Folch extraction for lipidomics studies in brain tissue of live animals has been completed in this study.

3.2. Introduction

Lipids are of importance in many brain diseases. For example, being able to extract and quantitate lipids is of great importance to further the understanding of neurodegenerative disorders including Parkinson's and Alzheimer's disease^[5-7] as well as mental illnesses such as depression^[14,119,131] and bipolar disorder^[132]. In addition to improving our understanding of the mechanisms and consequences of various diseases, measuring lipids in the brain may help to evaluate new drug delivery methods^[133,134], new treatments and their pharmacokinetics/pharmacodynamics and/or associated toxicity.

Conventional sample preparation techniques for lipid extraction from tissue samples involve a liquid-liquid extraction (LLE) and were originally developed by Folch^[46] and then adapted by Bligh and Dyer^[47]. The Folch method was developed in 1957^[46] and involves adding 20x excess of a 2:1 chloroform/methanol mixture to the tissue sample followed by the addition of water to yield a final ratio of 8:4:3 (v/v/v) of chloroform/methanol/water. The lipids partition into the lower, organic layer which is separated from the upper, aqueous layer by a protein interface. A modification to this protocol was made in 1959 by Bligh and Dyer^[47] who proposed the use of a ratio 1:2:0.8 (v/v/v) of chloroform/methanol/water instead. This modification was proposed to increase the recovery of lipids from muscle tissue and to reduce the amount of the toxic solvent, chloroform. However, Iverson *et al.* more recently demonstrated that for tissue with lipid content >2%, the Bligh and Dyer method underestimates the lipid content^[48]. Since a typical human brain has a lipid content ranging from 36% (grey matter) to 81% (myelin)^[135], the Folch method is the appropriate conventional method to extract brain lipids.

Recent additions to the LLE repertoire for the extraction of lipids include the methyl tert-butyl ether (MTBE) method developed by Matyash *et al.*^[50] and the butanol:methanol (BUME) method developed by Löfgren *et al.*^[49]. Matyash *et al.* showed their MTBE method had similar capabilities as the Folch and Bligh and Dyer methods to extract certain lipid classes from plasma and brain tissue samples, specifically glycerophospholipids (GP) and sphingolipids (SP). Methanol, MTBE and water are added step-wise in a ratio of 1.5:5:1.25 (v/v/v) to 0.2 (v) of sample. The aqueous phase is then re-extracted with MTBE/methanol/water (10:3:2.5, v/v/v) and the resulting organic phase is combined with the original organic phase. They found that >400 species from across 9 lipid subclasses: phosphatidylethanolamine (PE), PE-plasmalogen (PE O-),

phosphatidylserine (PS), phosphatidylglycerol (PG), phosphatidylcholine(PC), lysophosphatidylcholine (LPC), sphingomyelin (SM), and ceramide (Cer) were recovered with similar efficiencies to the Folch and Bligh and Dyer methods. MTBE is less dense than water meaning that the organic phase containing the lipids is on top of the biphasic system allowing easier recovery of the lipid-containing organic phase compared to LLE methods using chloroform which has the lipid-containing organic phase at the bottom necessitating the puncturing of an insoluble protein disk that separates the two phases. In addition to reducing the error this method also allows for the automation with use of robotic liquid handlers due to the fact that organic phase is the upper layer. Löfgren *et al.*^[49] developed the BUME method to extract lipids from plasma. This method first adds 300 μL uniphaseic butanol/methanol (3:1, v/v) to 10-100 μL plasma followed by the addition of 1% acetic acid and a two-phase extraction of the lipids into heptane/ethyl acetate (3:1, v/v). They compared their results to the Folch method and found that the BUME method extracted lipids from plasma with the same efficiency across several subclasses including cholesterol ester (CE), diacylglycerol (DG), triacylglycerols (TG), PC, LPC, SM, Cer and free cholesterol. This method successfully extracted glycerolipids (GL) unlike the MTBE method where Matyash *et al.*^[50] did not report GL recovery.

An alternative to the traditional, exhaustive LLE method is solid-phase microextraction. This non-exhaustive, microextraction sampling technique operates on the ability of the solid-phase coating on a fibre to extract lipids from the biological matrix on the basis of their distribution coefficients K_{fs} . SPME has been used in a wide range of *in vivo*, *ex vivo* and *in vitro* applications including: pharmacokinetic studies^[55,70,71], metabolomic studies^[136-138], measuring contaminants and pesticides in fish^[139,140], pharmaceuticals in fish^[141,142], and off-flavour contaminants in live fish^[72]. *In vivo* SPME was recently compared to *in vivo* microdialysis (MD) in study by Cudjoe *et al.* in order to evaluate the capability of SPME to monitor neurotransmitter changes in response to the drug fluoxetine^[55]. They showed that both SPME and MD displayed the same trends in neurotransmitter levels and that SPME had reduced error on the readings possibly due to a reduction of matrix effects. For this comparison, the same sampling time of 30 min was used for both methods, but in general MD has superior temporal resolution to SPME as it provides ability for continuous on-line monitoring of analyte concentrations. SPME, on the other hand, provides time-weighted average concentration over the sampling period. SPME has the potential to have superior spatial resolution due to the small size of the SPME fibres, currently 200 μm

core with 45 µm coating. To date, there have only been two lipidomic studies using SPME. The first focused on the measurement of polyunsaturated fatty acids (PUFA) in human and fish plasma^[73]. The study showed that C₁₈ SPME fibres directly immersed into plasma could successfully extract PUFAs and the method was validated with LOQs in the range of 5 – 12 ng/mL. The second study assessed the viability of SPME as a high throughput technique for analysis of a cellular lipidome^[74]. SPME was compared to Bligh and Dyer method and the lipid coverage obtained by the two methods was comparable. SPME also had the advantage of minimal matrix effects while the Bligh and Dyer method showed ionization suppression for low abundance species and ionization enhancement of abundant species. In this study, SPME was also shown to have better precision for several lipid subclasses: MG, LPC, SM and PC. Although the results of these two *ex vivo* studies appear promising and establish proof-of-concept, *in vivo* SPME has not been evaluated for lipidomics to date.

In light of this, the main goal of this study is to assess the viability of SPME as a tool for *in vivo* lipidomic studies in brain tissue for the first time. The Folch method was applied to brain tissue samples from the hippocampus and nucleus accumbens regions of rats. The Folch extracts obtained from the hippocampus region will be compared to *in vivo* SPME extracts from the hippocampus region by examining the lipid profiles obtained by both techniques. The main parameters used for evaluation will be lipid coverage, number and lipid subclass of confidently identified lipid species, signal intensity per lipid subclass, number of unique features observed only in *in vivo* SPME and matrix effects.

3.3. Materials and methods

3.3.1. Chemicals and materials

LC-MS grade solvents and mobile phase additives were purchased from Sigma-Aldrich, Oakville, Ontario, Canada. Lipid standards PS (17:0/17:0), LPS (17:1), PC (19:0/19:0), PE (17:0/17:0), PG (17:0/17:0), LPC (17:0), PE (12:0/13:0), PG (17:0/20:4(5Z,8Z,11Z,14Z)), PS (17:0/20:4(5Z,8Z,11Z,14Z)), PI (17:0/14:1(9Z)), LPA (13:0), sphingosine (SP) (d17:1), Cer (d18:1/25:0), Ceramide C25, SM (d18:1/12:0), LSM (d17:1), PA (17:0/20:4(5Z,8Z,11Z,14Z)), LPE (17:1(10Z)), MG(16:0), DG d₅ (15:0/15:0), DG d₅ (16:1/0:0/16:1), DG d₅ (18:0/0/18:0), DG d₅ (18:1/0:0/18:1), DG d₅ (18:2/0:0/18:2), TG d₅ (17:0/17:1/17:0) and TG (18:1(9Z)/18:1(6Z)/18:1(9Z)) were purchased from Avanti Polar Lipids, Alabaster, AL, USA.

Additional details including full lipid name, stock standard preparation and monoisotopic masses of observed ions are included in Appendix A Supplementary Tables A1 and A2. C₁₈ and mixed-mode (C₁₈ + benzenesulfonic acid) SPME fibers were obtained from Supelco as research samples.

3.3.2. Folch method for brain tissue samples

The rats (n=8, all male) were sacrificed and blood was collected from the entire body (ca. 3 mL) in tubes. The brains were removed immediately, divided to left and right hemispheres, and the nucleus accumbens (n=8) and hippocampus (n=8) regions of rat brains were dissected. The tissues were placed in aluminum foil pieces and left to be frozen on dry ice. They were shipped on dry ice to Concordia University and stored at -80°C until analysis.

The conventional extraction protocol was followed per the Folch procedure^[46]. Briefly, tissue samples were weighed (4.1-95.0 mg), immersed in liquid N₂ and then disrupted with a Bessman tissue pulverizer. Methanol was then added at a ratio of 100 µL of MeOH to 10 mg of tissue and homogenized with mechanical tissue grinder (Fisher Scientific). Chloroform was added at a 2:1 ratio chloroform:MeOH. The samples were then vortexed for 5 min and incubated at room temperature for 30 min. This was followed by centrifugation at 13,000 g for 20 mins at 4°C where a protein pellet was formed. The uniphaseic chloroform:MeOH mixture was transferred to a fresh microfuge tube where 0.9% NaCl was added to bring ratio to 8:4:3 (chloroform/methanol/water). This mixture was vortexed briefly and centrifuged at 2000 g for 15 min at 4°C to separate to a biphasic system. The lower organic layer was collected. The upper, aqueous layer was removed and 2:1 chloroform/MeOH was added to bring final ratio to 8:4:3. The mixture was vortexed briefly and centrifuged at 2000 g for 15 min at 4°C and placed on ice to help with phase separation. The bottom layer was removed and combined with the original, lower, organic layer. The resulting combined organic layers were separated into two aliquots (one for positive mode ESI analysis and one for negative mode ESI analysis), evaporated to dryness and stored at -80°C until analysis. Dried samples were reconstituted in 50:25:25 IPA:acetonitrile(ACN):H₂O with 200 ng/mL of IS mix II (Appendix A Supplementary Table A2). Blank extract was prepared using the full procedure but omitting the addition of tissue. Internal mix I (Appendix A Supplementary Table A1) to assess recovery was applied to the tissue prior to extraction. Each of the 8 samples per brain region had two technical replicates.

These replicates were obtained to assess extraction variability and were collected after the tissue homogenization step prior to the addition of 0.9% NaCl. Four of the nucleus accumbens samples did not form protein pellets and were therefore not used for analysis.

3.3.3. SPME extraction time optimization

Internal standard mix I (IS I) (Appendix A Supplementary Table A1) was spiked into tissue samples via a 25 μL syringe at a concentration of 10 $\mu\text{g}/(\text{g}$ of tissue) and left to incubate overnight at -80°C . *Mus musculus* whole brain samples were used for *ex vivo* SPME extraction time optimization. For SPME extraction time optimization experiments 15 mm SPME fibres coated with C_{18} extraction phase were conditioned for 1 hour in methanol/water (1:1, v/v) whilst being agitated at 450 rpm prior to extraction. Individual brain samples in HPLC vials with 250 μL glass insert at room temperature had one SPME fibre each placed in them to assess the effect of extraction time on the lipid profiles with two tissue samples for each time point. The time points were: 5 min, 15 min, 30 min, 1 hour, 2 hours and 20 hours. The two 20 hour samples then had one more fibre each placed in them for 5 min to assess the change in composition after 20 hours. Alongside the tissue samples, standard solution (500 ng/mL) in 20% methanol was extracted using the same time points (n=2). Blank extraction from 20% MeOH was performed for 5 min. After extraction, SPME fibres were briefly washed by dipping fibres into LC-MS grade water in glass HPLC vials for 5 seconds to remove any biological matter that remained on the fibre. Fibres were then placed into HPLC vials with 250 μL glass inserts containing 120 μL methanol/IPA (1/1, v/v) for 30 min in an orbital shaker at 450 rpm to perform the desorption.

3.3.4. SPME desorption time and desorption solvent optimization

15 mm SPME fibres coated with C_{18} extraction phase were conditioned for 1 hour in methanol/water (1:1, v/v) whilst being agitated at 450 rpm prior to extraction. Fibres were then placed in HPLC vials with 250 μL glass inserts containing 120 μL 200 ng/mL standard mix I in 20% MeOH for 30 min. Fibres were then desorbed into HPLC vials with 250 μL glass inserts containing 120 μL 100% MeOH for 30 min, 1 hour, 2 hours and 20 hours. Fibres that were desorbed into 100% MeOH for 30 mins were then sequentially desorbed into 120 μL 100% IPA to evaluate carryover. Additional fibres were also desorbed into 50%:50% MeOH/IPA and 20%:80% MeOH/IPA for 1 hour. Blank extraction was performed by placing fibres in 20%

MeOH. Samples were stored in -80°C until analysis. Samples were diluted to 70% organic with LC-MS grade water before analysis.

3.3.5. *In vivo* SPME sampling

All rats were male, 325 g/rat. They were anesthetized prior to sampling with halothane (and kept anesthetized through the entire period). Fibers were 4 mm mixed mode (200 µm core, 45 µm coating thickness). Prior to use, the fibers were kept in preconditioning solution at least for 30 min (50/50, ACN/H₂O). Prior to extraction, fibers were transferred in 300 µL ultrapure water.

For *in vivo* sampling, baseline collection was performed for 30 min (extraction with SPME), then rat was dosed with 10 mg/kg fluoxetine and two sequential samplings for 30 min were performed with the fibers. The SPME sampling was performed in hippocampus using a micropositioner to precisely control the position of the fiber in the brain. After extraction, fibers were first cleaned with kimwipe to remove mechanically the attached tissue residuals, then quickly washed in 300 µL ultrapure water and right away placed in -20°C freezer and kept there during the sampling day. At the end of the day, fibers were transferred to -80°C freezer and transferred to the University of Waterloo and Concordia University on dry ice without breaking the cold chain. Fibres were stored at -80°C until desorption. At Concordia University, desorption was performed for 1 hour into HPLC vials with 250 µL glass inserts containing 30 µL 100% MeOH containing 200 ng/mL of IS mix I. This was followed by a second desorption into 30 µL 100% IPA for 1 hour. All desorptions were performed in orbital shaker (Fisher Scientific, isotemp) at 450 rpm at room temperature. Samples were diluted to 70% organic with water prior to injection.

3.3.6. LC-MS/MS

Analysis of *in vivo* SPME, *ex vivo* SPME, and Folch extractions were performed on an Agilent 1200 LC system (Agilent Technologies, Santa Clara, CA, USA) connected to a LTQ-Orbitrap Velos (Thermo Fisher Scientific, Waltham, MA, USA) via a HESI source. Separation was performed on a Waters XSelect CSH C₁₈ reversed phase column with dimensions: 130Å, 2.5 µm, 2.1 mm x 75 mm (Waters, Milford, MA, USA). The refrigerated autosampler was set at 4°C and a column heater maintained at 55°C was used. The flow rate was 0.200 mL/min. The gradient program was as follows: 0-2 min 20% B, 2-3 min 20%-80% B, 3-16 min 80%-95% B, 16-24 min 95% B, 24-24.1 min 95%-20% B, 24.1-37 min 20% B. Injection volume was 10 µL.

LTQ orbitrap HESI source settings were as follow spray voltage: 3 kV, source temperature: 300°C, sheath gas flow rate: 10, Aux gas flow rate: 5, capillary temp: 275°C. A lock mass of 283.2643 (steric acid) was selected for internal mass calibration and S-Lens RF setting was 60%. Full MS¹ scan was performed with a m/z range of 280-1200, resolving power of 60,000, and AGC target of 1x10⁶ ions. This was followed by top 5 CID data-dependent-acquisition (DDA) for the 1st to the 5th most intense ion from the first scan event in the FTMS. The ion trap AGC MSⁿ target was 10,000. Dynamic exclusion settings were as follows: repeat count = 2, repeat duration = 20 seconds, and exclusion duration = 35 seconds. Collision energy = 35 V for DDA.

For desorption time and desorption solvent experiments an Agilent 1290 Infinity II UPLC system was connected to an Agilent 6550 iFunnel QTOF MS instrument with a Dual Agilent Jet Stream (AJS) electrospray ionization source (Agilent, Santa Clara, CA, USA). The system also incorporated a 1260 isocratic pump, which was used for continuous infusion of internal reference standard for internal mass calibration, which were 112.03632 (purine) and 980.016375 (HP-0921 acetate adduct) from Agilent mass reference solution. The refrigerated autosampler was set to 4°C. Separation was performed on the same Waters column used for Orbitrap experiments: Waters XSelect CSH C₁₈ reversed phase column. Column chamber was thermostatted to 55°C. The flow rate was 0.250 mL/min. The gradient was as follows: 0-4 min 40% B, 4-6 min 40-65% B, 6-14 min 65% B, 14-18 min 65-80% B, 18-24 min 80-87% B, 24-24.5 min 87-95% B, 24.5-26 min 95% B, 26-26.1 min 95-40 %B, 26.1-32 min 40% B. Injection volume was 10 µL.

The Dual AJS ESI source parameters for the Agilent 6550 iFunnel QTOF MS were: drying gas temp: 275°C, drying gas flow rate: 15 L/min, sheath gas temp: 300°C, sheath gas flow: 12 L/min, capillary voltage: 3500 V, nozzle voltage: 500 V. MS scan was collected in the range of 100-1200 m/z with 1 spectrum/s.

3.3.7. Data processing and analysis

Thermo Scientific Xcalibur (2.2 SP1.48) was used for targeted processing of Orbitrap data. To process Orbitrap data in an untargeted workflow Thermo Scientific SIEVE (2.2 SP2) was used with minimum intensity = 5000. The following criteria were applied to the datasets obtained from SIEVE: good quality peak shape (manual inspection), signal-to-noise ratio of 5 compared to the blank, and present in 66% of samples for *in vivo* and Folch extractions. Since n=2 signal had to be present in 100% of samples for *ex vivo* SPME extraction time samples. Features with

retention time of <2 or >25 min were omitted. Features with MW >1200 were omitted. *In vivo* SPME, *ex vivo* SPME, and Folch extractions after Orbitrap analysis were also processed using LipidSearch 4.1 to identify lipids. The high mass accuracy data from the MS¹ combined with the fragment MS² spectra are compared to a library of lipid ions and predicted lipid fragment patterns of over 1.5 million lipids^[99]. The “Product” search algorithm was used on data files with full scan and data-dependent-acquisition MS² spectra. The following settings were applied to the data files: precursor tolerance of 10 ppm and product tolerance of 0.5 Da and m-Score threshold = 5. The alignment settings were: alignment method = Mean, R.T. tolerance = 0.25 min, toprank filter = on, main node filter = all isomer peaks, m-score threshold = 5.0. The resulting datasets were manually curated to meet the following criteria: lipid had to have an A or B grade in at least one of the samples, visually inspected for good peak quality, and minimum signal-to-noise ratio of 5 compared to the blank. The ID quality of each identified lipid is assigned in grade form (A-D). A: lipid class and fatty acid chain composition completely identified; B: lipid class identified and fatty acid chain partially identified; C: lipid class or fatty acid chain identified; D: identification by other fragment loss (H₂O loss). Only lipids identified with either an A or B grade were reported. Principal Component Analysis (PCA) was performed by importing the MW, retention time and corresponding peak area list of features detected with SIEVE with the selection criteria outlined above into Umetrics SIMCA (14). Pareto scaling was used for all peak area data, and the autofit function was used to determine statistically relevant number of components that should be used for each PCA model.

For samples run on QTOF, targeted data processing was performed on Agilent Masshunter software (TOF Quantitative Analysis B.07.00, Qualitative Analysis B.07.00), using 20 ppm extraction window for monoisotopic masses of interest.

3.4. Results and discussion

Several parameters can influence the extraction efficiency of SPME including: coating, extraction time, desorption time, desorption solvent and volume, extraction pH, and temperature. Extraction pH, and temperature cannot be controlled *in vivo* and therefore were not further evaluated. The coatings for use during *in vivo* SPME must be biocompatible, and currently only C₁₈ and mixed-mode coatings are available in this format. Both coatings were found to work well for lipid extraction^[73,74], so were not further investigated. Therefore, the main parameters

investigated in current work were the effect of extraction time on the observed lipid coverage and selection of desorption conditions to ensure all lipids are completely desorbed from the fibres prior to LC-MS analysis.

3.4.1. *Ex vivo* SPME extraction from brain tissue and evaluation of extraction time

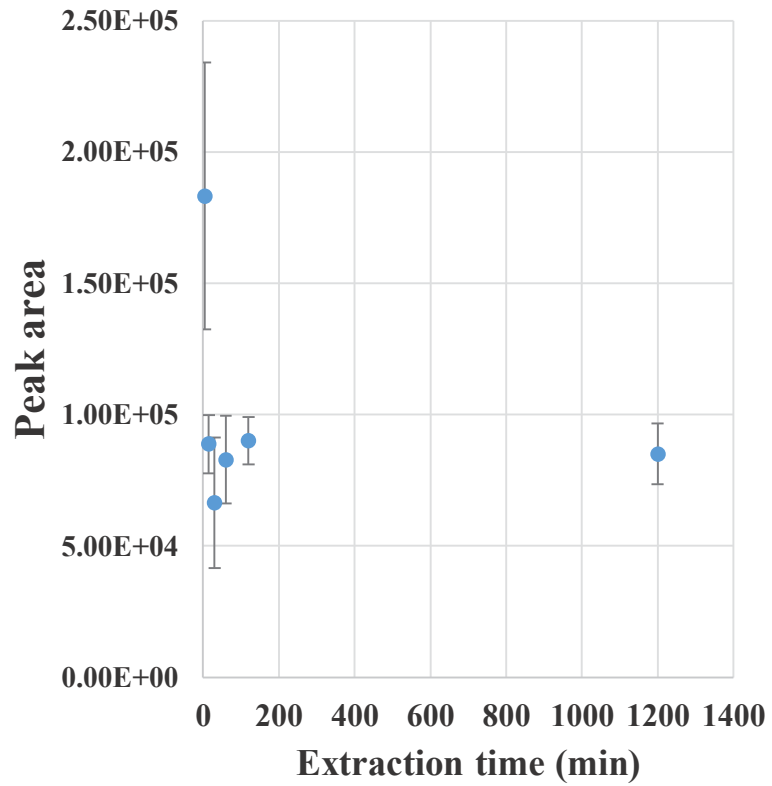
Microextraction methods such as SPME are based on equilibrium rather than being exhaustive extraction methods like LLE methods. An analyte is considered to have reached equilibrium when the amount extracted no longer increases as extraction time increases, within experimental error. Extraction time of lipids from standard solution in solvent and *ex vivo* from brain tissues spiked with IS mix II were assessed using the following extraction time points: 5 min, 15 min, 30 min, 1 hour, 2 hour and 20 hours. The tissue samples had one additional time point with a 5 min extraction after the 20 hours to assess the change of endogenous lipids due to exposure of the brain sample to air for 20 hours at room temperature. The resulting extraction profiles give information about displacement, degradation, and when lipids reached equilibrium with the fibre coating. Figure 3.1 (a) and (b) shows the extraction profiles for PS (17:0/17:0) obtained in standard solution and tissue sample. The results show that equilibrium is reached for standard solution in 15 min with the first time point, 5 min, being an outlier, while in tissue equilibrium is not reached even after 20 hours. Similar results were observed for other lipids such as PC (19:0/19:0) as summarized in Table 3.1. Figure 3.1(c-f) shows the results for LPS (17:0) lipid in standard solution and tissue, in both positive and negative ESI mode. The results for this lipid show that equilibrium is not reached in solution within 20 hours, while for tissue it is reached within 2 hours. In brain tissue the signal at the 20 hour mark is lower than the initial 5 min extraction. In the 5 min extraction performed after the 20 hour extraction a reduced signal is also observed. This suggests that there is degradation of LPS over time. These results also show good agreement between data collected in positive and negative ESI LC-MS. Results similar to LPS were observed for LPC (17:0) lipid. The extraction profiles of TG d₅ (17:0/17:1/17:0) in brain tissue shown in Figure 3.1 (m), show an increase up to 1 hour and then a marked decrease at 20 hours. TG was affected by solubility issues in the solvent, as TG lipids are not soluble in 20% methanol and therefore no extraction profile for TG in solvent was obtained. Increasing the proportion of organic solvent beyond 20% methanol was not feasible as this would lower K_{fs} values for the other lipids of interest.

The decrease in the amount extracted observed for PL and GL lipids at 20 hour time point can be due to several factors. It could represent displacement of lipids with lower K_{fs} by lipids with higher K_{fs} if the sorbent is becoming saturated. The drop could also be due to degradation of lipids at room temperature over the long extraction times employed in the experiment. To investigate this possibility, a second 5 min extraction was performed after the 20 hour extraction was complete. The inset graphs in Figure 3.1 show the comparison between initial and follow-up 5 min extraction, and allow us to conclude whether degradation occurred for the lipid in question. Lipid degradation was observed for LPS, whereas no change in lipid levels was observed for PS, LPC and TG. For LPC the same trend is observed in positive ESI mode and negative ESI mode but the difference in magnitude which could be due to either ion suppression or enhancement occurring in one mode but not the other. The decrease in TG signal at the 20 hour time point, Figure 3.1 (k), is therefore indicative of displacement rather than degradation. Table 3.1 summarizes the results for other spiked non-endogenous lipids as well, and * indicates that degradation at the 20 hour time point was observed. The average relative standard deviation (%RSD) for PS in the solvent samples is 20% while in brain tissue it is more than double that at 51%. The constant increase over time and larger RSD may be attributed to several factors: (i) heterogeneity of lipid tissue and exact location being sampled (ii) lipid diffusion through the tissue sample is more complex as the tissue sample is a complex, biological matrix and (iii) variability in the amount of sorbent immobilized on SPME fibers. In addition to the spiked non-endogenous lipid standards whose results were reported in Figure 3.1 and Table 3.1, brain samples can also be examined using untargeted lipidomics approach to monitor the effect of increasing the extraction time on other lipids beyond the lipids available as standards. This information can be used in order to glean information about the how the lipid profile changes over 20 hours when left at room temperature. These extracts were first processed using LipidSearch to use MS and MS/MS information to identify lipids observed in the samples.

After the 20 hour extraction, a significant increase in Cer peak area for 16 out of 43 Cer species was observed with a 5-71-fold increase in peak area. The 5 min extraction that followed the 20 hour extraction, also shows similar increase in Cer. It shows similar peak areas to the 20 hour extraction for those 16 Cer species that showed a drastic change in level at 20 hours. This confirms that there is a change in the lipid profile. This interpretation is further confirmed as not all Cer showed this change in level; those that did not show a drastic increase in the 20 hour

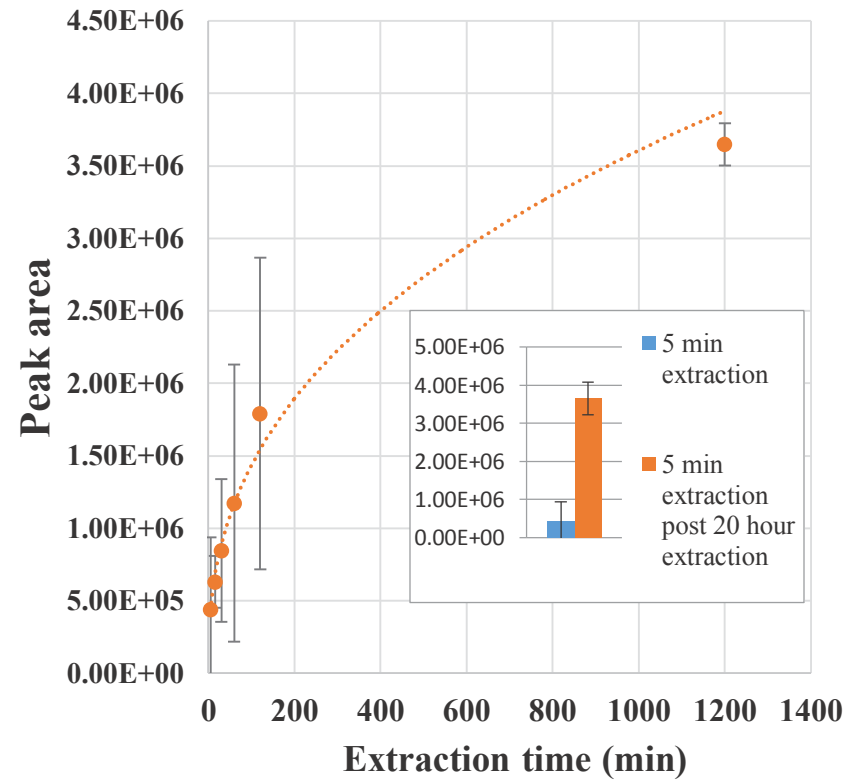
a

PS (17:0/17:0) positive mode standard in solvent



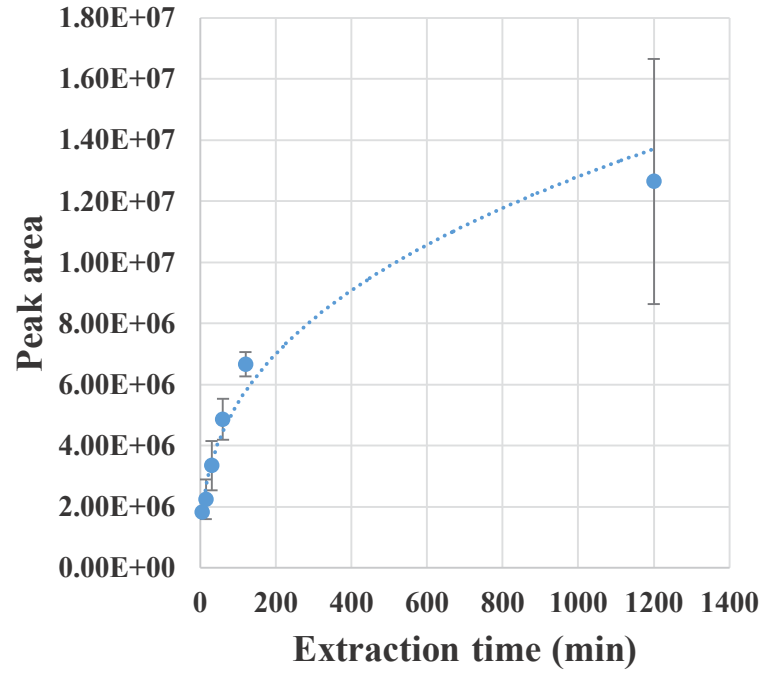
b

PS (17:0/17:0) positive mode standard in brain tissue



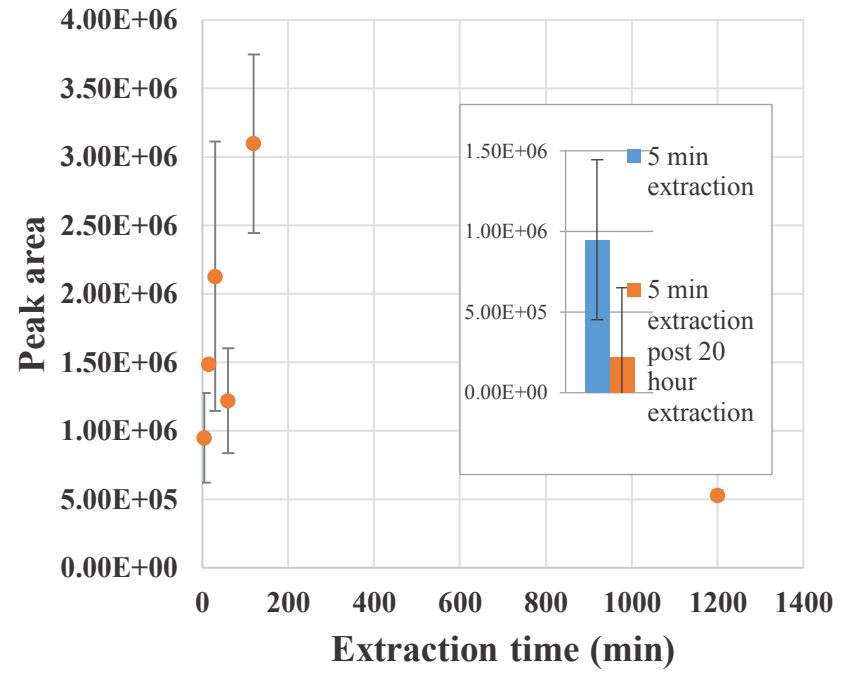
c

LPS (17:0) positive mode standard in solvent

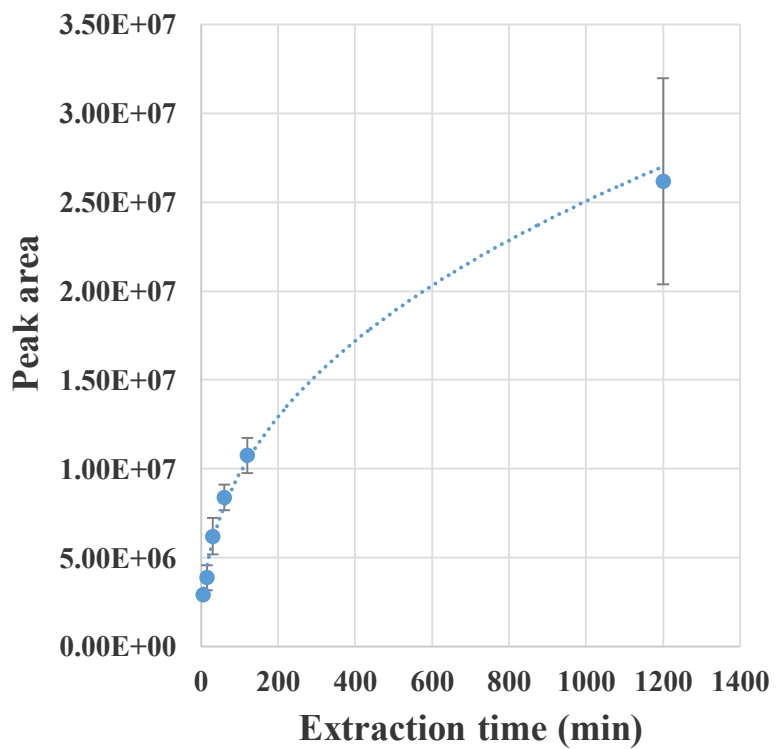


d

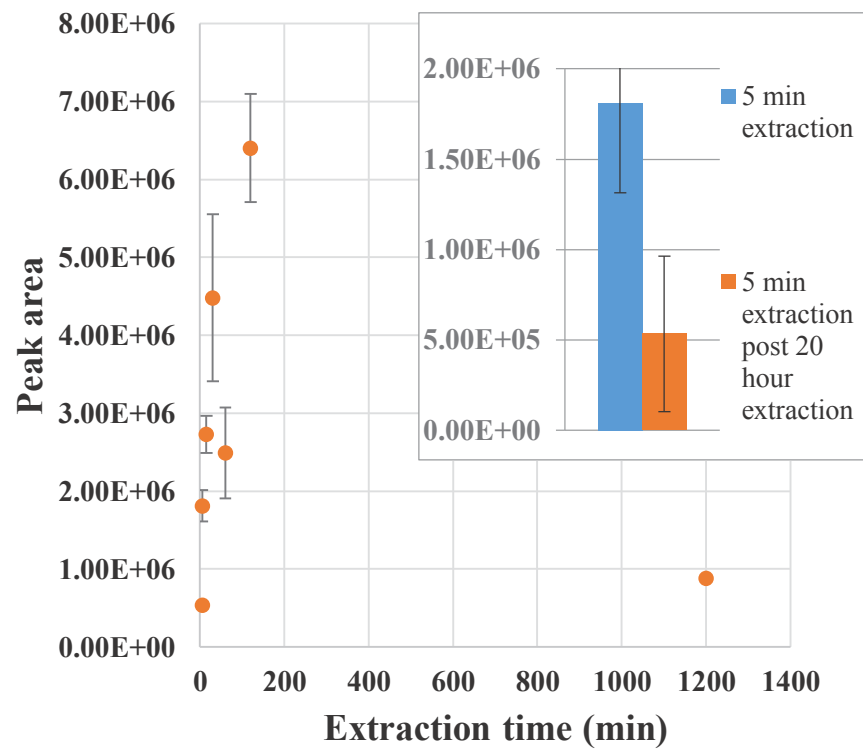
LPS (17:0) positive mode standard in brain tissue



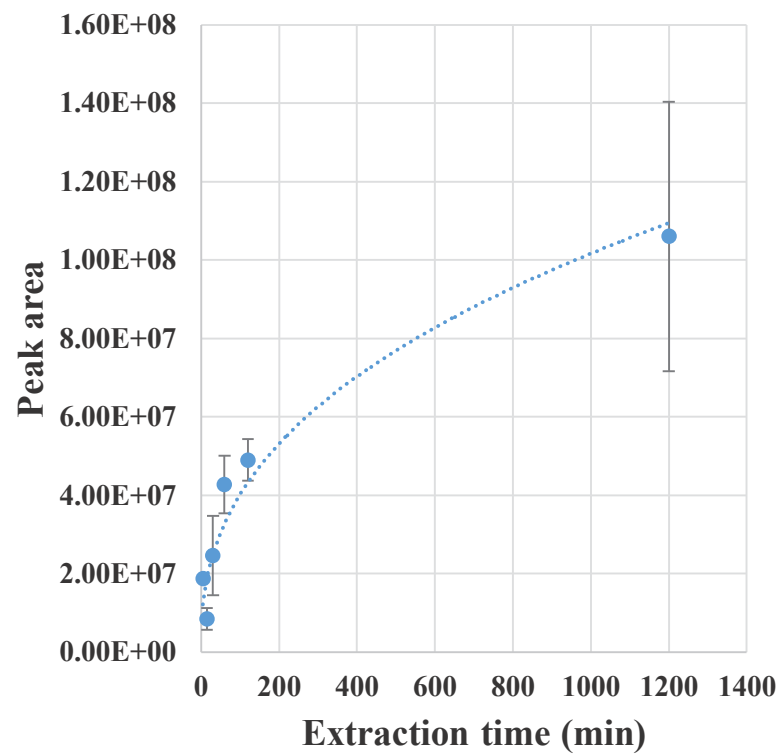
e LPS (17:0) negative mode standard in solvent



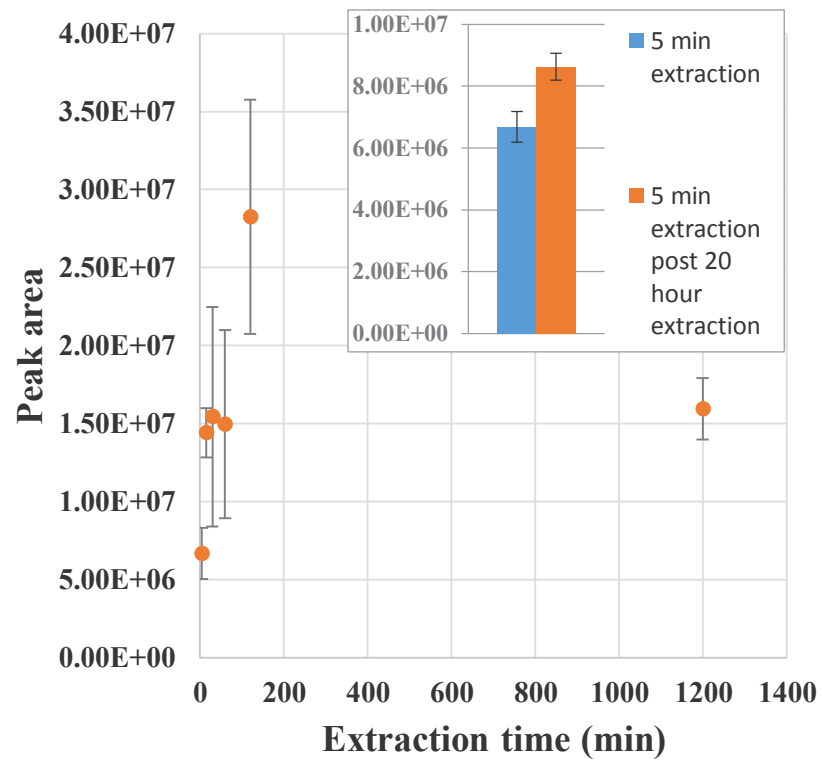
f LPS (17:0) negative mode standard in brain tissue



g LPC (17:0) positive mode standard
in solvent

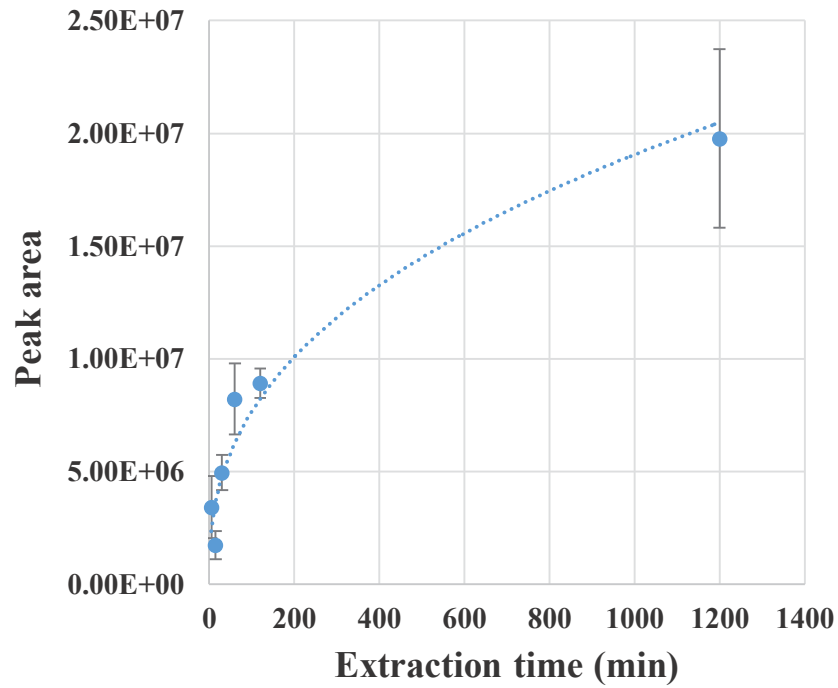


h LPC (17:0) positive mode standard
in brain tissue



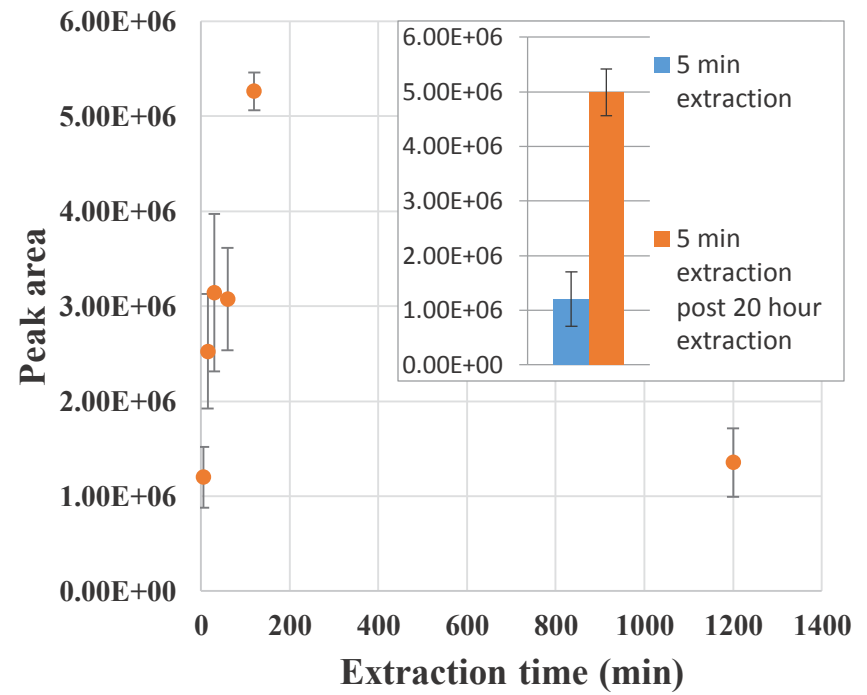
i

LPC (17:0) negative mode standard in solvent



j

LPC (17:0) negative mode standard in brain tissue



k

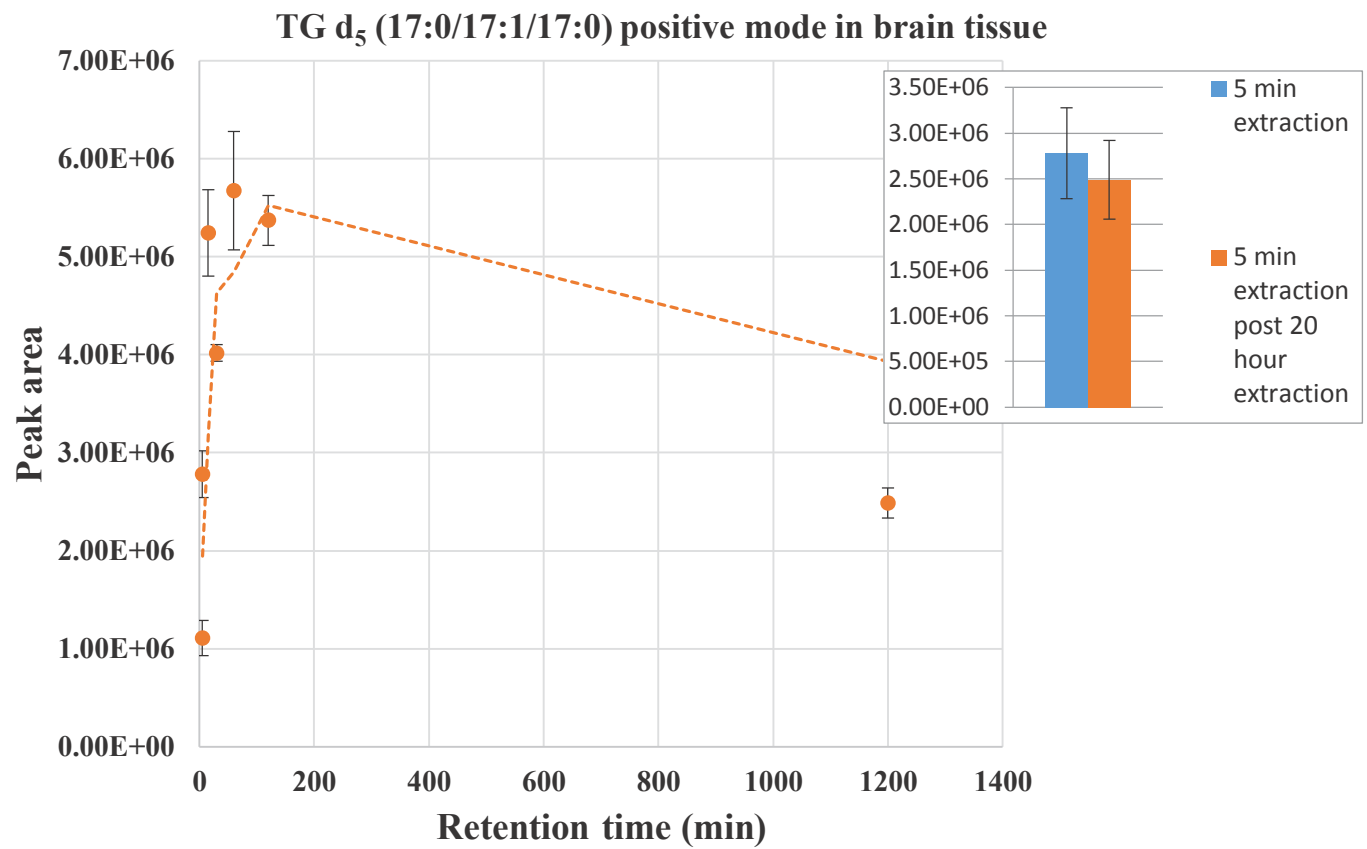


Figure 3.1 Example extraction time profiles of PS (17:0/17:0) (a-b), LPS (17:0)(c-f), LPC (17:0)(g-j) and TG d₅ (17:0/17:1/17:0)(k) obtained from the extraction of lipid standard mix (a, c, e, g, and i) and from lipid standard spiked into brain tissue (b, d, f, h, j, and k) extracted with SPME using six different extraction times: 5 min, 15 min, 30 min, 1 hour, 2 hours, and 20 hours. All extractions were performed in duplicate and analysed using a CSH C₁₈ column on an orbitrap.

Table 3.1 Summary of extraction times required to reach equilibrium in solvent and tissue samples for spiked non-endogenous lipids. *Degradation observed. †Release of PS was observed after 20 hours. ‡TG was not soluble in 20% MeOH.

Lipid standard	Time until equilibrium achieved in solvent	Time until equilibrium achieved in tissue
LPS (17:0)	Not reached	Inconclusive*
LPE (17:0)	Not reached	1 hour
LPC (17:0)	Not reached	2 hours
PS (17:0)	15 min	Not reached †
PE (17:0)	15 min	1 hour
PG (17:0/17:0)	15 min	2 hours
PC (19:0/19:0)	15 min	2 hours
DG d5 (15:0/15:0)	15 min	15 min
TG d ₅ (17:0/17:1/17:0)	N/A‡	1 hour

extraction times also did not show an increase in the 5 min extraction that verified sample stability. There is a release of Cer (d18:1/18:0) after 20 hours (Figure 3.2 (a)). This was not observed for all Cer as in the case of Cer (d20:0/23:2) (Figure 3.2 (c)). A similar release of PI was observed in the 20 hour and 5 min post 20 hour extractions (Figure 3.2 (b)).

A large difference in the PS (17:0/17:0) standard that was spiked into the brain tissue was observed (Figure 3.1 (b insert)). The 5 min extraction after 20 hours is approximately 6 times that of the 5 min extraction time point. This may be a lipid that is caused displacement observed in LPS (17:0) standard spiked into brain tissue. Since LPS has one less fatty acid chain they may diffuse through the tissue matrix more easily while PS having two fatty acid chains will have a higher overall affinity to the fibre sorbent.

One of the limitations of LipidSearch software is that only small number of lipids are identified with high degree of confidence. Therefore, the tissue samples were processed using SIEVE to determine total number of putative lipids detected depending on extraction time. These results are presented in Table 3.2. In the initial 5 min extraction 2158 and 3432 features were detected in positive and negative mode respectively. In ESI⁺, the number of putative lipids observed remains approximately stable (excluding the 15 min time point which is out of trend in both positive and negative mode) within experimental error at all time points including 20 hours. In negative ESI the number of putative lipids observed remains approximately stable from 5 min to 2 hours (excluding the 15 min time point which is an outside the experimental error tolerance in both

positive and negative mode) within experimental error. The increase observed at the 20 hour and the post 20 hour 5 min extraction is between 20-21% which is quite close to being within experimental error. However, this may indicate lipid degradation and perhaps release of lipids from membranes

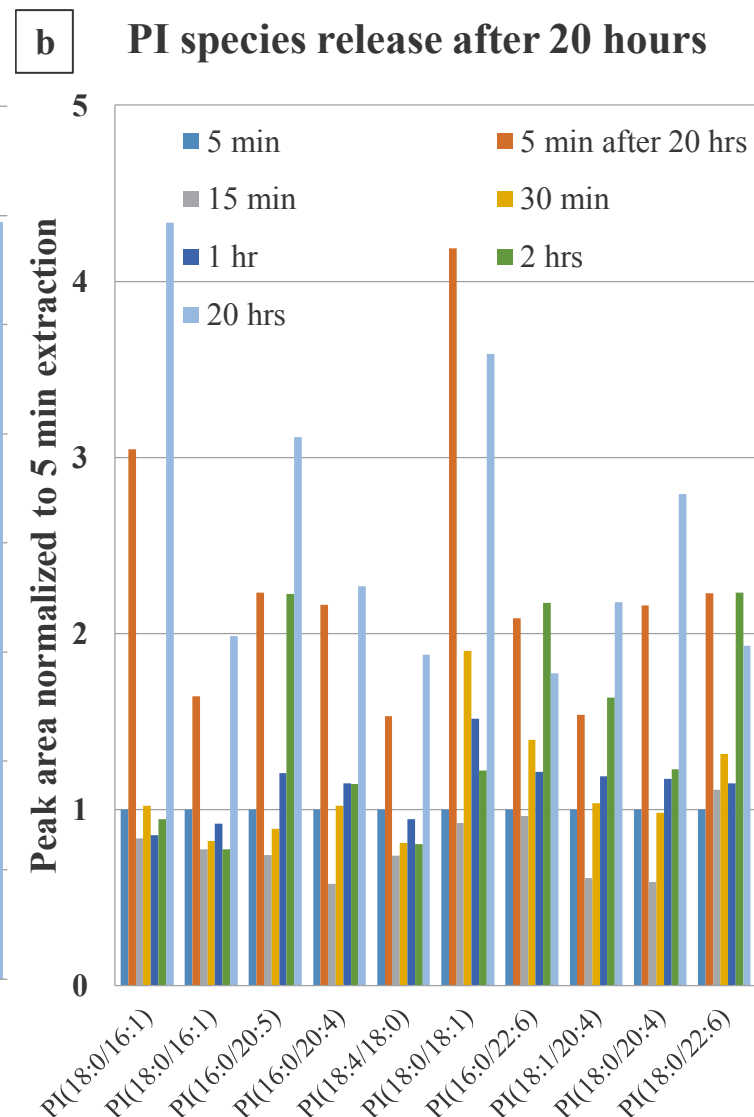
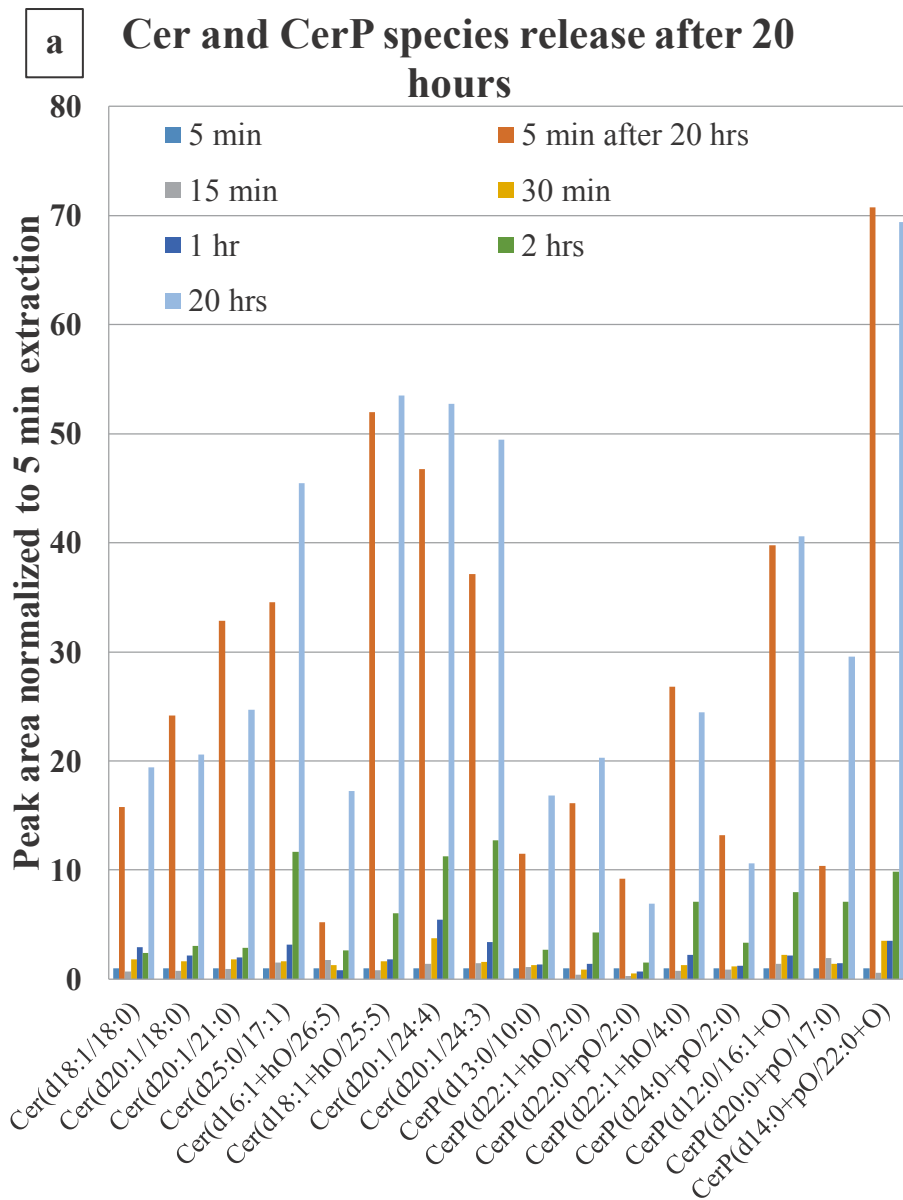
Table 3.2 Number of putative lipids detected using *ex vivo* SPME from brain tissue and the effect of extraction time on lipid coverage. The data was obtained using SIEVE software with the criteria for the feature to be included being: detected in both replicates of samples for each time point, good peak quality via manual inspection, and signal >5-times that of the blank, features with retention time <2 min and >25 min excluded, and features with MW >1200 excluded, n=2

	Number of features detected	Number of features detected
5 min	2158	3432
5 min after 20 hour extraction	2544	4239
15 min	1817	2700
30 min	2368	3511
1 hour	2115	3547
2 hour	2094	3392
20 hour	2592	4160

Table 3.1 shows that the 30 min extraction time used for following *in vivo* extractions was not sufficient for majority of lipids to reach equilibrium. *Ex vivo* results shown in Table 3.2 show that between 30 min to 2 hour there was not a drastic difference in the number of putative lipids detected. The release of lipids after 20 hours in the *ex vivo* will not play a role during an *in vivo* experiment. Not reaching equilibrium can lead to large variations in amounts of extracted lipids if time is not strictly controlled. Birjandi *et al.*^[74] found that for PUFAs equilibrium was achieved prior to 120 min and they therefore used 120 min as their extraction time. Brijandi *et al.*^[73] do not report extraction time profiles but use 90 min as their extraction time.

3.4.2. SPME desorption solvent and desorption time

To evaluate the effect of desorption time, extraction for 30 min was performed from lipid standard mix at a concentration of 200 ng/mL dissolved in 20% methanol. Fibres were desorbed into 100% MeOH for different times: 30 min, 1 hour, 2 hours and 20 hours to assess desorption time. Figure 3.3 (a) shows that longer desorption times did not cause an increase in the amount of lipid being desorbed meaning that desorption time of 30 minutes was enough time to desorb lipids from the fibres. In addition to desorption time, the effect of desorption solvent was also



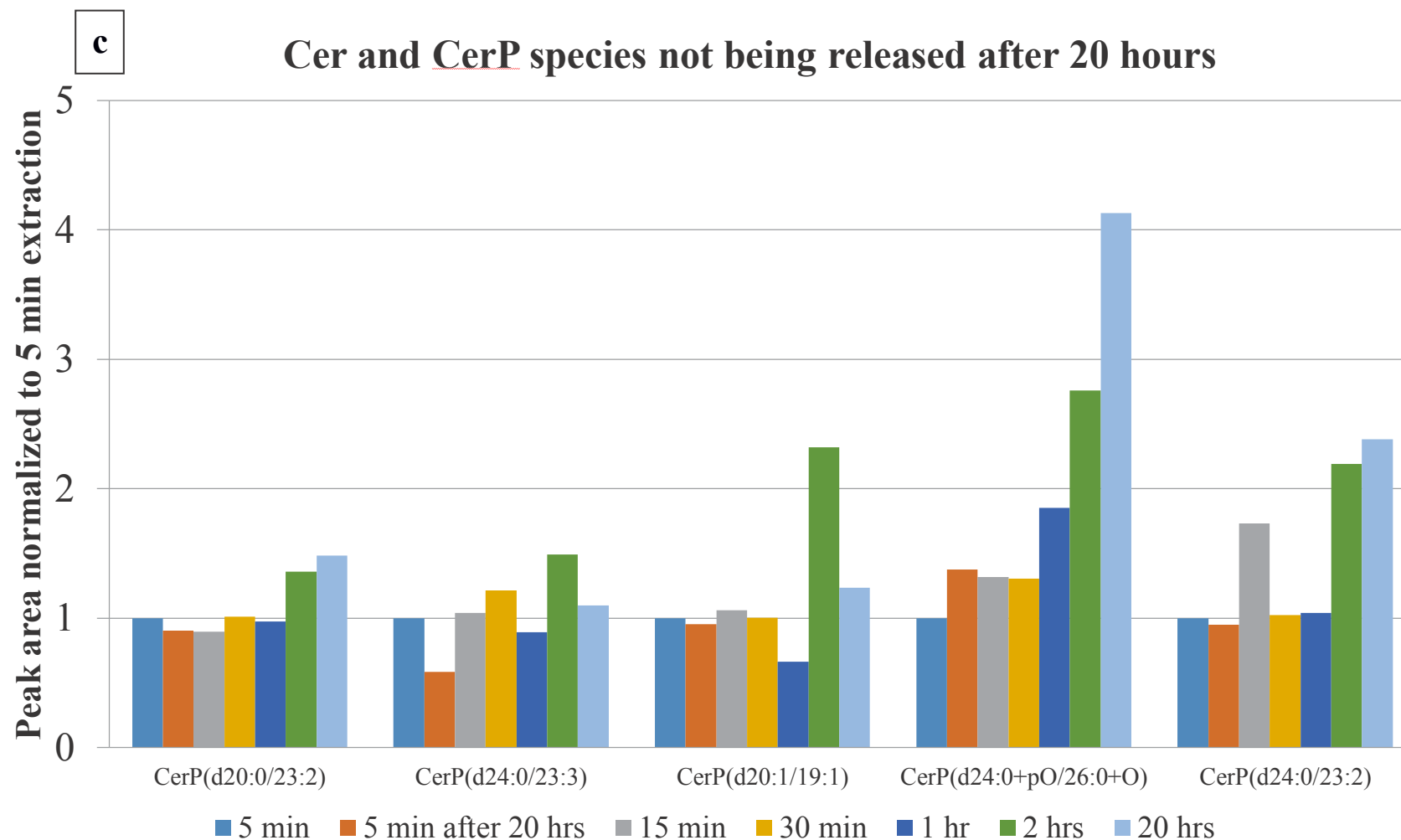
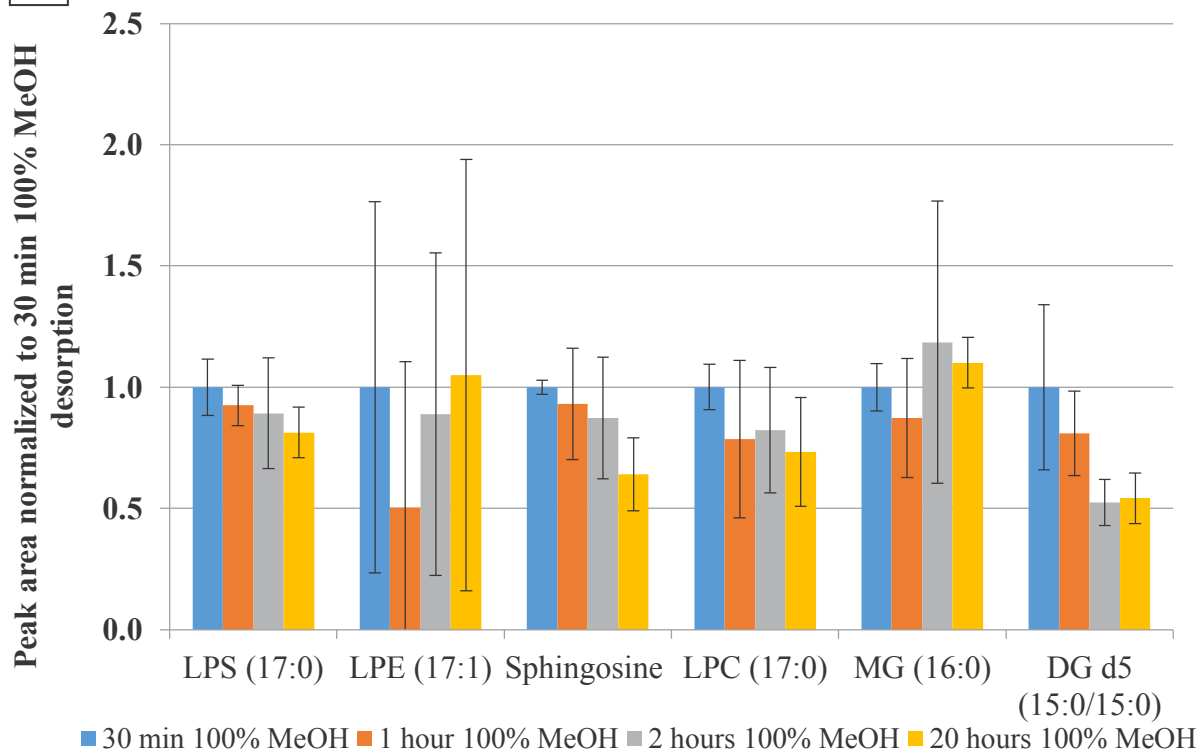
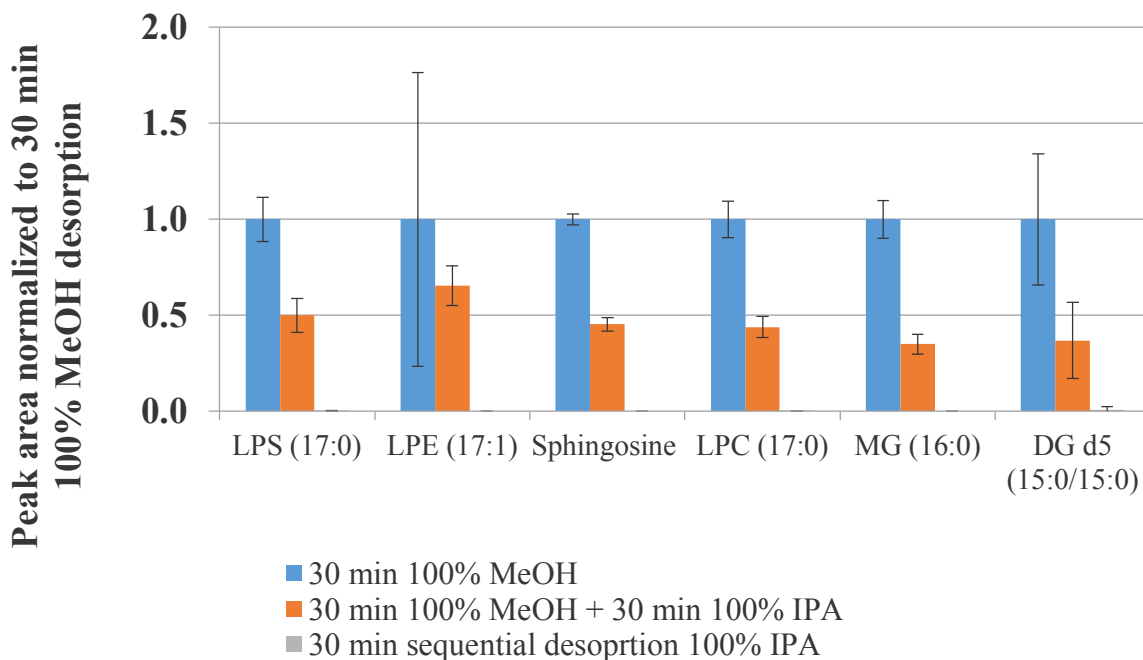


Figure 3.2 Comparison of 5 min SPME performed *ex vivo* immediately after thawing intact brain and the following the 20 hour extraction at room temperature. (a) shows a sub section of Cer and CerP that were released after 20 hours. (b) shows PIs that were released after 20 hours and (c) shows Cer and CerP species that did not exhibit release after 20 hours

assessed. These solvents included 100% MeOH (30 mins) and a sequential desorption into 100% IPA (30 min) after 100% MeOH. Figure 3.3 (b) shows that with sequential desorption into IPA no additional lipid is being desorbed into IPA. Combining the two fractions prior to LC-MS analysis: 100% MeOH and the sequential 100% IPA yielded the predicted results. The observed signal is half of that seen in 100% MeOH which is expected as it has been diluted 2-fold. The optimal desorption solvent should ideally be able to desorb all lipids efficiently during the initial desorption to avoid dilution effect from using two fresh portions of the solvent. Considering 100% methanol may not be able to completely desorb DG and TG classes, 1 hour desorptions into 100% MeOH, 50:50 MeOH/IPA, and 20:80 MeOH/IPA were also tested. The different combinations of MeOH and IPA show that the majority of lipids observed with the exception of LPE, desorb more readily into the 100% MeOH rather than the MeOH/IPA combinations. Based on standard results, 100% methanol and 30 min desorption were the options that were selected for SPME desorption. Considering standard solution did not contain TG due to solubility issues, *in vivo* SPME samples used for the extraction of lipids from the hippocampus region were first desorbed into 100% MeOH and then sequentially desorbed into 100% IPA. Figure 3.4 shows that the sequential desorption into IPA does in fact help to desorb lipids from the fibre to improve coverage. The IPA desorption was able to desorb lipids with larger $\log P$, as indicated by retention time increases. Table 3.3 shows that in positive ESI mode an extra 10 features are detected and in negative ESI mode an extra 186 features are detected. Table 3.3 reports 94 lipids common to both IPA and MeOH in positive mode and 427 in common in negative ESI mode. This causes the signal for these common lipids to be split across two desorption different fractions leading to a reduced signal in both fractions. This disadvantage of using sequential desorption required investigation into having a single desorption solvent.

3.4.3. Folch lipid profile of hippocampus and nucleus accumbens brain regions

Recovery standards that were applied to the tissue samples prior to extraction were not detected. This was addressed in the *ex vivo* extraction time samples by injection standards into the tissue samples via a syringe and incubating overnight at -80°C . Lipids from the nucleus accumbens and hippocampus regions of rat brains were extracted using the Folch method. Figure 3.5 shows ion maps created with data from the SIEVE data processing workflow. Table 3.4 shows the number

a**Evaluation of desorption time****b****Evaluation of sequential desorption**

c

Evaluation of desorption solvent combinations

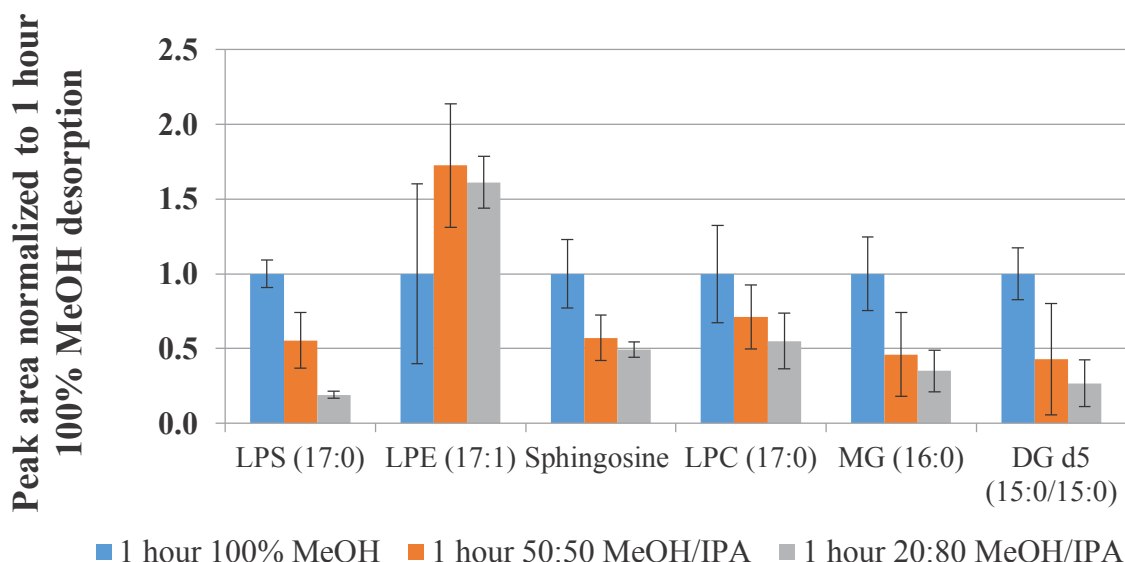


Figure 3.3 Evaluation of (a) desorption time (b) a sequential desorption from 100% MeOH into 100% IPA including analysis of the combined MeOH and IPA desorptions in a single LC-MS analysis and (c) different combinations of MeOH and IPA (100% MeOH; 50:50 MeOH/IPA; 20:80 MeOH:IPA). LC-MS analysis performed using a CSH C₁₈ column on QTOF, n=3.

Table 3.3 Number of putative lipids detected from *in vivo* SPME from hippocampus region using SIEVE software, features with >30% RSD in QC samples excluded, the criteria for the feature to be included being: detected in 66% of samples for each region, good peak quality via manual inspection, and signal >5-times that of the blank, features with retention time <2 min and >25 min excluded, and features with MW >1200 excluded, n=3

	Number of features detected in positive mode	Number of features detected in negative mode	Median RSD of positive mode (%)	Median RSD of negative mode (%)
MeOH desorption	137	451	52	41
Detected in IPA and MeOH desorptions	94	427	42	35
Features unique to IPA desorption	10	186	21	28
Total coverage	147	613		

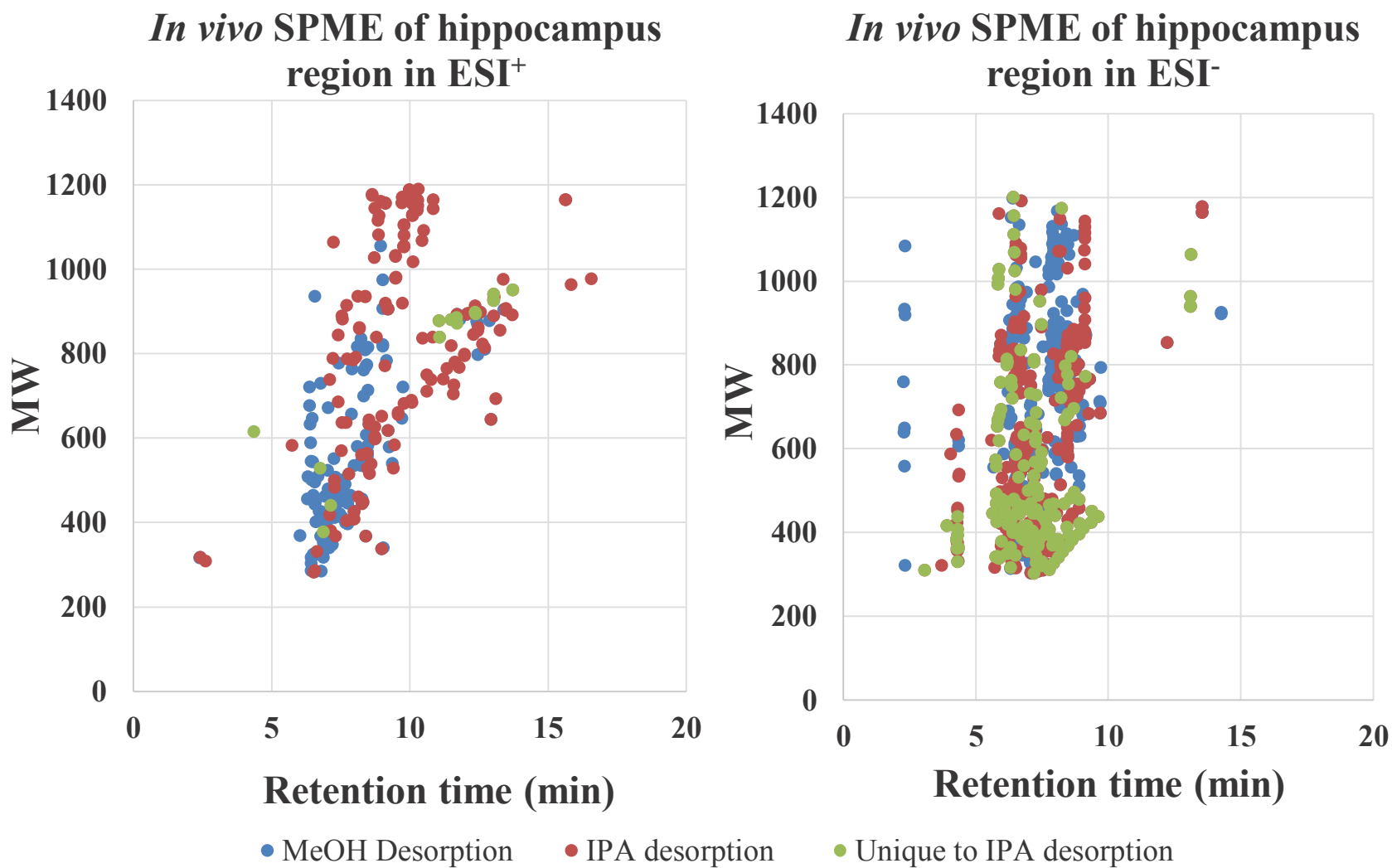


Figure 3.4 Ion maps of in vivo SPME extracts of hippocampus region (n=3) in (a) positive ESI mode and (b) negative ESI mode. Data was processed using SIEVE. The sequential desorption into IPA reveals unique features that were not detected in the MeOH extract.

of features detected in each region in each ESI mode. Both of the regions have a similar number of features with around 1400 in positive mode and around 1100 in negative mode. In the SIEVE data features with the same MW and RT were considered the same lipid. The two regions showed very similar lipid profiles according to the SIEVE data. In positive mode, the two regions had 1357 features with the same RT and MW which is over 99% feature overlap. In negative mode, there was an overlap of 884 features which accounts for 76% of the features.

Table 3.4 Number of putative lipids detected using SIEVE software in hippocampus (n=16) and nucleus accumbens (n=8) brain regions. The results shown are for high-quality data set whereby: features with >30% RSD in QC samples were excluded, features with retention time < 2 min and >25 min were excluded, and features with MW >1200 were excluded. In addition, each feature also had to meet the following criteria: detected in 66% of samples for either region, good peak quality via manual inspection, and signal >5-times that of blank.

Region	Number of features detected in positive mode	Number of features detected in negative mode
Hippocampus	1368	1161
Nucleus accumbens	1417	1159
Number of features common to both	1357	884

The median RSD across the biological replicates of the hippocampus region in negative mode is 45%. The median RSD of the technical replicates of the hippocampus region in negative mode ranges from 11-60% as shown in Table 3.5. This suggests that the high median observed in the biological replicates is due to the heterogeneity of the tissue samples rather than the extraction procedure, except in the case of H7 technical replicates where the median RSD is 82.0 and 60.6% in negative and positive mode respectively, indicating there was an issue with the repeatable extraction of this sample. Excluding the H7 technical replicates brings the median RSD of the biological replicates down to 40.1% and 41.7% supporting the hypothesis that the high median RSD observed may be attributed to the heterogeneity of the tissue samples. This is further confirmed by comparing the median RSD of QC samples (12.1 and 13.7%) which indicate the performance of LC-MS method over the long analytical batch. QC samples were used to assess instrumental drift and degradation of lipids over time by injection at the beginning

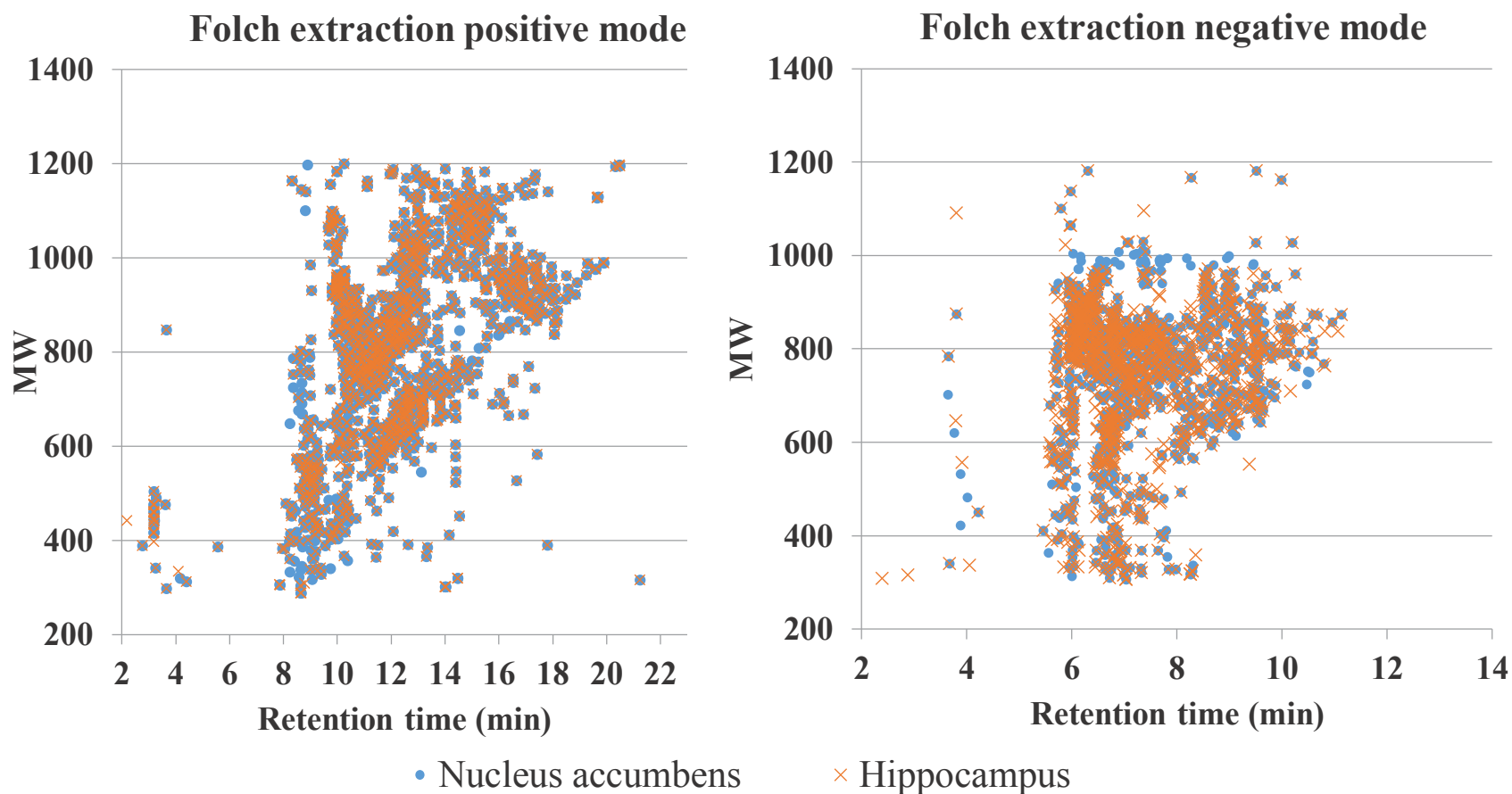


Figure 3.5 Ion maps of Folch extracts of hippocampus (8 biological replicates, n=2 technical replicates per sample) and nucleus accumbens (4 biological replicates, n=2 technical replicates per sample) regions after Orbitrap LC-MS analysis in (a) positive ESI mode and (b) negative ESI mode. Data was processed using SIEVE with the following criteria features with >30% RSD in QC samples were excluded, features with retention time <2 mins and >25 mins were excluded, features with MW >1200 were excluded. In addition, each feature also had to meet the following criteria: detected in 66% of samples for either region, good peak quality via manual inspection, and signal >5x that of blank.

of the analysis, throughout the analysis, and at the end of the analysis. No LC-MS instrument drift or lipid degradation was observed in the QC samples. The nucleus accumbens region in positive and negative mode exhibits the same high median RSD in the biological replicates at 49.7% and 40.0%. The median RSD for the technical replicates ranges from 25-67%, and among these samples the N1 technical replicates appear to be outliers. These tissue samples from the nucleus accumbens region were a lot smaller than the tissue samples for the hippocampus region which could explain the higher RSD observed in the technical replicates as sample processing errors would contribute more to the error observed in the technical replicates. Using only two technical replicates to calculate RSD is less than ideal but there was a need to assess the reproducibility of the replicates for over 1000 putative lipids. The loss of four samples was due to samples not forming protein pellets and the resulting organic phases containing large amounts of debris. Larger sample sizes could help alleviate this issue. Table 3.4 shows that the majority of lipids were detected in both samples. Where the two regions differ is the intensity of the identified lipids. Figure 3.6 shows a comparison of the summed total of the mean areas of each lipid subclass that were identified in the two regions. A value <0.5 shows that significantly less of that subclass is observed in the hippocampus region while a value >2 shows that significantly more of that lipid subclass is observed in the hippocampus regions. These values are larger than what is typically used in metabolomics studies (<0.66 and >1.5) due to the large biological variability observed in the tissue samples. From Figure 3.6 the lysophospholipids are seen in decreased amounts in the hippocampus regions in negative mode. Only three of the five lysophospholipids subclass were identified in positive mode, LPS, LPC and LPE and did not fall below the cut-off of 0.5. This discrepancy in the signal intensities could be due to ion suppression in negative mode. Another contributing factor is the identification of the lysophospholipids in negative mode. Fewer lysophospholipids were confidently identified in positive mode meaning that they are accounting for fewer of lipid species present in the sample. Ten LPEs were identified in negative mode while only four LPEs were confidently identified in positive mode. A full list of identified lipids, their integrated peak areas and LipidSearch grade are given in Appendix A Tables A5-8 of the supplementary information.

Green *et al.* ^[39] examined the phospholipid composition of a number of different regions of the brain including the nucleus accumbens using the Folch extraction method in combination with ¹H-NMR and ESI-MS/MS. Their ESI-MS/MS results examined four of the main GP subclasses:

PC, PE, PS and PI. They identified 15 species from the PC subclass with the most abundant being PC (34:1). Our analysis confidently (confident meaning grades of A or B after LipidSearch identification) identified seven PCs in the nucleus accumbens regions with the most abundant species being PC (34:1) agreeing with Green *et al.* According to Green *et al.*^[39] out of a total of 15 PEs, the most predominant PEs in the nucleus accumbens regions were PE (40:7) and PE (40:6). Our results obtained from LipidSearch identified 41 PE species confidently in the nucleus accumbens region. The most abundant PE was 40:6 which agrees with Green *et al.* study, but PE 40:7 was not identified in our results. Green *et al.*^[39] found PS (40:6) as the most abundant PS among seven PS identified. Our results show that PS (36:2) was the most abundant and PS (40:6) was not identified among a total of 22 PSs confidently identified in the nucleus accumbens region. Green *et al.*^[39] identified a total of five PIs with PI (38:4) being the most abundant. Our analysis identified four PIs in the nucleus accumbens region with the most abundant being PI (38:4) in agreement with Green *et al.*

Almeida *et al.*^[36] analysed six regions of rat brain including the hippocampus region using shotgun MS approach. They identified 32 PCs and 34 PC O- species with PC (34:1) and PC O- (34:1) being the most abundant. Our analysis agreed with respect to PC (34:1) being the most abundant PC. We identified PC O- (20:3) as the most abundant PC O- species. However, we only confidently identified four PC species and one PC-O species in the hippocampus region which is drastically different to coverage provided by Almeida *et al.* This shows that future work needs to examine how to boost the number of confident identifications using LipidSearch. Their PE coverage includes 22 PE species and 22 PE O- with PE (40:6) and PE O- (40:7) being the most abundant^[36]. Our coverage identified 24 PE species and 24 PE O- species with PE (38: 4) and PE (40:6) being equally the most abundant PE species and PE O- (38:6) and PE O- (40:6) being equally the most abundant of the PE O- species in the hippocampus region with PE O- (40:7) being the 9th most abundant PE O- species in the hippocampus region. Almeida *et al.* identified 12 members of the PS subclass with PS (40:6) being the most abundant compared to our analysis which confidently identified 18 PS species with PS (36:2) being most abundant. Notably, PS (40:6) was identified in our analysis as one of the least abundant PS species and it is not clear what is causing this discrepancy in results. For PG subclass, Almeida *et al.* identified 12 PGs with PG (34:1) being most abundant while our analysis confidently identified 10 PGs with PG (34:4) being the most abundant with PG (34:1) being the second most abundant. Eight

Table 3.5 Technical and biological variability of lipid measurement using Folch extraction method for hippocampus and nucleus accumbens brain regions. The table shows median %RSD of the signal intensity of all lipids detected in different biological and technical replicates of the Folch extractions of the hippocampus and nucleus accumbens regions to assess the heterogeneity of the tissue sample and repeatability of extraction procedure. *Low sample volume prevented analysis of the 2nd technical replicate of N3.

Region		Median RSD% in positive mode	Median RSD% in negative mode	
Hippocampus	H1	17.0	20.6	
	H2	20.5	27.1	
	H3	14.1	19.9	
	Technical replicates	H4	18.6	23.3
		H5	17.6	11.6
	H6	42.2	42.1	
	H7	82.0	60.6	
	H8	26.5	26.8	
	Biological replicates	46.2	45.1	
	Biological replicates excluding H7	40.1	41.7	
Nucleus accumbens	N1	66.5	64.6	
	Technical replicates	N2	27.2	25.5
		N3	59.9	N/A*
	N4	35.0	30.4	
	Biological replicates	49.7	40.0	
	Biological replicates excluding N1	44.5	27.3	
	Quality control	12.1	13.7	

PIs were identified by Almeida *et al.* with PI (34:1) being the most abundant^[36]. Our analysis identified only four PIs with PI (38:4) being the most abundant. Almeida *et al.* identified 12 LPC species with LPC (16:0) being the most abundant. Our coverage of LPC identified three species with only species, LPC (18:0) being detected in negative mode and the two other species, LPC (18:1) and LPC (20:4), at similar abundance, being only detected in positive mode. Almeida *et*

al. identified five Cer with Cer (d36:1) being the most abundant. In contrast, our analysis identified four Cer in positive mode and six Cer in negative mode with Cer (d16:0) and Cer (d46:7) being the most abundant in each mode. For the SM subclass Almeida *et al.* identified 15 SM with SM d36:1 being the most abundant. Our analysis only confidently identified one SM in the hippocampus region, SM (d30:1) showing we need to work further to improve our confident identifications of this subclass. Finally, they identified eight cholesterol esters (CE) with CE (20:4) being the most abundant while we only identified one: CE (22:6) which was the 2nd most abundant CE identified by Almeida *et al.*^[36]. Almeida *et al.* did not report any LGP except for LPC while our analysis confidently identified 11 LPEs, four LPGs, four LPIs and two LPSs in the hippocampus region. In addition, our analysis also detected 17 DGs and 56 TGs.

The PCAs in Figure 3.7 show that the QCs group well at the centre of the plot indicating repeatable LC-MS conditions throughout the analyses. The comparison of positive versus negative mode PCA (PC1 versus PC2) shows that there is better grouping of the regions and separation along the x-axis using ESI data. According to Table 3.5 in positive mode the outliers were H7 (which was omitted from PCA) and N1. The PCA reported that N1 was not an outlier and that N3 was. The PCA for negative mode classified H8 and N1 as outliers. According to Table 3.5 H7, not H8 was an outlier and N1 in agreement with the PCA was an outlier. The positive PCA is described by five components which account for a cumulative R2X of 0.715. The negative mode PCA is described by four components accounting for a cumulative R2X of 0.686. Pareto scaling was used. This ensures that the PCA is less dominated by lipids with the highest intensity by using the square root of the standard deviation rather than just the standard deviation which is used in autoscaling^[143]. The loading plots were examined and the features contributing most were entered into LIPID MAPS database in order to obtain tentative identification. A list of these compounds that were downregulated in the hippocampus region with respect to nucleus accumbens and their tentative IDs is given in Table 3.6. They are mostly species belonging to the GP class. Given the mass accuracy of the Orbitrap is often <1 ppm the correctness of these identifications, especially those with mass error above 10 ppm is questionable, and may indicate co-elution of two species. The most promising feature is PI (38:5)

Comparison of identified lipid sub classes by region in the brain

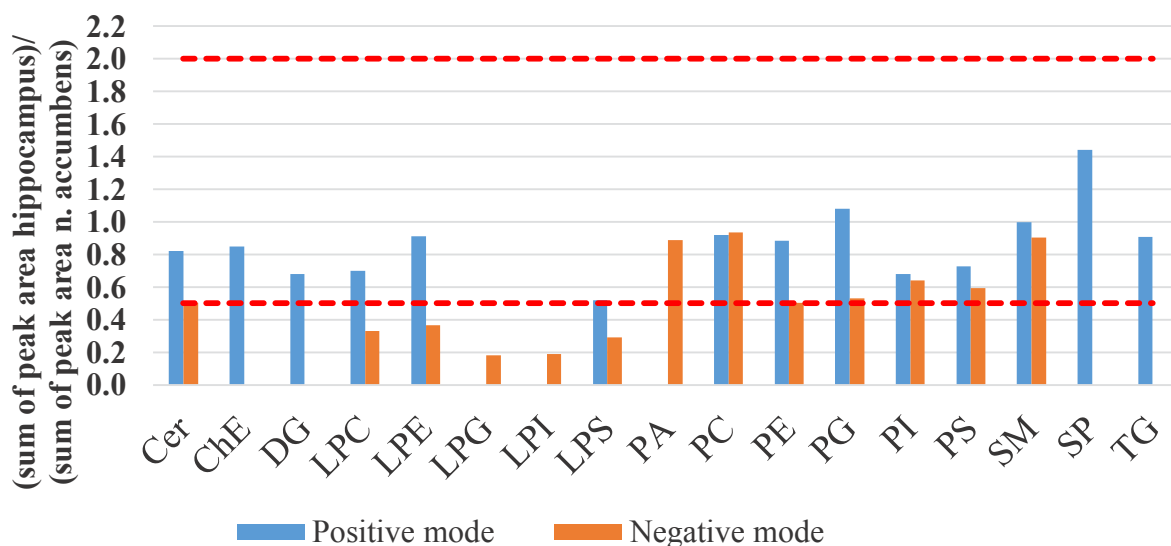


Figure 3.6 Comparison of lipid signal intensities observed for hippocampus and nucleus accumbens. The mean peak area of each of the identified lipid sub classes were summed. The sum of peak areas in the hippocampus region/sum of peak areas in the nucleus accumbens region were compared. A value <0.5 (indicated by red dash) shows that significantly less of that subclass is observed in the hippocampus region while a value >2 (indicated by red dash) shows that significantly more of that lipid subclass is observed in the hippocampus region. Lipid areas were corrected using IS MIX II on a subclass basis. Folch extracts of hippocampus (8 biological replicates, n=2) and nucleus accumbens(4 biological replicates, n=2) regions were analysed on an using as CSH C₁₈ column on an Orbitrap.

with a mass error of <3 ppm. PI (38:5) was the only lipid from this list identified by Green *et al.*^[39]. They identified it as the 4th most abundant lipid in the nucleus accumbens. Almeida^[36] *et al.* also identified PI (38:5) in the hippocampus area as the 3rd most abundant PI. They also identified PC (30:1) and PE O-(34:3) in very low amounts. Table 3.7 is the list of compounds that were upregulated in hippocampus region. All of these tentatively identified lipids belong to the GP class. None of these hits had a fold change greater than the cut-off of 2 except for PS (27:1). Lipids with odd chains are not produced in mammals suggesting this lipid may not originate endogenously. Considering the poor separation of the two regions in the positive mode PCA the top 10 compounds were not queried.

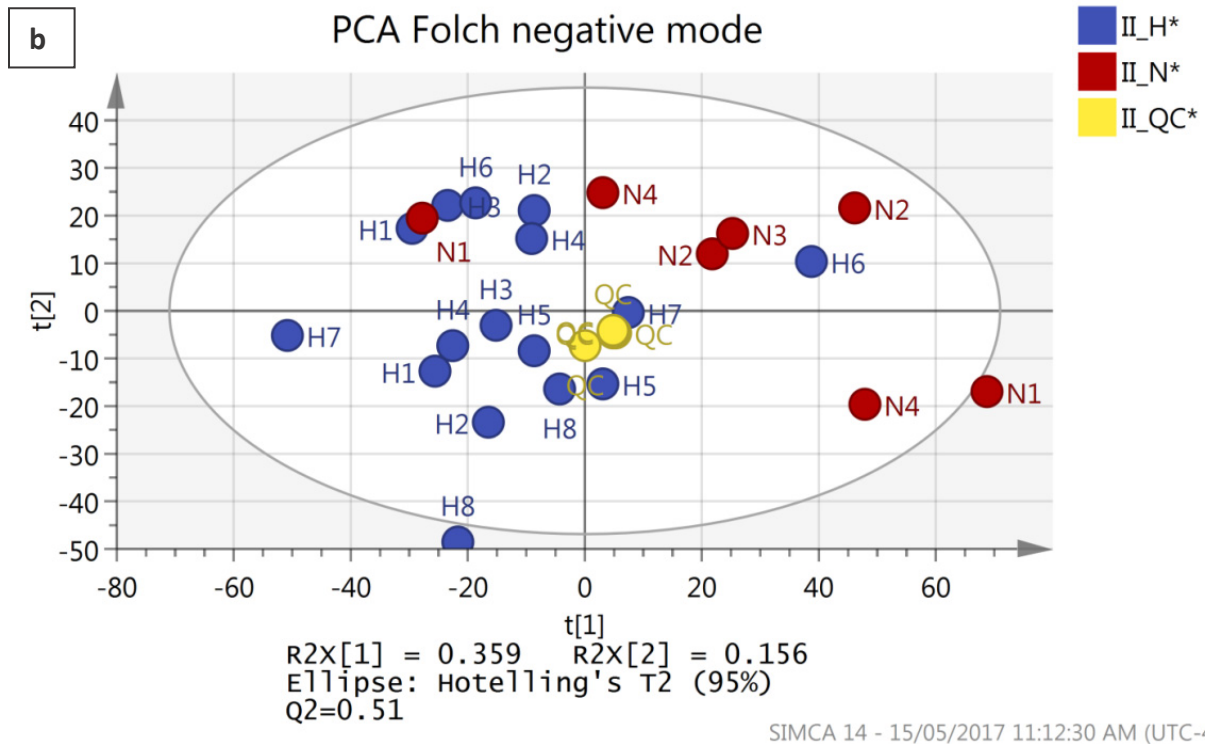
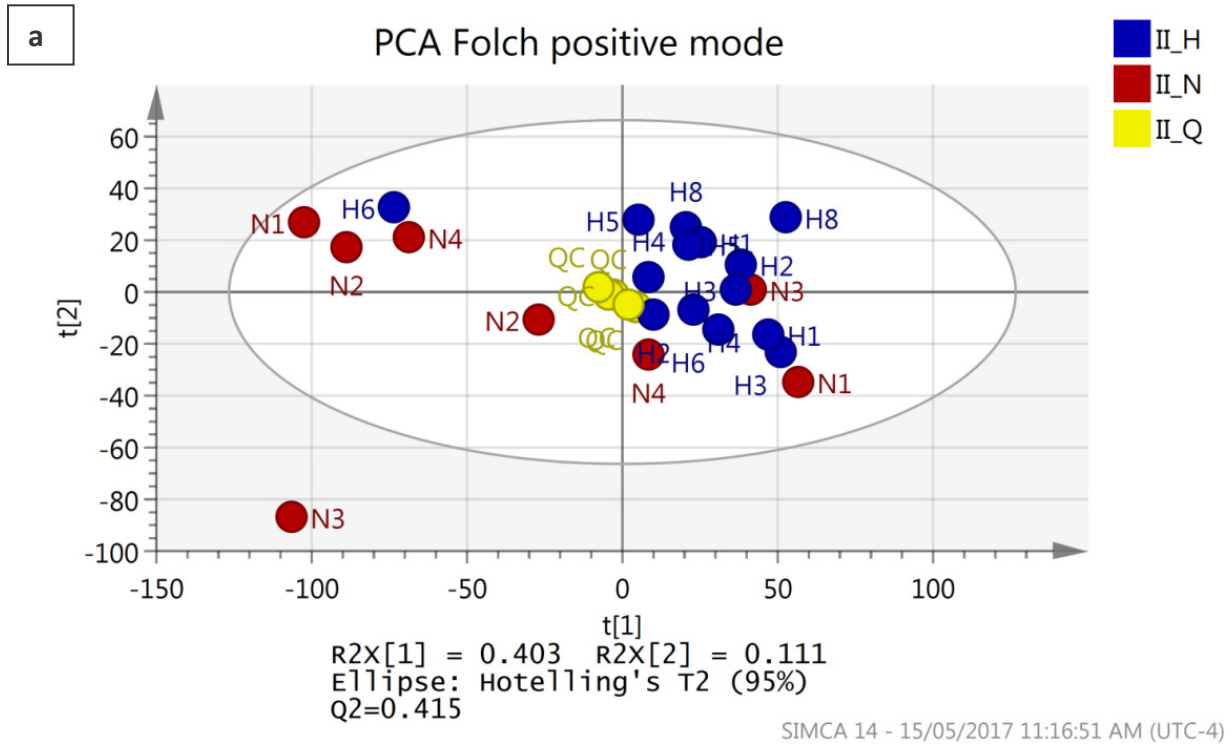


Figure 3.7 The PCA plots from (a) positive ESI mode and (b) negative ESI mode of the Folch extracts of the two brain regions hippocampus $n=16$ (blue), nucleus accumbens (red) $n=8$ and QC (yellow) $n=5$. (H7 replicates omitted from positive mode PCA due to high RSD)

Table 3.6 Top 10 compounds contributing most to negative mode PCA separation along x-axis along with tentative ID's queried from LIPID MAPS database that were downregulated in hippocampus with respect to nucleus accumbens

Observed	RT (min)	Fold-	Tentative ID	Exact	Mass error
887.559	9.5	0.6	PS(44:8)	887.5676	9.7
884.539	6.2	0.6	PI(38:5)	884.5415	2.8
885.542	6.3	0.6	No hit		
824.549	6.3	0.4	PG(40:5)	824.5567	9.3
391.275	6.2	0.7	N-(5Z,8Z,11Z,14Z-eicosatetraenoyl)-L-serine	391.2723	6.9
496.389	7.4	0.4	No hit		
683.598	9.1	0.5	No hit		
699.61	9.4	0.3	No hit		
703.552	6.5	0.5	No hit		
751.49	5.9	0.3	No hit		

Table 3.7 Top 10 compounds contributing most to negative mode PCA separation along x-axis along with tentative ID's queried from LIPID MAPS database that were upregulated in hippocampus with respect to nucleus accumbens

Observed	RT (min)	Fold-	Tentative ID	Exact	Mass error
752.368	8.3	1.8	No hits		
784.526	6.4	1.2	PG(37:4)	784.5254	0.7
767.519	6.9	1.2	PS O-(36:5)	767.5101	11.6
785.529	6.9	1.2	PS (36:3)	785.5207	10.6
593.406	7.1	1.8	PC (22:0)	593.4057	0.5
681.56	8.3	1.7	No hits		
689.622	9.4	1.1	No hits		
799.531	7.0	4.4	PS (27:1)	799.5363	6.6
805.677	9.8	1.6	No hits		
1093.72	8.2	1.3	No hits		

3.4.4. *In vivo* SPME lipid profile of hippocampus

SPME was performed *in vivo* in the hippocampus region of rat brain to extract lipids for 30 min. Figure 3.4 shows the ion maps of the features detected in both positive and negative mode using the SIEVE workflow. Table 3.3 shows the number of features detected in each ESI mode. These fibres extracted less than the *ex vivo* fibres used in the extraction time optimization step. The *in vivo* SPME extracted 147 compounds in positive mode compared to the 769 extracted by the *ex vivo* SPME according to SIEVE, Table 3.2. In negative mode the *in vivo* SPME extracted 613 putative lipids compared to the *ex vivo* SPME where 1336 putative lipids were observed, Table

3.2. The fibres used for the *in vivo* extractions had a coating length of only 4 mm as compared to the fibres used for the extraction time optimization experiments *ex vivo* that had coating length of 15 mm. The 4 mm coated fibre has 0.13 mm³ volume of extraction phase while the volume of extraction phase on the 15 mm is four times that of the extraction phase on the 4 mm fibre with 0.52 mm³ of coating. In addition the *in vivo* fibres were mixed mode: C₁₈ + benzenesulfonic acid (strong cation exchange) compared to the 15 mm fibres which were only C₁₈. This could lead to different coverage of the two different types of fibre due to the distribution coefficient of the analyte between the fibre and the sample system changing due to the different extraction phase. These two factors explain the reduction of features detected using *in vivo* SPME. The main reason why coating length was reduced to 4 mm was to obtain better spatial resolution for *in vivo* studies. The University of Waterloo is also working on further miniaturizing the diameter of the fibres, which would further reduce the amount of lipids extracted. To counteract these, performing LC-MS analysis on more recent and more sensitive models of mass spectrometers could help regain the coverage. Other options include using nanoLC, and/or increasing injection volume to ensure enough of material is available for MS detection.

The *in vivo* lipid profile obtained from LipidSearch was compared to the 30 min *ex vivo* time point extraction. In ESI⁺, 164 lipids were identified in the *ex vivo* SPME extractions while the *in vivo* SPME identified 128 lipids with the LipidSearch. There were 34 out of the 147 lipids identified in the *in vivo* profile that were also identified in the *ex vivo* tissue samples: 3 Cer, 1 DG, 17 PE, 1 PS, and the remaining 13 were TGs. In negative mode, 46 out of the 58 lipids identified in the *in vivo* lipid profile were also identified in the *ex vivo* tissue samples: 9 LPE, 1 LPS, 7 PC, 21 PE, 2 PG, 4 PI, 1 PS and 1 SM. The total number of lipids identified with LipidSearch in ESI⁻ in the *ex vivo* samples was 123 lipids which is more than twice the number of lipids identified in the *in vivo* samples which was 55.

3.4.5. Folch versus *in vivo* SPME

Table 3.8 and Table 3.9 compare the lipid species identified with LipidSearch in the Folch extraction to those extracted with *in vivo* SPME fibres in positive mode and negative mode, respectively. These data sets were run independently on the LipidSearch platform. This was done to evaluate how many lipids can be confidently identified from *in vivo* SPME extracts, where lower amount extracted and signal intensity is expected to be observed. For Folch extracts, there was sufficient sample to also perform MS/MS analysis with HCD fragmentation which can

Table 3.8 Comparison of species identified with the Folch extraction method (n=16) to in vivo SPME (n=3) method of the hippocampus region with LipidSearch in positive ESI mode on Orbitrap. Lipids were considered identified if they contained an A or B grade in one of the samples from each of the stated extraction methods

Lipid class	Lipid subclass	Number species identified in Folch extraction from hippocampus	Number of species identified in SPME from hippocampus
GL	DG	21	4
	TG	59	86
GP	LPC	2	0
	LPE	4	0
	LPS	2	0
	PC	7	0
	PE	30	23
	PS	9	1
	PG	2	0
	PI	1	0
SL	SM	1	0
	SP	1	2
	Cer	5	11
Cholesterol	ChE	1	0
Total		145	127

Table 3.9 Comparison of species identified with the Folch extraction method (n=16) to in vivo SPME (n=3) method of the hippocampus region with LipidSearch in negative ESI mode on Orbitrap. Lipids were considered identified if they contained an A or B grade in one of the samples from each of the stated extraction methods

Lipid class	Lipid subclass	Number species identified in Folch extraction from hippocampus	Number of species identified in SPME from hippocampus
GP	LPC	1	0
	LPE	10	9
	LPS	2	2
	LPG	4	0
	LPI	4	0
	PC	5	10
	PE	39	21
	PS	14	4
	PG	8	2
	PI	4	7
	PA	3	0
SL	Cer	6	1
	SM	1	2
Total		99	57

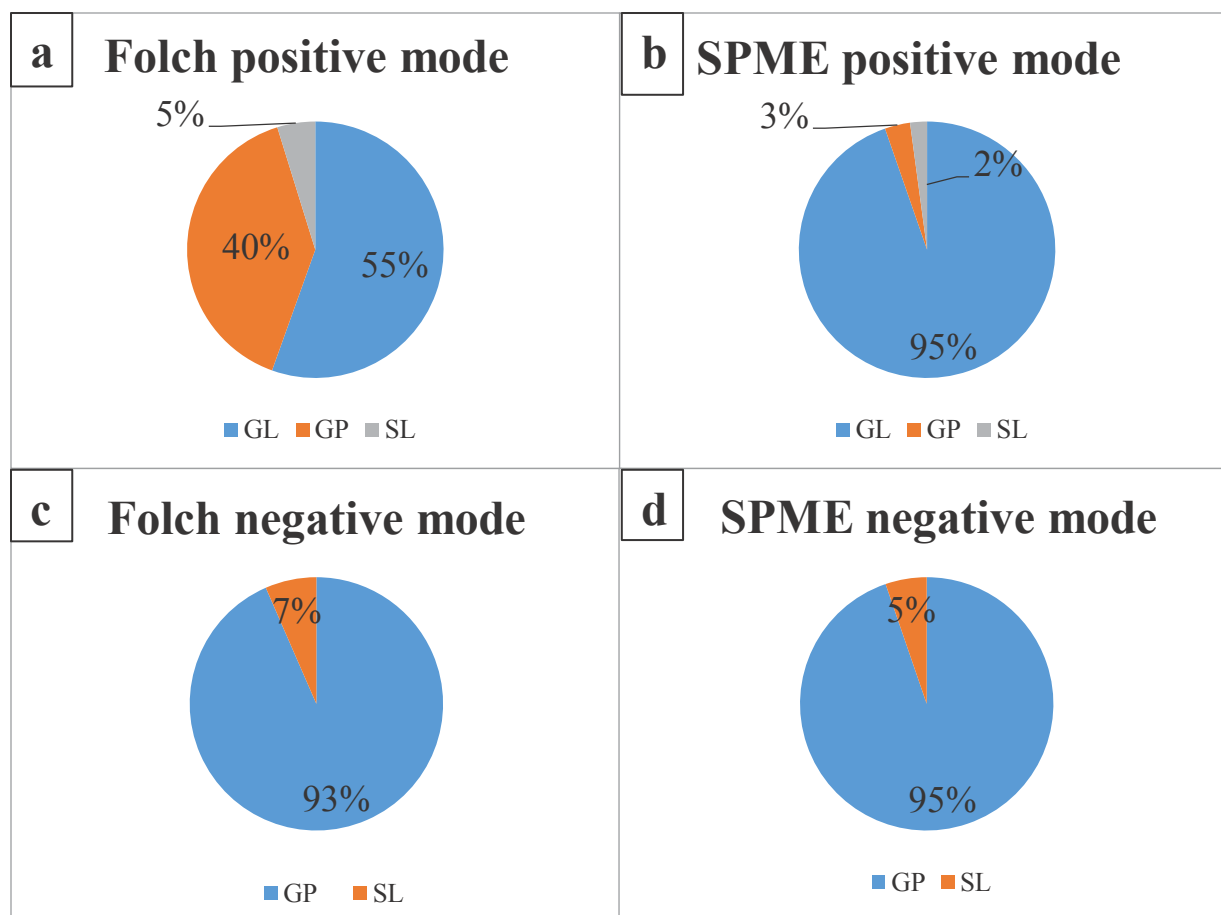


Figure 3.8 (a-b) Composition of the hippocampus according to the number of lipid species confidently identified with LipidSearch from the Folch extraction and *in vivo* SPME in positive mode. According to LipidSearch SPME extracts contain mostly GL, 95%, while in Folch GPs make up 40% of the lipids. (c-d) show the same comparison but in negative mode. Here both methods show a similar % of GPs and SLs.

further help improve the number of identifications. However, for SPME samples there was not sufficient sample to do this, so to do fair comparison, HCD data collected for Folch extraction will be excluded here to allow a levelled comparison. The Folch extraction had 147 lipids identified in positive mode with the majority belonging to the GL lipid class. These TGs and DGs accounted for 55% of the lipid species identified. The SPME identified 120 lipids with 74% of these belonging to the GL lipid class. 56 of the lipids identified in the SPME analysis were also among the lipids seen in the Folch extraction. In negative mode, only half as many lipids are identified by SPME when compared to Folch, 55 vs. 99 respectively. 17 of these lipids were also identified in the Folch samples. The Folch method is an exhaustive extraction method compared to SPME which is a non-exhaustive method. The fewer number of features observed from the SIEVE data from *in vivo* SPME is to be expected. SPME doesn't extract lipids that are bound to

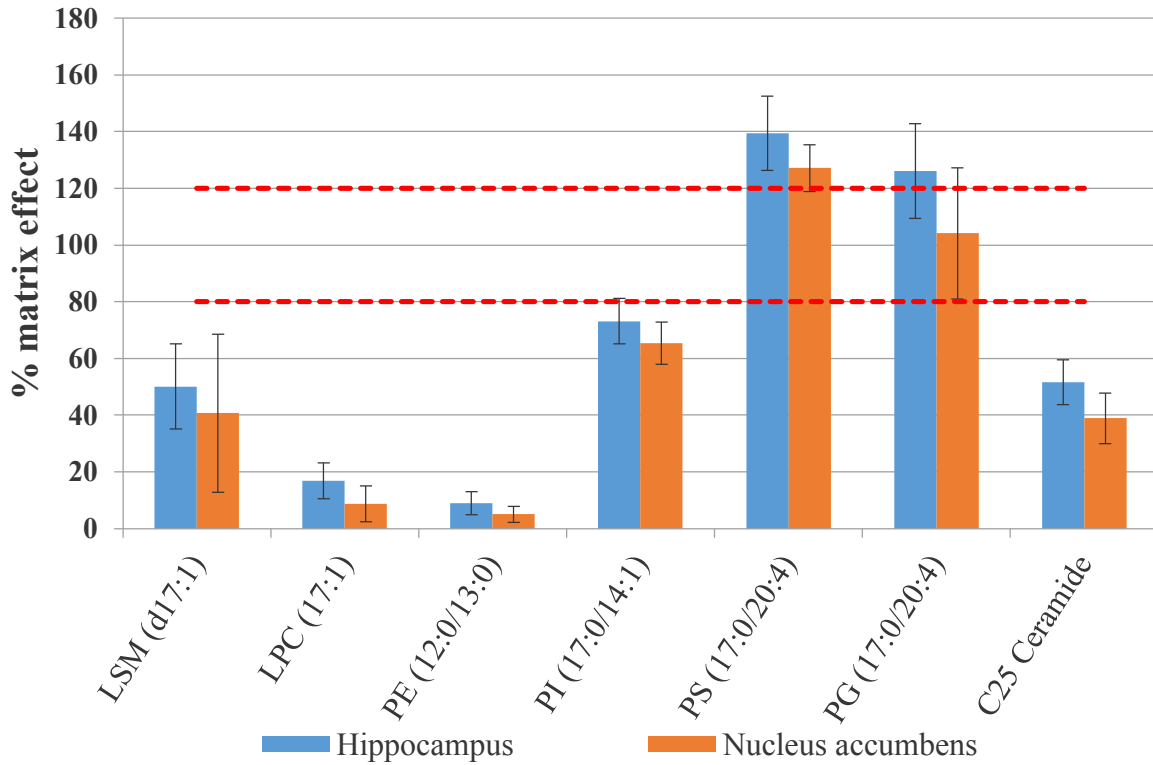
proteins while the Folch extraction will denature proteins and disrupt the binding of lipids to proteins due to the excess of organic solvent. Figure 3.8 shows the distribution of the identified lipids in Folch and *in vivo* SPME in both positive and negative mode. The two methods show quite different lipid profiles for positive mode but show very similar lipid class profiles in negative mode. The Folch method had a lot more GPs identified in it in the positive mode samples possibly due to the bioavailability of the GPs observed in the Folch extract. The large number of Cer identified in the *ex vivo* samples compared to the small number of Cer identified in the *in vivo* sample is partially due to the larger sample size of the *ex vivo* data set. The large number of Cers observed in the *ex vivo* samples may be due to exposure of the samples to air and release of the Cer that would be otherwise be bound e.g. in the *in vivo* samples as Cer are signalling molecules associated with, among other things, apoptosis^[144].

3.4.6. Matrix effects

Matrix effects were assessed by monitoring the signal of standards spiked post-extraction into both the Folch extracts and the SPME extracts. This standard mixture contained lipids from across GL, GP and SP classes and included: LPA, LPC, PE, PI, PS, PG, PA, LSM, SP, SM Cer, DG and TG. For the Folch extractions LPA, SP, LPC, PS, and Cer show signal suppression in positive mode with TG showing signal enhancement. LSM, PE, SM, and PI are within the acceptable range. In negative mode LSM, LPC and PE show signal suppression while PG and PS show signal enhancement with PG falling within the acceptable range in the nucleus accumbens samples. The trends were comparable for both hippocampus and nucleus accumbens region. SPME method shows less pronounced matrix effects compared to the Folch method. LPE and PS fall just outside the criterion of 80%. In positive mode LPS, LPC, PG, DG, and TG all fall within the acceptable range of 80-120%. PE shows a large amount of signal suppression with signal intensity of 6% compared to standards in solvent. PC shows signal enhancement with signal intensity of 440% compared to standards in solvent. In negative mode LPE, LPC and PG show no suppression or enhancement. LPS shows no suppression within experimental error and PE shows significant suppression at 5%. PC shows significant enhancement at 240% signal in solvent.

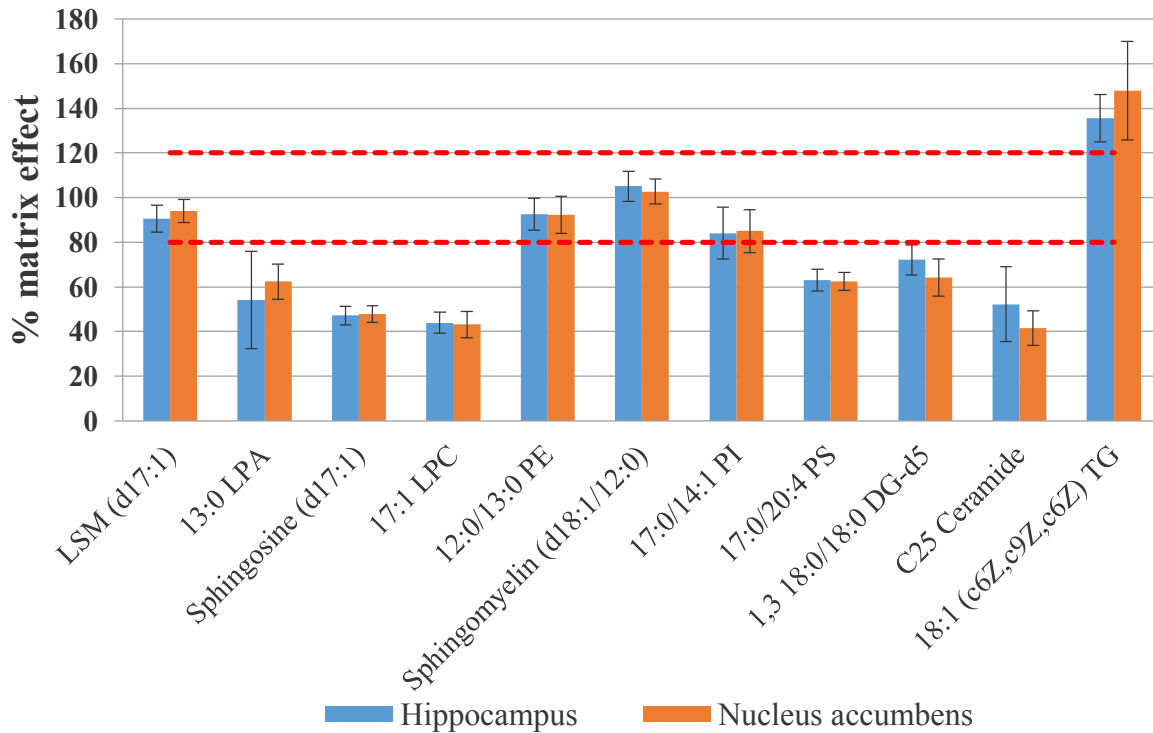
a

Matrix effect of Folch negative mode



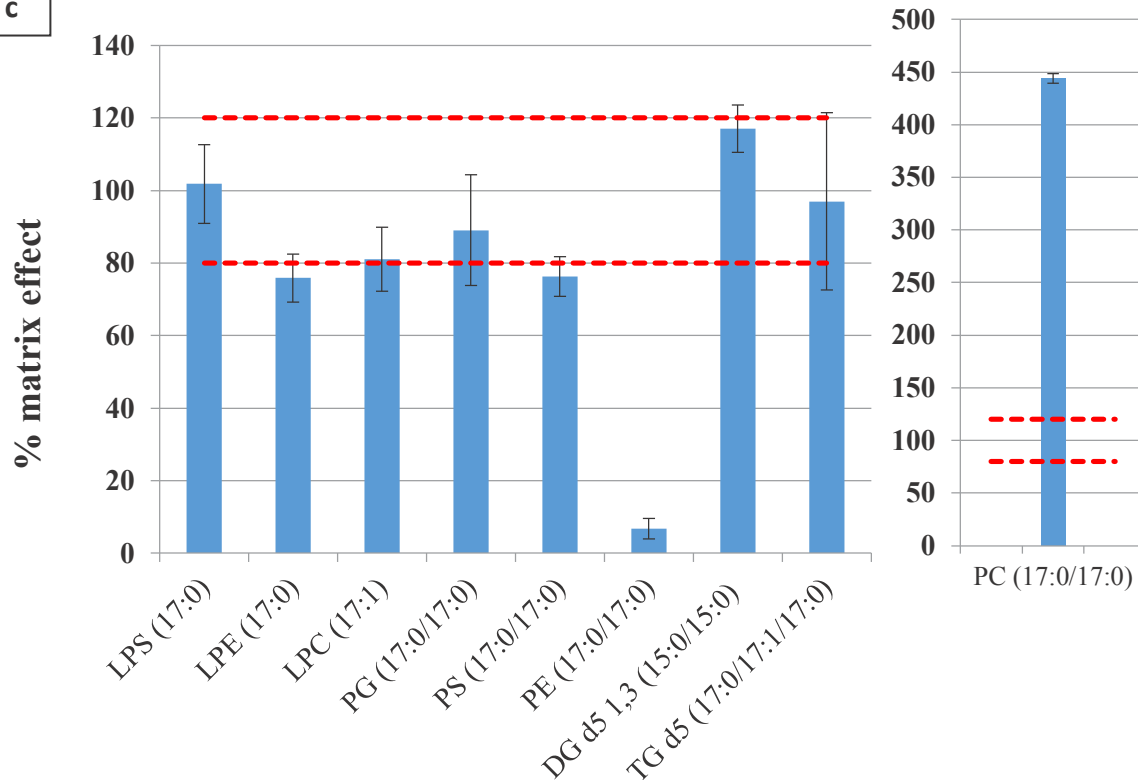
b

Matrix effect of Folch positive mode



c

Matrix effect in vivo SPME positive mode



d

Matrix effect in vivo SPME negative mode

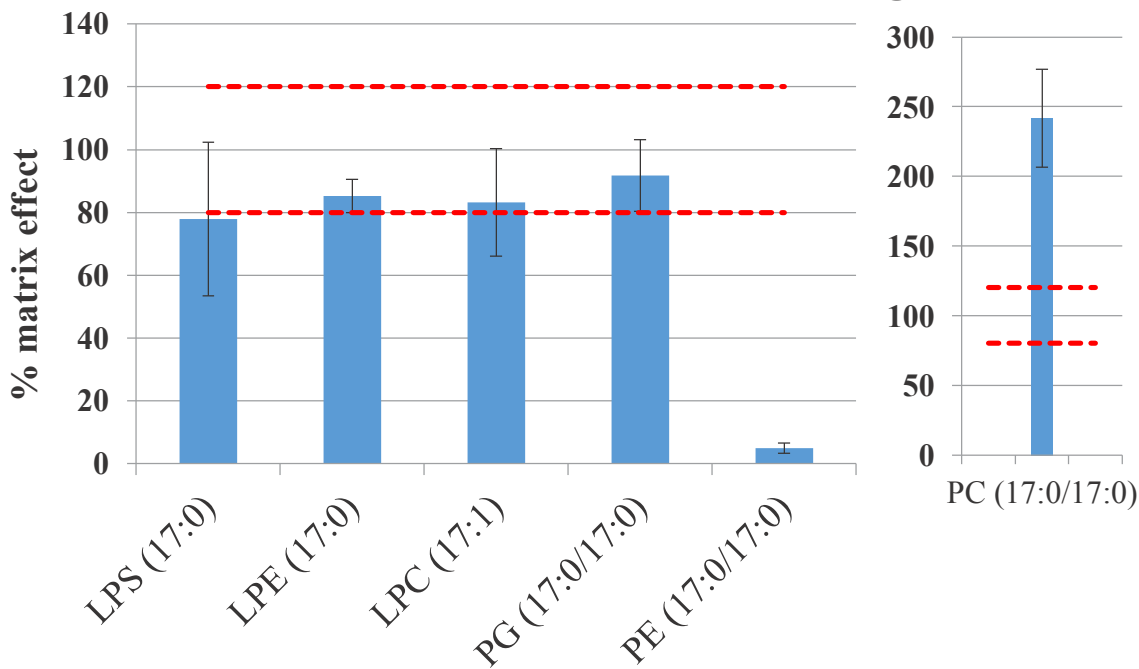


Figure 3.9 Response of standard mix spiked post extraction to monitor matrix effects in Folch extracts (a-b) and in vivo SPME extracts (c-d)

3.5. Conclusions

This study has demonstrated the ability of *in vivo* SPME fibres to successfully extract lipids from brain tissue. In positive mode, a similar number of lipids were identified to a traditional Folch extraction 127, and 145 respectively. The SIEVE analysis detected vastly fewer features, 145 for SPME, than the Folch extraction with 1368 features. In negative mode 57 lipids were identified in the *in vivo* SPME fibre extracts while the Folch method had 99 lipids identified. Processing the data with SIEVE detected 613 features in the *in vivo* SPME extracts and 1161 in the Folch extracts. The lipid profile observed in the SPME extracts showed similarities to the Folch extract identifying some of the most abundant lipid species identified in the Folch extract. This demonstrates the potential ability of SPME to capture a relevant snapshot of a lipid profile. SPME is a non-exhaustive, equilibrium based method that extracts free lipids. Folch is an exhaustive extraction method that disrupts the binding of lipids to proteins and/or membranes hence the greater number of features detected with SIEVE and identified with LipidSearch.

Acknowledgments;

The authors gratefully acknowledge financial support for this project from CQDM, Ontario Brain Institute (OBI), Brain Canada and participating members (as financial contributors) Pfizer Canada Inc. and Merck Canada Inc. for the project entitled “Solid phase microextraction-based integrated platform for untargeted and targeted *in vivo* brain studies.”. The authors would like to thank Millipore Sigma for providing *in vivo* SPME fibres.

4. Conclusions and future work

4.1. Conclusions

SPME had been used in *ex vivo* lipidomic studies but has not been previously used for *in vivo* lipidomic studies. This study's major aim was to evaluate SPME viability for use as an *in vivo* method to extract lipids from brains of live animals.

The results of this thesis clearly demonstrate that SPME can extract similar lipids to what is observed with Folch extractions of the same region of brain, the hippocampus. However, total lipid coverage of the miniaturized *in vivo* SPME resulted in a drastic difference in detected features with only 147 features detected in positive mode compared to 1368 detected in the Folch extract. In negative mode ESI, difference in detected features was not as pronounced with 613 features detected in the SPME extract compared to the 1161 features detected in the Folch extracts. Despite the large difference in detected features, these results are exciting as they represent the first time that lipids were measured directly *in vivo* in living animals to the best of my knowledge. This opens up new possibilities to monitor the effect of drugs, disease, genetic mutations or other stimuli on *in vivo* lipid concentrations in different regions of the brain.

The main reasons behind lower coverage of *in vivo* SPME are both biological and analytical. From the biological perspective SPME only extracts free lipids. Lipids, due to their hydrophobic nature, are highly bound, so their free concentrations are very low. From the analytical perspective, the SPME fibres' small dimensions mean that only small amounts of analyte are extracted. This in turn requires very sensitive analytical instrumentation with low LOD. Using a more powerful MS would be expected to decrease the LOD leading to an increase in SPME coverage. Additionally, MS instrumentation is still improving resulting in an overall increase in SPME coverage.

When comparing the number of lipids confidently identified with LipidSearch software, despite very small amounts of lipids extracted by SPME, good quality MS/MS spectra were acquired resulting in confident identification of 127 lipids versus 145 lipids identified in Folch extract in positive ESI mode. In positive mode, 37 of the 127 lipids identified with LipidSearch in the *in vivo* samples were among some of the most abundant 145 lipids identified in the Folch extracts. In negative mode, 34 lipids identified with LipidSearch in the *in vivo* samples were also identified in the Folch extracts. This shows that lipid concentration, as expected, is important

contributing factor to whether a given lipid will be detected by SPME. However, clearly lipid binding status and/or incorporation into membrane can result in highly abundant lipids detected by Folch method, not being identified in the *in vivo* SPME extracts of the same brain region. SPME may therefore allow determination of complementary information regarding the free concentrations of lipid species which cannot be obtained from a Folch extraction. It is interesting to note that although more putative lipids were detected in negative mode only half the number of lipids were confidently identified compared to positive mode. This decrease in identification of lipids in negative mode may be due to the problem of “chimera” MS/MS spectra where lipids with the same *m/z* and retention time are chosen for fragmentation at the same time leading to incomplete identification. This could be addressed by extending the LC separation time to attempt to separate co-eluting lipid species.

In positive ESI, SPME and Folch extracts showed a large difference in lipid class profile as only 3% of the identified lipids in the SPME extracts were GP while this number was much larger in the Folch extracts at 40%. This is possibly due to the GP not being available for extraction by SPME due to membrane binding and/or incorporation in the membrane. Another possibility is that the GP are present in very low concentrations and in the SPME fractions they are below the LOD of the instrument. In negative ESI, SPME and Folch extraction had a similar lipid subclass profile. The % of lipid classes in the SPME and Folch extracts were very similar with 5% SL and 93% GP in the SPME extracts and 7% SL and 93% GP in the Folch extracts. The matrix effects of both extracts were examined. As expected, the non-exhaustive SPME technique reduced the amount of matrix effects observed compared to the exhaustive, LLE Folch method. Matrix effects for only LPE, PS, PE in ESI⁺ and LPS, PE, and PC ESI⁻ were observed for SPME among the lipid standards tested.

A consequence of optimizing the LC-MS for lipidomics to achieve as high SPME lipid coverage as possible was the finding that the use of acetic acid as a mobile phase additive in ESI⁻ can help increase signal intensity and lipid coverage. To investigate this, 0.02% AA was compared to three other popular additive choices that are part of a wide range of mobile phases are used in the literature for lipidomic studies: 10 mM AmAc, 10 mM AmAc with 0.02% AA and 0.014-0.05% AmOH. Our work supports previous targeted and metabolomic studies' conclusion that AA is a superior choice as a weak acid additive in ESI⁻, and expands it for the first time to lipids. Our investigation showed that AA contributes to the ionization efficiency via solution-phase, gas-

phase and droplet-surface interactions with the analytes. It caused an increase in signal of up to 1000-fold when compared to AmOH and up to 19-fold when compared to AmAc. The increase was dependent on lipid subclass with significant improvements observed for 11 lipid subclasses. For two subclasses, there was a decrease in ionization efficiency: ceramide and PC. Peak shape of PA and PS deteriorated with the use of AA but was compensated by an increase in peak height, still resulting in improved S/N ratios. No peak shape deterioration was observed for any of the other GPs and SLs observed. In addition to benefits of increased ionization efficiency the use of AA allowed for an increase in detected features by 60% when compared to AmAc and from 40-200% when compared to various concentrations of AmOH.

The effect of pH on negative ESI ionization has been investigated for only a small number of compounds which did not include lipids. As pH plays a role on ionization efficiency, this study will help contribute to the overall understanding of the role of pH and ESI. Computational modelling of the complex interaction of an additive in gas-phase, solution-phase and at the surface of the ESI droplet may help to predict which mobile phase additive best suits the analysis of a given analyte.

4.2. Future work

This study of *in vivo* SPME viability as a technique for brain lipidomics is a first preliminary step in the evaluation and validation of the technique.

Extraction time profiles of lipids showed some interesting results such as possible displacement of TG and degradation of LPS. These experiments need to be repeated so that more accurate extraction time profiles can be obtained to get a better understanding of a lipids extraction from a complex biological matrix like brain tissue. Inter-fibre reproducibility should be assessed and using only reliable fibres should improve the overall quality of the experiment by reducing the error on observations due to fibre irreproducibility. Additional time points between 2 and 20 hours would help to plot and interpret lipid extraction profiles. The fact that displacement was observed in tissue samples but not solvent samples in conjunction with the difference in extraction time on overall lipid coverage shows that optimization in tissue samples is crucial.

The recovery and K_{fs} values of different lipid classes will allow a more complete picture of the efficacy of SPME as an extraction method. Once these values are known it will determine for

which lipid classes SPME C₁₈ is suitable for and guide the choice of sorbent for other lipid classes that are not suited to C₁₈. For these reasons these two parameters need to be evaluated.

A more direct comparison of *in vivo* SPME to Folch with a larger number of samples is required. This comparison will use brain tissue sample from the same rats that the *in vivo* SPME has been performed on compensating for the biological heterogeneity observed in this study. The sample size will also be increased allowing for better data quality and interpretation. *In vivo* SPME has previously been shown to capture unstable metabolites prone to enzymatic conversion. This is potentially the case for lipidomics as well as lipids were identified in *in vivo* SPME samples that were not identified in the Folch extracts.

The disparity between the number of features detected with SIEVE and the number of confidently identified lipids with LipidSearch is very large and warrants further investigation such as comparing the amount of MS/MS spectra that are triggered and collected versus how many confident identifications are being obtained. If there are many “chimera” spectra being obtained due to co-elution of lipid species with the same m/z LC run-time may be lengthened to improve separation and increase the amount of high quality MS/MS spectra that are obtained. Only one collision energy was used in this study. Altering the collision energy can help improve identification of lipids by improving the spectra obtained. For larger lipids increasing the collision energy may result in successful fragmentation that is not possible at lower collision energies.

References

- [1] X. Han. *Lipidomics Comprehensive Mass Spectrometry of Lipids*. **2016**.
- [2] A. D. Watson. Thematic review series: Systems Biology Approaches to Metabolic and Cardiovascular Disorders. Lipidomics: a global approach to lipid analysis in biological systems. *J. Lipid Res.* **2006**, *47*, 2101.
- [3] M. Ståhlman, J. Boren, K. Ekroos. *Lipidomics: Technologies and Applications, Chapter 3*. Wiley-VCH, **2012**.
- [4] M. M. Siddique, S. A. Summers. *Lipidomics: Technologies and Applications, Chapter 9*. Wiley-VCH, **2012**.
- [5] M. Söderberg, C. Edlund, I. Alafuzoff, K. Kristensson, G. Dallner. Lipid composition in different regions of the brain in Alzheimer's disease/senile dementia of Alzheimer's type. *J. Neurochem.* **1992**, *59*, 1646.
- [6] M. Puppolo, D. Varma, S. A. Jansen. A review of analytical methods for eicosanoids in brain tissue. *J. Chromatogr. B* **2014**, *964*, 50.
- [7] R. B. Chan, T. G. Oliveira, E. P. Cortes, L. S. Honig, K. E. Duff, S. A. Small, M. R. Wenk, G. Shui, G. Di Paolo. Comparative Lipidomic Analysis of Mouse and Human Brain with Alzheimer Disease. *J. Biol. Chem.* **2012**, *287*, 2679.
- [8] M. Jové, A. Naudí, M. Portero-Otin, R. Cabré, S. Rovira-Llopis, C. Bañuls, M. Rocha, A. Hernández-Mijares, V. M. Victor, R. Pamplona. Plasma lipidomics discloses metabolic syndrome with a specific HDL phenotype. *FASEB J.* **2014**, *28*, 5163.
- [9] R. L. Kozlowski, T. W. Mitchell, S. J. Blanksby. A rapid ambient ionization-mass spectrometry approach to monitoring the relative abundance of isomeric glycerophospholipids. *Sci. Rep.* **2015**, *5*.
- [10] M. C. Thomas, T. W. Mitchell, D. G. Harman, J. M. Deeley, J. R. Nealon, S. J. Blanksby. Ozone-induced dissociation: Elucidation of double bond position within mass-selected lipid ions. *Anal. Chem.* **2008**, *80*, 303.
- [11] G. F. Gibbons, K. Islam, R. J. Pease. Mobilisation of triacylglycerol stores. *Biochim. Biophys. Acta - Mol. Cell Biol. Lipids* **2000**, *1483*, 37.
- [12] R. A. Coleman, D. P. Lee. Enzymes of triacylglycerol synthesis and their regulation. *Prog. Lipid Res.* **2004**, *43*, 134.
- [13] H. Mulder, L. S. Holst, H. Svensson, E. Degerman, F. Sundler, B. Ahrén, P. Rorsman, C. Holm. Hormone-sensitive lipase, the rate-limiting enzyme in triglyceride hydrolysis, is expressed and active in β -cells. *Diabetes* **1999**, *48*, 228.
- [14] C. P. Müller, M. Reichel, C. Mühle, C. Rhein, E. Gulbins, J. Kornhuber. Brain membrane lipids in major depression and anxiety disorders. *Biochim. Biophys. Acta - Mol. Cell Biol. Lipids* **2015**, *1851*, 1052.
- [15] B. Payrastre, K. Missy, S. Giuriato, S. Bodin, M. Plantavid, M. P. Gratacap. Phosphoinositides: Key players in cell signalling, in time and space. *Cell. Signal.* **2001**, *13*, 377.
- [16] M. G. Waugh. PIPs in neurological diseases. *Biochim. Biophys. Acta - Mol. Cell Biol. Lipids* **2015**, *1851*, 1066.

- [17] F. Sabourdy, L. Astudillo, C. Colacios, P. Dubot, M. Mrad, B. Segui, N. Andrieu-Abadie, T. Levade. Monogenic neurological disorders of sphingolipid metabolism. *Biochim. Biophys. Acta - Mol. Cell Biol. Lipids* **2014**, *1851*, 1040.
- [18] D. S. Menaldino, A. Bushnev, A. Sun, D. C. Liotta, H. Symolon, K. Desai, D. L. Dillehay, Q. Peng, E. Wang, J. Allegood, S. Trotman-Pruett, M. C. Sullards, A. H. Merrill. Sphingoid bases and de novo ceramide synthesis: Enzymes involved, pharmacology and mechanisms of action. *Pharmacol. Res.* **2003**, *47*, 373.
- [19] A. N. Moore, A. W. Kampfl, X. Zhao, R. L. Hayes, P. K. Dash. Sphingosine-1-phosphate induces apoptosis of cultured hippocampal neurons that requires protein phosphatases and activator protein-1 complexes. *Neuroscience* **1999**, *94*, 405.
- [20] M. Jatana, S. Giri, A. K. Singh. Apoptotic positive cells in Krabbe brain and induction of apoptosis in rat C6 glial cells by psychosine. *Neurosci. Lett.* **2002**, *330*, 183.
- [21] I. Galve-Roperh, C. Sánchez, M. L. Cortés, T. G. Del Pulgar, M. Izquierdo, M. Guzmán. Anti-tumoral action of cannabinoids: Involvement of sustained ceramide accumulation and extracellular signal-regulated kinase activation. *Nat. Med.* **2000**, *6*, 313.
- [22] J. R. Van Brocklyn, C. A. Letterle, P. J. Snyder, T. W. Prior. Sphingosine-1-phosphate stimulates human glioma cell proliferation through Gi-coupled receptors: role of ERK MAP kinase and phosphatidylinositol 3-kinase β . *Cancer Lett.* **2002**, *181*, 195.
- [23] A. Kimura, T. Ohmori, R. Ohkawa, S. Madoiwa, J. Mimuro, T. Murakami, E. Kobayashi, Y. Hoshino, Y. Yatomi, Y. Sakata. Essential Roles of Sphingosine 1-Phosphate/S1P1 Receptor Axis in the Migration of Neural Stem Cells Toward a Site of Spinal Cord Injury. *Stem Cells* **2007**, *25*, 115.
- [24] S. Shirao, S. Kashiwagi, M. Sato, S. Miwa, F. Nakao, T. Kurokawa, N. Todoroki-Ikeda, K. Mogami, Y. Mizukami, S. Kuriyama, K. Haze, M. Suzuki, S. Kobayashi. Sphingosylphosphorylcholine Is a Novel Messenger for Rho-Kinase-Mediated Ca^{2+} Sensitization in the Bovine Cerebral Artery. *Circ. Res.* **2002**, *91*, 112 LP.
- [25] B. M. Altura, A. Gebrewold, T. Zheng, B. T. Altura. Sphingomyelinase and ceramide analogs induce vasoconstriction and leukocyte-endothelial interactions in cerebral venules in the intact rat brain: Insight into mechanisms and possible relation to brain injury and stroke. *Brain Res. Bull.* **2002**, *58*, 271.
- [26] D. A. Butterfield, J. Drake, C. Pocernich, A. Castegna. Evidence of oxidative damage in Alzheimer's disease brain: central role for amyloid β -peptide. *Trends Mol. Med.* **2001**, *7*, 548.
- [27] B. T. Hyman, G. W. Van Hoesen, A. R. Damasio, C. L. Barnes. Alzheimer's disease: cell-specific pathology isolates the hippocampal formation. *Science* **1984**, *225*, 1168.
- [28] J. D. Bremner, M. Narayan, E. R. Anderson, L. H. Staib, H. L. Miller, D. S. Charney. Hippocampal Volume Reduction in Major Depression. *Am. J. Psychiatry* **2000**, *157*, 115.
- [29] P. Videbech, B. Ravnkilde. Hippocampal Volume and Depression: A Meta-Analysis of MRI Studies. *Am. J. Psychiatry* **2004**, *161*, 1957.
- [30] B. Knutson, C. M. Adams, G. W. Fong, D. Hommer. Anticipation of increasing monetary reward selectively recruits nucleus accumbens. *J. Neurosci.* **2001**, *21*, RC159.
- [31] T. W. Robbins, B. J. Everitt. Drug addiction: bad habits add up. *Nature* **1999**, *398*, 567.
- [32] G. Di Chiara, V. Bassareo, S. Fenu, M. A. De Luca, L. Spina, C. Cadoni, E. Acquas, E. Carboni,

- V. Valentini, D. Lecca. Dopamine and drug addiction: the nucleus accumbens shell connection. *Neuropharmacology* **2004**, *47*, 227.
- [33] J. S. O. Brien, E. L. Sampson. Lipid composition of the normal human brain: gray matter, white matter and myelin. *J. Lipid Res.* **1965**, *6*.
- [34] M. Sud, E. Fahy, D. Cotter, A. Brown, E. A. Dennis, C. K. Glass, A. H. Merrill, R. C. Murphy, C. R. H. Raetz, D. W. Russell. LMSD: lipid maps structure database. *Nucleic Acids Res.* **2007**, *35*, D527.
- [35] R. Almeida, J. K. Pauling, E. Sokol, H. K. Hannibal-Bach, C. S. Ejsing. Comprehensive lipidome analysis by shotgun lipidomics on a hybrid quadrupole-orbitrap-linear ion trap mass spectrometer. *J. Am. Soc. Mass Spectrom.* **2014**, *26*, 133.
- [36] R. Almeida, Z. Berzina, E. C. Arnspang, J. Baumgart, J. Vogt, R. Nitsch, C. S. Ejsing. Quantitative spatial analysis of the mouse brain lipidome by pressurized liquid extraction surface analysis. *Anal. Chem.* **2015**, *87*, 1749.
- [37] I. Rappley, D. S. Myers, S. B. Milne, P. T. Ivanova, M. J. Lavoie, H. A. Brown, D. J. Selkoe. Lipidomic profiling in mouse brain reveals differences between ages and genders, with smaller changes associated with α -synuclein genotype. *J. Neurochem.* **2009**, *111*, 15.
- [38] O. Quehenberger, A. M. Armando, A. H. Brown, S. B. Milne, D. S. Myers, A. H. Merrill, S. Bandyopadhyay, K. N. Jones, S. Kelly, R. L. Shaner, C. M. Sullards, E. Wang, R. C. Murphy, R. M. Barkley, et al. Lipidomics reveals a remarkable diversity of lipids in human plasma. *J. Lipid Res.* **2010**, *51*, 3299.
- [39] P. Green, N. Anyakoha, G. Yadid, I. Gispan-Herman, A. Nicolaou. Arachidonic acid-containing phosphatidylcholine species are increased in selected brain regions of a depressive animal model: Implications for pathophysiology. *Prostaglandins Leukot. Essent. Fat. Acids* **2009**, *80*, 213.
- [40] M. H. Sarafian, M. Gaudin, M. R. Lewis, F. P. Martin, E. Holmes, J. K. Nicholson, M. E. Dumas. Objective set of criteria for optimization of sample preparation procedures for ultra-high throughput untargeted blood plasma lipid profiling by ultra performance liquid chromatography-mass spectrometry. *Anal. Chem.* **2014**, *86*, 5766.
- [41] A. Triebel, M. Trötz Müller, J. Hartler, T. Stojakovic, H. C. Köfeler. Lipidomics by ultrahigh performance liquid chromatography-high resolution mass spectrometry and its application to complex biological samples. *J. Chromatogr. B Anal. Technol. Biomed. Life Sci.* **2017**, *1053*, 72.
- [42] W. Hewelt-Belka, J. Nakonieczna, M. Belka, T. Baczek, J. Namieśnik, A. Kot-Wasik. Comprehensive methodology for *Staphylococcus aureus* lipidomics by liquid chromatography and quadrupole time-of-flight mass spectrometry. *J. Chromatogr. A* **2014**, *1362*, 62.
- [43] A. Reis, A. Rudnitskaya, G. J. Blackburn, N. M. Fauzi, A. R. Pitt, C. M. Spickett. A comparison of five lipid extraction solvent systems for lipidomic studies of human LDL. *J. Lipid Res.* **2013**, *54*, 1812.
- [44] K. Jurowski, K. Kochan, J. Walczak, M. Barańska, W. Piekoszewski, B. Buszewski. Comprehensive review of trends and analytical strategies applied for biological samples preparation and storage in modern medical lipidomics: State of the art. *TrAC Trends Anal. Chem.* **2017**, *86*, 276.
- [45] T. Cajka, O. Fiehn. Toward Merging Untargeted and Targeted Methods in Mass Spectrometry-Based Metabolomics and Lipidomics. *Anal. Chem.* **2016**, *88*, 524.
- [46] J. Folch, M. Lees, G. Stanley. A simple method for the isolation and purification of total lipids

- from animal tissues. *J Biol Chem. J. Biol. Chem.* **1957**, 226, 497.
- [47] E. G. Bligh, W. J. Dyer. A rapid method of total lipid extraction and purification. *Can. J. Biochem. Physiol.* **1959**, 37, 911.
- [48] S. J. Iverson, S. L. Lang, M. H. Cooper. Comparison of the Bligh and Dyer and Folch methods for total lipid determination in a broad range of marine tissue. *Lipids* **2001**, 36, 1283.
- [49] L. Löfgren, M. Ståhlman, G.-B. G.-B. Forsberg, S. Saarinen, R. Nilsson, G. I. Hansson. The BUMÉ method: a novel automated chloroform-free 96-well total lipid extraction method for blood plasma. *J. Lipid Res.* **2012**, 53, 1690.
- [50] V. Matyash, G. Liebisch, T. V Kurzchalia, A. Shevchenko, D. Schwudke. Lipid extraction by methyl-tert-butyl ether for high-throughput lipidomics. *J. Lipid Res.* **2008**, 49, 1137.
- [51] J. Sheng, R. Vannela, B. E. Rittmann. Evaluation of methods to extract and quantify lipids from *Synechocystis* PCC 6803. *Bioresour. Technol.* **2011**, 102, 1697.
- [52] D. J. Weiss, C. E. Lunte, S. M. Lunte. In vivo microdialysis as a tool for monitoring pharmacokinetics. *TrAC - Trends Anal. Chem.* **2000**, 19, 606.
- [53] A. N. Khramov, J. A. Stenken. Enhanced microdialysis extraction efficiency of ibuprofen in vitro by facilitated transport with beta-cyclodextrin. *Anal. Chem.* **1999**, 71, 1257.
- [54] C. Carneheim, L. Stähle. Microdialysis of Lipophilic Compounds: A Methodological Study. *Pharmacol. Toxicol.* **1991**, 69, 378.
- [55] E. Cudjoe, B. Bojko, I. de Lannoy, V. Saldivia, J. Pawliszyn. Solid-Phase Microextraction: A Complementary In Vivo Sampling Method to Microdialysis. *Angew. Chemie Int. Ed.* **2013**, 52, 12124.
- [56] M. I. Davies, J. D. Cooper, S. S. Desmond, C. E. Lunte, S. M. Lunte. Analytical considerations for microdialysis sampling. *Adv. Drug Deliv. Rev.* **2000**, 45, 169.
- [57] M. I. Davies. A review of microdialysis sampling for pharmacokinetic applications. *Anal. Chim. Acta* **1999**, 379, 227.
- [58] P. Nandi, S. M. Lunte. Recent trends in microdialysis sampling integrated with conventional and microanalytical systems for monitoring biological events: A review. *Anal. Chim. Acta* **2009**, 651, 1.
- [59] A. Stefani, V. Trendafilov, C. Liguori, E. Fedele, S. Galati. Subthalamic nucleus deep brain stimulation on motor-symptoms of Parkinson's disease: Focus on neurochemistry. *Prog. Neurobiol.* **2017**, 151, 157.
- [60] S. Nomura, T. Inoue, H. Imoto, E. Suehiro, Y. Maruta, Y. Hirayama, M. Suzuki. Effects of focal brain cooling on extracellular concentrations of neurotransmitters in patients with epilepsy. *Epilepsia* **2017**, 58, 627.
- [61] K. Antoniou, A. Polissidis, F. Delis, N. Pouliou. The impact of cannabinoids on motor activity and neurochemical correlates. *Neuromethods* **2017**, 121, 341.
- [62] A. Kastellakis, J. Radke, K. Thermos. Functional mapping of somatostatin receptors in brain: In vivo microdialysis studies. *Neuromethods* **2017**, 121, 317.
- [63] É. A. Souza-Silva, R. Jiang, A. Rodríguez-Lafuente, E. Gionfriddo, J. Pawliszyn. A critical review of the state of the art of solid-phase microextraction of complex matrices I. Environmental analysis. *TrAC - Trends Anal. Chem.* **2015**, 71, 224.

- [64] É. A. Souza-Silva, E. Gionfriddo, J. Pawliszyn. A critical review of the state of the art of solid-phase microextraction of complex matrices II. Food analysis. *TrAC - Trends Anal. Chem.* **2015**, *71*, 236.
- [65] É. A. Souza-Silva, N. Reyes-Garcés, G. A. Gómez-Ríos, E. Boyaci, B. Bojko, J. Pawliszyn. A critical review of the state of the art of solid-phase microextraction of complex matrices III. Bioanalytical and clinical applications. *TrAC - Trends Anal. Chem.* **2015**, *71*, 249.
- [66] G. Ouyang, D. Vuckovic, J. Pawliszyn. Nondestructive sampling of living systems using in vivo solid-phase microextraction. **2011**, *111*, 2784.
- [67] D. Vuckovic, I. De Lannoy, B. Gien, R. E. Shirey, L. M. Sidisky, S. Dutta, J. Pawliszyn. In vivo solid-phase microextraction: Capturing the elusive portion of metabolome. *Angew. Chemie - Int. Ed.* **2011**, *50*, 5344.
- [68] J. C. Y. Yeung, I. de Lannoy, B. Gien, D. Vuckovic, Y. Yang, B. Bojko, J. Pawliszyn. Semi-automated in vivo solid-phase microextraction sampling and the diffusion-based interface calibration model to determine the pharmacokinetics of methoxyfenoterol and fenoterol in rats. *Anal. Chim. Acta* **2012**, *742*, 37.
- [69] F. M. Musteata, I. de Lannoy, B. Gien, J. Pawliszyn. Blood sampling without blood draws for in vivo pharmacokinetic studies in rats. *J. Pharm. Biomed. Anal.* **2008**, *47*, 907.
- [70] D. Vuckovic, I. de Lannoy, B. Gien, Y. Yang, F. M. Musteata, R. Shirey, L. Sidisky, J. Pawliszyn. In vivo solid-phase microextraction for single rodent pharmacokinetics studies of carbamazepine and carbamazepine-10,11-epoxide in mice. *J. Chromatogr. A* **2011**, *1218*, 3367.
- [71] X. Zhang, A. Es-haghi, J. Cai, J. Pawliszyn. Simplified kinetic calibration of solid-phase microextraction for in vivo pharmacokinetics. *J. Chromatogr. A* **2009**, *1216*, 7664.
- [72] Z. Bai, A. Pilote, P. K. Sarker, G. Vandenberg, J. Pawliszyn. In vivo solid-phase microextraction with in vitro calibration: Determination of off-flavor components in live fish. *Anal. Chem.* **2013**, *85*, 2328.
- [73] A. P. Birjandi, F. S. Mirnaghi, B. Bojko, M. Wąsowicz, J. Pawliszyn. Application of solid phase microextraction for quantitation of polyunsaturated Fatty acids in biological fluids. *Anal. Chem.* **2014**, *86*, 12022.
- [74] A. P. Birjandi, B. Bojko, Z. Ning, D. Figeys, J. Pawliszyn. High throughput solid phase microextraction: A new alternative for analysis of cellular lipidome? *J. Chromatogr. B Anal. Technol. Biomed. Life Sci.* **2016**, *1043*, 12.
- [75] T. Cajka, O. Fiehn. Comprehensive analysis of lipids in biological systems by liquid chromatography-mass spectrometry. *TrAC - Trends Anal. Chem.* **2014**, *61*, 192.
- [76] D. C. Harris. *Quantitative Chemical Analysis*. Macmillan, **2010**.
- [77] P. Jiang, C. A. Lucy. Coupling normal phase liquid chromatography with electrospray ionization mass spectrometry: strategies and applications. *Anal. Methods* **2016**, *8*, 6478.
- [78] N. Christinat, D. Morin-Rivron, M. Masoodi. High-Throughput Quantitative Lipidomics Analysis of Nonesterified Fatty Acids in Human Plasma. *J. Proteome Res.* **2016**, *15*, 2228.
- [79] T. Cajka, O. Fiehn. Increasing lipidomic coverage by selecting optimal mobile-phase modifiers in LC-MS of blood plasma. *Metabolomics* **2016**, *12*, 34.
- [80] C. W. N. Damen, G. Isaac, J. Langridge, T. Hankemeier, R. J. Vreeken. Enhanced lipid isomer

- separation in human plasma using reversed-phase UPLC with ion-mobility/high-resolution MS detection. *J. Lipid Res.* **2014**, *55*, 1772.
- [81] N. Abbassi-Ghadi, E. A. Jones, M. Gomez-Romero, O. Golf, S. Kumar, J. Huang, H. Kudo, R. D. Goldin, G. B. Hanna, Z. Takats. A Comparison of DESI-MS and LC-MS for the Lipidomic Profiling of Human Cancer Tissue. *J. Am. Soc. Mass Spectrom.* **2016**, *27*, 255.
- [82] M. Ghaste, R. Mistrik, V. Shulaev. Applications of fourier transform ion cyclotron resonance (FT-ICR) and orbitrap based high resolution mass spectrometry in metabolomics and lipidomics. *Int. J. Mol. Sci.* **2016**, *17*, DOI 10.3390/ijms17060816.
- [83] R. J. Malott, C. H. Wu, T. D. Lee, T. J. Hird, N. F. Dalleska, J. E. A. Zlosnik, D. K. Newman, D. P. Speert. Fosmidomycin decreases membrane hopanoids and potentiates the effects of colistin on burkholderia multivorans clinical isolates. *Antimicrob. Agents Chemother.* **2014**, *58*, 5211.
- [84] K. D. Wyndham, J. E. O’Gara, T. H. Walter, K. H. Glose, N. L. Lawrence, B. A. Alden, G. S. Izzo, C. J. Hudalla, P. C. Iraneta. Characterization and evaluation of C18HPLC stationary phases based on ethyl-bridged hybrid organic/inorganic particles. *Anal. Chem.* **2003**, *75*, 6781.
- [85] J. Zeleny. The electrical discharge from liquid points, and a hydrostatic method of measuring the electric intensity at their surfaces. *Phys. Rev.* **1914**, *3*, 69.
- [86] J. Zeleny. Instability of electrified liquid surfaces. *Phys. Rev.* **1917**, *10*, 1.
- [87] J. B. Fenn, M. Mann, C. K. Meng, S. F. Wong, C. M. Whitehouse. Electrospray ionization for mass spectrometry of large biomolecules. *Science (80-.)*. **1989**, *246*, 64.
- [88] R. Kostianen, T. J. Kauppila. Effect of eluent on the ionization process in liquid chromatography-mass spectrometry. *J. Chromatogr. A* **2009**, *1216*, 685.
- [89] Lord Rayleigh. XX. On the equilibrium of liquid conducting masses charged with electricity. *Philos. Mag. Ser. 5* **1882**, *14*, 184.
- [90] L. Konermann, E. Ahadi, A. D. Rodriguez, S. Vahidi. Unraveling the mechanism of electrospray ionization. *Anal. Chem.* **2013**, *85*, 2.
- [91] E. Ahadi, L. Konermann. Ejection of Solvated Ions from Electrosprayed Methanol / Water Nanodroplets Studied by Molecular Dynamics Simulations. *J. Am. Chem. Soc.* **2011**, *133*, 9354.
- [92] Agilent. Agilent 6200 Series TOF and 6500 Series Q-TOF LC / MS System Concepts Guide. **2012**, 17.
- [93] S. Lacorte, A. R. Fernandez-Alba. Time of flight mass spectrometry applied to the liquid chromatographic analysis of pesticides in water and food. *Mass Spectrom. Rev.* **2006**, *25*, 866.
- [94] A. W. T. Bristow, K. S. Webb. Intercomparison study on accurate mass measurement of small molecules in mass spectrometry. *J. Am. Soc. Mass Spectrom.* **2003**, *14*, 1086.
- [95] A. Makarov. Electrostatic Axially Harmonic Orbital Trapping: A High-Performance Technique of Mass Analysis. **2000**, *72*, 1156.
- [96] S. Eliuk, A. Makarov. Evolution of Orbitrap Mass Spectrometry Instrumentation. *Annu. Rev. Anal. Chem.* **2015**, *8*, 61.
- [97] J. V Olsen, J. Schwartz, J. Griep-Raming, M. L. Nielsen, E. Damoc, E. Denisov, O. Lange, P. Remes, D. Taylor, M. Splendore, E. R. Wouters, M. Senko, A. Makarov, M. Mann, et al. A dual pressure linear ion trap Orbitrap instrument with very high sequencing speed. *Mol. Cell. Proteomics* **2009**, *8*, 2759.

- [98] M. Katajamaa, M. Orešič. Data processing for mass spectrometry-based metabolomics. *J. Chromatogr. A* **2007**, *1158*, 318.
- [99] R. Taguchi, M. Ishikawa. Precise and global identification of phospholipid molecular species by an Orbitrap mass spectrometer and automated search engine Lipid Search. *J. Chromatogr. A* **2010**, *1217*, 4229.
- [100] M. Koivusalo, P. Haimi, L. Heikinheimo, R. Kostainen, P. Somerharju. Quantitative determination of phospholipid compositions by ESI-MS: effects of acyl chain length, unsaturation, and lipid concentration on instrument response. *J. Lipid Res.* **2001**, *42*, 663.
- [101] S. Milne, P. Ivanova, J. Forrester, H. Alex Brown. Lipidomics: An analysis of cellular lipids by ESI-MS. *Methods* **2006**, *39*, 92.
- [102] C. R. Mallet, Z. Lu, J. R. Mazzeo. A study of ion suppression effects in electrospray ionization from mobile phase additives and solid-phase extracts. *Rapid Commun. Mass Spectrom.* **2004**, *18*, 49.
- [103] N. B. Cech, C. G. Enke. Practical implications of some recent studies in electrospray ionization fundamentals. *Mass Spectrom. Rev.* **2001**, *20*, 362.
- [104] B. A. Huffman, M. L. Poltash, C. A. Hughey. Effect of polar protic and polar aprotic solvents on negative-ion electrospray ionization and chromatographic separation of small acidic molecules. *Anal. Chem.* **2012**, *84*, 9942.
- [105] T. Henriksen, R. K. Juhler, B. Svensmark, N. B. Cech. The relative influences of acidity and polarity on responsiveness of small organic molecules to analysis with negative ion electrospray ionization mass spectrometry (ESI-MS). *J. Am. Soc. Mass Spectrom.* **2005**, *16*, 446.
- [106] J. Liigand, A. Laaniste, A. Kruve. pH Effects on Electrospray Ionization Efficiency. *J. Am. Soc. Mass Spectrom.* **2016**, *28*, 461.
- [107] A. Kruve, K. Kaupmees, J. Liigand, I. Leito. Negative electrospray ionization via deprotonation: Predicting the ionization efficiency. *Anal. Chem.* **2014**, *86*, 4822.
- [108] A. M. Kamel, P. R. Brown, B. Munson. Effects of mobile-phase additives, solution pH, ionization constant, and analyte concentration on the sensitivities and electrospray ionization mass spectra of nucleoside antiviral agents. *Anal. Chem.* **1999**, *71*, 5481.
- [109] B. M. Ehrmann, T. Henriksen, N. B. Cech. Relative Importance of Basicity in the Gas Phase and in Solution for Determining Selectivity in Electrospray Ionization Mass Spectrometry. *J. Am. Soc. Mass Spectrom.* **2008**, *19*, 719.
- [110] O. Yanes, R. Tautenhahn, G. J. Patti, G. Siuzdak. Expanding coverage of the metabolome for global metabolite profiling. *Anal. Chem.* **2011**, *83*, 2152.
- [111] X. J. Yang, Y. Qu, Q. Yuan, P. Wan, Z. Du, D. Chen, C. Wong. Effect of ammonium on liquid- and gas-phase protonation and deprotonation in electrospray ionization mass spectrometry. *Analyst* **2013**, *138*, 659.
- [112] B. a. Mansoori, D. a. Volmer, R. K. Boyd. "Wrong-way-round" Electrospray Ionization of Amino Acids. *Rapid Commun. Mass Spectrom.* **1997**, *11*, 1120.
- [113] K. Schug, H. M. McNair. Adduct formation in electrospray ionization. Part 1: Common acidic pharmaceuticals. *J. Sep. Sci.* **2002**, *25*, 759.
- [114] S. Zhou, K. D. Cook. Protonation in Electrospray Mass Spectrometry : Wrong-Way-Round or

- Right-Way-Round? *J. Am. Soc. Mass Spectrom.* **2000**, *11*, 961.
- [115] Z. R. Wu, W. Q. Gao, M. A. Phelps, D. Wu, D. D. Miller, J. T. Dalton. Favorable effects of weak acids on negative-ion electrospray ionization mass spectrometry. *Anal. Chem.* **2004**, *76*, 839.
- [116] X. Zhang, M. R. Clausen, X. Zhao, H. Zheng, H. C. Bertram. Enhancing the power of liquid chromatography-mass spectrometry-based urine metabolomics in negative ion mode by optimization of the additive. *Anal. Chem.* **2012**, *84*, 7785.
- [117] M. Ovčáčíková, M. Lisa, E. Cífková, M. Holčapek. Retention behavior of lipids in reversed-phase ultrahigh-performance liquid chromatography-electrospray ionization mass spectrometry. *J. Chromatogr. A* **2016**, *1450*, 76.
- [118] L. Wang, C. Hu, S. Liu, M. Chang, P. Gao, L. Wang, Z. Pan, G. Xu. Plasma lipidomics investigation of hemodialysis effects by using liquid chromatography-mass spectrometry. *J. Proteome Res.* **2016**, *15*, 1986.
- [119] S. Chen, C. Wei, P. Gao, H. Kong, Z. Jia, C. Hu, W. Dai, Y. Wu, G. Xu. Effect of Allium macrostemon on a rat model of depression studied by using plasma lipid and acylcarnitine profiles from liquid chromatography/mass spectrometry. *J. Pharm. Biomed. Anal.* **2014**, *89*, 122.
- [120] D. Y. Bang, M. H. Moon. On-line two-dimensional capillary strong anion exchange/reversed phase liquid chromatography-tandem mass spectrometry for comprehensive lipid analysis. *J. Chromatogr. A* **2013**, *1310*, 82.
- [121] A. I. Ostermann, I. Willenberg, N. H. Schebb. Comparison of sample preparation methods for the quantitative analysis of eicosanoids and other oxylipins in plasma by means of LC-MS/MS. *Anal. Bioanal. Chem.* **2015**, *407*, 1403.
- [122] Y. Wang, A. M. Armando, O. Quehenberger, C. Yan, E. A. Dennis. Comprehensive ultra-performance liquid chromatographic separation and mass spectrometric analysis of eicosanoid metabolites in human samples. *J. Chromatogr. A* **2014**, *1359*, 60.
- [123] O. Uhl, C. Glaser, H. Demmelmair, B. Koletzko. Reversed phase LC/MS/MS method for targeted quantification of glycerophospholipid molecular species in plasma. *J. Chromatogr. B* **2011**, *879*, 3556.
- [124] D. Y. Bang, S. Lim, M. H. Moon. Effect of ionization modifiers on the simultaneous analysis of all classes of phospholipids by nanoflow liquid chromatography/tandem mass spectrometry in negative ion mode. *J. Chromatogr. A* **2012**, *1240*, 69.
- [125] M. Nazari, D. C. Muddiman. Polarity Switching Mass Spectrometry Imaging of Healthy and Cancerous Hen Ovarian Tissue Sections by Infrared Matrix-Assisted Laser Desorption Electrospray Ionization (IR-MALDESI). *Analyst* **2016**, *141*, 595.
- [126] E. P. Hunter, S. G. Lias. Proton Affinity Evaluation in: NIST Chemistry WebBook, NIST Standard Reference Database Number 69, Linstrom PJ, Mallard WG, Eds. National Institute of Standards and Technology, Gaithersburg MD, 20899. can be found under <http://cccbdb.nist.gov/palistx.asp#webbook>, **2016**.
- [127] D. Marsh. *Handbook of Lipid Bilayers*. CRC Press, **2013**.
- [128] V. Wewer, I. Dombrink, K. vom Dorp, P. Dörmann. Quantification of sterol lipids in plants by quadrupole time-of-flight mass spectrometry. *J. Lipid Res.* **2011**, *52*, 1039.
- [129] A. Kiontke, A. Oliveira-Birkmeier, A. Opitz, C. Birkemeyer. Electrospray ionization efficiency is dependent on different molecular descriptors with respect to solvent pH and instrumental

- configuration. *PLoS One* **2016**, *11*, 1.
- [130] K. Hiraoka, K. MURATA, I. Kudaka. Do the Electrospray Mass Spectra Reflect the Ion Concentrations in Sample Solution? *J. Mass Spectrom. Soc. Jpn.* **1995**, *43*, 127.
- [131] R. Faria, M. M. Santana, C. A. Avelaira, C. Simões, E. Maciel, T. Melo, D. Santinha, M. M. Oliveira, F. Peixoto, P. Domingues, C. Cavadas, M. R. M. Domingues. Alterations in phospholipidomic profile in the brain of mouse model of depression induced by chronic unpredictable stress. *Neuroscience* **2014**, *273*, 1.
- [132] E. Sigitova, Z. Fišar, J. Hroudová, T. Cikánková, J. Raboch. Biological hypotheses and biomarkers of bipolar disorder. *Psychiatry Clin. Neurosci.* **2016**, *77*.
- [133] C. Portioli, M. Bovi, D. Benati, M. Donini, M. Perduca, A. Romeo, S. Dusi, H. L. Monaco, M. Bentivoglio. Novel functionalization strategies of polymeric nanoparticles as carriers for brain medications. *J. Biomed. Mater. Res. - Part A* **2017**, *105*, 847.
- [134] A. Sarkar, I. Fatima, Q. M. S. Jamal, U. Sayeed, M. K. A. Khan, S. Akhtar, M. A. Kamal, A. Farooqui, M. H. Siddiqui. Nanoparticles as a carrier system for drug delivery across blood brain barrier. *Curr. Drug Metab.* **2017**, *18*, 129.
- [135] J. S. O'Brien, E. L. Sampson. Fatty acid and fatty aldehyde composition of the major brain lipids in normal human gray matter, white matter, and myelin. *J. Lipid Res.* **1965**, *6*, 545.
- [136] C. C. Loureiro, A. S. Oliveira, M. Santos, A. Rudnitskaya, A. Todo-Bom, J. Bousquet, S. M. Rocha. Urinary metabolomic profiling of asthmatics can be related to clinical characteristics. *Allergy Eur. J. Allergy Clin. Immunol.* **2016**, *71*, 1362.
- [137] S. E. Ali, M. A. Farag, P. Holvoet, R. S. Hanafi, M. Z. Gad. A Comparative Metabolomics Approach Reveals Early Biomarkers for Metabolic Response to Acute Myocardial Infarction. *Sci. Rep.* **2016**, *6*, DOI 10.1038/srep36359.
- [138] M. A. Farag, S. Fahmy, M. A. Choucry, M. O. Wahdan, M. F. Elsebai. Metabolites profiling reveals for antimicrobial compositional differences and action mechanism in the toothbrushing stick "miswak" *Salvadora persica*. *J. Pharm. Biomed. Anal.* **2017**, *133*, 32.
- [139] S. Wang, K. D. Oakes, L. M. Bragg, J. Pawliszyn, G. Dixon, M. R. Servos. Validation and use of in vivo solid phase micro-extraction (SPME) for the detection of emerging contaminants in fish. *Chemosphere* **2011**, *85*, 1472.
- [140] J. Xu, J. Luo, J. Ruan, F. Zhu, T. Luan, H. Liu, R. Jiang, G. Ouyang. In vivo tracing uptake and elimination of organic pesticides in fish muscle. *Environ. Sci. Technol.* **2014**, *48*, 8012.
- [141] O. P. Togunde, K. D. Oakes, M. R. Servos, J. Pawliszyn. Optimization of solid phase microextraction for non-lethal in vivo determination of selected pharmaceuticals in fish muscle using liquid chromatography-mass spectrometry. *J. Chromatogr. A* **2012**, *1261*, 99.
- [142] O. P. Togunde, K. D. Oakes, M. R. Servos, J. Pawliszyn. Determination of pharmaceutical residues in fish bile by solid-phase microextraction couple with liquid chromatography-tandem mass spectrometry (LC/MS/MS). *Environ. Sci. Technol.* **2012**, *46*, 5302.
- [143] R. a van den Berg, H. C. J. Hoefsloot, J. a Westerhuis, A. K. Smilde, M. J. van der Werf. Centering, scaling, and transformations: improving the biological information content of metabolomics data. *BMC Genomics* **2006**, *7*, 142.
- [144] C. Mencarelli, P. Martinez-Martinez. Ceramide function in the brain: When a slight tilt is enough. *Cell. Mol. Life Sci.* **2013**, *70*, 181.

Appendix A Supplementary information for Chapter 2 and 3.

Supplementary Table A1. Internal standard mix 1 (IS mix I), Stock solution concentration = 6 µg/mL in 100% MeOH. **Most intense ion.** NA (lipid does not ionize in negative mode)

	Avanti Lipids cat. no.	Lipid abbreviation	[M-H]⁻	[M+CH₃COO]⁻	Purchased form/solution
1-(10Z-heptadecenoyl)-2-hydroxy- <i>sn</i> -glycero-3-[phospho-L-serine] (sodium salt)	858141	17:1 LPS	508.2681	568.2892	Powder
1-(10Z-heptadecenoyl)- <i>sn</i> -glycero-3-phosphoethanolamine	110699	17:1 LPE	464.2783	524.2994	Chloroform
1-heptadecanoyl-2-hydroxy- <i>sn</i> -glycero-3-phosphocholine	855676	17:0 LPC	508.3407	568.362	Chloroform
1,2-diheptadecanoyl- <i>sn</i> -glycero-3-phospho-(1'- <i>rac</i> -glycerol) (sodium salt)	830456	17:0/17:0 PG	749.5338	809.5549	CHCl ₃ /MeOH/H ₂ O (65:35:8)
1,2-dinonadecanoyl- <i>sn</i> -glycero-3-phosphocholine	850367	19:0/19:0 PC	816.6488	876.6699	Chloroform
1,2-diheptadecanoyl- <i>sn</i> -glycero-3-phospho-	840028	17:0/17:0 PS	762.5291	822.5502	Powder

L-serine (sodium salt)					
1,2-diheptadecanoyl-sn-glycero-3-phosphoethanolamine	830756	17:0/17:0 PE	718.5392	778.5603	Chloroform
1,3(d ₅)-dipentadecanoyl-glycerol	110536	15:0/15:0 DG d ₅	NA		Powder
1,3(d ₅)-diheptadecanoyl-2-(10Z-heptadecenoyl)-glycerol	110544	17:0/17:1/17:0 TG d ₅	NA		Powder

Supplementary Table A2. Internal standard mix 2 (IS mix II), Stock solution concentration = 400 ng/mL in 100% MeOH. **Most intense ion.** NA (lipid does not ionize in negative mode)

	Avanti Lipids cat. no.	Lipid abbreviation	[M-H]⁻	[M+CH₃COO]⁻	Note	Purchased form/solution
1-tridecanoyl-sn-glycero-3-phosphate (ammonium salt)	LM-1700	LPA (13:0)	367.1891	427.2102		Methanol
1-(10Z-heptadecenoyl)-sn-glycero-3-phosphocholine	LM-1601	LPC (17:1)	506.3252	566.3463	Both adducts have similar abundance	Methanol
1-dodecanoyl-2-tridecanoyl-sn-glycero-3-phosphoethanolamine	LM-1100	PE (12:0/13:0)	592.3984	652.4195		Methanol
1-heptadecanoyl-2-(9Z-tetradecenoyl)-sn-glycero-3-phospho-(1'-myo-inositol) (ammonium salt)	LM-1504	PI (17:0/14:1)	793.4873	853.5084		Methanol
1-heptadecanoyl-2-(5Z,8Z,11Z,14Z-eicosatetraenoyl)-sn-glycero-3-phospho-L-serine (ammonium salt)	LM-1302	PS (17:0/20:4)	796.5134	856.5345		Methanol

1-heptadecanoyl-2-(5Z,8Z,11Z,14Z-eicosatetraenoyl)-sn-glycero-3-phospho-(1'-rac-glycerol) (ammonium salt)	LM-1202	PG (17:0/20:4)	783.5182	843.5393		Methanol
1-heptadecanoyl-2-(5Z,8Z,11Z,14Z-eicosatetraenoyl)-sn-glycero-3-phosphate (ammonium salt)	LM-1402	PA (17:0/20:4)	709.4814	769.5025		Methanol
heptadeca-sphing-4-enine-1-phosphocholine	LM-2320	Lyso Sphingomyelin (d17:1)	449.315	509.3361	Not detected in AA plasma samples	Ethanol
heptadeca-sphing-4-enine	LM-2000	Sphingosine (d17:1)	284.2595	344.2806		Ethanol
N-(dodecanoyl)-sphing-4-enine-1-phosphocholine	LM-2312	Sphingomyelin (d18:1/12:0)	645.4977	705.5188		Ethanol
N-(pentacosanoyl)-sphing-4-enine	LM-2225	Ceramide C25	662.6457	722.6668		Ethanol
	LM-6004	DG d ₅ mix		NA	contains: DG d ₅ - (16:1/0:0/16:1), DG d ₅ -(18:0/0/18:0), DG d ₅ - (18:1/0:0/18:1), DG d ₅ -(18:2/0:0/18:2)	Toluene/Methanol

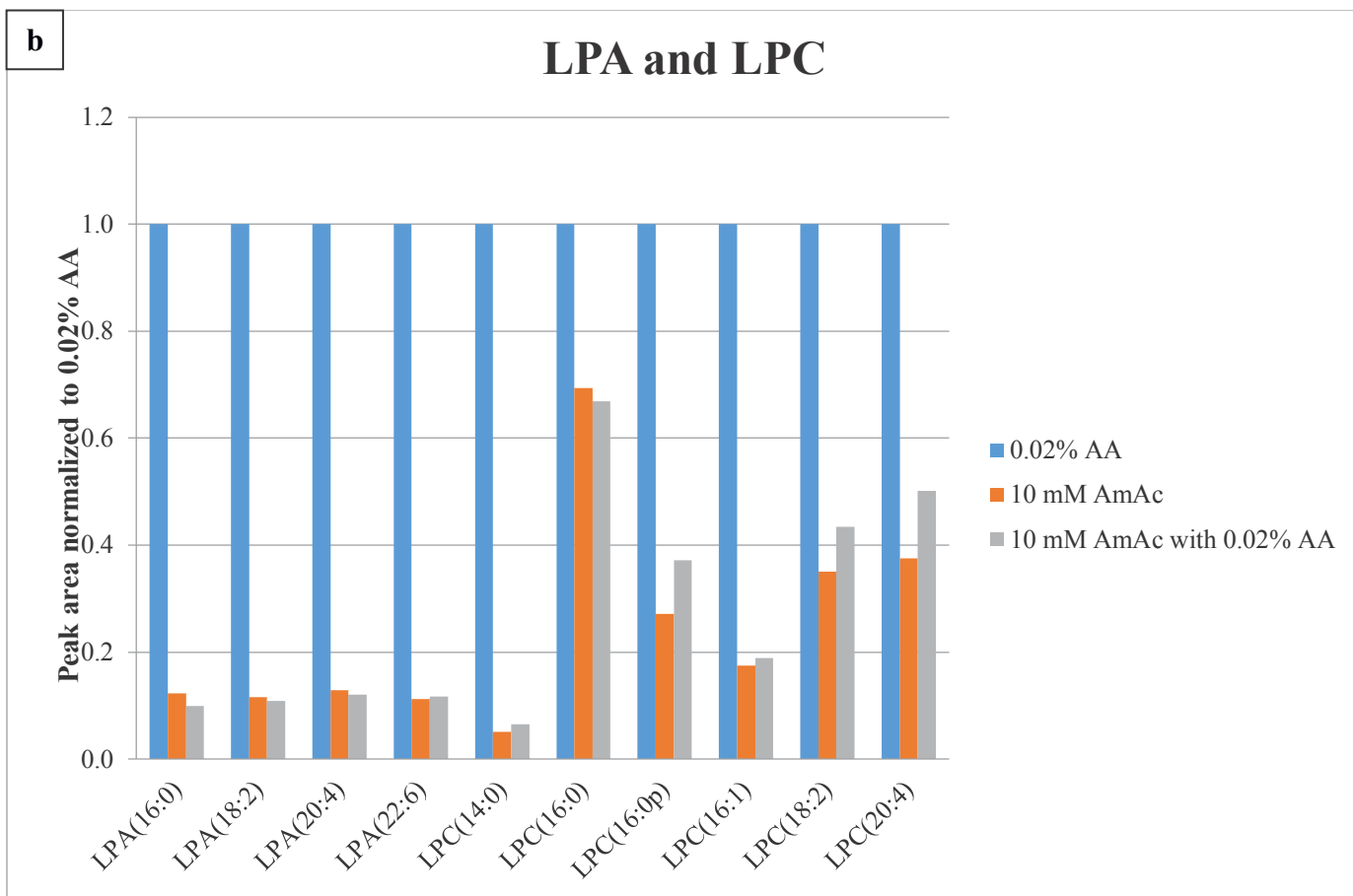
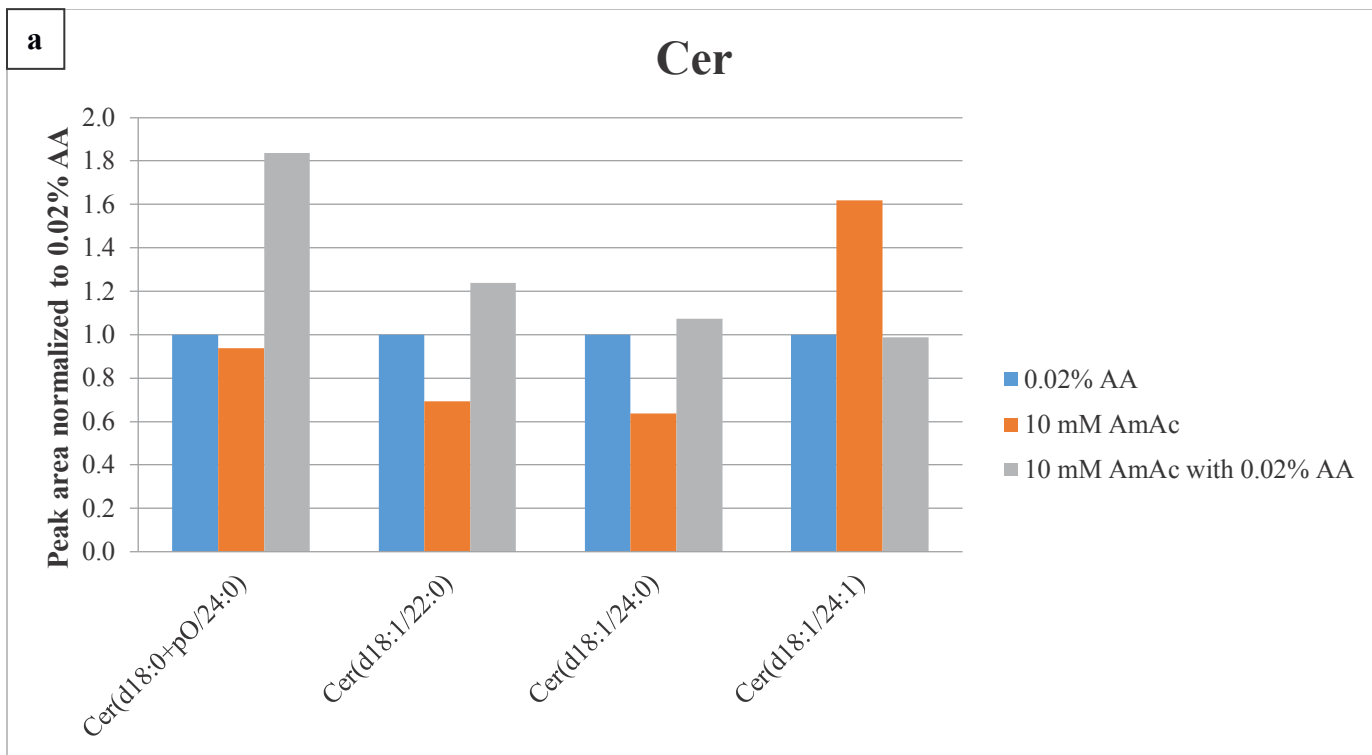
Supplementary Table A3. Standard mix I Stock solution concentration = 1 µg/mL in 100% MeOH. **Most intense ion.** NA (lipid does not ionize in negative mode). ND (lipid should ionize in negative mode but not detected)

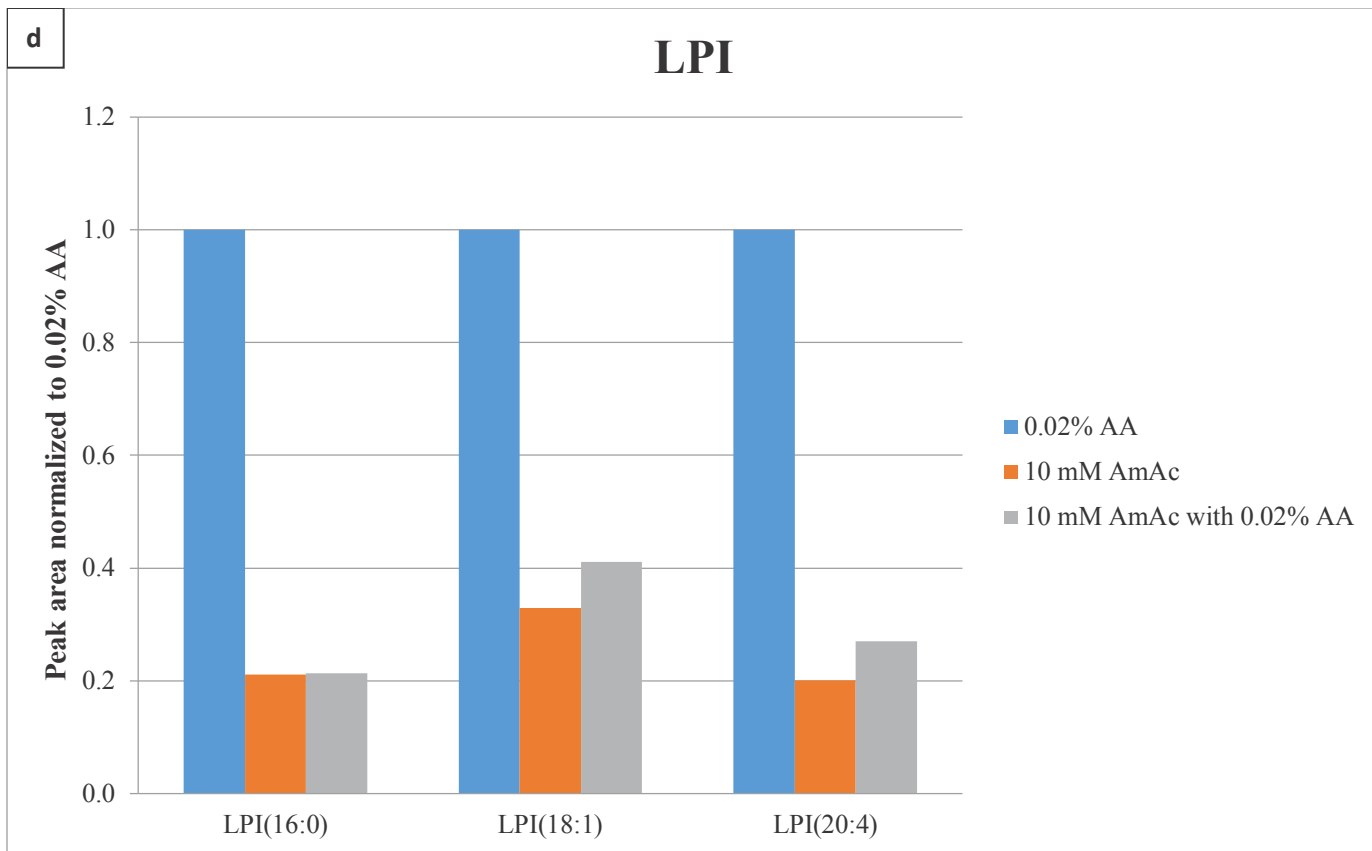
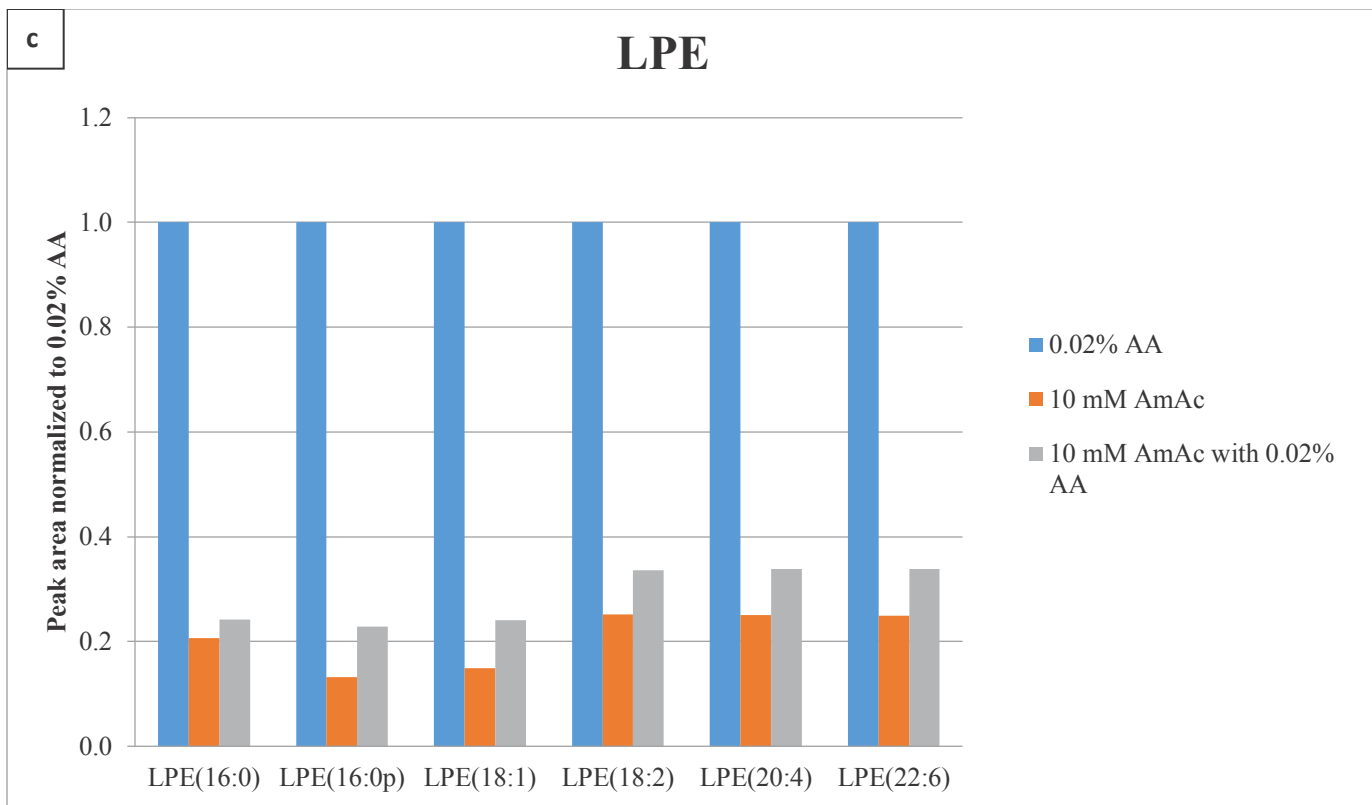
	Avanti Lipids cat. no.	Lipid abbreviation	[M-H]⁻	[M+CH₃COO]⁻	Note	Purchased form/solution
1-(10Z-heptadecenoyl)-2-hydroxy- <i>sn</i> -glycero-3-[phospho-L-serine] (sodium salt)	858141	LPS (17:1)	508.2681	568.2892		Powder
1-(10Z-heptadecenoyl)- <i>sn</i> -glycero-3-phosphoethanolamine	110699	LPE (17:1)	464.2783	524.2994		Chloroform
1-heptadecanoyl-2-hydroxy- <i>sn</i> -glycero-3-phosphocholine	855676	LPC (17:0)	508.3407	568.362		Chloroform
1,2-distearoyl- <i>sn</i> -glycero-3-phospho-(1'- <i>rac</i> -glycerol) (sodium salt)	840465	PG (18:0/18:0)	777.5651	837.5862		Chloroform
1,2-diheptadecanoyl- <i>sn</i> -glycero-3-phosphoethanolamine	830756	PE (17:0/17:0)	718.5392	778.5603		Chloroform
1,2-diheptadecanoyl- <i>sn</i> -glycero-3-phospho-L-serine (sodium salt)	840028	PS (17:0/17:0)	762.5291	822.5502		Powder
1,2-dinonadecanoyl- <i>sn</i> -glycero-3-phosphocholine	850367	PC (19:0/19:0)	816.6488	876.6699		Chloroform
N-stearoyl-D- <i>erythro</i> -sphingosine	860518	Cer (d18:1/18:0)	564.5361	624.5572		Powder

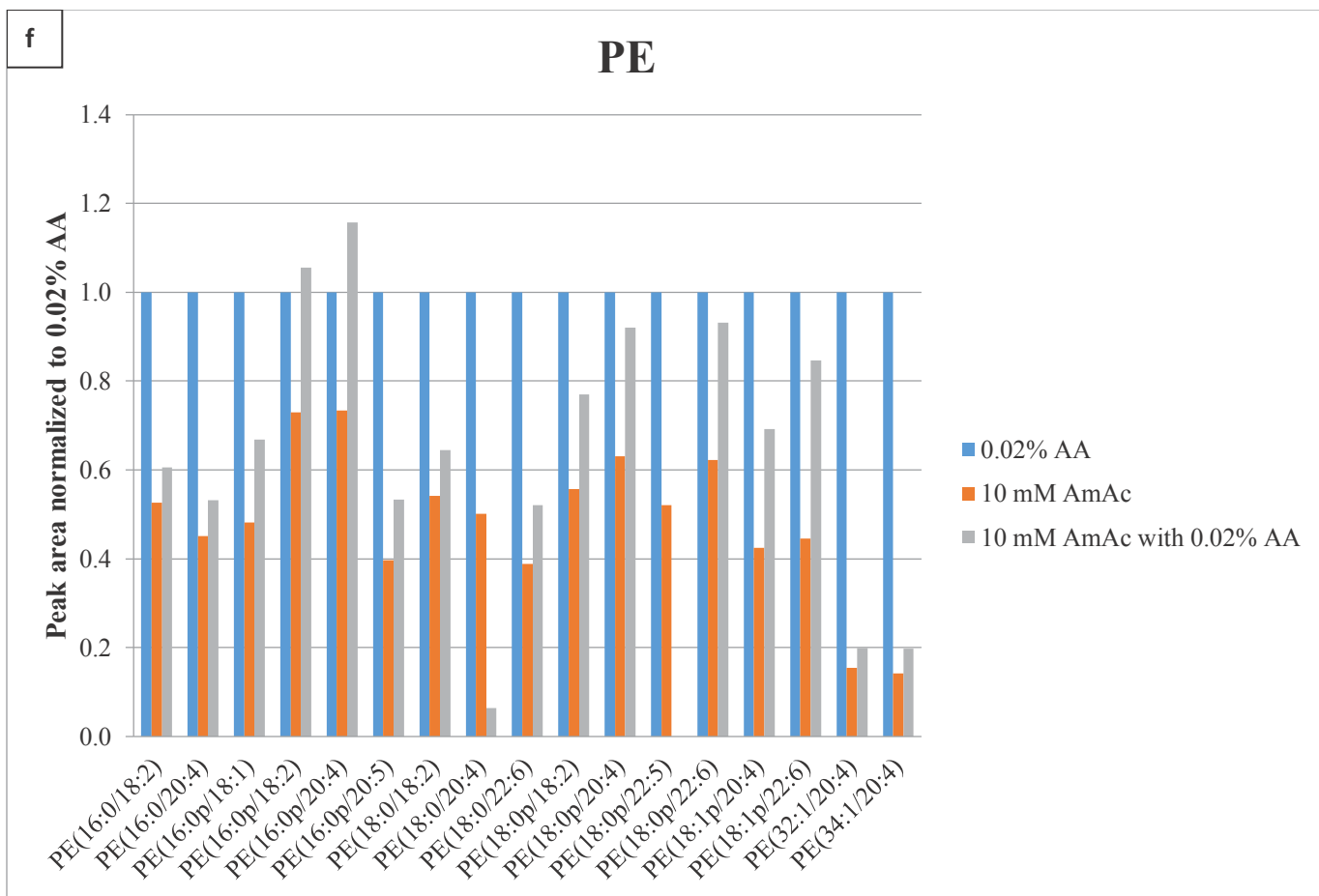
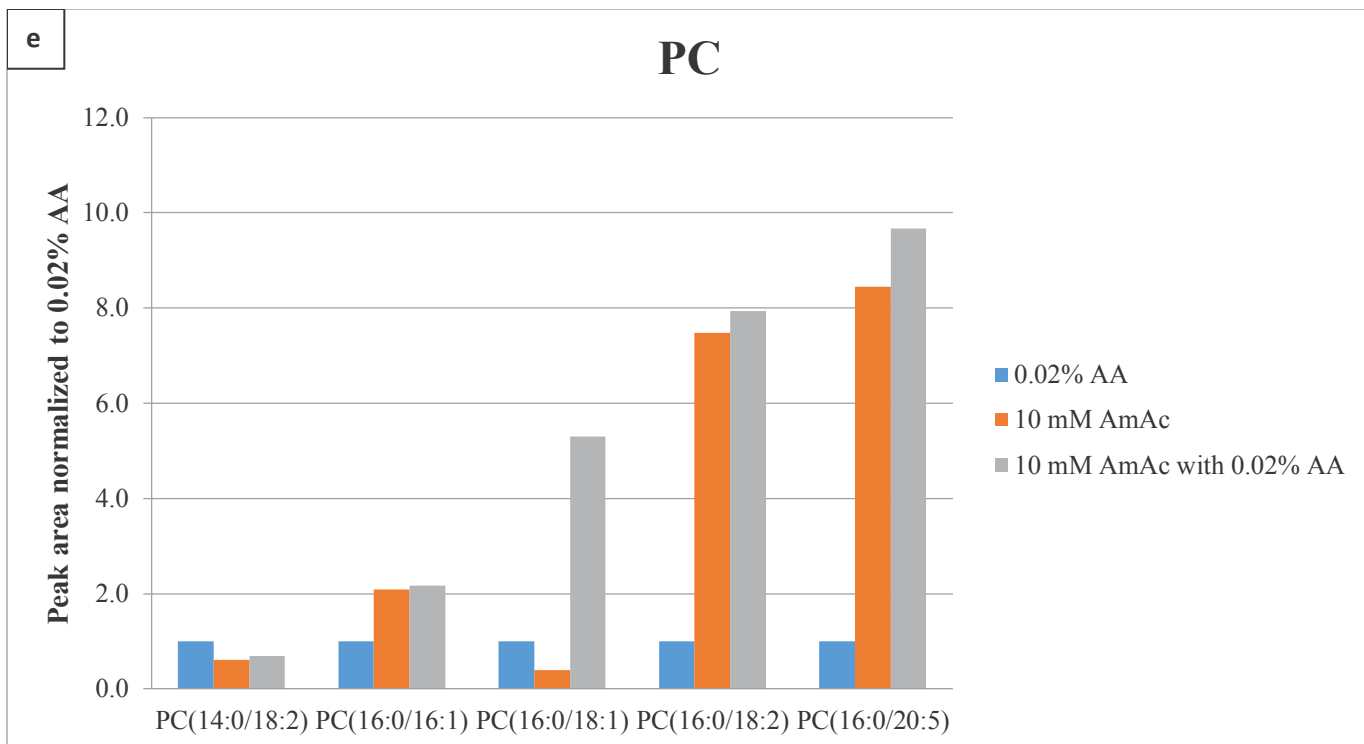
N-stearoyl-D- <i>erythro</i> -sphingosylphosphorylcholine	860586	SM (d18:1/18:0)	729.5916	789.6127		Powder
D- <i>erythro</i> -sphingosine	860490	Sphingosine (d18:1)		ND		Powder
1,2-distearoyl- <i>sn</i> -glycero-3-phosphate (sodium salt)	830865	PA (18:0/18:0)		ND		CHCl ₃ /MeOH/H ₂ O (65:35:8)
1-hexadecanoyl- <i>rac</i> -glycerol	110606	MG (16:0)		NA		Chloroform
1,3(d5)-dipentadecanoyl-glycerol	110536	DG d5 (15:0/15:0)		NA		Powder
1,3(d5)-diheptadecanoyl-2-(10Z-heptadecenoyl)-glycerol	110544	TG d5 (17:0/17:1/17:0)		NA		Powder
Total Cerebrosides (Brain, Porcine)	131303	Natural cerebrosides		ND	781.953 (average based on fatty acid distribution in product)	Powder

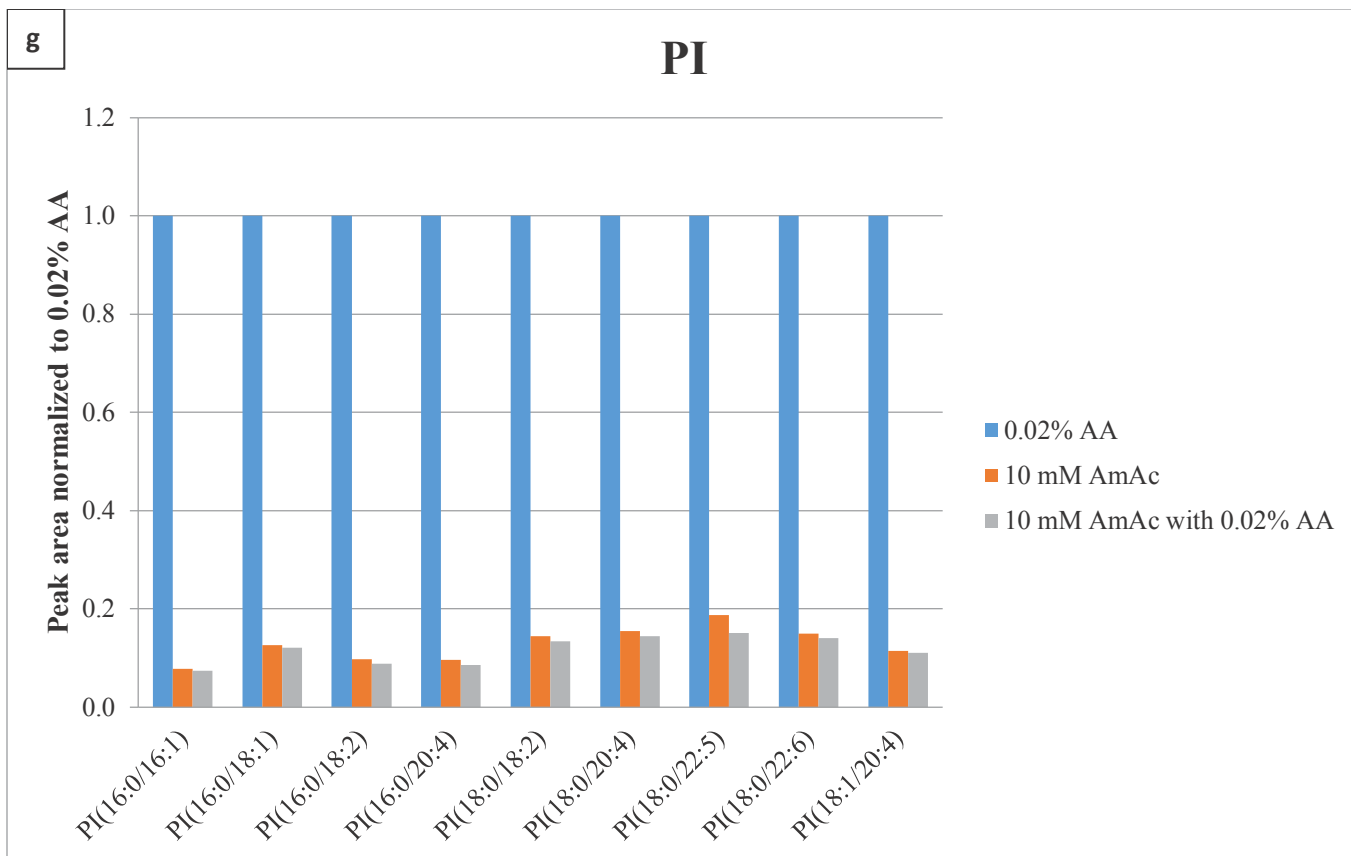
Supplementary Table A4. Number of lipid species identified by LipidSearch in plasma samples analysed on Orbitrap (n=4) using each of the three different mobile phase compositions

Lipid subclass	0.02% AA	10 mM AmAc	10 mM AmAc and 0.02% AA
Cer	7	11	10
LPA	6	7	6
LPC	6	7	8
LPE	10	6	7
LPG	2	0	0
LPI	7	3	3
LPS	1	0	0
PA	1	2	2
PC	18	26	23
PE	25	28	32
PG	1	0	0
PI	14	12	10
SM	2	2	2
Total	101	104	103

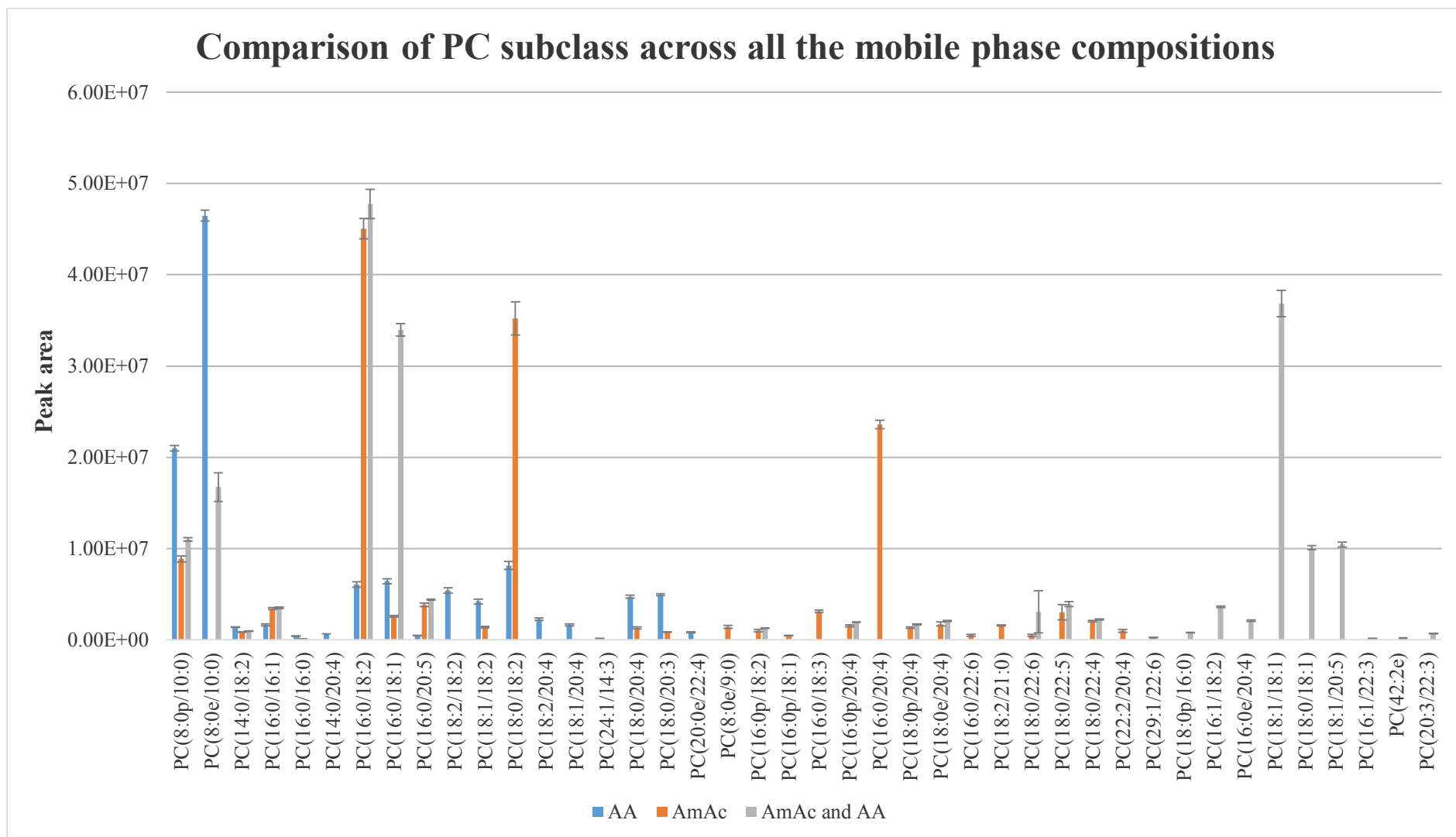








Supplementary Figure A1. Signal enhancements for each-subclass (a-g) showing effects of AA on signal intensity of lipids belonging to that subclass that were identified in all three mobile phase compositions: 0.02% AA, 10 mM AmAc and 10 mM AmAc with 0.02% AA. Signal normalised to AA containing mobile phase. Plasma samples analysed on Orbitrap, n=4.



Supplementary Figure A2. Signal changes of PC subclass showing intra-class changes in signal intensity. Plasma samples analysed on Orbitrap, n=4.

Supplementary Table A5 Lipids extracted from hippocampus by **Folch method** and confidently identified using LipidSearch in **negative** mode. n=16

Detected in SPME	Lipid Identity	Calc Mass	RT (min)	Main ion	Mean Peak area
No	PC(18:4/18:0)	781.5622	7.787	[M+CH ₃ COO] ⁻	3.70E+06
No	PE(16:0p/20:3)	725.5359	8.133	[M-H] ⁻	2.56E+06
No	PE(18:0/20:1)	773.5935	8.788	[M-H] ⁻	1.15E+06
No	PE(18:0p/16:0)	703.5516	8.542	[M-H] ⁻	9.11E+05
No	PE(18:1p/21:1)	769.5985	8.899	[M-H] ⁻	2.51E+05
No	PE(20:0p/22:4)	807.6142	8.997	[M-H] ⁻	3.57E+06
No	PE(20:4/22:6)	811.5152	7.726	[M-H] ⁻	1.27E+06
No	PG(18:0/18:2)	774.5411	9.467	[M-H] ⁻	1.91E+05
No	Cer(d18:1+hO/28:6)	709.6009	10.17	[M-H] ⁻	5.94E+05
No	Cer(d18:1+hO/30:6)	737.6322	10.762	[M-H] ⁻	4.66E+05
No	Cer(d18:1/25:0)	663.6529	9.778	[M-H] ⁻	3.00E+05
No	Cer(d20:0+pO/28:2)	747.7105	7.945	[M-H] ⁻	1.07E+04
No	Cer(d20:0+pO/31:1)	791.7731	8.107	[M-H] ⁻	8.02E+03
No	Cer(d20:1+hO/27:6)	723.6166	10.448	[M-H] ⁻	4.39E+05
Yes	LPE(16:0)	453.2855	6.483	[M-H] ⁻	1.03E+07
Yes	LPE(16:0p)	437.2906	6.587	[M-H] ⁻	8.83E+06
Yes	LPE(18:0)	481.3168	6.706	[M-H] ⁻	4.84E+07
Yes	LPE(18:0p)	465.3219	6.826	[M-H] ⁻	2.47E+07
Yes	LPE(18:1)	479.3012	6.508	[M-H] ⁻	7.53E+07
Yes	LPE(18:1p)	463.3063	6.636	[M-H] ⁻	3.14E+07
No	LPE(20:1)	507.3325	6.708	[M-H] ⁻	1.45E+07
Yes	LPE(20:4)	501.2855	6.462	[M-H] ⁻	1.29E+07
No	LPE(22:4)	529.3168	6.561	[M-H] ⁻	2.62E+07
Yes	LPE(22:6)	525.2855	6.461	[M-H] ⁻	1.45E+07
No	LPG(16:0)	484.2801	5.581	[M-H] ⁻	2.58E+05

No	LPG(18:1)	510.2958	5.623	[M-H] ⁻	8.72E+05
No	LPG(20:4)	532.2801	3.883	[M-H] ⁻	9.28E+04
No	LPG(22:6)	556.2801	3.916	[M-H] ⁻	1.00E+05
No	LPI(16:0)	572.2962	4.218	[M-H] ⁻	3.14E+04
No	LPI(18:0)	600.3275	5.703	[M-H] ⁻	6.88E+06
No	LPI(18:1)	598.3118	5.593	[M-H] ⁻	7.06E+05
No	LPI(20:4)	620.2962	3.653	[M-H] ⁻	9.46E+05
No	LPS(18:1)	523.291	5.889	[M-H] ⁻	8.26E+05
Yes	LPS(22:6)	569.2754	5.757	[M-H] ⁻	3.64E+06
No	PA(16:0/16:0)	648.473	11.581	[M-H] ⁻	1.39E+06
No	PA(16:0/20:4)	696.473	11.924	[M-H] ⁻	3.77E+06
No	PA(18:1/18:1)	700.5043	9.421	[M-H] ⁻	2.41E+06
Yes	PC(16:0/18:1)	759.5778	7.993	[M+CH ₃ COO] ⁻	6.69E+06
Yes	PC(16:0/22:6)	805.5622	7.744	[M+CH ₃ COO] ⁻	1.95E+06
No	PC(16:0p/23:1)	813.6611	8.711	[M+CH ₃ COO] ⁻	2.04E+06
No	PC(18:0/12:0)	705.5309	7.656	[M+CH ₃ COO] ⁻	4.33E+05
Yes	PE(16:0/20:4)	739.5152	7.868	[M-H] ⁻	2.20E+07
Yes	PE(16:0/22:6)	763.5152	7.84	[M-H] ⁻	6.32E+07
No	PE(16:0p/16:1)	673.5046	7.937	[M-H] ⁻	9.83E+05
Yes	PE(16:0p/18:1)	701.5359	8.246	[M-H] ⁻	2.46E+07
Yes	PE(16:0p/20:4)	723.5203	8.02	[M-H] ⁻	2.57E+07
Yes	PE(16:0p/22:4)	751.5516	8.364	[M-H] ⁻	4.27E+07
Yes	PE(16:0p/22:6)	747.5203	7.992	[M-H] ⁻	6.27E+07
No	PE(16:1/18:1)	715.5152	7.857	[M-H] ⁻	8.94E+05
Yes	PE(18:0/18:1)	745.5622	8.405	[M-H] ⁻	1.35E+07
Yes	PE(18:0/20:4)	767.5465	8.167	[M-H] ⁻	7.92E+07
Yes	PE(18:0/22:4)	795.5778	8.436	[M-H] ⁻	1.30E+07
No	PE(18:0/22:5)	793.5622	8.336	[M-H] ⁻	2.76E+06
Yes	PE(18:0/22:6)	791.5465	8.13	[M-H] ⁻	7.36E+07

Yes	PE(18:0p/18:1)	729.5672	8.598	[M-H]	2.30E+07
Yes	PE(18:0p/20:1)	757.5985	9.014	[M-H]	1.52E+07
No	PE(18:0p/22:1)	785.6298	9.47	[M-H]	3.95E+06
Yes	PE(18:0p/22:4)	779.5829	8.666	[M-H]	1.89E+07
Yes	PE(18:0p/22:6)	775.5516	8.355	[M-H]	5.91E+07
Yes	PE(18:1/18:1)	743.5465	8.113	[M-H]	1.13E+07
No	PE(18:1/18:2)	741.5309	8.393	[M-H]	3.24E+05
Yes	PE(18:1/20:4)	765.5309	7.912	[M-H]	3.22E+07
No	PE(18:1/22:6)	789.5309	7.89	[M-H]	1.83E+07
No	PE(18:1/24:0)	829.6561	9.666	[M-H]	6.82E+05
No	PE(18:1p/16:1)	699.5203	8.012	[M-H]	1.74E+06
Yes	PE(18:1p/18:1)	727.5516	8.353	[M-H]	3.86E+07
Yes	PE(18:1p/20:1)	755.5829	8.724	[M-H]	8.71E+06
Yes	PE(18:1p/20:4)	749.5359	8.08	[M-H]	2.69E+07
No	PE(18:1p/22:1)	783.6142	9.084	[M-H]	3.06E+06
No	PE(18:1p/22:4)	777.5672	8.371	[M-H]	1.24E+07
Yes	PE(18:1p/22:6)	773.5359	8.052	[M-H]	1.98E+07
No	PE(18:1p/24:1)	811.6455	9.522	[M-H]	1.39E+06
No	PE(22:4/20:4)	815.5465	7.932	[M-H]	1.40E+06
No	PE(32:1/18:1)	939.7656	7.655	[M-H]	6.43E+05
No	PE(34:1/20:4)	989.7813	7.652	[M-H]	6.02E+05
No	PG(16:0/16:0)	722.5098	6.378	[M-H]	1.90E+07
Yes	PG(16:0/18:1)	748.5254	6.394	[M-H]	9.61E+07
No	PG(16:0/20:4)	770.5098	6.307	[M-H]	2.99E+07
No	PG(18:0/18:1)	776.5567	6.478	[M-H]	1.61E+07
No	PG(18:0/20:4)	798.5411	6.409	[M-H]	4.74E+07
No	PG(20:4/22:6)	842.5098	6.171	[M-H]	8.24E+06
No	PG(22:6/22:6)	866.5098	6.16	[M-H]	2.94E+07
Yes	PI(16:0/20:4)	858.5258	6.143	[M-H]	2.19E+08

No	PI(16:0/22:6)	882.5258	6.138	[M-H] ⁻	1.99E+07
Yes	PI(18:0/20:4)	886.5571	6.236	[M-H] ⁻	1.00E+09
No	PI(18:0/20:5)	884.5415	6.841	[M-H] ⁻	2.01E+07
No	PS(16:0/18:1)	761.5207	6.883	[M-H] ⁻	3.10E+07
No	PS(16:0/20:4)	783.505	6.834	[M-H] ⁻	5.36E+06
No	PS(16:0/22:6)	807.505	6.84	[M-H] ⁻	1.47E+07
No	PS(18:0/20:3)	813.552	7.238	[M-H] ⁻	1.01E+07
No	PS(18:0/22:3)	841.5833	7.786	[M-H] ⁻	3.70E+06
No	PS(18:0p/22:6)	819.5414	7.213	[M-H] ⁻	1.69E+06
No	PS(18:1/18:1)	787.5363	6.952	[M-H] ⁻	7.82E+07
No	PS(18:1/20:4)	809.5207	6.845	[M-H] ⁻	1.77E+07
No	PS(18:1/22:0)	845.6146	8.733	[M-H] ⁻	5.71E+05
No	PS(18:1/22:1)	843.5989	7.641	[M-H] ⁻	3.93E+06
No	PS(18:1/22:6)	833.5207	6.843	[M-H] ⁻	3.62E+07
No	PS(18:1/24:1)	871.6302	8.773	[M-H] ⁻	5.77E+05
No	PS(20:0/22:6)	863.5676	7.242	[M-H] ⁻	2.34E+06
No	PS(20:4/22:6)	855.505	6.829	[M-H] ⁻	7.16E+06
No	PS(22:4/22:6)	883.5363	6.846	[M-H] ⁻	3.63E+07
No	PS(22:6/22:6)	879.505	7.787	[M+CH ₃ COO] ⁻	1.46E+07

Supplementary Table A6 Lipids extracted from hippocampus by *in vivo* SPME method and confidently identified using LipidSearch in **negative** mode. n=3

Unique to SPME	Lipid Identity	Calc Mass	RT (min)	Main Ion	Mean peak area
No	LPE(16:0)	453.2855	6.60	[M-H] ⁻	1.01E+06
No	LPE(16:0p)	437.2906	6.72	[M-H] ⁻	6.16E+05
No	LPE(18:0)	481.3168	6.83	[M-H] ⁻	3.36E+06
No	LPE(18:0p)	465.3219	6.95	[M-H] ⁻	1.04E+06
No	LPE(18:1)	479.3012	6.66	[M-H] ⁻	2.15E+06
No	LPE(18:1p)	463.3063	6.77	[M-H] ⁻	9.46E+05
No	LPE(20:4)	501.2855	6.51	[M-H] ⁻	1.31E+06
No	LPE(22:6)	525.2855	6.50	[M-H] ⁻	1.32E+06
No	LPS(22:6)	569.2754	5.87	[M-H] ⁻	7.64E+05
Yes	PC(16:0/16:0)	733.5622	8.05	[M+CH ₃ COO] ⁻	2.33E+06
Yes	PC(16:0/16:1)	731.5465	7.85	[M+CH ₃ COO] ⁻	3.57E+05
No	PC(16:0/18:1)	759.5778	8.11	[M+CH ₃ COO] ⁻	3.32E+06
Yes	PC(16:0/18:2)	757.5622	7.92	[M+CH ₃ COO] ⁻	7.20E+05
Yes	PC(16:0/20:4)	781.5622	7.92	[M+CH ₃ COO] ⁻	1.39E+06
No	PC(16:0/22:6)	805.5622	7.89	[M+CH ₃ COO] ⁻	5.59E+05
Yes	PC(18:0/16:0)	761.5935	8.37	[M+CH ₃ COO] ⁻	5.11E+05
Yes	PC(18:0/18:1)	787.6091	8.42	[M+CH ₃ COO] ⁻	9.92E+05
Yes	PC(18:1p/21:0)	813.6611	8.66	[M+CH ₃ COO] ⁻	3.23E+05
Yes	PC(20:0p/21:1)	841.6924	9.02	[M+CH ₃ COO] ⁻	7.69E+05

Yes	PE(16:0/18:1)	717.5309	8.19	[M-H] ⁻	5.97E+05
No	PE(16:0/20:4)	739.5152	7.99	[M-H] ⁻	8.04E+05
No	PE(16:0/22:6)	763.5152	7.97	[M-H] ⁻	2.49E+06
No	PE(16:0p/18:1)	701.5359	8.39	[M-H] ⁻	1.20E+06
No	PE(16:0p/20:4)	723.5203	8.18	[M-H] ⁻	1.67E+06
No	PE(16:0p/22:4)	751.5516	8.51	[M-H] ⁻	4.44E+06
No	PE(16:0p/22:6)	747.5203	8.15	[M-H] ⁻	2.30E+06
No	PE(18:0/18:1)	745.5622	8.52	[M-H] ⁻	1.09E+06
No	PE(18:0/20:4)	767.5465	8.31	[M-H] ⁻	5.92E+06
No	PE(18:0/22:4)	795.5778	8.57	[M-H] ⁻	1.12E+06
No	PE(18:0/22:6)	791.5465	8.27	[M-H] ⁻	5.44E+06
No	PE(18:0p/18:1)	729.5672	8.74	[M-H] ⁻	1.58E+06
No	PE(18:0p/20:1)	757.5985	9.13	[M-H] ⁻	2.42E+05
No	PE(18:0p/22:4)	779.5829	8.78	[M-H] ⁻	1.74E+06
No	PE(18:0p/22:6)	775.5516	8.47	[M-H] ⁻	3.97E+06
No	PE(18:1/18:1)	743.5465	8.25	[M-H] ⁻	7.58E+05
No	PE(18:1/20:4)	765.5309	8.06	[M-H] ⁻	7.19E+05
No	PE(18:1p/18:1)	727.5516	8.47	[M-H] ⁻	1.58E+06
No	PE(18:1p/20:1)	755.5829	8.80	[M-H] ⁻	3.50E+05
No	PE(18:1p/20:4)	749.5359	8.24	[M-H] ⁻	1.54E+06
No	PE(18:1p/22:6)	773.5359	8.20	[M-H] ⁻	1.04E+06
No	PG(16:0/18:1)	748.5254	6.42	[M-H] ⁻	7.93E+05

Yes	PI(16:0/18:1)	836.5415	6.35	[M-H] ⁻	4.63E+05
Yes	PI(16:0/18:2)	834.5258	6.29	[M-H] ⁻	3.54E+05
No	PI(16:0/20:4)	858.5258	6.29	[M-H] ⁻	3.54E+06
Yes	PI(18:0/18:1)	864.5728	6.43	[M-H] ⁻	4.94E+05
Yes	PI(18:0/18:2)	862.5571	6.37	[M-H] ⁻	4.91E+05
No	PI(18:0/20:4)	886.5571	6.37	[M-H] ⁻	2.06E+07
Yes	PI(18:1/20:4)	884.5415	6.31	[M-H] ⁻	1.76E+06
No	PS(18:0/22:6)	835.5363	7.52	[M-H] ⁻	9.82E+05
Yes	SM(d18:0/18:1)	730.5989	8.02	[M+CH ₃ COO] ⁻	9.24E+05
Yes	SM(d18:1/16:0)	702.5676	7.74	[M+CH ₃ COO] ⁻	7.46E+05
Yes	Cer(d14:1/24:6)	581.4808	8.45	[M-H] ⁻	3.02E+05
No	PS(18:0/22:6)	835.5363	7.52	[M-H] ⁻	9.82E+05

Supplementary Table A7 Lipids extracted from hippocampus by **Folch method** and confidently identified using LipidSearch in **positive** mode. n=16. *This ID requires further confirmation with authentic standards, as $[M+NH_4]^+$ adduct should typically be observed for TG lipids.

Detected in SPME	Lipid Identity	Calc Mass	RT (min)	Main ion	Mean Peak area
No	Cer(d14:0/2:0)	287.246	4.92	$[M+H]^+$	1.20E+07
No	Cer(d20:0+pO/18:0)	611.5853	13.07	$[M+H]^+$	2.68E+06
No	Cer(d20:1+hO/18:0+O)	625.5645	12.24	$[M+NH_4]^+$	9.93E+06
No	Cer(d20:1+hO/20:1+O)	651.5802	13.07	$[M+H]^+$	5.83E+06
No	Cer(d22:0/18:2+2O)	651.5802	13.07	$[M+H]^+$	5.81E+06
No	ChE(22:6)	696.5845	16.53	$[M+NH_4]^+$	3.77E+06
No	DG(16:0/18:1)	594.5223	12.11	$[M+NH_4]^+$	5.23E+07
No	DG(16:0/20:4)	616.5067	11.78	$[M+NH_4]^+$	2.84E+07
No	DG(18:0/16:0)	596.538	12.51	$[M+NH_4]^+$	9.05E+06
No	DG(18:0/18:1)	622.5536	12.63	$[M+NH_4]^+$	5.54E+07
No	DG(18:0/20:3)	646.5536	12.59	$[M+NH_4]^+$	6.53E+06
Yes	DG(18:0/20:4)	644.538	12.28	$[M+NH_4]^+$	2.39E+08
No	DG(18:1/22:0)	678.6162	13.82	$[M+NH_4]^+$	6.51E+06
No	DG(18:1/22:1)	676.6006	13.26	$[M+NH_4]^+$	2.39E+06
No	DG(18:1/24:0)	706.6475	14.51	$[M+NH_4]^+$	9.83E+06
No	DG(18:1/24:1)	704.6319	13.88	$[M+NH_4]^+$	7.39E+06
No	DG(20:0/18:1)	650.5849	13.16	$[M+NH_4]^+$	5.34E+06

No	DG(22:0/20:4)	700.6006	13.84	[M+H] ⁺	2.30E+06
No	DG(22:1/22:1)	732.6632	14.55	[M+NH ₄] ⁺	1.53E+06
No	DG(24:0/20:4)	728.6319	14.54	[M+H] ⁺	3.20E+06
No	DG(24:1/20:4)	726.6162	13.86	[M+H] ⁺	2.49E+06
No	DG(4:0/14:2)	368.2563	14.01	[M+Na] ⁺	8.33E+05
No	DG(4:0/14:3)	366.2406	14.16	[M+Na] ⁺	5.54E+04
No	LPC(20:4)	543.3325	8.84	[M+H] ⁺	4.74E+06
No	LPE(18:0p)	465.3219	9.56	[M+H] ⁺	3.73E+06
No	LPE(20:3)	503.3012	8.89	[M+Na] ⁺	5.41E+06
No	LPE(22:6)	525.2855	8.89	[M+H] ⁺	5.42E+06
No	LPS(22:6)	569.2754	8.51	[M+H] ⁺	7.77E+05
Yes	PE(16:0p/18:1)	701.5359	11.44	[M+H] ⁺	1.56E+08
Yes	PE(16:0p/20:4)	723.5203	11.17	[M+H] ⁺	7.79E+07
No	PE(16:0p/22:4)	751.5516	11.52	[M+H] ⁺	1.89E+08
Yes	PE(16:0p/22:6)	747.5203	11.13	[M+H] ⁺	1.36E+08
Yes	PE(18:0/20:4)	767.5465	11.35	[M+H] ⁺	3.96E+08
Yes	PE(18:0p/18:1)	729.5672	11.85	[M+H] ⁺	2.58E+08
No	PE(18:0p/20:1)	757.5985	12.31	[M+H] ⁺	9.85E+07
No	PE(18:0p/20:3)	753.5672	11.75	[M+H] ⁺	2.61E+07
No	PE(18:0p/22:1)	785.6298	12.81	[M+H] ⁺	8.11E+06
Yes	PE(18:0p/22:4)	779.5829	11.91	[M+H] ⁺	1.82E+08
No	PE(18:0p/22:5)	777.5672	11.75	[M+H] ⁺	2.84E+07

Yes	PE(18:0p/22:6)	775.5516	11.53	[M+H] ⁺	2.56E+08
No	PE(18:1/18:1)	743.5465	11.03	[M+Na] ⁺	5.62E+07
No	PE(18:1p/18:1)	727.5516	11.50	[M+H] ⁺	2.01E+08
No	PE(18:1p/20:1)	755.5829	11.93	[M+H] ⁺	9.08E+07
No	PE(18:1p/20:4)	749.5359	11.24	[M+H] ⁺	9.11E+07
No	PE(18:1p/22:6)	773.5359	11.20	[M+H] ⁺	6.37E+07
No	PE(18:1p/24:0)	813.6611	14.40	[M+H] ⁺	1.49E+07
No	PE(18:1p/24:1)	811.6455	12.90	[M+H] ⁺	3.27E+06
No	PE(25:1/9:0)	717.5309	11.20	[M+H] ⁺	5.92E+07
No	PE(26:0/18:1)	857.6874	12.70	[M+H] ⁺	5.65E+07
No	PE(27:1/9:0)	745.5622	11.63	[M+H] ⁺	1.09E+08
No	PE(28:0/18:1)	885.7187	13.26	[M+H] ⁺	1.71E+07
No	PE(28:1/18:1)	883.703	12.74	[M+H] ⁺	8.38E+06
No	PE(33:1/9:0)	829.6561	13.06	[M+H] ⁺	3.01E+06
No	PE(8:0e/12:1)	507.3325	8.94	[M+H] ⁺	2.19E+07
No	PG(23:1/14:3)	784.5254	10.57	[M+NH ₄] ⁺	5.95E+08
No	PI(16:0/20:4)	858.5258	10.26	[M+NH ₄] ⁺	3.57E+07
No	PS(18:1/18:1)	787.5363	10.48	[M+H] ⁺	3.24E+07
No	PS(20:1/22:6)	861.552	9.94	[M+Na] ⁺	5.15E+06
No	PS(23:0/11:1)	761.5207	10.48	[M+H] ⁺	1.36E+07
No	PS(25:0/11:1)	789.552	10.80	[M+H] ⁺	1.65E+08
Yes	PS(27:0/11:3)	813.552	10.59	[M+Na] ⁺	4.86E+08

No	PS(27:1/11:3)	811.5363	10.52	[M+Na] ⁺	1.94E+07
No	SM(d18:1/12:0)	646.505	10.00	[M+H] ⁺	3.31E+07
No	So(d18:0+pO)	317.293	6.40	[M+H] ⁺	5.01E+05
No	TG(12:0e/18:0/18:0)	792.7571	11.26	[M+NH ₄] ⁺	1.99E+05
No	TG(12:0p/10:3/18:0)*	672.5693	13.17	[M+H] ⁺	2.33E+06
No	TG(14:0p/10:2/18:1)	700.6006	13.82	[M+H] ⁺	1.94E+06
No	TG(16:0/16:0/16:0)	806.7363	16.97	[M+NH ₄] ⁺	9.98E+06
Yes	TG(16:0/16:0/16:1)	804.7207	16.39	[M+NH ₄] ⁺	3.45E+06
Yes	TG(16:0/16:0/18:1)	832.752	17.10	[M+NH ₄] ⁺	1.75E+07
No	TG(16:0/16:0/18:3)*	828.7207	16.97	[M+H] ⁺	2.55E+06
No	TG(16:0/16:0/20:4)	854.7363	16.56	[M+NH ₄] ⁺	5.15E+06
Yes	TG(16:0/16:0/22:6)	878.7363	16.44	[M+NH ₄] ⁺	9.68E+06
Yes	TG(16:0/16:1/18:1)	830.7363	16.58	[M+NH ₄] ⁺	5.40E+06
No	TG(16:0/16:1/18:2)	828.7207	16.04	[M+NH ₄] ⁺	1.33E+06
No	TG(16:0/16:1/22:6)	876.7207	15.86	[M+NH ₄] ⁺	1.47E+06
Yes	TG(16:0/18:1/18:1)	858.7676	17.22	[M+NH ₄] ⁺	1.68E+07
Yes	TG(16:0/18:1/18:2)	856.752	16.73	[M+NH ₄] ⁺	8.08E+06
Yes	TG(16:0/18:1/18:3)*	854.7363	17.11	[M+H] ⁺	4.40E+06
Yes	TG(16:0/18:1/20:4)	880.752	16.46	[M+NH ₄] ⁺	3.75E+06
Yes	TG(16:0/18:1/22:6)	904.752	16.55	[M+NH ₄] ⁺	1.26E+07
Yes	TG(16:0/18:2/18:2)	854.7363	16.25	[M+NH ₄] ⁺	3.39E+06
No	TG(16:0/18:2/18:3)	852.7207	15.80	[M+NH ₄] ⁺	6.95E+05

No	TG(16:0/18:3/22:6)*	900.7207	16.42	[M+H] ⁺	2.20E+06
No	TG(16:0/20:4/20:4)	902.7363	16.13	[M+NH ₄] ⁺	5.75E+06
Yes	TG(16:0/20:4/22:6)	926.7363	16.02	[M+NH ₄] ⁺	4.86E+06
No	TG(16:0/22:6/22:6)	950.7363	15.90	[M+NH ₄] ⁺	3.74E+06
No	TG(16:1/18:2/18:3)	850.705	15.72	[M+NH ₄] ⁺	4.97E+05
No	TG(16:1p/12:4/14:4)	688.5067	10.67	[M+NH ₄] ⁺	1.02E+08
Yes	TG(18:0/16:0/16:0)	834.7676	17.69	[M+NH ₄] ⁺	5.83E+06
Yes	TG(18:0/16:0/18:0)	862.7989	18.39	[M+NH ₄] ⁺	1.95E+06
Yes	TG(18:0/16:0/18:1)	860.7833	17.80	[M+NH ₄] ⁺	1.19E+07
No	TG(18:0/16:0/18:3)*	856.752	17.70	[M+H] ⁺	1.42E+06
No	TG(18:0/16:0/20:1)	888.8146	18.48	[M+NH ₄] ⁺	1.86E+06
No	TG(18:0/16:0/20:4)	882.7676	17.29	[M+NH ₄] ⁺	7.65E+06
Yes	TG(18:0/16:0/22:6)	906.7676	17.16	[M+NH ₄] ⁺	6.19E+06
Yes	TG(18:0/18:0/20:4)	910.7989	17.87	[M+NH ₄] ⁺	1.76E+06
Yes	TG(18:0/18:1/18:1)	886.7989	17.92	[M+NH ₄] ⁺	5.09E+06
No	TG(18:0/18:1/20:1)	914.8302	18.58	[M+NH ₄] ⁺	7.53E+05
Yes	TG(18:0/18:1/20:4)	908.7833	17.21	[M+NH ₄] ⁺	1.98E+06
Yes	TG(18:0/18:1/22:6)	932.7833	17.26	[M+NH ₄] ⁺	2.24E+06
No	TG(18:0/20:3/20:4)	932.7833	16.86	[M+NH ₄] ⁺	1.56E+06
No	TG(18:0/20:4/20:4)	930.7676	16.69	[M+NH ₄] ⁺	2.49E+06
No	TG(18:0/20:4/22:6)	954.7676	16.56	[M+NH ₄] ⁺	1.19E+06
Yes	TG(18:1/18:1/18:1)	884.7833	17.54	[M+NH ₄] ⁺	6.15E+07

Yes	TG(18:1/18:1/18:2)	882.7676	16.88	[M+NH ₄] ⁺	3.33E+06
No	TG(18:1/18:1/20:4)	906.7676	16.82	[M+NH ₄] ⁺	3.70E+06
No	TG(18:1/20:4/20:4)	928.752	16.274	[M+NH ₄] ⁺	2.32E+06
No	TG(18:1/20:4/22:6)	952.752	15.981	[M+NH ₄] ⁺	9.46E+05
No	TG(18:1p/10:3/14:1)*	696.5693	11.696	[M+H] ⁺	4.32E+04
No	TG(18:1p/12:1/14:1)*	728.6319	14.501	[M+H] ⁺	3.16E+06
No	TG(18:1p/14:4/14:4)	744.5693	11.426	[M+NH ₄] ⁺	4.33E+08
Yes	TG(18:2/18:2/18:2)	878.7363	15.892	[M+NH ₄] ⁺	1.50E+06
No	TG(18:2p/10:4/22:4)	798.6162	11.937	[M+NH ₄] ⁺	1.19E+08
No	TG(18:2p/12:4/14:4)	714.5223	10.763	[M+NH ₄] ⁺	2.82E+08
No	TG(18:2p/20:4/20:5)	908.7258	13.595	[M+NH ₄] ⁺	1.48E+06
No	TG(20:1p/10:3/22:6)	826.6475	12.451	[M+NH ₄] ⁺	1.15E+08
No	TG(20:1p/10:4/14:4)	716.538	11.024	[M+NH ₄] ⁺	1.30E+09
No	TG(6:0/18:1/20:4)	740.5955	11.108	[M+Na] ⁺	3.03E+07

Supplementary Table A8 Lipids extracted from hippocampus by *in vivo* SPME method and confidently identified using LipidSearch in **positive** mode. n=3. *This ID requires further confirmation with authentic standards, as $[M+NH_4]^+$ adduct should typically be observed for TG lipids.

Unique to SPME	Lipid Identity	Calc Mass	RT (min)	Main Ion	Mean area
No	Cer(d20:0+pO/2:0)	387.3349	7.21	$[M+H]^+$	1.19E+06
Yes	CerP(d16:0+pO/23:2)	701.5359	12.78	$[M+NH_4]^+$	1.59E+06
Yes	CerP(d18:1+hO/22:0+O)	733.5622	8.03	$[M+H]^+$	5.88E+05
Yes	CerP(d18:1+hO/30:2)	825.6611	8.69	$[M+H]^+$	1.11E+06
No	CerP(d20:0+pO/17:0)	677.5359	12.93	$[M+NH_4]^+$	4.73E+06
Yes	CerP(d20:0+pO/31:0+O)	889.75	13.52	$[M+NH_4]^+$	8.29E+05
Yes	CerP(d22:0+pO/18:2+O)	731.5465	7.82	$[M+H]^+$	5.58E+06
Yes	CerP(d24:0+pO/16:0+O)	735.5778	7.89	$[M+Na]^+$	1.63E+07
No	DG(14:0p/15:0)	510.4648	8.46	$[M+NH_4]^+$	1.07E+07
No	DG(18:0/20:4)	644.538	9.04	$[M+NH_4]^+$	1.93E+06
Yes	DG(21:0/10:2)	550.4597	8.46	$[M+NH_4]^+$	1.04E+07
Yes	PE(16:0/19:0)	733.5622	8.03	$[M+H]^+$	9.34E+07
Yes	PE(16:0/21:0)	761.5935	8.32	$[M+H]^+$	1.73E+07
No	PE(16:0p/18:1)	701.5359	8.34	$[M+H]^+$	2.81E+06
No	PE(16:0p/20:4)	723.5203	8.13	$[M+H]^+$	4.83E+06
No	PE(16:0p/22:6)	747.5203	8.10	$[M+H]^+$	7.06E+06
No	PE(18:0/20:4)	767.5465	8.26	$[M+H]^+$	9.48E+06

Yes	PE(18:0e/19:1)	745.5985	8.28	[M+H] ⁺	8.27E+06
No	PE(18:0p/18:1)	729.5672	8.68	[M+H] ⁺	2.70E+06
Yes	PE(18:0p/20:4)	751.5516	8.45	[M+H] ⁺	7.08E+06
No	PE(18:0p/22:4)	779.5829	8.71	[M+H] ⁺	2.13E+06
No	PE(18:0p/22:6)	775.5516	8.42	[M+H] ⁺	8.06E+06
Yes	PE(18:1/21:0)	787.6091	8.34	[M+H] ⁺	4.10E+07
Yes	PE(18:1/21:1)	785.5935	8.16	[M+H] ⁺	2.19E+07
Yes	PE(19:0/18:1)	759.5778	8.04	[M+H] ⁺	1.70E+08
Yes	PE(19:0/18:2)	757.5622	7.90	[M+H] ⁺	1.63E+07
Yes	PE(19:0/20:4)	781.5622	7.90	[M+H] ⁺	3.87E+07
No	PE(19:0/22:0)	817.6561	9.02	[M+H] ⁺	1.69E+07
Yes	PE(19:0/22:6)	805.5622	7.89	[M+H] ⁺	1.91E+07
Yes	PE(20:0p/17:0)	745.5985	8.20	[M+H] ⁺	8.27E+06
Yes	PE(30:1/11:3)	809.5935	8.19	[M+H] ⁺	3.27E+07
Yes	PE(8:0p/9:0)	465.2855	6.52	[M+H] ⁺	1.10E+07
No	PS(27:0/11:3)	813.552	7.73	[M+Na] ⁺	3.77E+06
Yes	So(d17:1+hO)	301.2617	6.19	[M+H] ⁺	6.31E+05
Yes	So(d18:1)	299.2824	6.54	[M+H] ⁺	5.27E+06
Yes	TG(12:0/14:0/14:0)	694.6111	10.60	[M+NH ₄] ⁺	6.81E+05
Yes	TG(14:0p/11:4/17:0)*	698.5849	9.88	[M+H] ⁺	2.04E+06
Yes	TG(15:0/14:0/16:0)	764.6894	12.09	[M+NH ₄] ⁺	1.24E+06
Yes	TG(15:0/14:0/16:1)	762.6737	11.68	[M+NH ₄] ⁺	9.48E+05

Yes	TG(15:0/14:1/16:1)	760.6581	11.23	[M+NH ₄] ⁺	1.32E+05
Yes	TG(15:0/15:0/16:0)	778.705	12.47	[M+NH ₄] ⁺	2.25E+06
Yes	TG(15:0/16:0/16:0)	792.7207	12.76	[M+NH ₄] ⁺	1.41E+06
No	TG(15:0/16:0/16:1)	790.705	12.24	[M+NH ₄] ⁺	1.57E+06
Yes	TG(15:0/16:0/24:0)	904.8459	15.35	[M+NH ₄] ⁺	1.75E+05
Yes	TG(15:0/16:1/16:1)	788.6894	11.82	[M+NH ₄] ⁺	9.19E+05
Yes	TG(16:0/12:0/14:0)	722.6424	11.20	[M+NH ₄] ⁺	6.82E+05
Yes	TG(16:0/12:0/14:3)*	716.5955	10.60	[M+H] ⁺	3.18E+05
Yes	TG(16:0/13:0/14:0)	736.6581	11.40	[M+NH ₄] ⁺	5.47E+05
Yes	TG(16:0/14:0/14:0)	750.6737	11.81	[M+NH ₄] ⁺	1.26E+06
Yes	TG(16:0/14:0/14:1)	748.6581	11.36	[M+NH ₄] ⁺	7.72E+05
Yes	TG(16:0/14:0/16:1)	776.6894	11.99	[M+NH ₄] ⁺	1.72E+06
Yes	TG(16:0/14:0/18:3)*	800.6894	12.46	[M+H] ⁺	9.74E+05
No	TG(16:0/16:0/16:1)	804.7207	12.62	[M+NH ₄] ⁺	2.51E+06
No	TG(16:0/16:0/18:1)	832.752	13.24	[M+NH ₄] ⁺	2.66E+06
No	TG(16:0/16:0/22:6)	878.7363	12.61	[M+NH ₄] ⁺	5.96E+05
Yes	TG(16:0/16:0/24:0)	918.8615	15.74	[M+NH ₄] ⁺	2.13E+05
No	TG(16:0/16:1/16:1)	802.705	12.18	[M+NH ₄] ⁺	1.67E+06
Yes	TG(16:0/16:1/17:0)	818.7363	12.93	[M+NH ₄] ⁺	1.39E+06
Yes	TG(16:0/16:1/17:1)	816.7207	12.47	[M+NH ₄] ⁺	1.04E+06
No	TG(16:0/16:1/18:1)	830.7363	12.79	[M+NH ₄] ⁺	2.31E+06
Yes	TG(16:0/16:1/24:0)	916.8459	15.26	[M+NH ₄] ⁺	1.24E+05

No	TG(16:0/18:1/18:1)	858.7676	13.35	[M+NH ₄] ⁺	3.15E+06
No	TG(16:0/18:1/18:2)	856.752	12.89	[M+NH ₄] ⁺	3.50E+06
No	TG(16:0/18:1/18:3)*	854.7363	13.24	[M+H] ⁺	1.36E+06
No	TG(16:0/18:1/20:4)*	880.752	13.36	[M+H] ⁺	1.62E+06
No	TG(16:0/18:1/22:6)	904.752	12.73	[M+NH ₄] ⁺	1.30E+06
No	TG(16:0/18:2/18:2)	854.7363	12.44	[M+NH ₄] ⁺	1.38E+06
Yes	TG(16:0/18:2/22:6)	902.7363	12.28	[M+NH ₄] ⁺	9.99E+05
No	TG(16:0/20:4/22:6)	926.7363	12.24	[M+NH ₄] ⁺	4.50E+05
Yes	TG(16:0/8:0/12:0)	638.5485	9.55	[M+NH ₄] ⁺	1.58E+06
Yes	TG(16:1/10:4/14:2)	680.5016	4.88	[M+NH ₄] ⁺	7.10E+04
Yes	TG(16:1/12:0/14:0)	720.6268	10.73	[M+NH ₄] ⁺	2.41E+05
Yes	TG(16:1/14:0/14:1)	746.6424	10.95	[M+NH ₄] ⁺	2.50E+05
Yes	TG(16:1/14:0/16:1)	774.6737	11.55	[M+NH ₄] ⁺	7.85E+05
Yes	TG(16:1/16:1/17:1)	814.705	12.03	[M+NH ₄] ⁺	3.43E+05
Yes	TG(16:1/16:1/18:1)	828.7207	12.31	[M+NH ₄] ⁺	9.13E+05
Yes	TG(16:1/16:1/24:0)	914.8302	14.70	[M+NH ₄] ⁺	2.21E+05
Yes	TG(16:1/18:1/24:0)	942.8615	15.36	[M+NH ₄] ⁺	1.63E+05
Yes	TG(18:0/14:0/16:0)	806.7363	13.11	[M+NH ₄] ⁺	1.66E+06
Yes	TG(18:0/15:0/16:0)	820.752	13.30	[M+NH ₄] ⁺	7.77E+05
No	TG(18:0/16:0/16:0)	834.7676	13.78	[M+NH ₄] ⁺	1.45E+06
No	TG(18:0/16:0/18:0)	862.7989	14.44	[M+NH ₄] ⁺	8.72E+05
No	TG(18:0/16:0/18:1)	860.7833	13.89	[M+NH ₄] ⁺	2.37E+06

No	TG(18:0/16:0/18:1)	860.7833	13.89	[M+NH ₄] ⁺	2.47E+05
No	TG(18:0/16:0/18:3)*	856.752	13.52	[M+H] ⁺	4.02E+05
Yes	TG(18:0/16:0/19:0)	876.8146	14.78	[M+NH ₄] ⁺	2.26E+05
Yes	TG(18:0/16:0/20:0)	890.8302	15.09	[M+NH ₄] ⁺	3.70E+05
Yes	TG(18:0/16:0/20:3)*	884.7833	14.44	[M+H] ⁺	4.89E+05
No	TG(18:0/16:0/22:6)	906.7676	13.27	[M+NH ₄] ⁺	9.23E+05
Yes	TG(18:0/17:0/18:1)	874.7989	14.22	[M+NH ₄] ⁺	1.89E+05
Yes	TG(18:0/18:0/18:1)	888.8146	14.55	[M+NH ₄] ⁺	8.27E+05
Yes	TG(18:0/18:0/20:3)*	912.8146	15.09	[M+H] ⁺	1.94E+05
No	TG(18:0/18:0/20:4)	910.7989	14.07	[M+NH ₄] ⁺	3.33E+05
No	TG(18:0/18:1/18:1)	886.7989	14.01	[M+NH ₄] ⁺	1.46E+06
Yes	TG(18:0/18:1/20:3)*	910.7989	14.55	[M+H] ⁺	3.99E+05
No	TG(18:0/18:1/20:4)	908.7833	14.02	[M+H] ⁺	6.98E+05
Yes	TG(18:0/18:1/22:4)	936.8146	13.98	[M+NH ₄] ⁺	3.20E+05
No	TG(18:0/18:1/22:6)	932.7833	13.38	[M+NH ₄] ⁺	1.02E+06
No	TG(18:1/18:1/18:1)	884.7833	13.50	[M+NH ₄] ⁺	2.30E+06
No	TG(18:1/18:1/18:2)	882.7676	13.00	[M+NH ₄] ⁺	1.20E+06
Yes	TG(18:1/18:2/18:2)	880.752	12.55	[M+NH ₄] ⁺	8.54E+05
Yes	TG(18:1/18:2/20:4)*	904.752	13.04	[M+H] ⁺	5.00E+05
No	TG(18:2/18:2/18:2)	878.7363	12.12	[M+NH ₄] ⁺	5.34E+05
Yes	TG(18:2p/12:3/14:4)	716.538	8.03	[M+NH ₄] ⁺	9.30E+07
Yes	TG(18:4/15:0/16:1)*	810.6737	11.87	[M+H] ⁺	3.02E+05

Yes	TG(18:4/16:0/16:1)*	824.6894	12.18	[M+H] ⁺	7.84E+05
Yes	TG(25:0/16:0/16:1)	930.8615	15.54	[M+NH ₄] ⁺	1.63E+05
Yes	TG(25:0/16:0/18:1)	958.8928	16.12	[M+NH ₄] ⁺	7.18E+04
Yes	TG(26:0/15:0/16:0)	932.8772	15.91	[M+NH ₄] ⁺	1.90E+05
Yes	TG(26:0/16:0/16:1)	944.8772	15.86	[M+NH ₄] ⁺	1.58E+05
Yes	TG(4:0/16:0/18:0)	666.5798	10.05	[M+NH ₄] ⁺	1.03E+06
Yes	TG(4:0/16:0/18:3)	660.5329	9.55	[M+H] ⁺	5.90E+05
Yes	TG(8:0/12:0/12:0)*	582.4859	8.74	[M+NH ₄] ⁺	8.73E+05
Yes	TG(8:0/12:0/14:0)	610.5172	9.13	[M+NH ₄] ⁺	1.31E+06

Appendix B Systematic Assessment of Seven Solvent and Solid-Phase
Extraction Methods for Metabolomics Analysis of Human Plasma by
LC-MS

Dmitri G. Sitnikov, Cian S. Monnin and Dajana Vuckovic

SCIENTIFIC REPORTS

OPEN

Systematic Assessment of Seven Solvent and Solid-Phase Extraction Methods for Metabolomics Analysis of Human Plasma by LC-MS

Received: 04 May 2016
Accepted: 10 November 2016
Published: 21 December 2016

Dmitri G. Sitnikov^{1,2}, Cian S. Monnin¹ & Dajana Vuckovic^{1,2}

The comparison of extraction methods for global metabolomics is usually executed in biofluids only and focuses on metabolite coverage and method repeatability. This limits our detailed understanding of extraction parameters such as recovery and matrix effects and prevents side-by-side comparison of different sample preparation strategies. To address this gap in knowledge, seven solvent-based and solid-phase extraction methods were systematically evaluated using standard analytes spiked into both buffer and human plasma. We compared recovery, coverage, repeatability, matrix effects, selectivity and orthogonality of all methods tested for non-lipid metabolome in combination with reversed-phased and mixed-mode liquid chromatography mass spectrometry analysis (LC-MS). Our results confirmed wide selectivity and excellent precision of solvent precipitations, but revealed their high susceptibility to matrix effects. The use of all seven methods showed high overlap and redundancy which resulted in metabolite coverage increases of 34–80% depending on LC-MS method employed as compared to the best single extraction protocol (methanol/ethanol precipitation) despite 7x increase in MS analysis time and sample consumption. The most orthogonal methods to methanol-based precipitation were ion-exchange solid-phase extraction and liquid-liquid extraction using methyl-tertbutyl ether. Our results help facilitate rational design and selection of sample preparation methods and internal standards for global metabolomics.

The objective of global metabolomics is to analyze all small-molecular-weight species ($\leq 1,500$ Da) in a biological sample¹. LC-MS is currently the method of choice for global metabolomics studies because it provides the highest metabolite coverage using a single analytical technique². Typically, several hundred to thousand(s) metabolites can be detected in a single analysis³. The size of human metabolome is currently unknown, but is projected to exceed the conservative estimate of 4229 endogenous metabolites in concentrations spanning 11 orders of magnitude⁴. The most recent estimates predict 8500 endogenous metabolites⁵, and up to 40000 additional exogenous metabolites, such as drugs, additives and toxins that may be present in human samples⁶. Considering the typical coverage of untargeted metabolomics analysis, it is clear that metabolome complexity is overwhelming the capacity of modern metabolomics methods. Therefore, new strategies to increase metabolome coverage are required.

The most widely used protocol for global metabolomics of plasma is solvent precipitation using cold methanol or methanol/ethanol (1/1, v/v) with a plasma-to-solvent ratio of 1 to 3 or 4^{7–10}. Cold solvent is added to minimize the extent of enzymatic conversion of metabolites and to precipitate the proteins. The removal of proteins from plasma also prevents protein build-up on LC column which improves LC column lifetime and significantly increases the number of detected metabolites through disruption of protein binding and minimizing number of signals originating from proteins¹¹. Methanol and methanol/ethanol are the solvents of choice due to high metabolite coverage as shown by several studies^{8,9,11}. However, the wide selectivity of such solvent-based precipitations results in highly complex samples which precludes the detection of lower abundance metabolites. Liquid-liquid extraction (LLE) using methyl-tertbutyl ether (MTBE) has become a popular alternative in recent years for its ability to provide good coverage of both polar and lipid metabolomes and compatibility with robotic

¹Department of Chemistry and Biochemistry, Concordia University, 7141 Sherbrooke St. W., Montréal, Québec, H4B 1R6, Canada. ²PERFORM Centre, Concordia University, 7141 Sherbrooke St. W., Montréal, Québec, H4B 1R6, Canada. Correspondence and requests for materials should be addressed to D.V. (email: dajana.vuckovic@concordia.ca)

systems^{13,14}. In contrast, solid-phase extraction (SPE) methods are often avoided in global metabolomics of plasma due to their increased selectivity comparative to methanol-based extraction methods. SPE methods, thus, tend to decrease overall metabolite coverage¹¹ but may improve data quality through improved repeatability^{11,15} and reduced matrix effects^{12,16}. For instance, optimized HybridSPE™ successfully removed phospholipids in order to lower matrix effects while maintaining acceptable recoveries and repeatability¹¹. In order to increase metabolome coverage beyond what can be achieved with methanol-based precipitations, multiple orthogonal extraction methods can be combined in a sequential manner as successfully shown in lipidomics where 2-fold improvement in coverage was achieved using different SPE fractionation approaches^{7,17}. However, no similar sequential extraction approaches exist to date for non-lipid metabolome. To systematically design such sequential extraction protocol(s), it is necessary to directly compare coverage of various solvent precipitation, LLE and SPE methods. However, only a limited number of studies compared solvent precipitation methods to SPE and LLE to date^{7,11,12}. Based on these published evaluations of extraction methods in real samples, a few limitations should be highlighted. None of these studies examine the orthogonality of SPE and MTBE methods to methanol-based methods in side-by-side fashion and comparison across the studies is not possible due to the different instrumentation and data processing strategies used. Most of these studies focus on metabolome coverage and extraction repeatability only, and no simultaneous evaluation of matrix effects and recovery in biological matrix has been performed to date. Recovery studies are crucial in order to design sequential extraction methods that are fully orthogonal and minimize splitting of the signal between multiple fractions. In addition, semi-quantitative comparisons of metabolite signal intensities between extraction methods can be misleading because variations in analyte signals due to matrix effects are not properly taken into account using the addition of stable isotope labeled (SIL) analytes^{18,19}, fully isotopically-labeled complex matrices, or standard addition calibration. The latter approach was successfully employed to monitor and compare absolute recovery of sequential extraction by hybrid and mixed-mode SPE in untargeted metabolomics²⁰. The underappreciated advantages of standard addition method become obvious when comparing different extraction methods. It is well-established that the slopes of calibration curves for biofluids originating from multiple populations can show significant differences²¹. Similarly, different matrix effects are expected in samples originating from extraction methods with different selectivity. In such cases, signal intensity changes may be driven by matrices alone leading to erroneous conclusions regarding the extraction performance. Although matrix effects are extensively studied in targeted bioanalysis, this issue has not been addressed in global metabolomics of biofluids except in one study where post-column infusion experiment was performed to identify region of significant ion suppression¹⁶. However, anecdotal evidence across multiple comparison studies shows potentially significant matrix effects with huge differences in signal intensity observed when using different extraction methods^{15,20,22}. Therefore, the quantification of absolute recovery and matrix effects using a systematic set of standard analytes when evaluating multiple extraction methods is missing from comparisons to date, leaving a critical gap in our knowledge.

Following an extraction, the most frequently used LC separation in global metabolomics is the parallel use of C18 reversed-phase (RP) chromatography and hydrophilic interaction chromatography (HILIC) to achieve good coverage of non-polar and polar metabolome respectively^{23,24}. More recently, mixed-mode chromatographic materials combining RP and ion-exchange mechanisms in low-bleed MS-compatible stationary phases provide improved retention of a broad spectrum of metabolites^{25,26}. The major objective of this study was to perform the first side-by-side comparison of three conventional solvent precipitation methods to test the effect of small changes in solvent polarity (methanol, methanol-ethanol, and methanol-MTBE), one LLE (MTBE) method and three post-deproteinization SPE methods (C18, mixed cation-anion exchange (IEX) and divinylbenzene-pyrrolidone (PEP2)) for LC-MS metabolomics of human plasma. Absolute recovery and matrix effects for standard analytes were evaluated for all seven extraction methods using standard addition method. The repeatability and selectivity/orthogonality of extraction methods were compared using both targeted metabolites and on global basis in combination with RP and mixed-mode IEX/RP (Scherzo) LC-MS. These data pave the way for the rational selection of the best and most complementary extraction methods of the human plasma metabolome and clearly show the effect of using multiple sample preparation methods in a given study design on metabolome coverage.

Methods

Solvents and reagents. LC-MS grade solvents/mobile phase additives and analyte standards were purchased from Sigma-Aldrich (Oakville, ON, Canada) unless stated otherwise. ACTH (1–39) was obtained from Anaspec (Fremont, CA, USA). Norepinephrine (d_6), cholic acid (d_4), epinephrine (d_3), dopamine (d_4), melatonin (d_4), 4-aminobutanoic acid (d_6) and phenylalanine (d_5) were obtained from CDN Isotopes (Point-Claire, QC, Canada), while $^{13}C_6$ - thyroxine was purchased from Toronto Research Chemicals (Toronto, ON, Canada). MTBE was bought from Fisher Scientific (Toronto, ON, Canada), while all phospholipids were obtained from Avanti Polar Lipids (Alabaster, Alabama, USA). Kynurenine and D-erythro-sphingosine (further mentioned as sphingosine for brevity) were purchased from Cayman Chemicals (Ann Arbor, MI, USA). Solid stationary phases (PEP2, ODS-C18 and divinylbenzene conjugated with sulfonic acid and quaternary amine moieties (IEX)) were obtained from Agela Technologies (Wilmington, DE, USA). Citrated pooled human plasma was obtained from Bioreclamation (Baltimore, MD, USA) and was collected in accordance with the company's code of ethics. All reagents were of analytical or higher grade.

Standard analyte mix. The chemical diversity of metabolome is enormous both in terms of polarity and charge^{27,28}. Using predicted octanol/water partition values, metabolites in human plasma cover a polarity range from -5 (polyamines, amino acids) to 10 (fatty acids) to 35 (triacylglycerides)²⁷. For the charge state, metabolites can be separated into acidic, basic, neutral and zwitterion classes. For instance, the study analyzing charge properties of 2553 non-lipid human metabolites from Human Metabolome Database, found that approximately

22% of metabolites are neutral, while 46.5 and 18.2% contain acidic carboxylic and phosphate groups, respectively. Basic aliphatic amines and aromatic heterocyclic nitrogen groups were found in 16 and 24.5% of non-lipid metabolites, while 13.8% of compounds were zwitterions²⁹. The focus of current work is non-lipid metabolome, so standard metabolite selection was confined to metabolites with high to intermediate polarity typically found in blood plasma. A few lipids were also included in the mix to help in the assessment of matrix effects and method selectivity towards lipids, but systematic evaluation of extraction performance for lipids was beyond the scope of this study. Therefore, we evaluated extraction methods using standards with limited but systematic set of chemical properties that (i) resembled class composition of a target samples and included acids, bases, neutrals, zwitterions, lipids and small peptides, (ii) were systematic and scalable in terms of chemical properties (Log P range of -3.9 to 11.5 , MW range of 105 to 900 Da), and (iii) amenable to the RP and mixed-mode LC-MS analytical methods employed in the study. All individual stock solutions were prepared in appropriate solvents as summarized in Supplementary Table 1, divided into aliquots and stored at below -70°C , while working standards were prepared at appropriate concentrations prior to analysis. Standard mix was prepared at $5\ \mu\text{g}/\text{mL}$ from appropriate stock solutions using 20% methanol unless otherwise specified.

Extraction of analyte standard from buffer. The standard mix was prepared at $5\ \mu\text{g}/\text{mL}$ of each compound in 25 mM ammonium acetate, pH 6.5 buffer. This high concentration was required to avoid non-specific adsorptive losses. Buffer composition was selected to obtain suitable pH and ionic strength for IEX stationary phases in order to achieve maximum recovery of analytes, while ensuring MS compatibility. The standard mix was extracted in six replicates by solvent-precipitation (methanol/ethanol (1/1, v/v), methanol, methanol/MTBE (1/1, v/v), liquid-liquid extraction (MTBE) and solid-phase extraction (PEP2, C18, IEX). In solvent precipitations and LLE, $100\ \mu\text{L}$ of standard mix was extracted with $400\ \mu\text{L}$ of ice-cold solvent, vortexed for 30 min and centrifuged for 15 min at $15000 \times g$. All steps were executed at 4°C . After centrifugation, $350\ \mu\text{L}$ of the upper layer was dried and stored at below -70°C until analysis. For SPE, $100\ \mu\text{L}$ of standard mix was loaded on a 3 mL SPE cartridge containing 100 mg (C18, IEX) or 60 mg (PEP2) sorbent. The cartridges were washed with 1 mL of sample buffer and eluted into glass tubes with 1.5 mL of elution solvent specific for every sorbent: C18 with 0.1% formic acid in 100% acetonitrile, PEP2 with 150 mM ammonium acetate, pH 6.8 in 94% methanol and IEX with 400 mM ammonium acetate pH 6.8 in 42% methanol. Eluted samples were evaporated to dryness under vacuum, and stored at below -70°C . Before analysis, all samples were reconstituted in $10\ \mu\text{L}$ of 20% methanol containing 2.5 mM ammonium acetate (pH 6.5), sonicated at ambient temperature for 5 min, vortexed for 10 min, diluted with $90\ \mu\text{L}$ of 2.5 mM ammonium acetate, pH 6.5, sonicated and vortexed for 5 and 10 min and centrifuged at $15000 \times g$ for 30 s.

Extraction of plasma samples spiked with standard analytes. Solvent precipitations and LLE were carried out as described above using (i) the sample buffer (composed of 2% acetonitrile in 2.5 mM ammonium acetate pH 6.5) to obtain a blank extract for each method, (ii) plasma samples spiked with standard analytes to yield approximately 800 ng/ml before extraction and 100 ng/mL at LC-MS step in six replicates and (iii) unspiked plasma samples in 12 replicates to be pooled on per-method basis and used to build calibration curves for each method. Prior to SPE extraction, replicates of plasma and sample buffer were precipitated using methanol as described above, evaporated to dryness, reconstituted in the sample buffer, pooled as appropriate, and divided into replicates equivalent to $100\ \mu\text{L}$ of plasma. Six of these replicates were spiked with the standard analytes at 800 ng/mL per each of three SPE methods. All samples were extracted by three SPE sorbents in parallel following the protocols described above to generate the sample sets similar to the one prepared for precipitation and LLE, i.e. blank extracts (i), spiked plasma extracts (ii), and unspiked plasma extracts (iii). All samples were dried under vacuum and stored at below -70°C .

Preparation of plasma extracts for LC-MS analysis. All plasma extracts were reconstituted in $30\ \mu\text{L}$ of 20% methanol as described for standard analytes and further dissolved in $270\ \mu\text{L}$ of 2.5 mM ammonium acetate. Standard addition calibration curves were prepared for each extraction method by adding $30\ \mu\text{L}$ of the sample buffer or the mix of standard analytes to yield matrix calibration curve with 0 or 62.5, 125, 250 and 500 ng/mL, respectively. For the assessment of matrix effect, an external standard calibration curve in 2.5 mM ammonium acetate pH 6.5, 2% acetonitrile was also prepared in the same concentration range.

LC-MS analysis. All extracts ($10\ \mu\text{L}$ injection volume) were analyzed on 1290 UPLC chromatograph (Agilent Technologies, Santa Clara, CA) using $3.0\ \mu\text{m}$, mixed-mode Scherzo SM-C18, 2×150 mm column (Imtakt, Portland, OR) and $1.8\ \mu\text{m}$ Zorbax Eclipse octadecyl 2×200 mm column coupled to Agilent 6550 iFunnel Q-TOF mass spectrometer in positive and negative ESI in the mass range 100–1000 m/z. Additional details including LC-MS settings are provided in SI.

Data analysis. TOF Quant software (version B.07.00 SP1, Agilent) was used for the determination of absolute recovery of standard metabolites from buffer and plasma. Raw data was extracted at 15 ppm mass accuracy, aligned within ± 0.15 min retention time, integrated and corresponding adducts were summarized. Protonated and deprotonated ions were used for all other analytes in positive and negative ESI, respectively except for melatonin in positive ESI where sodiated adduct was also found. Quantitation was executed using external calibration curves in buffer and standard addition calibration in plasma. The recoveries of each analyte for each extraction method were hierarchically clustered using the Euclidian distance method with CIMminer online analysis at <http://discover.nci.nih.gov/cimminer/oneMatrix.do>³⁰. The recoveries of analytes below 5 and above 80% were assigned to 0 and 100%, respectively for correct visualization. Matrix effect was calculated by dividing the peak area of an analyte in matrix calibration standard spiked post-extraction by the area in the calibration standard

prepared in the sample buffer at the same analyte concentration and converting to percentage. The subtraction of endogenous signals was performed using signal obtained in unspiked plasma extracts. The final results reported for matrix effect represent the mean value obtained across four different concentrations tested for each analyte. Pooled QC samples for all target analytes in all analytical batches showed $RSD \leq 25\%$. QC data showed no evidence of analyte degradation in extracted plasma samples except possibly for histamine and sphingosine both of which showed systematic 20–30% decrease of signal intensity throughout the long analytical batches. For the global evaluation of the extraction methods, peak picking, deconvolution, alignment and integration were executed on Profinder (Agilent) with the following parameters: ion mass threshold of ± 15 ppm, relative height of $MS + 1/MS$ isotope abundance 15%, RT threshold ± 0.15 min, minimum peak height 200 and 2000 counts for $M + 1$ and M peaks, respectively. The selectivity and repeatability analyses were carried out on Mass Profiler Professional (MPP, Agilent) with integration and binning parameters similar to Profinder, after removal of low quality metabolite signals that (i) were not at least 5x higher than the signal in blank and (ii) that were not found in at least 5 out of 6 replicates of a given extraction method. The data were manually verified and found to include 2–3% duplicate entries (a feature split between multiple entries by the peak picking algorithm). Therefore, the accuracy of putative metabolite coverage is $\pm 3\%$. The orthogonality of extraction methods in global metabolomics approach was evaluated in a pairwise manner using the above high-quality data. Number of matched features for all possible paired combinations were used for hierarchical clustering using CIMiner online tool.

Results and Discussion

Seven different extraction methods are compared based on the absolute recovery of standard analytes from buffer and human plasma, repeatability, selectivity and matrix effects in parallel with global LC-MS based metabolomics analysis. The overall experimental design is shown in Supplementary Figure 1. To the best of our knowledge, this is the first side-by-side comparison of the quality of sample preparation from blood plasma by conventional solvent precipitations (methanol-ethanol, methanol, methanol-MTBE), LLE (MTBE) and SPE (C18, IEX, PEP2) methods in a single study.

Targeted Analysis

Recovery, repeatability and selectivity of metabolite extraction from buffer. Analyte recovery is summarized in Fig. 1a and Supplementary Table 2. The analytes are listed by increasing logP values retrieved from Chempidder database predicted using ACD Laboratories algorithm. The extraction methods are arranged according to the results of hierarchical analysis. As expected, methanol, methanol/ethanol and methanol/MTBE extractions clustered closely together and provided the broadest coverage and the highest recovery across the wide range of metabolite classes tested. IEX provided high recovery only for polar charged metabolites, while MTBE provided high recovery for hydrophobic neutral metabolites. Among SPE methods, PEP2 provided broader metabolite coverage than C18 (Table 1), due to its ability to retain some of the polar metabolites. The highest selectivity in buffer was demonstrated by IEX, followed by C18 and MTBE. Moreover, IEX and C18/MTBE methods demonstrated little overlap, which can be exploited in sequential sample preparations for global and targeted metabolomics. None of the tested analytes exhibited $\geq 50\%$ recovery in all of the extraction methods (Supplementary Table 2). Supplementary Table 4 summarizes the main performance characteristics of all extractions methods tested. The recovery of $\geq 80\%$ is considered exhaustive and quantitative bioanalytical methods permit method precision of up to $\leq 20\%$ RSD at lower limit of quantitation. However, very few metabolites can meet these most stringent criteria for any of the tested methods as shown in Supplementary Table 4. Global metabolomics methods are considered semi-quantitative, so applying more relaxed criteria of $\geq 50\%$ recovery and $\leq 30\%$ RSD is a reasonable compromise between method coverage and method performance. Using this criteria, methanol-based precipitations can provide acceptable performance for 17 out of 22 metabolites. Overall, metabolite recovery correlated to the predicted LogP values and the expected selectivity of the extraction methods. Neutral metabolites such as melatonin demonstrated the best quantitative ($\geq 80\%$) recoveries amongst all standard metabolites. The best repeatability was demonstrated by methanol-based precipitations (Supplementary Table 4). SPE and LLE methods demonstrated lower repeatability than methanol blends with the poorest performance by MTBE and C18 SPE (Supplementary Table 4). This poor repeatability of MTBE is attributed to irreproducible partitioning of some metabolites between organic and aqueous phases, and was most pronounced for pantothenic acid, thyroxine and phenylalanine.

Recovery, repeatability and selectivity of metabolite extraction from plasma. The high recovery ($\geq 80\%$) was demonstrated by thyrotropin releasing hormone and melatonin in 6 out of 7 methods tested (Fig. 1b, Supplementary Table 3). Ionic compounds such as histamine, tyrosine and kynurenine with low molecular weight and LogP values demonstrated quantitative recovery in only 1 out of 7 methods. In addition, better recovery of triiodothyronine, thyroxine and the large peptide neurotensin (in contrast to tripeptide thyrotropin releasing hormone) was observed on RP SPE comparative to solvent based extractions (Supplementary Table 3A). The recovery of some analytes from plasma changed drastically in plasma *versus* buffer. The recovery of neutral compounds (cortisol, cortisone) by MTBE, PEP2 and C18 was decreased in plasma but the recovery in methanol-based solvents increased (Supplementary Tables 2A and 3A). This clearly shows the importance of performing recovery studies in biofluid matrix. The extraction repeatability (Supplementary Table 3B) showed similar trends to what was seen in buffer with methanol-based methods outperforming both SPE and LLE methods. However, SPE and LLE methods showed significant deterioration of method precision. For instance, MTBE method provided acceptable precision ($\leq 30\%$ RSD) for only melatonin, cortisol and triiodothyronine. Hierarchical clustering results shown in Fig. 1b confirm wide metabolite coverage of gold standard methanol-based solvent precipitation methods with high recovery across metabolite classes. The results also show the selectivity of MTBE is narrowed

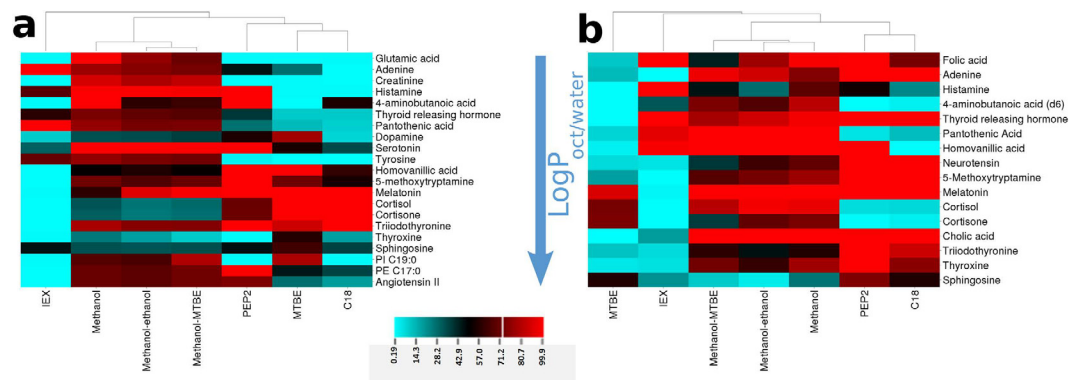


Figure 1. Hierarchical analyses and heat maps show the recovery of standard analytes from buffer (a) and human plasma (b). All extraction methods were hierarchically clustered using Euclidian distance method. The intensity of each cell represents range of recovery of an analyte relative to the initial amount spiked prior extraction. Recoveries below 5 and above 80% were assigned to 0 and 100%, for visualization purposes. The order of analytes corresponds to the increase in octanol-water partition coefficients, except for angiotensin II which did not have predicted value.

Evaluation of matrix effects	RP LC-MS analysis							Scherzo mixed-mode LC-MS analysis						
	Methanol-ethanol	Methanol-MTBE	Methanol	MTBE	IEX	PEP2	C18	Methanol-ethanol	Methanol-MTBE	Methanol	MTBE	IEX	PEP2	C18
Suppressed (+ESI)	6	6	6	4	7	9	5	4	4	4	4	4	7	5
Enhanced (+ESI)	5	5	5	4	2	4	2	11	11	11	7	7	3	2
Total affected (+ESI)	11	11	11	8	9	13	7	15	15	15	11	11	10	7
Total unaffected (+ESI)	6	6	6	12	7	4	10	2	2	1	8	4	7	10
Suppressed (-ESI)	3	3	5	0	1	1	1	7	4	9	1	10	5	3
Enhanced (-ESI)	2	2	2	2	4	7	8	4	3	2	5	1	4	2
Total affected (-ESI)	5	5	7	2	5	8	9	11	7	11	6	11	9	5
Total unaffected (-ESI)	5	5	3	10	9	6	5	2	6	2	8	1	4	9

Table 1. Summary of total number of standard analytes which experienced matrix effect (suppression or enhancement) across different extraction methods in combination with either RP or mixed-mode LC-MS analysis. Analytes ($n = 24$, including SIL analogues for some of the metabolites) were counted if they were detected in buffer and at least one of the post-extraction spiked calibration standards. For metabolites detected at all concentration levels the mean matrix effect obtained across all concentration levels is reported. A metabolite was considered to be enhanced if its matrix effect ratio exceeded 120% or suppressed if it was less than 80%. The species that were not detected in either matrix were not counted, because matrix effect could not be properly determined for such cases. Supplementary Table 7 shows full results for matrix effect evaluation.

to uncharged species with $\text{LogP} \geq 1.4$ and confirm orthogonal selectivity of IEX and MTBE methods previously observed for buffer. This can be used for the removal of hydrophobic compounds in sequential sample preparations. The effect of adding a second MTBE extraction step was also investigated to examine if this will further improve the metabolite recovery. The results of this experiment are shown in Supplementary Table 5. Only the recovery of folic acid and adenine increased when the second extraction step is included. For the remaining metabolites, no significant changes within experimental error were observed as expected theoretically due to high polarity of many of the metabolites within standard mix. Finally, methanol-based methods provide the most comprehensive and reproducible extraction of standard analytes from plasma (Fig. 1) as indicated by much lower mean RSD values than observed for other extractions (Supplementary Table 4). The more selective methods of SPE and LLE show good performance only for a narrow range of metabolites that are best suited to each extraction method depending on their polarity and charge characteristics. In both Supplementary Tables 2 and 3, some metabolites show recoveries above 120% in some of SPE methods. This result was surprising, considering the similar matrix composition of standard addition calibration and unknown samples, so it was investigated further. The first possibility considered was different adduct formation in buffer versus plasma. No such differences were found, so this was eliminated as contributing factor. Melatonin and melatonin d_4 both had similar high recoveries in PEP2 and C18 SPE, which pointed to the fact this result may be due to co-suppression of spiked metabolites. The only compositional difference between calibration standards and samples used to evaluate recovery is the number of spiked metabolites present. Calibration standards were spiked after extraction and will therefore

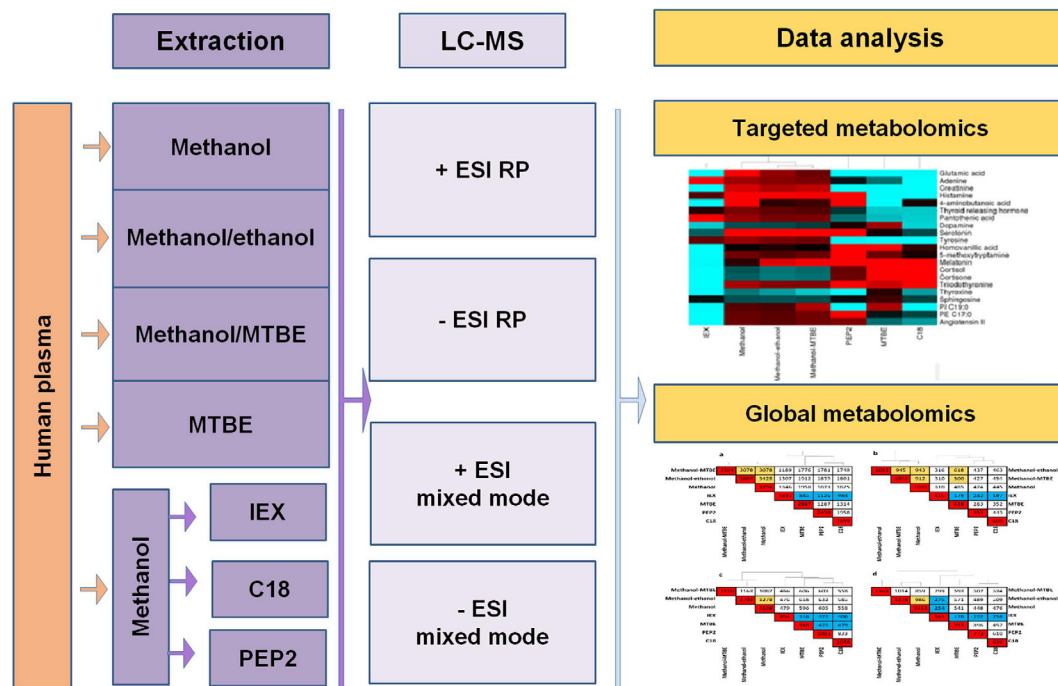


Figure 2. Overview of experimental design to compare seven extraction methods for untargeted metabolomics analysis of human plasma.

contain all metabolites of the standard mix, whereas the recovery samples were spiked before extraction and will remove or incompletely extract some of the metabolites from standard mix depending on the extraction method selectivity. This was further verified by re-analyzing the same extracts on longer chromatographic method (60 min analysis time), and proper quantitative recovery (80–120%) was obtained in all instances. These results clearly show that global metabolomics methods are extremely susceptible to matrix effects and that semi-quantitative performance of these methods can be affected by minor differences in matrix composition.

Extraction preferences of standard analytes. Two groups of analytes emerged based on our recovery studies in buffer and plasma (Fig. 1). Analytes with LogP below 0.4 (above tyrosine) show poor recovery in MTBE and good recovery in methods suitable for extraction of polar species such as PEP2 and methanol-based solvent precipitations (Group I). The second group consists of less polar analytes ($\text{LogP} \geq 0.4$) which demonstrate good recovery in MTBE, PEP2 and C18 (Group II). Interestingly, Group II analytes had recoveries $\geq 50\%$ in most solvent and SPE methods in contrast to their recoveries from buffer. This difference in recovery is attributed to adsorptive losses in buffer. In the experiments with buffer we tried to minimize these losses by using high metabolite concentrations, but clearly adsorptive losses were still considerable especially for metabolites such as thyroxine, cortisone and cortisol. In conclusion, side-by-side systematic comparison of the absolute recovery of extraction methods was possible using standard addition calibration and showed clearly the critical importance of recovery determination in biofluids.

Matrix effects. Matrix effects were evaluated using the post-extraction spike method at up to four different concentration levels. This evaluation was performed using both RP and mixed-mode LC-MS methods in positive and negative ESI. Ion suppression was observed for metabolites with lower LogP values (melatonin, 4-aminobutanoic acid, adenine and homovanillic acid) in methanol-based extractions in RP. Neutral analytes of intermediate polarity with LogP of 1.2 (cortisol and cortisone) were not affected in any extraction method, while signals from more hydrophobic metabolites ($\text{LogP} \geq 1.4$, triiodothyronine and thyroxine) were enhanced in all solvent-based extracts, suppressed in IEX and PEP2 and remained unaffected in C18 SPE. The suppression in solvent-based extractions in -ESI RP (Supplementary Figure 2, Supplementary Tables 6 and 7) affected wider range of analytes than in +ESI and extends toward neutral mid-hydrophobic analytes (cortisol and cortisone), while organic acids (folic, pantothenic, homovanillic and cholic) remained unaffected. The suppression of polar analytes in RP analysis in both positive and negative ESI is not surprising and could be explained by the co-elution of large number of un-retained metabolites. However, mixed-mode LC-MS analysis which is capable of chromatographically separating the majority of these charged species also shows very significant problems with ionization suppression and/or enhancement depending on the analyte and extraction method tested. Previous studies have also shown that HILIC methods are also highly susceptible to matrix effects even when using microextraction format²². Matrix effect could be partially decreased via improved resolution at LC-MS step by the decrease of stationary phase particle size ($< 2 \mu\text{m}$) or drastic increase of column length and chromatography time to limits which may be impractical in real study³¹. Therefore, there is no simple solution to

implement to address this major problem. Finally, methanol-based extracts demonstrated higher number of analytes affected by matrix effect. In contrast, the more selective MTBE and C18 SPE methods showed matrix effects for fewer metabolites and less pronounced extent of suppression/enhancement if matrix effects were present (Table 1, Supplementary Figure 2). The higher suppression matrix effect observed for methanol blends is most likely caused by higher matrix complexity as compared to MTBE and C18 SPE methods which are more selective as shown by our recovery experiments. Overall, the results of this comparison show that matrix effects pose a significant challenge in all extraction protocols and can have significant impact on biomarker discovery efforts. Additional ways to reduce and evaluate matrix effects during such studies should be explored and implemented. Table 1 also shows that the analyses performed using mixed-mode chromatography are more susceptible to signal enhancement. The observed enhancement of signal response (for example, triiodothyronine and thyroxine in Scherzo analysis (Supplementary Figure 2) may be explained by: (i) true matrix effect; (ii) the presence of co-eluting isobaric contaminants whose signals were mistakenly included due to insufficient resolution of QTOF; (iii) formation of significant amount of adducts in buffer but not in matrix calibration points and/or (iv) limited solubility of standard analytes in buffer calibration samples versus plasma extracts. To evaluate possibility (ii), the matrix effect experiment was repeated for +ESI Scherzo LC analysis using Orbitrap Velos™ mass spectrometer with mass resolution of 100,000. The same enhancement results were observed, so we can conclude that the cause of observed ion enhancement is not co-elution of species with similar m/z to the analytes of interest. Next, Na^+ and NH_4^+ adduct formation was compared for buffer samples versus plasma extract samples. No significant differences in adduct formation were found for any analytes except for melatonin where sodiated adduct with the intensity similar to protonated ions was formed in buffer calibration points. To correct for sodiated adduct formation, total area of sodiated and protonated ions was used in calculations of matrix effect for melatonin. Finally, the observation of large differences between matrix effects in Scherzo and RP despite identical sample preparation protocols between these two methods exclude the involvement of partial solubility. Thus, it is plausible to conclude that the enhancement effect observed in mixed-mode LC analysis (and occasionally in RP analysis) is based on true difference in ionization process between plasma-based and buffer-based samples. This is further supported by the fact that for both analytes that exhibit ion enhancement, their isotopically labelled standards also confirm the same extent of enhancement showing high quality of the collected data.

Selection of internal standards for global metabolomics. Our recovery and matrix effects results can be used to guide the selection of the best internal standards for quality control for human plasma metabolomics. Standards that show no susceptibility to matrix effects make ideal internal standards (as SIL analogues) to spike before extraction in order to monitor extraction recovery. These include 5-methoxytryptamine, folic acid, thyrothypin releasing hormone and cortisol for +ESI RP; and pantothenic and cholic acids for -ESI RP all of which showed no matrix effects across all seven extraction methods tested as shown in Supplementary Table 6. These can be supplemented with additional standards spiked post extraction to monitor for matrix effects such as SIL analogues of adenine and thyroxine for \pm ESI RP; neurotensin, melatonin, thyroxine and cortisol for +ESI Scherzo and homovanillic acid, melatonin and thyroxine -ESI Scherzo. These analytes show large differences in matrix effects between different extraction methods as shown in Supplementary Figure 2 which suggests their ionization is susceptible to presence of possible co-eluting interferences, and do not overlap with proposed recovery standards. The use of matrix effect standards is suggested to evaluate relative matrix effects between individual samples but it should be noted that they would only reflect the extent of ion suppression at that specific moment of chromatographic run. Finally, the above internal standard suggestions are valid for the exact extraction methods, plasma loading and LC methods tested in this study. Further testing is required to extrapolate the use of these specific standards to other experimental conditions. In general, for any combination of extraction method and LC-MS analysis, standards with high recovery in that extraction method and no matrix effects across all extractions for the chosen LC-MS method would make ideal recovery standards, while standards highly susceptible to ion suppression/enhancement would make useful internal standards for monitoring of matrix effects across individual samples.

Global Metabolite Analysis

Seven extraction protocols were compared using four LC-MS analyses in order to assess metabolite coverage, extraction repeatability and method overlap (orthogonality) as shown in Fig. 2. Table 2 summarizes metabolite coverage and extraction repeatability of all extraction methods tested. As expected, the highest number of putative metabolites was extracted by methanol-based solvent precipitation methods, with the highest number of putative metabolites (3804) detected for methanol/ethanol. The analysis of organic MTBE fraction resulted in 2887 putative metabolites as revealed by +ESI RP analysis. Approximately 30% less metabolite features were detected in C18 and PEP2 SPE extracts while only 1835 putative metabolites were observed for IEX SPE. The table also shows median RSD of signals across all extraction methods for each LC-MS analysis. Methanol-ethanol and methanol extractions demonstrated the best repeatability versus all other extraction methods independently of LC-MS method employed. PEP2 and IEX had acceptable repeatability for global metabolomics. On the other hand, MTBE and C18 extraction methods demonstrated the worst repeatability independent of LC-MS analysis (Table 2). The high proportion of irreproducible features in these two methods requires the application of rigorous quality controls and in-depth investigation for the sources of such irreproducibility. Previous C18 SPE studies for plasma metabolomics indicate conflicting evidence regarding C18 repeatability for this application. In the first study on this topic, Michopoulos *et al.* showed 48% and 55% of features detected in C18 SPE and methanol precipitation had $\text{RSD} \leq 30\%$ respectively, which implied both methods have similar repeatability¹⁵. Rico *et al.* also observed similar repeatability between methanol and C18 SPE with approximately 80% of features which met 30% RSD criteria for both methods¹¹. Our results show that only 42% of features extracted by C18 SPE met

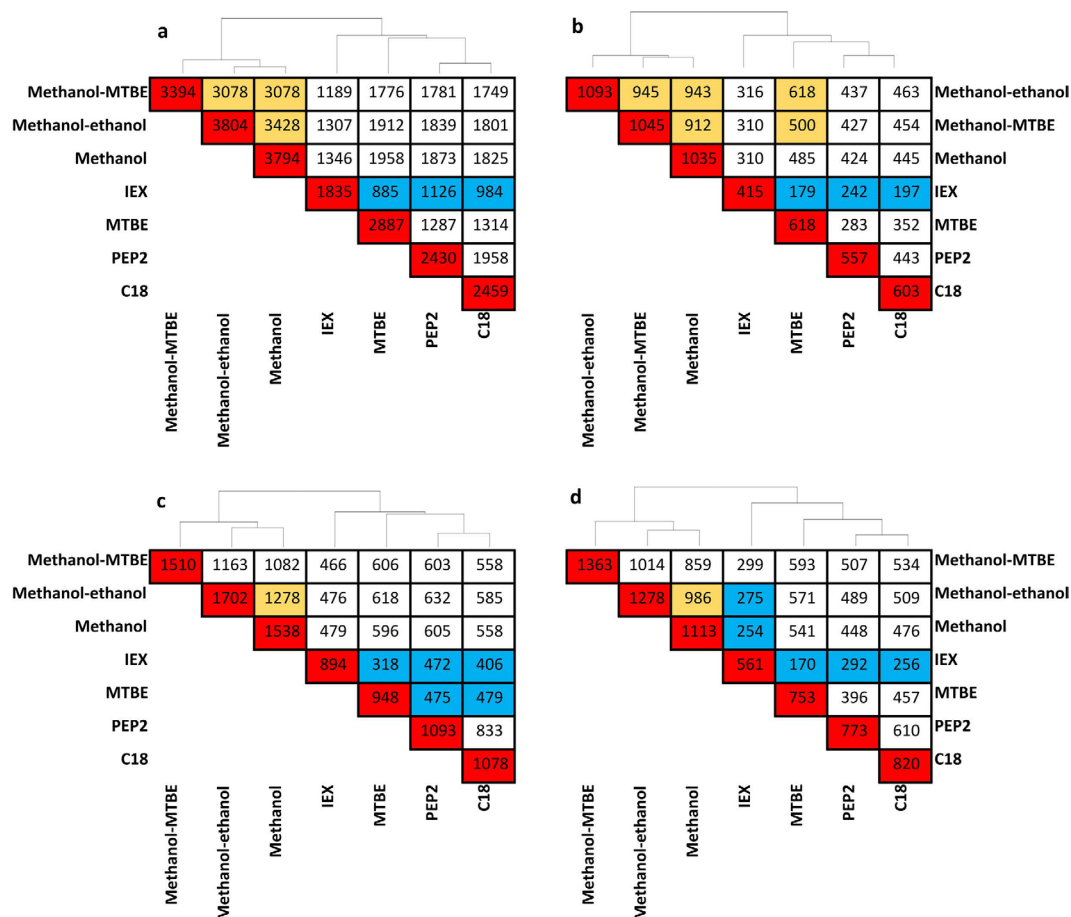


Figure 3. Hierarchical clustering of the number of putative metabolites detected in plasma extracts and pairwise overlap coverage of seven extraction methods. Samples were analyzed using +ESI RP (a) –ESI RP (b), +ESI Scherzo (c) and –ESI Scherzo (d). Red colour boxes located across the diagonal show the total number of putative metabolites detected with that extraction method from plasma. Yellow, white and cyan blue colors designate high (99.9–80% overlap), medium (79.9–50.0%) and low (50.0–0% overlap) of putative metabolite populations observed by the two extraction methods specified. Therefore, the methods indicated with cyan blue boxes are the most orthogonal pairs of methods across all of the seven extraction methods tested.

Extraction method	+ESI RP			–ESI RP			+ESI Scherzo			–ESI Scherzo		
	M	Median % RSD	M ₃₀	M	Median % RSD	M ₃₀	M	Median % RSD	M ₃₀	M	Median % RSD	M ₃₀
Methanol-ethanol	3804	12.8	3306	1093	13.4	1051	1702	22.3	1087	1278	18.7	930
Methanol-MTBE	3394	17.7	2389	1055	12.7	849	1510	25.2	877	1363	21	897
Methanol	3795	11.5	3483	1035	11.4	940	1538	19	1089	1113	17.9	802
IEX	1835	17.5	1406	415	12.5	364	894	23.2	571	561	23.1	373
MTBE	2887	37.9	1037	618	26.9	362	948	39.1	326	753	31.7	345
PEP2	2430	21	1635	557	14.5	444	1093	24.9	651	773	21.5	498
C18	2459	34.6	1032	603	22.7	394	1078	41.4	318	820	33.2	357
Total metabolome coverage	5853			1466			3072			2229		

Table 2. Metabolite coverage and repeatability of extraction methods assessed by global metabolomics analysis. This table shows total number of putative metabolites (M) detected in minimum 5 out of 6 extraction replicates analyzed using RP or Scherzo mixed-mode LC-MS after removal of features present in blank extracts, median RSD of signal intensity across all putative metabolite features detected in the extraction method and the number of metabolites for which extraction method was highly repeatable with RSD ≤ 30% for n = 6 independent extractions (M₃₀). RSD for each putative metabolite feature was calculated using raw signal intensities in extraction replicates (n = 6). Number of features with RSD ≤ 30% (between replicates) represent high quality features that could be used for biomarker discovery and pathway analysis in global metabolomics projects.

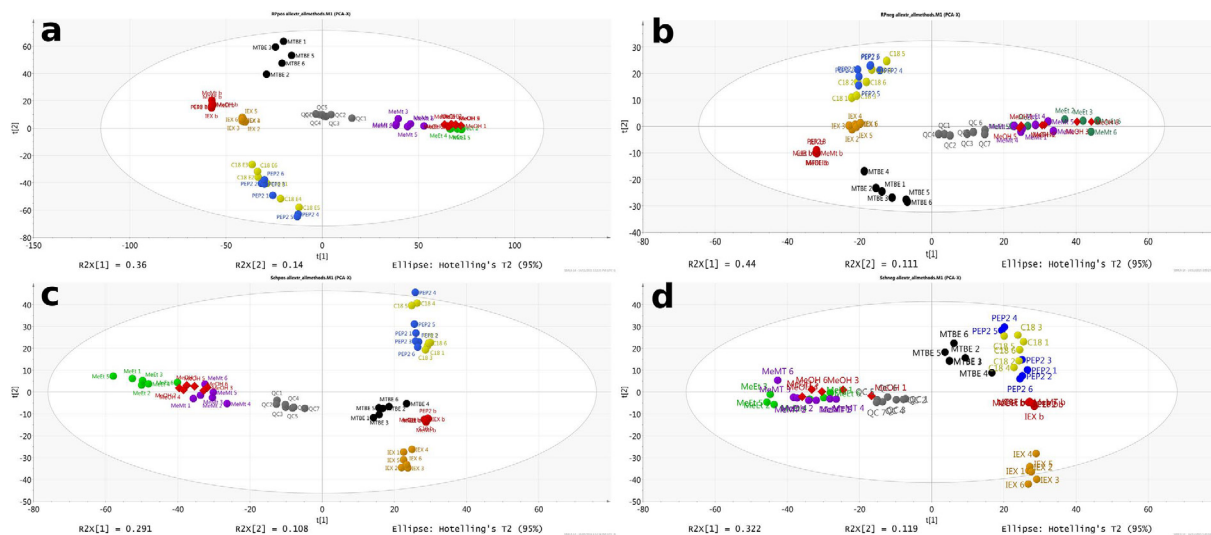


Figure 4. PCA analysis of seven extraction methods and quality control samples analyzed on four LC-MS methods (**a,b** – reversed phase analysis; **c,d** – Scherzo mixed-mode analysis in positive and negative ESI, respectively) executed on all metabolites that satisfy criteria described in main text (not present in blank, and present in minimum of 5 out of 6 replicates of at least one extraction method). The graph displays colored spheres for blank (red), QC (dark grey), IEX (dark gold), C18 (yellow), PEP2 (blue), MTBE (black), methanol-MTBE (violet), methanol-ethanol (green) extraction replicates and red diamonds for methanol extraction replicates. The plots show the top two principal components. Numbering of replicates corresponds to their sequential injection order in a given LC-MS analysis. Analysis was executed using multivariate analysis software SIMCA (v 14.1.64, Umetrics, San Jose, CA, USA) after Pareto scaling.

the repeatability criteria which is consistent with Michopoulos *et al.* study¹⁵. However, our results also show vast superiority of methanol repeatability where 92% of features were highly repeatable with $RSD \leq 30\%$ for $n = 6$ extraction replicates. Considering this discrepancy across the studies for C18 SPE, further investigation of the factors affecting repeatability is required. Such contributing factors may include lack of automation used in our study and the exact selection of sorbent characteristics and wash/elution conditions. For instance, our study employed acetonitrile, whereas both Michopoulos *et al.* and Rico *et al.* used methanol as elution solvent which may have contributed to the poor precision^{11,15}. Our MTBE results are in contrast to good precision obtained when using MTBE with in-vial dual extraction method where $\geq 80\%$ of features had $RSD \leq 30\%$ for $n = 3$ extraction replicates¹⁴. The same authors observed poor precision of MTBE LLE with evaporation/reconstitution step whereby only 56% of detected features exhibited $RSD \leq 30\%$. The latter result is consistent with the results of the current study where evaporation/reconstitution step was employed. During their evaluation of optimum method for lipidomics, Sarafian *et al.* also showed poor repeatability of MTBE in comparison to methanol with a similar 2-fold deterioration of mean RSD and the numbers of highly reproducible lipids³² consistent with what was observed in current study. During further investigation of MTBE extraction repeatability, the repeatability of solvent pipetting was investigated and found not to be significant contributing factor to overall method performance. Next, the +ESI RP LC-MS analysis of newly-prepared aqueous and organic layers obtained after MTBE extraction found that aqueous extracts had repeatability similar to that of methanol (median RSD of 15.7% for MTBE aqueous) versus 16.0% RSD for methanol obtained during this follow-up experiment. In contrast, organic extracts had median RSD of 36.4% which is consistent with 37.9% median RSD obtained in our initial experiment presented in Table 2. Detailed investigation of this data showed clear dependence of RSD on retention time: large proportion of peaks eluting with retention time of >20 min had RSDs greater than 50% in both methanol and MTBE extracts. Methanol had large number of peaks with retention time <20 min which exhibited good repeatability, which resulted in good median RSDs observed for the global metabolomics data. MTBE, on the other hand, had only small number of metabolites eluting with retention time <20 min, and very high proportion of metabolites with retention time >20 min, which resulted in overall higher median RSDs observed in Table 2. Based on this evidence, it is believed that poor MTBE repeatability observed in our study may not arise from the extraction method itself, but from poor match between the composition of MTBE extract and RP and mixed-mode LC separation methods employed in this study which would not adequately separate lipids extracted by MTBE. This conclusion is further supported by the observed increase in median RSD from 35.4 to 50.9% when one-step MTBE and two-step MTBE extractions were compared. Although 2-step extraction increased recovery of few mid-polar metabolites, this also increased the extent of co-elution thus causing further deterioration in RSD.

Further analysis of Table 2 across LC-MS methods demonstrated inferior reproducibility of Scherzo analysis comparative to RP. This is attributed to lower resolution of Scherzo column (larger particle size than RP column) and larger matrix effect than in RP as shown in Matrix Effects section. Finally, hierarchical analysis was performed to determine pairwise orthogonality of each of the methods tested. The results are shown in Fig. 3. The hierarchical clustering confirms the high orthogonality of IEX and MTBE to other methods observed in targeted

Extraction method	Recovery	Matrix effects	Repeat ability	Metabolome coverage
Methanol/ethanol	+++	++	+++	++++
Methanol	++++	++	++++	++++
Methanol/MTBE	+++	++	+++	+++
MTBE	++	++++	+	++
C18	+++	++++	+	++
PEP2	+++	++	++	++
IEX	+	+++	++	+

Table 3. Summary of method performance for extraction of plasma. Number of pluses represent the scoring of method performance where + is the worst and ++++ is the best.

analysis, similarity between methanol-based extractions and similarity between C18 and PEP2 SPE methods. Our orthogonality results for methanol and C18 SPE (1825/2459 putative metabolites = 74% overlap using data shown in Fig. 3) are consistent with what was reported by Rico *et al.* who observed 58–68% overlap between the two methods and ability to detect 600 additional features when comparing SPE to methanol precipitation¹⁰. Using +ESI RP analysis, total of 5853 non-redundant putative metabolite features were detected across all seven extraction methods tested. This represents only 54% improvement over the single best extraction method of methanol/ethanol (3804 putative metabolites) or methanol (3795 putative metabolites). Therefore, 7x increase in MS analysis time and the use of LLE and SPE with widely different selectivity mechanisms did not provide a huge boost in our ability to detect low abundance metabolome. Similar results were observed for other LC-MS methods where the increases were 34% (–ESI RP LC-MS), 80% (+ESI mixed mode LC-MS) and 74% (–ESI mixed mode LC-MS). These results clearly show that simply using multiple extraction methods in parallel is not the best way to increase metabolite coverage and that sequential extractions should be explored to further boost metabolome coverage. Figure 4 shows principal component analysis results for all extraction and LC-MS methods further illustrating that IEX and MTBE are the most complementary methods to methanol-based solvent precipitation.

Conclusions

For the first time, absolute analyte recoveries and matrix effects in plasma were systematically assessed for seven solvent precipitations, LLE and SPE methods using standard addition calibration. In addition, method repeatability, orthogonality and metabolome coverage were compared in combination with two reversed-phased and mixed-mode LC-MS methods. Our results confirm wide selectivity of methanol-based precipitation methods versus LLE and SPE, with the best results observed using methanol or methanol/ethanol as shown in Table 3. However, methanol-based methods suffer from severe matrix effects which negatively impacts data quality and may result in inaccurate selection of tentative biomarkers. We also show that IEX and PEP2 SPE provide acceptable performance for global metabolomics studies of plasma, and can be employed depending on the desired coverage of the metabolome for a given application. Our analysis platform revealed high orthogonality of MTBE and IEX to each other and other methods, providing the possibility of increased metabolome coverage via sequential application of these methods.

References

- Ceglarek, U. *et al.* Challenges and developments in tandem mass spectrometry based clinical metabolomics. *Mol. Cell. Endocrinol.* **301**, 266–271 (2009).
- Vuckovic, D. Current trends and challenges in sample preparation for global metabolomics using liquid chromatography – mass spectrometry. *Anal. Bioanal. Chem.* **403**, 1523–1548 (2012).
- Kraly, J. R., Telu, K. H., Yan, X., Wallace, W. E., Stein, S. E. & Simón-Manso, Y. Analysis of human plasma metabolites across different liquid chromatography/mass spectrometry platforms: Cross-platform transferable chemical signatures. *Rapid Commun. Mass Spectrom.* **30**, 581–593 (2016).
- Psychogios, N. *et al.* The Human Serum Metabolome. *PLoS One* **6**, 1–23 (2011).
- Wishart, D. S. Advances in metabolite identification. *Bioanalysis* **3**, 1769–1782 (2011).
- Wishart, D. S. *et al.* HMDB 3.0—The Human Metabolome Database in 2013. *Nucleic Acids Res.* **41**, D801–D807 (2013).
- Yang, Y. *et al.* New sample preparation approach for mass spectrometry-based profiling of plasma results in improved coverage of metabolome. *J. Chromatogr. A* **1300**, 217–226 (2013).
- Bruce, S. J. *et al.* Investigation of human blood plasma sample preparation for performing metabolomics using ultrahigh performance liquid chromatography/mass spectrometry. *Anal. Chem.* **81**, 3285–96 (2009).
- Want, E. J. *et al.* Solvent-dependent metabolite distribution, clustering, and protein extraction for serum profiling with mass spectrometry. *Anal. Chem.* **78**, 743–752 (2006).
- Gika, H. & Theodoridis, G. Sample preparation prior to the LC-MS-based metabolomics/metabonomics of blood-derived samples. *Bioanalysis* **3**, 1647–61 (2011).
- Rico, E., González, O., Blanco, M. E. & Alonso, R. M. Evaluation of human plasma sample preparation protocols for untargeted metabolic profiles analyzed by UHPLC-ESI-TOF-MS. *Anal. Bioanal. Chem.* **406**, 7641–7652 (2014).
- Tulipani, S., Llorach, R., Urpi-Sarda, M. & Andres-lacueva, C. Comparative analysis of sample preparation methods to handle the complexity of the blood fluid metabolome: when less is more. *Anal. Chem.* **85**, 341–348 (2013).
- Matyash, V., Liebisch, G., Kurzchalia, T. V., Shevchenko, A. & Schwudke, D. Lipid extraction by methyl-tert-butyl ether for high-throughput lipidomics. *J. Lipid Res.* **49**, 1137–46 (2008).
- Whiley, L., Godzien, J., Ruperez, F. J., Legido-Quigley, C. & Barbas, C. In-vial dual extraction for direct LC-MS analysis of plasma for comprehensive and highly reproducible metabolic fingerprinting. *Anal. Chem.* **84**, 5992–9 (2012).
- Michopoulos, F., Lai, L., Gika, H., Theodoridis, G. & Wilson, I. UPLC-MS-based analysis of human plasma for metabonomics using solvent precipitation or solid phase extraction. *J. Proteome Res.* **8**, 2114–21 (2009).

16. Tulipani, S. *et al.* New and vintage solutions to enhance the plasma metabolome coverage by LC-ESI-MS untargeted metabolomics: the not-So-simple process of method performance evaluation. *Anal. Chem.* **87**, 2639–2647 (2015).
17. Skov, K., Hadrup, N., Smedsgaard, J. & Frandsen, H. LC-MS analysis of the plasma metabolome—A novel sample preparation strategy. *J. Chromatogr. B* **978–979**, 83–88 (2015).
18. Berg, T. *et al.* Evaluation of ^{13}C - and ^2H -labeled internal standards for the determination of amphetamines in biological samples, by reversed-phase ultra-high performance liquid chromatography-tandem mass spectrometry. *J. Chromatogr. A* **1344**, 83–90 (2014).
19. Bueschl, C., Krska, R., Kluger, B. & Schuhmacher, R. Isotopic labeling-assisted metabolomics using LC – MS. *Anal. Bioanal. Chem.* **405**, 27–33 (2013).
20. David, A., Abdul-Sada, A., Lange, A., Tyler, C. R. & Hill, E. M. A new approach for plasma (xeno)metabolomics based on solid-phase extraction and nanoflow liquid chromatography-nanoelectrospray ionisation mass spectrometry. *J. Chromatogr. A* **1365**, 72–85 (2014).
21. Matuszewski, B. K. Standard line slopes as a measure of a relative matrix effect in quantitative HPLC-MS bioanalysis. *J. Chromatogr. B. Analyt. Technol. Biomed. Life Sci.* **830**, 293–300 (2006).
22. Vuckovic, D. & Pawliszyn, J. Systematic evaluation of solid-phase microextraction coatings for untargeted metabolomic profiling of biological fluids by liquid chromatography-mass spectrometry. *Anal. Chem.* **83**, 1944–1954 (2011).
23. Theodoridis, G. *et al.* Mass spectrometry-based holistic analytical approaches for metabolite profiling in systems biology studies. *Mass Spectrom Rev.* **30**, 884–906 (2011).
24. Noga, S. & Buszewski, B. Hydrophilic interaction liquid chromatography (HILIC) — a powerful separation technique. *Anal. Bioanal. Chem.* **402**, 231–247 (2012).
25. Van De Steene, J. & Lambert, W. Validation of a solid-phase extraction and liquid chromatography – electrospray tandem mass spectrometric method for the determination of nine basic pharmaceuticals in wastewater and surface water samples. *J. Chromatogr. A* **1182**, 153–160 (2008).
26. Yanes, Oscar Tautenhahn, Ralf Patti J. & Suizdak, G. Expanding coverage of the metabolome for global metabolite profiling. *Anal. Chem.* **83**, 2152–2161 (2011).
27. Cajka, T. & Fiehn, O. Toward merging untargeted and targeted methods in mass spectrometry-based metabolomics and lipidomics. *Anal. Chem.* **88**, 524–545 (2016).
28. Contrepois, K., Jiang, L. & Snyder, M. Optimized analytical procedures for the untargeted metabolomic profiling of human urine and plasma by combining hydrophilic interaction (HILIC) and reverse-phase liquid chromatography (RPLC)-mass spectrometry. *Mol. Cell. Proteomics* **14**, 1684–1695 (2015).
29. Manallack, D. T. *et al.* The acid/base profile of the human metabolome and natural products. *Mol. Inform.* **32**, 505–515 (2013).
30. Weinstein, J. N. *et al.* An information-intensive approach to the molecular pharmacology of cancer. *Science* **275**, 343–349 (1997).
31. Shi, T. *et al.* Long-gradient separations coupled with selected reaction monitoring for highly sensitive, large scale targeted protein quantification in a single analysis. **85**, 1–16 (2013).
32. Sarafian, M. H. *et al.* Objective set of criteria for optimization of sample preparation procedures for ultra-high throughput untargeted blood plasma lipid profiling by ultra performance liquid chromatography-mass spectrometry. *Anal. Chem.* **86**, 5766–5774 (2014).

Acknowledgements

The authors thank Natural Sciences and Engineering Research Council of Canada for research funding and D.S. thanks PERFORM Centre at Concordia University for Ph.D. scholarship funding.

Author Contributions

D.G.S. and C.S.M. executed all experimental and analysis work, D.G.S. and D.V. designed the study, interpreted results and co-wrote the manuscript. All authors reviewed and revised the manuscript.

Additional Information

Supplementary information accompanies this paper at <http://www.nature.com/srep>

Competing financial interests: The authors declare no competing financial interests.

How to cite this article: Sitnikov, D. G. *et al.* Systematic Assessment of Seven Solvent and Solid-Phase Extraction Methods for Metabolomics Analysis of Human Plasma by LC-MS. *Sci. Rep.* **6**, 38885; doi: 10.1038/srep38885 (2016).

Publisher's note: Springer Nature remains neutral with regard to jurisdictional claims in published maps and institutional affiliations.



This work is licensed under a Creative Commons Attribution 4.0 International License. The images or other third party material in this article are included in the article's Creative Commons license, unless indicated otherwise in the credit line; if the material is not included under the Creative Commons license, users will need to obtain permission from the license holder to reproduce the material. To view a copy of this license, visit <http://creativecommons.org/licenses/by/4.0/>

© The Author(s) 2016